MS&A – Modeling, Simulation and Applications 15

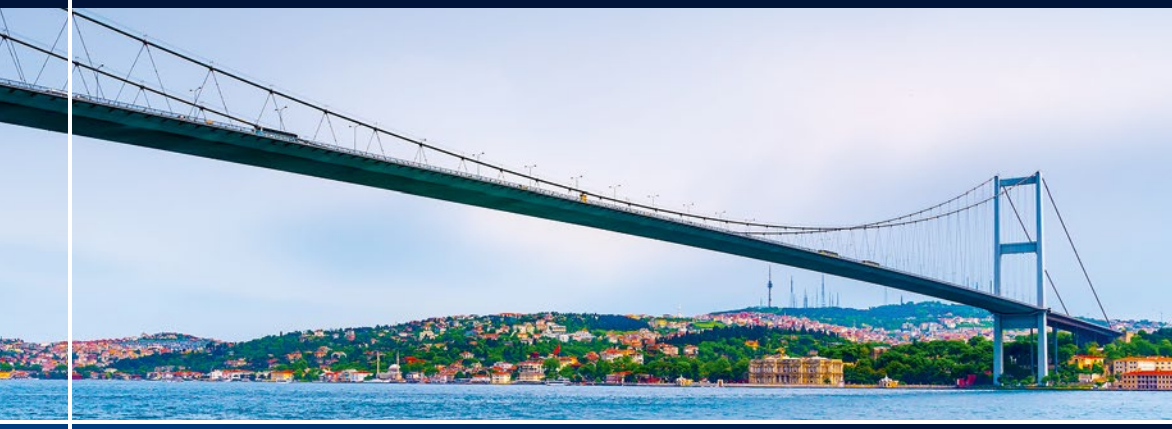

Filippo Gazzola

Mathematical Models for Suspension Bridges

Nonlinear Structural Instability

Springer

MS&A

Volume 15

Editor-in-Chief

A. Quarteroni

Series Editors

T. Hou
C. Le Bris
A.T. Patera
E. Zuazua

More information about this series at
http://www.springer.com/series/8377

Filippo Gazzola

Mathematical Models for Suspension Bridges

Nonlinear Structural Instability

Springer

Filippo Gazzola
Dipartimento di Matematica
Politecnico di Milano
Milano
Italy

ISSN 2037-5255 ISSN 2037-5263 (electronic)
MS&A - Modeling, Simulation & Applications
ISBN 978-3-319-15433-6 ISBN 978-3-319-15434-3 (eBook)
DOI 10.1007/978-3-319-15434-3

Library of Congress Control Number: 2015940339

Springer Cham Heidelberg New York Dordrecht London

Cover illustration: Istanbul Bosphorus Bridge, ©imagIN.gr photography/Shutterstock.com

Printed on acid-free paper

Springer International Publishing AG Switzerland is part of Springer Science+Business Media (www.springer.com)

Dedicated to Chiara, Francesco, Alberto

. . . l'acqua scorre tranquilla
sotto il ponte che oscilla . . .

Preface

Several years ago, I was intensively studying semilinear biharmonic elliptic equations, a topic quite far away from suspension bridges. In 2009, I was invited at a conference in Bertinoro (Italy) and I had the occasion to listen to a talk by Joe McKenna. I had already met Joe several times, including during a beautiful visit to the Corcovado in Rio de Janeiro, and I had also heard some of his talks. But it was on that occasion that I realized that a fourth order equation that he used to describe traveling waves in suspension bridges was identical to an equation that I obtained, after some change of variables, when studying radial entire solutions of semilinear biharmonic equations at critical growth, see [122]. That day I understood that some beautiful pieces of mathematics were certainly hidden into suspension bridges models.

Suddenly, I started getting interested in suspension bridges, in their history, in their mysteries. I spent some time in digging in the engineering literature and I found very interesting debates with divergent opinions leading quite naturally to open problems, of great appeal also for mathematicians. I soon discovered that problems related to structures, and therefore to nonlinear elasticity, are awfully complicated and very little information may be derived from a correct mathematical model. My personal challenge became to find reasonably simple mathematical models able to describe some of the phenomena visible in actual bridges and also able to give reliable responses to designers. This challenge had started some years earlier with the work by McKenna, followed by several other colleagues.

In this book I collected some of the historical material that I found in literature as well as the material that I produced in recent years, thanks to a wide and nice team of collaborators. Hopefully more mathematicians will find some interest in the models and in the open problems presented here, much work is still to be done, many improvements are needed on the models discussed in this monograph. And hopefully engineers will take advantage of several mathematical tools available for the study of nonlinear phenomena and, even better, use them for their future plans.

The main purpose of this book is to observe the static and dynamic behavior of suspension bridges and to try to fit them in suitable mathematical models. Several models suggested in literature are too poor both to describe with sufficient accuracy

the behavior of actual bridges and to give reliable responses. Classical mechanics tells us that **the models should be nonlinear with enough degrees of freedom** but, due to their difficulty, many tools of nonlinear analysis have been developed only in recent years. As a simple but extremely meaningful example, consider the classical Hill [141] equation

$$\ddot{y}(t) + a(t)y(t) = 0 \tag{1}$$

where a is a periodic function. For more than one century, mathematicians have sought refined criteria for the stability of the trivial solution $y \equiv 0$ of (1) but only in recent time, see e.g. [213], the stability of the trivial solution has been studied for nonlinear versions of the Hill equation. I come back to this problem with more details in Chap. 3.

Throughout the book I will discuss classical linear models and revisit them by placing suitable nonlinearities into the equations. Then I analyze the qualitative behavior of the solutions while it is not a primary scope of this book to reach exact quantitative responses. The following step should be to improve further the models and to put the correct values of all the parameters involved, in order to obtain also precise quantitative information and practical suggestions for future plans: some parameters may be determined theoretically whereas other parameters need to be determined experimentally. This step is usually called structural analysis and consists in studying the design and, for given structural geometry, materials and sizes. But this is beyond the scope of this book.

In order to shorten the exposition and to concentrate on the main core, I decided to drop all the proofs and I merely give precise references where to find most of them. Throughout the book I distinguish between Theorems (rigorous statements with all the assumptions) and Propositions (informal statements with qualitative assumptions). The parts of the text written in a smaller type are quotations taken from literature. The parts of the text written in **bold face** and entered in a minibox are statements by myself. One further remark: I give some biographical information only about the authors of historical and old contributions, the whole list of biographies being in the index named "Historical Biographies".

In the next few pages I describe in some detail the purposes and the contents of this book.

Milan, Italy Filippo Gazzola
December 2014

Acknowledgements

The author is grateful to his mathematician colleagues, friends, and collaborators Mohammed Al-Gwaiz, Gianni Arioli, Vieri Benci, Elvise Berchio, Alberto Ferrero, Antonio Giorgilli, Mohamed Jleli, Paschalis Karageorgis, Joseph McKenna, Raffaella Pavani, Bessem Samet, Yongda Wang, and Chiara Zanini for inspiring discussions and sharing ideas. He is also grateful to the engineers Gianni Bartoli, Fabio Biondini, Antonio Capsoni, Giorgio Diana, Walter Lacarbonara, Pier Giorgio Malerba, Paolo Mantegazza, Federico Perotti, Giuseppe Rega, Ferruccio Resta, Maurizio Zanotti, and Alberto Zasso for their interest and for fruitful discussions and suggestions on the engineering part of the models.

The author also thanks the master civil engineering students Davide Baccarin, Pierre Bergot, and Luca Civati for their enthusiasm and work on some of the models presented in this book. Moreover, the author is grateful to Esperia Ferrara for taking care of the copyright duties and to Francesca Bonadei for her highly professional assistance.

Last but not least, the author is willing to thank several anonymous referees for their criticisms which lead to an improvement of some parts of this book and the Editors of the MS&A Springer series for their encouragements and suggestions.

Essential parts of this book are based on the work published in different form before. The author thanks all his collaborators for their contributions which are reported in this book. Detailed information on the sources are given in the bibliographical notes at the end of each chapter.

About this book

For later use, let us explain how we name the different components of a suspension bridge, see Fig. 1. The roadway is supported from below by a girder which is often composed by stiffening trusses. Four high towers sustain two parallel cables which in turn sustain the hangers: we will emphasize the importance of cables by calling them sustaining cables. At their lower endpoint the hangers are linked to the roadway and sustain it from above. A suspension bridge is usually erected starting from the anchorages and the towers. Then the sustaining cables are installed between the two couples of towers. Once the cables are in position, they furnish a stable working base from which the roadway and the stiffening truss can be raised from floating barges. The hangers are hooked to the cables and the roadway is hooked to the hangers; this deforms the cable and stretches the hangers which start their restoring action on the roadway. We refer to [221, Section 15.23] for full details. We are here concerned with the main span, namely the part of the roadway between the four towers. It has a rectangular shape with two long free edges (of the order of 1 km) and two shorter edges (of the order of 20 m) fixed and hinged between the towers.

The complex composition of a suspension bridge yields two major difficulties: firstly it appears aerodynamically quite vulnerable, secondly it appears very hard to

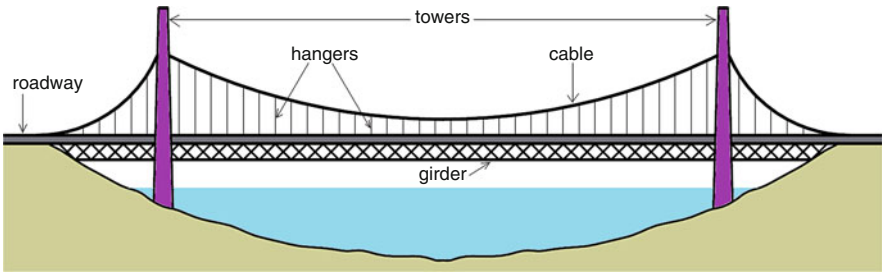

Fig. 1 Sketch of a suspension bridge

describe its behavior through simple and reliable mathematical models. In this book we suggest some new models and discuss whether the existing mathematical models are suitable to describe a suspension bridge or if they need some improvements. From classical mechanics we learn that any mathematical model aiming to describe the behavior of suspension bridges needs to have enough degrees of freedom and to contain some nonlinearity. As should be expected, nonlinearities allow to view some hidden phenomena. In particular, we will show that nonlinear models exhibit a critical energy, depending only on the structural parameters, which, if exceeded, gives rise to uncontrolled vibrations within the structure: the critical energy coincides with the onset of structural instability. This suggests us to give a definition of flutter based on the internal energy, and not on the strength of an external wind as in most classical approaches.

Nowadays, the dominant explanation for the instability of suspension bridges relies on the so-called aerodynamic forces generated by the wind-structure interaction (see Billah-Scalan [47]). These forces act in several different ways according to how far is the structure from equilibrium, in particular how large is the torsional angle, and may generate self-excitation and negative damping effects. Our attention is focused on the cause of wide torsional oscillations. In this book we emphasise a structural instability and explain why large vertical oscillations may instantaneously switch to the more destructive torsional ones. In order to achieve this task, we need to strip the model of any interaction with external effects such as the action of the wind, damping and dissipation, and aerodynamic forces. This enables us to show that, in several models representing ideally isolated bridges in vacuum, a structural instability may occur provided enough energy is initially put inside the structure. The wind and vortex shedding are usually responsible for introducing energy within the structure, and our analysis starts after that the energy is inserted. The structural instability highlighted in this book is then combined with the well-known aerodynamic effect. Let us now make a detailed summary of the contents of each chapter. In turn, each chapter starts with a preface explaining its contents.

Brief History of Suspension Bridges

Any reliable theory needs experimental observations but since any experiment on an actual bridge is extremely expensive, we observe what has occurred in history. In this chapter we recall some historical events and testimony concerning oscillations in suspension bridges. Most of the early bridges, from the dawn of the nineteenth century until the Tacoma Narrows Bridge collapse in 1940, did not have strong enough stiffening girders and the roadway displayed several forms of oscillations. Longitudinal oscillations (which we simply call vertical oscillations in the sequel) were expected, but, in flexible bridges, these could suddenly transform into more dangerous oscillations, such as torsional oscillations. We revisit the main events where this phenomenon occurred, as well as many attempts of explanations, mostly of aerodynamic nature. None of these explanations seems to be unanimously

accepted in the scientific community, and some fundamental questions still appear to be unanswered. We conclude the chapter by giving strong evidence of the necessity of more reliable mathematical models describing the nonlinear structural behavior of suspension bridges.

One-Dimensional Models

The first mathematical equations aiming to describe suspension bridges or some parts of it (such as the roadway, the cables, and the towers) appear in two milestone contributions by Navier [210] and Melan [199]. Due to the difficulties of models with more degrees of freedom, the equations suggested were essentially ODEs. In this chapter we describe in detail these models and we derive the corresponding equations by recalling what is known in literature. In many models the roadway is seen as a one-dimensional beam and the equations are linearized. It was McKenna with several coauthors [134, 168, 196] who first introduced nonlinearities in the equations: we illustrate his models and contributions. We then show that nonlinear beam equations may display self-excited oscillations, that is, solutions with oscillations having increasing and thinning amplitude and blowing up in finite space length. From a physical point of view, this leads to the fracture of the beam. We also show how the nonlinearities increase the number of vibrations of the beam.

A Fish-Bone Beam Model

The same phenomenon of self-excited oscillations may be displayed in models with more degrees of freedom. A linear model suggested by Moore [205] describes the roadway as a plate having a center beam with rigid cross sections. In this chapter we modify this model by considering nonlinear interactions between different kinds of oscillations, and we show that vertical oscillations may suddenly transform into torsional oscillations. This occurs when enough energy is present within the structure. We call this energy threshold the flutter energy. The full model is then approximated with a finite number of degrees of freedom through a Galerkin approximation. This enables us to show that the flutter energy depends on the nonlinear modes of oscillation. The analysis is here performed both theoretically (with a detailed study of the stability of nonlinear Hill equations) and numerically. An explanation of how the stability is lost is also given; this enables us to give an effective method to compute the flutter energy, at least in some simplified models.

Models with Interacting Oscillators

The Newton equation for a simple rod model representing the cross section of the roadway was introduced by McKenna [191] and subsequently improved by McKenna-Tuama [195]. In this chapter we slightly modify this model both by considering multiple cross sections interacting with the adjacent ones and by considering isolated systems, with energy conservation. We are so able to show that in nonlinear models with interacting oscillators, the sudden transition from vertical oscillations to torsional oscillations is intrinsic within the structure and does not depend on the external forcing term acting on it. The sudden transition may occur only when the internal energy is larger than some critical energy threshold, which we call again flutter energy. The flutter energy depends on the oscillating modes and we give an effective way to compute it. This phenomenon has a sound explanation in terms of the behavior of suitable evolution maps which, in the simplest case of one cross section, may be taken to be Poincaré maps. It turns out that the starting spark for torsional oscillations is a resonance between nonlinear oscillators which can occur when the internal energy is larger than the flutter energy.

Plate Models

In this chapter we model the roadway as a long and narrow rectangular thin plate. We first recall some models from classical elasticity theory, both linear and nonlinear. Since fully nonlinear equations appear mathematically untractable and since linear equations are unreliable, as a compromise we consider several semilinear and quasilinear differential equations. For each problem we set up the variational formulation, we go through a careful study of the spectrum of the differential operator involved, and we end up with the evolution equation modeling the bridge. The study of the spectrum enables us to fully describe the oscillating modes of a bridge and to explain how the cables may induce vertical oscillations to switch to torsional ones. The first model, with no stretching energy, leads to a semilinear equation for which, once more, large vertical oscillations may suddenly transform into destructive torsional oscillations: we estimate the flutter energy through a finite dimensional approximation of the phase space. We are so able to provide an explanation why the oscillations at the Tacoma Narrows Bridge switched from the tenth vertical mode to the second torsional mode. Then we revisit a quasilinear system due to von Kármán which appears suitable for large deformations of the plate: it requires the introduction of the Airy function and a careful choice of the boundary conditions. For this system, the stretching energy comes naturally within the model. But in case of prestressed structures, suitable stretching terms should be included in the model. In this respect, we suggest three different stretching terms: the first one leads to another semilinear equation, while the other two lead to quasilinear equations which take into account the strength of prestressing.

Conclusions

In this final section we answer to the questions raised in the first chapter and we draw our conclusions. All the models considered display the same phenomenon and yield the same explanation: besides the well-known aerodynamic instability there exists also a structural instability which is the cause of many troubles for suspension bridges. Thus we formally suggest a definition of flutter energy, which is the energy threshold above which the structural instability appears.

Contents

Notations

$D^2u =$ Hessian matrix of the function u.
$[\phi, \psi] = \phi_{xx}\psi_{yy} + \phi_{yy}\psi_{xx} - 2\phi_{xy}\psi_{xy}$, the Monge-Ampère operator, see Sect. 5.2.2.
$C_c^\infty(\Omega) = \{f \in C^\infty(\Omega);\ \text{supp}(f) \text{ is compact in } \Omega\}$.
$L^p(\Omega) = \{f : \Omega \to \mathbb{R};\ \int_\Omega |f|^p < \infty\}$, Lebesgue space of p-th power integrable functions: the norm is denoted by $\|\cdot\|_p$ or $\|\cdot\|_{L^p}$.
$L^\infty(\Omega) = \{f : \Omega \to \mathbb{R};\ \sup_\Omega |f| < \infty\}$, Lebesgue space of essentially bounded functions: the norm is denoted by $\|\cdot\|_\infty$ or $\|\cdot\|_{L^\infty}$.
$H^1(\Omega) = \{f : \Omega \to \mathbb{R};\ \int_\Omega (|\nabla f|^2 + f^2) < \infty\}$, first order Sobolev space of squared integrable functions with squared integrable gradient.
$H_0^1(\Omega) = \{f \in H^1(\Omega);\ f = 0 \text{ on } \partial\Omega \text{ in the sense of traces}\}$.
$H^2(\Omega) = \{f \in H^1(\Omega);\ \int_\Omega |D^2 f|^2 < \infty\}$, second order Sobolev space of functions with squared integrable derivatives up to order 2.
$H_*^2(\Omega) = \left\{f \in H^2(\Omega);\ f = 0 \text{ on } \{0,\pi\}\times(-\ell,\ell)\right\}$ when $\Omega = (0,\pi)\times(-\ell,\ell) \subset \mathbb{R}^2$, see Sect. 5.3.1.
$W^{4,1}(\Omega) = \{f : \Omega \to \mathbb{R};\ \int_\Omega (|D^4 f| + |f|) < \infty\}$, fourth order Sobolev space of integrable functions with integrable derivatives up to order 4, see Sect. 2.5.2.
$C^0([0,T]; X) =$ space of functions continuous in time with respect to the X-norm in space; $u \in C^0([0,T]; X)$ if and only if $\|u(t) - u(t_0)\|_X \to 0$ as $t \to t_0$. Similarly, for the spaces $C^1([0,T]; X)$ and $C^2([0,T]; X)$.
TNB = Tacoma Narrows Bridge, see Sect. 1.4.
(GPCM) = General Principle of Classical Mechanics, see Sect. 1.8.

Chapter 1
Brief History of Suspension Bridges

The sound modeling of any mechanical system requires careful experimental observations. For complex structures such as suspension bridges, the observations have to be taken from history and not just from lab experiments. In this chapter we survey several historical events and we attempt to classify the observed phenomena in suitable categories. The most instructive event is certainly the Tacoma Narrows Bridge collapse which is analysed in great detail, together with many different attempts of explanations. None of them seems to answer to all the questions raised by the collapse.

We explain why nonlinear modeling seems unavoidable for suspension bridges and we conclude the chapter with some hints on how to proceed in order to reach more reliable models.

1.1 First Suspension Bridges

Who really had the first idea of suspension bridge is hard to say. In [273, Chap. I], the Canadian engineer John Alexander Low Waddell (1854–1938) suggests that we should go

> ... back to the days when our arboreal ancestors formed living chains of their own bodies, holding to each other with arms, legs, and tails, thus constructing suspension bridges across the water from the overhanging branches of opposite trees, in order to let their tribe pass over in safety to the other side...

Instead of animals (monkeys) one can also attribute the original ideas to plants: Pugsley [227, p. 1] writes that

> ... the suspension bridge owes its origin to the extravagancies of ropes of creepers, vines and other trailing plants in warm countries.

But, of course, the modern feeling of a suspension bridge is fairly different.

F. Gazzola, *Mathematical Models for Suspension Bridges*, MS&A 15,
DOI 10.1007/978-3-319-15434-3_1

In 1433, Thangtong Gyalpo built eight bridges in eastern Bhutan but his iron chain bridges did not include a suspended deck bridge as in all modern suspension bridges. Instead, both the railing and the walking layer of Gyalpo bridges used wires and the stress points that carried the screed were reinforced by the iron chains. This is the reason why Gyalpo is not considered the first designer of a suspension bridge. A diagram of one of the Gyalpo bridges was published by the British explorer Laurence Austine Waddell in 1905 in the report [274]: the diagram is represented in Fig. 1.1. Gerner [132] describes Thangtong Gyalpo as *an iron chain suspension bridge builder, a universal genius with supernatural abilities*.

The first design of a modern suspension bridge is attributed by Navier [210, p. 7] and Kawada [153, p. 16] to the Italian engineer Fausto Veranzio (1551–1617) in the year 1595, see [265]; this is also the oldest reference in our bibliography. Veranzio proposed an iron bridge (Pons Ferreus) which is somehow a compromise between a suspension bridge and a cable-stayed bridge, see Fig. 1.2.

He also designed a wooden bridge deck suspended by hemp ropes (Pons Canabeus) which is quite similar to modern suspension bridges, see Fig. 1.3. None of these bridges was ever built.

The first suspension bridges were erected only about two centuries later. As far as we are aware, the first one was the Jacob Creek Bridge, built in Pennsylvania in 1801 by the Irish judge and engineer James Finley (1756–1828). This is the first example of a suspension bridge using wrought iron chains and with a level deck, see the picture in Fig. 1.4.

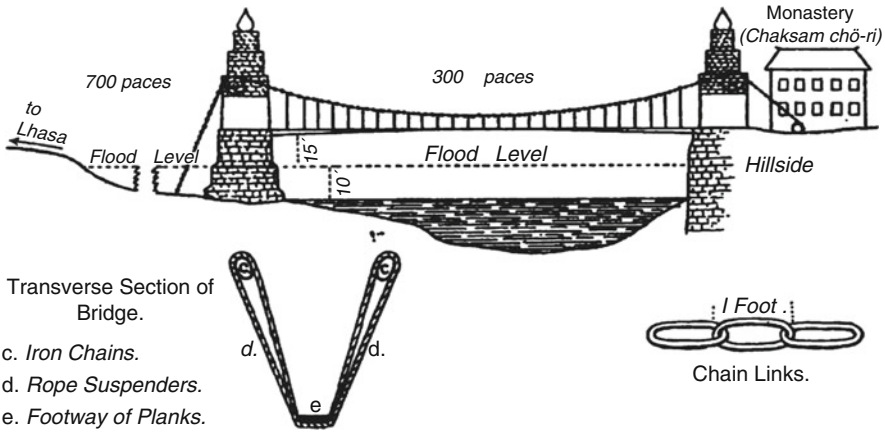

Fig. 1.1 Picture of the Chushul Chakzam suspension bridge (*Source*: [274], http://commons.wikimedia.org/wiki/File:Chakzampa.png)

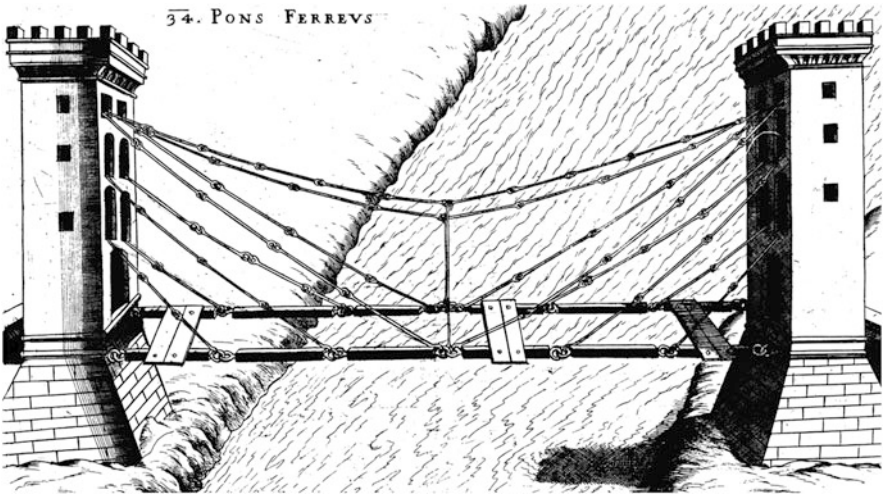

Fig. 1.2 Picture of the Pons Ferreus by Fausto Veranzio (1595) (Reproduced with permission from Fondazione Biblioteca di via Senato, Milano, Italy)

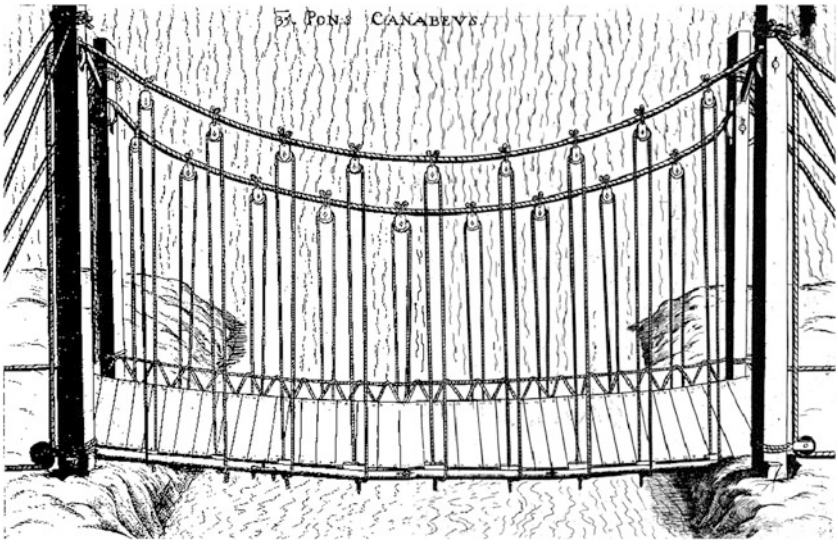

Fig. 1.3 Picture of the Pons Canabeus by Fausto Veranzio (1595) (Reproduced with permission from Fondazione Biblioteca di via Senato, Milano, Italy)

Fernández Troyano [109, p. 544] writes that Finley

> . . . built a series of them similar to the Chinese but making the deck separate from the main cables and this was probably never done in Eastern bridges even though the method is in F. Veranzio's drawings.

Fig. 1.4 View of the Jacob Creek Bridge (1801) (*Source*: [112, p. 441], http://commons.wikimedia.org/wiki/File:Jacobs-creek-bridge-1.jpg)

Several suspension bridges were erected in Great Britain during the nineteenth century. Quite soon they showed to be quite pregnable in presence of strong winds. Between 1818 and 1889, ten suspension bridges suffered major damages or collapsed in windstorms, see [105, Table 1, p. 13], which is commented by

> An examination of the British press for the 18 years between 1821 and 1839 shows it to be more replete with disastrous news of suspension bridges troubles than Table 1 reveals, since some of these structures suffered from the wind several times during this period and a number of other suspension bridges were damaged or destroyed as a result of overloading.

It is not our purpose to give a detailed list of all the collapses for which we refer to the bibliographical notes in Sect. 1.9. In the next sections, we merely describe those events which are particularly meaningful for our purposes. As we shall see, the mathematical models suggested in this monograph, well describe these events and enable us to give reliable explanations of them.

1.2 Collapses Due to an External Resonance

In this section we show that an external forcing, even if fairly weak, may considerably amplify the oscillations of a bridge. This happens if the force is somehow "able to adapt itself" to the already existing oscillations. This is what we call external resonance, namely a precise matching between the frequency of the forcing term and a natural frequency of the structure. An external resonance yields a strongly cooperative interaction between the forcing and the oscillations of a bridge, the so-called negative damping effect. We point out that the analysis of this phenomenon is not among the scopes of the present monograph. However, since many people tend to attribute to an external resonance the failure of some suspension bridges, we think it is of some interest to focus on it. This will enable us to avoid misunderstanding: in the next sections we will explain in detail why an external resonance cannot be the culprit of bridges collapses in presence of windstorms.

The Broughton Suspension Bridge, close to Manchester, was built in 1826 and collapsed in 1831 due to an external resonance. A troop was marching over the bridge in step. According to [10],

> Shortly after they got upon the bridge, the men, who were marching four abreast, found that the structure vibrated in unison with the measured step with which they marched; and as this vibration was by no means unpleasant, they were inclined to humour it by the manner in which they stepped. As they proceeded, and as a greater number of them got upon the bridge, the vibration went on increasing.

And when the vibration was of large amplitude a bolt in one of the stay-chains snapped, causing the bridge to collapse at one end. No lives were lost but 40 men fell into the river. Then the report [10] analyses the causes of the collapse:

> There is no doubt that the immediate cause was the powerful vibration communicated to the bridge by the measure and uniform step of the soldiers. If the same, or a much larger number of persons had passed over in a crowd, and without observing any regular step, in all probability the accident would not have happened, because the tread of one person would have counteracted the vibration arising from that of another. But the soldiers all stepping at the same time, and at regular intervals, communicated, as we mentioned in describing the accident, a powerful vibration to the bridge, which went on increasing with every successive step.

This description corresponds to what we call external resonance. Finally, [10] concludes with the following recommendation:

> We hope the commanding officer will take the precaution of dismissing his men from their ranks before they attempt to cross: indeed, that precaution should be observed by troops crossing all chain bridges, however small they may be.

And indeed, as a consequence of the Broughton incident, the British Army issued an order that troops should "break step" when crossing a bridge.

This collapse well explains what we mean by external resonance. From a mathematical point of view, the probability that the step frequency of a troop coincides exactly with a natural frequency of a bridge is zero. However, as also occurred in further events, if the two frequencies almost coincide then, unconsciously, the step of the humans tends to approach a natural frequency of the structure.

The Angers Suspension Bridge over the Maine River in France was built in 1839 and collapsed in 1850, see Fig. 1.5. The collapse occurred while a battalion of French soldiers was marching across it, killing 226 of them. The soldiers had been ordered to break step and to space themselves farther apart than normal. But the battalion arrived during a thunderstorm when the wind was making the bridge oscillate and their efforts to match the swaying and keep their balance had caused them to involuntarily march with the same cadence, contributing to the resonance: they were in step at a natural frequency of the bridge. This is well described in the Report [101]:

> Les soldats avaient peine à se tenir en équilibre; ils ont déclaré qu'ils marchaient comme des hommes ivres, craignant de tomber tantôt à droite, tantôt à gauche. Il est à croire qu'ainsi ballottés sous l'influence d'une cause qui se faisait sentir à tous de la même manière, ils ont donné involontairement à leur pas une certaine cadence d'accord avec le va et vient des oscillations. C'est un mouvement instinctif auquel il est difficile et dangereux de résister sous d'autres rapports.

In some sense, the soldiers were forced to walk at the same frequency of the oscillating bridge. And also [101] names this phenomenon as a resonance:

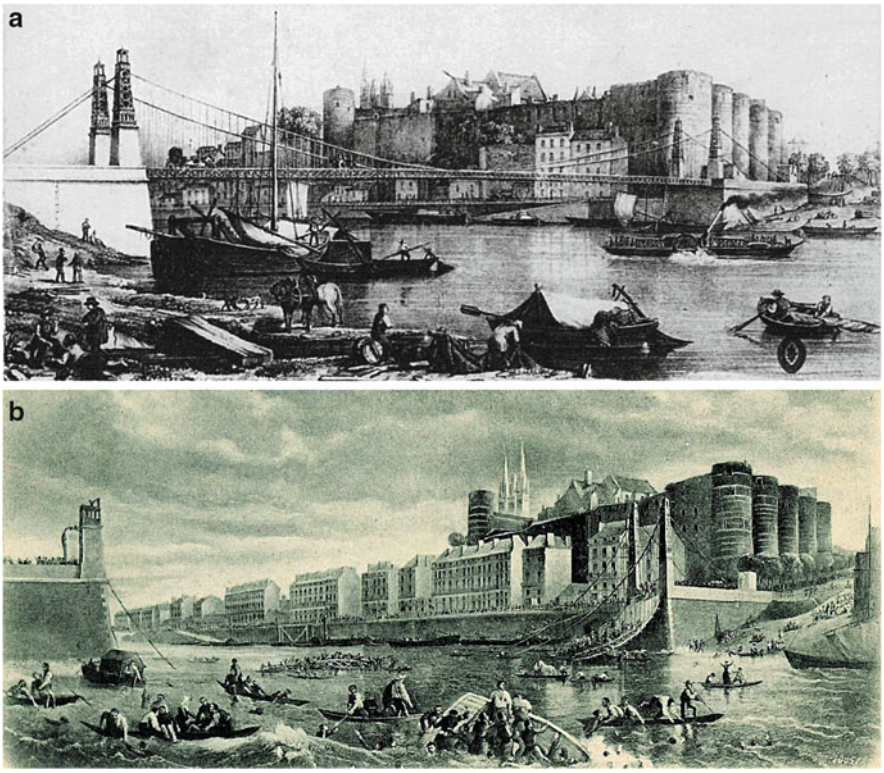

Fig. 1.5 Collapse of the Angers Bridge (1850)
(*Source*: (**a**) http://commons.wikimedia.org/wiki/File:Pont1839.jpg;
(**b**) http://commons.wikimedia.org/wiki/File:Pont_de_la_Basse-Chaîne_(7).jpg)

> C'est un effet de mécanique bien connu que quand un corps oscillant reste soumis pendant quelque temps à la force qui produit les oscillations, son amplitude va toujours en croissant, les efforts faits successivement s'ajoutent aux efforts antérieurs et occasionnent des effets de plus en plus considérables.

This is also the opinion of more recent reports, see [109, p. 63]:

> Why the bridge broke up is not precisely known ... but it is now thought that the phenomenon of resonance must have been involved.

The Angers Bridge tragedy had significant implications: France abandoned the use of suspension bridges during the following decades.

In 1886, the Austrian bridge over the Ostrawitza River collapsed when a troop of Uhlan cavalry charged over it. The load merely consisted of 26 soldiers, 16 horses, 2 carts, who were probably all moving synchronously at a natural frequency of the bridge; see [11, 181] and also [50, p. 7], [234, p. 93]. According to [185, pp. 52–53],

> The structure gave way so suddenly that the whole troop was precipitated into the river among the ruins, six men being killed instantly.

The word "suddenly" is alarming and is certainly the reason why lives were lost.

Fig. 1.6 The London Millennium Bridge (2000) (Reproduced with permission from Nadja Levtsenko, http://myself113.deviantart.com/art/Millenium-Bridge-97396006)

Let us now skip forward until June 2000. The very same day of the opening of the London Millennium Bridge, see Fig. 1.6. The crowd streamed on it and the bridge started to sway from side to side: the pedestrians fell spontaneously into step with the vibrations, thereby amplifying them. The bridge was closed in order to prevent a possible tragedy. The specialist of vibration Parker [214] confirmed that pedestrian behavior could be at the root of the problem:

> A pedestrian's centre of gravity is about 1m above his feet and as he walks normally he puts his feet alternately about 100mm each side of a centre line. Thus each pedestrian exerts a cyclic lateral force of about 8% of body weight at a frequency of around 1Hz. If a large number of people walk - not in step - across a bridge, the resultant mean lateral force would be the force from one pedestrian multiplied by the square root of the total number. This would probably be enough to start the bridge swaying at the critical frequency. At this point more and more pedestrians would find it more comfortable to walk in phase with the movement, feeding more and more lateral energy into the structure.

The bridge wobble was due to the way people balanced themselves, rather than the timing of their steps, see [2, 179, 236]. The pedestrians acted as negative dampers, adding energy to the bridge natural sway. The London Millennium Bridge was re-opened after the addition of positive dampers. Since then, only tiny oscillations have been detected. Also this event may be classified as external resonance.

1.3 Collapses Due to Unexpected Oscillations

In this section we recall several collapses of suspension bridges, occurred in the nineteenth century, as described by some witnesses. As we shall see, they all exhibit some common features. The nonlinear mathematical models that we suggest in the next chapters are able to reproduce the destructive oscillations described in this section.

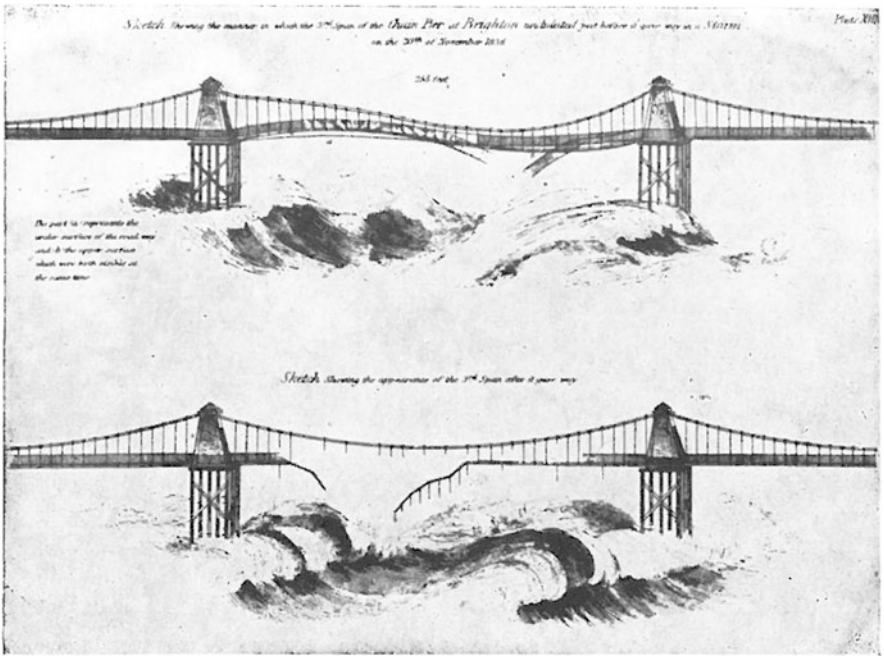

Fig. 1.7 Collapse of the Brighton Chain Pier (1836) (Reproduced with permission from the Library of Royal Engineers, Kent)

A first event deserving to be mentioned is the collapse of the Brighton Chain Pier, built in 1823. It collapsed a first time in 1833, it was rebuilt and partially destroyed once again in 1836. Both the collapses are attributed to violent windstorms. For the second collapse a witness, the British Royal engineer Col. William Reid (1791–1858) reported valuable observations and sketched a picture illustrating the destruction [230], see Fig. 1.7. The report by Reid [230] also describes the collapse as follows:

> For a considerable time, the undulations of all the spans seemed nearly equal ... but soon after midday the lateral oscillations of the third span increased to a degree to make it doubtful whether the work could withstand the storm; and soon afterwards the oscillating motion across the roadway, seemed to the eye to be lost in the undulating one, which in the third span was much greater than in the other three; the undulatory motion which was along the length of the road is that which is shown in the first sketch; but there was also an oscillating motion of the great chains across the work, though the one seemed to destroy the other.

This description highlights the presence of different oscillations, including a torsional one. More comments about this collapse, and on Reid report, are due to Russell [235] who claims, in particular, that

> the remedies I have proposed, are those by which such destructive vibrations would have been rendered impossible.

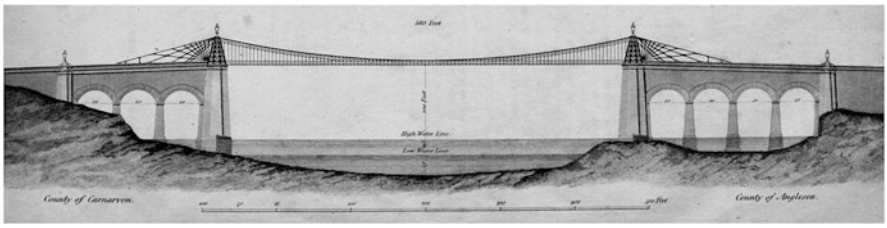

Fig. 1.8 The suspension bridge over the Menai Straits (1826) (Reproduced with permission from Menai Heritage, www.menaibridges.co.uk)

His remedies were to alter the place of the cross bars and to put stays below the bridge which should be put *at distances not perfectly equal*. The scope is to break symmetry in the vertical oscillating modes of the roadway. As we shall see in the next chapters, he had seen right!

A second event deserving mention is the inauguration of the Menai Straits Bridge, in 1826. The project of the bridge was due to Thomas Telford and the opening of the bridge is considered as the beginning of a new science nowadays known as "Structural Engineering". In Fig. 1.8 we show the Telford original design. The construction of this bridge had a huge impact in the English society, a group of engineers founded the "Institution of Civil Engineers" and Telford was elected the first president of this association. In 1839 the Menai Bridge collapsed due to a hurricane. In that occasion, unexpected oscillations appeared; Provis [225] provided the following description:

> the character of the motion of the platform was not that of a simple undulation, as had been anticipated, but the movement of the undulatory wave was oblique, both with respect to the lines of the bearers, and to the general direction of the bridge.

One year later, Provis [226] pointed out that the Menai Bridge collapse had generated many erroneous and contradictory reports; therefore, he clarifies several aspects which appear quite important for our purposes. He writes:

> The motion which had been anticipated was that of simple undulation flowing in waves at right angles to the length of the bridge; and had this been the only motion, the bearers, it is apprehended, would not have been injured by the gale. They would have been equally raised or depressed throughout their lengths as the wave rolled forward, and been subjected to no strain which they were not fully competent to resist.

Whence, vertical oscillations were expected and the bridge would have been safe if only these oscillations would have shown up. The bridge was not ready to resist to strain, that is, to other kinds of oscillations. Then Provis continues by writing:

> The movement of this undulatory wave, however, was oblique with the lines of the bearers and their suspending rods as well as with the general direction of the bridge.

Doubtless, this comment describes a combination of vertical and torsional oscillations. Summarising, Provis tells us that vertical oscillations were expected and harmless, while torsional oscillations were unexpected at that time and turned out to be destructive.

The Wheeling Suspension Bridge was erected in 1849 in West Virginia; it collapsed in 1854 during a violent storm. From [255] we quote the following dramatic description of the collapse:

> About 3 o'clock we walked up towards the Suspension Bridge, and went upon it, intending to take a walk across it for pleasure, as we have frequently done, enjoying the cool breeze and the undulating motion of the bridge ... as it began to sway violently we thought it prudent to retrace our steps. We had been off the flooring only two minutes ... just in time to see the whole structure of cables and flooring heaving and dashing with tremendous force. For a few moments we watched it with breathless anxiety, lunging like a ship in the storm; at one time it rose to nearly the height of the towers then fell, and twisted and writhed, and was dashed almost bottom upward. At last there seemed to be a determined twist along the entire span, about one half of the flooring being nearly reversed, and down went the immense structure from its dizzy height to the stream below, with an appalling crash and roar. ... We witnessed the terrific scene and saw that it was brought about by the tremendous violence of the gale. The great body of the flooring and the suspenders, forming something like a basket swung between the towers, was swayed to and from, like the motion of a pendulum.

Quite luckily no lives were lost. Also this terrific description is very useful for our purposes. In particular, we underline the movement which was "twisted and writhed" (which yields the keyword "torsional") and the timing "only two minutes" (which yields the keyword "suddenly").

What we learned from these three collapses may be summarised as follows. Vertical oscillations are to be expected in suspension bridges and do not appear dangerous for the structure. Different kinds of oscillations, in particular torsional oscillations, may suddenly appear and destroy the bridge. So, we learned that

destructive oscillations may appear suddenly in suspension bridges.

By "destructive" we mean any kind of oscillation which is different from the vertical oscillations. As we have seen, these are mostly torsional oscillations. In Fig. 1.9 we sketch vertical and torsional oscillations in a suspension bridge.

Some decades before the above described collapses, at the end of the eighteenth century, the German physicist Ernst Chladni (1756–1827) was touring Europe and showing, among other things, the nodal line patterns of vibrating plates, see Fig. 1.10. The Chladni experiment, first published in [77], consisted of creating vibrations in a square-shaped metal plate whose surface was covered with light sand. The plate was bowed until it reached resonance, when the vibration caused the sand to concentrate along the nodal lines of vibrations: this experiment is still

Fig. 1.9 Vertical (*left*) and torsional (*right*) oscillations in suspension bridges

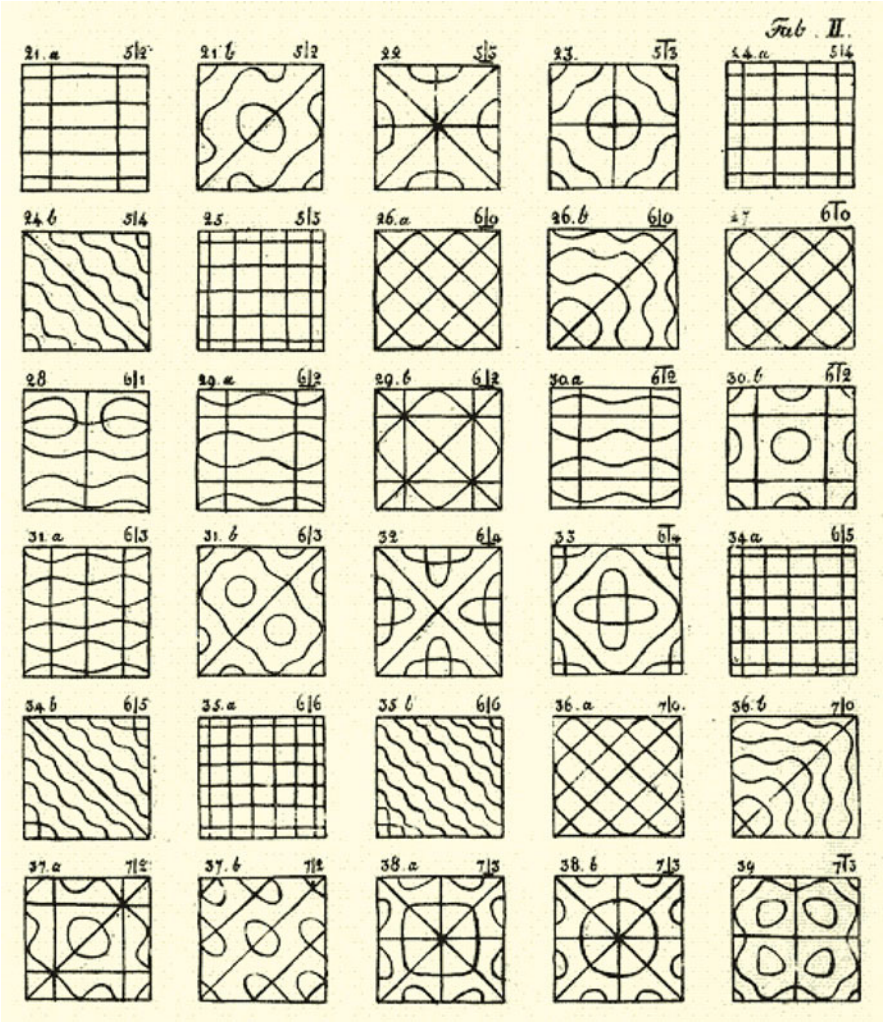

Fig. 1.10 Chladni patterns in a vibrating plate (*Source*: http://it.wikipedia.org/wiki/File:Ernst_Chladni_tab_II.gif)

in use nowadays and the videos are easily found on the web. This simple but very effective way to display the nodal lines of vibrations was seen by Navier [209] as

> Les curieuses expériences de M. Chaldni sur les vibrations des plaques.

It appears quite clearly from Fig. 1.10 how complicated may be the vibrations of a thin plate and hence of a bridge. And, indeed, the just described events testify that, besides the somehow expected vertical oscillations, also different kinds of oscillations may appear. The description of different coexisting forms of oscillations

within the structure is probably the most challenging problem in suspension bridges. The pattern of oscillations depends both on the forcing and on the conditions at the boundary of the plate. In Sect. 5.3.3 we analyse the eigenfunctions of plates modeling suspension bridges.

The reasons of the failures described in the present section are completely different from the ones described in Sect. 1.2. In this section the external force was violent and disordered whereas in Sect. 1.2 it was light and precise. A random and variable wind does not adapt itself to a natural frequency of a bridge and cannot create an external resonance.

1.4 The Tacoma Narrows Bridge Collapse

The history of bridges, suspended and not, contains many further dramatic events (see Sect. 1.9), an amazing amount of bridges had troubles for different reasons. Among them, the most celebrated is certainly the Tacoma Narrows Bridge (TNB), collapsed in 1940 just a few months after its opening, both because of the impressive video available on the web [253] and because of the large number of studies that it has inspired.

The TNB was considered very light and flexible. Not only this was apparent to traffic after the opening, but also it was felt during the construction. According to [241, pp. 46–47],

> ... during the final stages of work, an unusual rhythmic vertical motion began to grip the main span in only moderate winds ... these gentle but perceptible undulations were sufficient to induce both bridgeworker nausea and engineering concern.

The undulatory motion of the span attracted the local interest and

> ... motorists ventured onto the TNB to observe vehicles ahead of them slowly disappearing in the trough of a wave.

So, it was not surprising that vertical oscillations were visible on the day of the collapse. On November 7, 1940, around 8.30 a.m.

> the bridge appeared to be behaving in the customary manner ... oscillating in a four noded manner ... these motions, however, were considerably less than had occurred many times before...

See [9, Appendix V-3]. Nevertheless, a sudden change in the motion was alarming, a violent destructive torsional movement started. All this happened under not extremely strong winds, about 80 km/h, and under a relatively high frequency of oscillation, about 36 cpm, see [105, p. 23]. A witness to the collapse was Farquharson, the man escaping in the video [253]. According to his detailed testimony in [104],

> ... a violent change in the motion was noted. This change appeared to take place without any intermediate stages and with such extreme violence that the span appeared to be about to roll completely over.

Farquharson then continues with an important description of the modes:

> The motion, which a moment before had involved a number of waves (nine or ten) had shifted almost instantly to two.

This fundamental observation establishes the following unquestionable facts:

the oscillations in suspension bridges are not periodic in time, (1.1)

vertical and torsional oscillations are not independent, (1.2)

since, otherwise, vertical oscillations would not transform into torsional oscillations. This justifies both the conclusions (1.1) and (1.2).

Figure 1.11 shows the original TNB with its torsional oscillations. This picture should be compared with Fig. 1.7. And the description in the present section should be compared with the descriptions in Sect. 1.3: although the TNB collapse is the most widely studied bridge failure, it is not an isolated event. In this respect, Rocard [234, p. 99] writes

> the oscillation of the Tacoma Bridge then corresponded exactly to Lt.-Col. Reid's description of the Brighton Chain Pier.

After the TNB accident three engineers (Ammann, von Kármán, and Woodruff) were assigned to investigate the collapse and report to the Public Works Administration. Their Report [9] contains several answers to major questions such as technical details on the project and comments on the flexibility. The Report considers

> the crucial event in the collapse to be the sudden change from a vertical to a torsional mode of oscillation;

see [241, p. 63]. In the Report [9, p. 28] one finds a letter by Durkee, a project engineer, which states that

> There appears to be no difference in the motion whether the wind is steady or gusty.

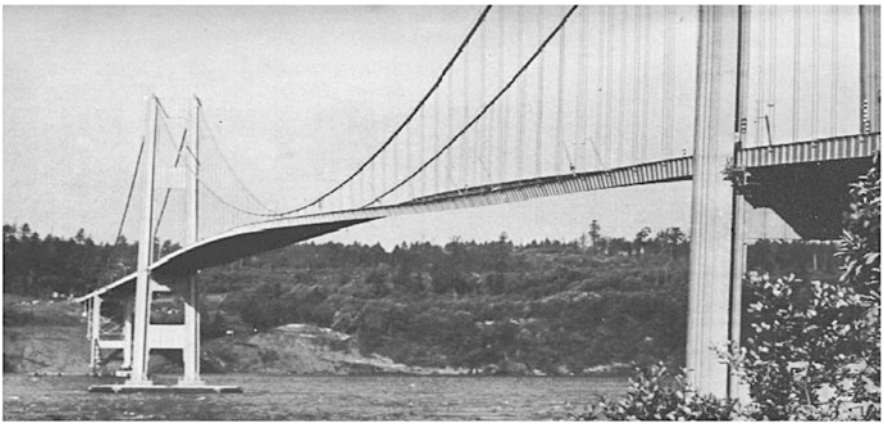

Fig. 1.11 The collapsed Tacoma Narrows Bridge (1940) (From [9, p. 6], reproduced with permission from the University of Washington Libraries, Special Collections)

As we shall see in the next chapters, also this observation is of crucial importance, it suggests that

the qualitative behavior of the wind plays no direct role,

what counts is the amount of energy that it inserts in the structure. (1.3)

1.5 Some Bridges That Did Not Collapse

In this section we analyse three bridges which were built at the same time as the TNB but which were more lucky since they still stand. We emphasise the main differences with the TNB and we raise some questions.

The Golden Gate Bridge was inaugurated in 1937. It is usually classified as "very flexible" although it is strongly stiffened by a thick girder, see Fig. 1.12. The original roadway was heavy and made with concrete; the weight was reduced in 1986 when a new roadway was installed. Nowadays, in spite of the girder, the bridge can swing more than an amazing 8 m and flex about 3 m under big loads, which explains why the bridge is classified as very flexible. Due to high winds around 120 km/h, the Golden Gate Bridge has been closed, without suffering structural damage, only three times: in 1951, 1982, 1983, always during the month of December. Wide vertical oscillations were well visible in 1938: in [9, Appendix IX], the chief engineer of the Golden Gate Bridge writes

> I observed that the suspended structure of the bridge was undulating vertically in a wavelike motion of considerable amplitude.

Fig. 1.12 The Golden Gate Bridge (1937) with its stiffening trusses (*Source*: http://commons.wikimedia.org/wiki/File:Golden_Gate_Bridge_from_underneath.jpg by Ambush Commander)

See also the related detailed description in [197, Sect. 1]. Hence, even in presence of stiffening trusses, one should expect vertical oscillations although the truss seems to prevent these oscillations to be transformed into torsional oscillations. Some people believe that trusses do not solve completely the problem and that torsional oscillations might still appear but, of course, only in presence of very large energy inputs. In this respect, we quote from [105, p. 13] a comment on suspension bridges strengthened by stiffening trusses:

> That significant motions have not been recorded on most of these bridges is conceivably due to the fact that they have never been subjected to optimum winds for a sufficient period of time.

So, it is expected that under prolonged winds, not necessarily hurricanes, or heavy and synchronised traffic loads, a stiffening truss may become useless. The replacement of the original TNB opened in 1950 with stiffening trusses, see [107] for the description of the plans, and still stands today as the westbound lanes of the present-day twin bridge complex, the eastbound lanes opened in 2007. Figure 1.13 shows the bridge as it is today. It should be compared with the one in Fig. 1.11.

The Deer Isle Bridge, see Fig. 1.14, is a suspension bridge in the state of Maine which encountered wind stability problems similar to those of the original TNB. Before the bridge was finished, in 1939, the wind induced motion in the relatively lightweight roadway. Diagonal stays running from the sustaining cables to the stiffening girders on both towers were added to stabilize the bridge. Nevertheless, the oscillations of the roadway during some windstorms in 1942 caused extensive damage and destroyed some of the stays. At that time everybody had the collapse of the TNB in mind, so that stronger and more extensive longitudinal and transverse diagonal stays were added. In her report, Moran [206] wrote

> Like the Tacoma Narrows, Maine's Deer Isle Bridge was designed long and thin and turned out to be dangerously unstable. Unlike the Tacoma Narrows, it's still standing.

Fig. 1.13 The current twins Tacoma Bridges (1950 and 2007) (Reproduced with permission from Michael Goff, Oregon Department of Transportation, US, http://structurae.de/photos/index.cfm?id=100618)

Fig. 1.14 The Deer Isle Bridge (1939) (Reproduced with permission from Thaddeus Roan, https://www.flickr.com/photos/80651083@N00/164141206/)

Fig. 1.15 The Bronx-Whitestone Bridge (1939) (Reproduced with permission from Jason Joel Photography, www.jasonjoelphotography.com)

This shows a strong dependence of the response of a bridge on its structure: even if two bridges are almost similar they can react very differently to external forcing. Is there a correct mathematical model able to justify how small structural differences may generate highly different responses? We will try to give an answer to this question in the next chapters. In particular, in Sect. 3.6 we show how small variations of the natural frequencies may have a huge consequence on the stability behavior.

The Bronx-Whitestone Bridge displayed in Fig. 1.15, was built in New York in 1939 and has shown an intermitted tendency to mild vertical motion from the time the floor system was installed. The reported motions have never been very large,

Fig. 1.16 The Akashi Kaikyo Bridge (1998) (From http://commons.wikimedia.org/wiki/File:Akashi_Bridge.JPG. Permission is granted by GNU Free Documentation License)

but were noticeable to the traveling public. Several successive steps were taken to stabilize the structure, see [12]. Midspan diagonal stays and friction dampers at the towers were first installed; these were later supplemented by diagonal stayropes from the tower tops to the roadway level. However, even these devices were not entirely adequate and in 1946 the roadway was stiffened by the addition of truss members mounted above the original plate girders, the latter becoming the lower chords of the trusses [8, 215]. This is an example of bridge built without considering all the possible external effects, subsequently stiffened and damped by means of several additional components.

Nowadays suspension bridges are quite safe precisely because stiffening trusses rule out the possibility of the appearance of torsional motions. We show here two recent beautiful suspension bridges which are certainly well-known among engineers; our purpose is to convince mathematicians of their beauty and elegance. The Akashi Kaikyo Bridge was built in Japan in 1998, see Fig. 1.16. With its 3,911 m, and main span of 1,991 m, the Akashi Bridge is so far the longest suspension bridge in the world. A curiosity is that, during its construction an earthquake increased the distance between towers of about 1 m. A description of the plans of the Akashi Bridge, in particular of the stiffening trusses, may be found in the monograph by Kawada [153]. Even more recent is the Aizhai Bridge in China opened to traffic in 2012, see Fig. 1.17. The Aizhai Bridge is one of the highest suspension bridges in the world and it has a unique span of 1,146 m.

What we have seen in this section enables us to draw the following conclusions.

1. In a suspension bridge vertical oscillations may appear under strong winds.
2. Vertical oscillations may transform into destructive torsional oscillations; this transformation requires more external energy if the roadway is stiffened.
3. Structural solutions may improve considerably the stability of bridges.
4. The aerodynamic response of a bridge strongly depends on its structure.

Fig. 1.17 The Aizhai Bridge (2012) (Reproduced with permission from Eric Sakowski, HighestBridges.com)

1.6 Some Doubts and Questions

The events described in Sects. 1.3 and 1.4 taught us that not only vertical oscillations appear in bridges but also that they can partially switch to torsional oscillations, see the pictures in Fig. 1.18 which display (from top to bottom) the first two vertical modes and a combined vertical-torsional mode with a node at midspan: in each picture the position of the roadway is compared with equilibrium.

The possible appearance of torsional oscillations was already noticed in [9, 50] (see also [241, pp. 50–51]):

> large vertical oscillations can rapidly change, almost instantaneously, to a torsional oscillation.

However, a careful look at [253] shows that vertical oscillations continue also after the appearance of torsional oscillations; in the video, one sees that in the first part of the bridge the street-lamps oscillate in opposition of phase when compared with the street-lamps in the second part of the bridge. This behavior is confirmed by the description of the events in Sect. 1.3 which also show that torsional oscillations are destructive. And this means that a combined vertical-torsional configuration may indeed occur; throughout this book we will bring evidence that this occurs when vertical oscillations become too large. This configuration is represented in the lowest picture in Fig. 1.18: in Sect. 5.3.3 we will explain why the torsional oscillations appear in this precise form. In fact, what really occurs is better described by:

large vertical oscillations can rapidly create, almost instantaneously, additional torsional oscillations.

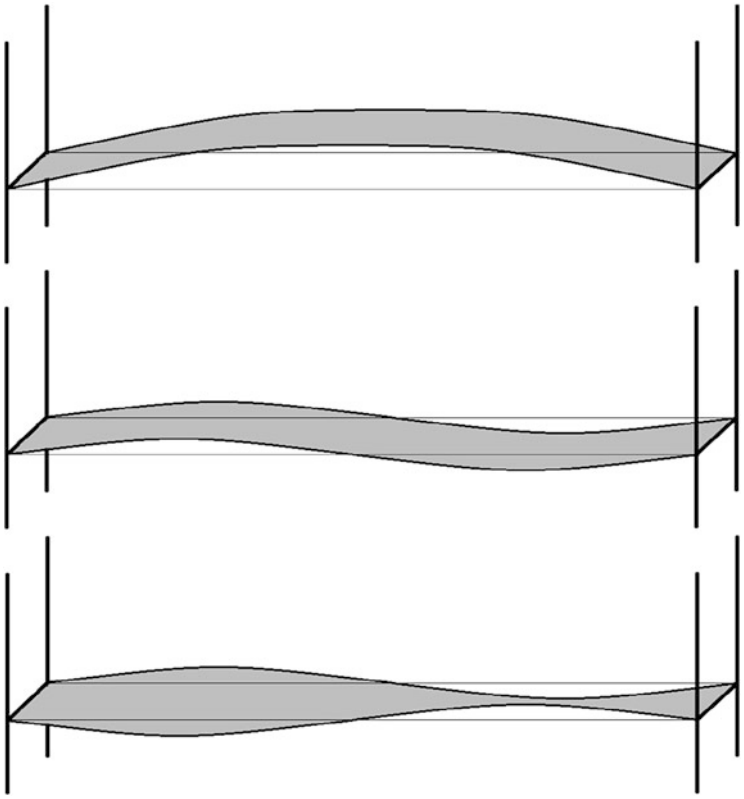

Fig. 1.18 Some possible oscillations of a bridge roadway

Scott [241, p. 53] raises two fundamental questions about the TNB collapse:

– How could a span designed to withstand 161 km/h winds and a static horizontal wind pressure of 146 kg/m^2 succumb under a wind of less than half that velocity imposing a static force one-sixth the design limit?
– How could horizontal wind forces be translated into dynamic vertical and torsional motion?

In view of what we just discussed, the answer to the first question is that the TNB was ready to withstand 161 km/h wind provided that the oscillations would have been vertical, but since torsional oscillations appeared, this considerably lowered the critical speed of the wind. Therefore, the two above questions reduce to the following main question:

(Q1) why do torsional oscillations appear suddenly in suspension bridges?

Further questions, still without an answer, were raised about the TNB in the Report [9, p. 125]:

(Q2) why the self-induced oscillations did not appear at earlier occasions when high wind velocity prevailed?

(Q3) why have self-induced oscillations not been observed in other modern bridges?

Some attempts to give an answer to the above questions were made soon after the TNB collapse. Let us quote the following comments by Bleich-McCullough-Rosecrans-Vincent [50, Appendix D]:

> If vertical and torsional oscillations occur, they must be caused by vertical components of wind forces or by some structural action which derives vertical reactions from a horizontally acting wind.

This part is continued in [50] by stating that there exist references to both alternatives and that

> A few instrumental measurements have been made ... which showed the wind varying up to 8 degrees from the horizontal. Such variation from the horizontal is not the only, and perhaps not the principal source of vertical wind force on a structure.

Not much progress was made since then. In 1978, Scanlan [237, p. 209] writes

> The original Tacoma Narrows Bridge withstood random buffeting for some hours with relatively little harm until some fortuitous condition "broke" the bridge action over into its low antisymmetrical torsion flutter mode.

In 1999, the mathematician McKenna [191, Sect. 2.3] writes that

> there is no consensus on what caused the sudden change to torsional motion.

In 2001, Scott [241] writes

> Opinion on the exact cause of the Tacoma Narrows Bridge collapse is even today not unanimously shared.

So, there seems to be no convincing explanation why torsional oscillations appear: of course, a "fortuitous condition" is not an explanation. In [121] we suggested that there might exist a strong instability of the vertical oscillatory motion as if, after reaching some critical energy threshold, an impulse generated a new unexpected oscillation. Roughly speaking, we believe that part of the energy responsible of vertical oscillations switches to another energy which generates torsional oscillations; the switch occurs without intermediate stages. As we shall see in the next three chapters, it is precisely a bifurcation occurring for large energy which is the onset for torsional oscillations in nonlinear mechanical systems.

Many other attempts to give an answer to the above questions have been made but, after 75 years, a full explanation of the reasons of the TNB collapse is not available. Any possible explanation has received criticisms and none of them is unanimously considered conclusive. Many further bridges failures, including recent events, still remain without explanations, see [5]. For instance, the Matukituki Bridge collapse, which occurred in April 1977 just 12 days after completion during

a windstorm, is described in [149] with words such as *believed* and *suspected* leaving some incertitude on the reasons of the failure, although it was officially attributed to an aeroelastic instability; further information about this small bridge and some pictures of the injured structure may be found in the book [252]. Irvine [149, Example 4.6, p. 180] describes the oscillations of the Matukituki Suspension Footbridge as

> ... the deck persisted in lurching and twisting wildly until failure occurred, and for part of the time a node was noticeable at midspan.

The last part of this comment is well represented in Figs. 1.7 and 1.11, as well as in the lowest picture of Fig. 1.18. According to the detailed analysis on the TNB by Smith-Vincent [245, p. 21], this form of torsional oscillations seems to be the only possible one:

> The only torsional mode which developed under wind action on the bridge or on the model is that with a single node at the center of the main span.

This immediately raises a further natural question: why do torsional oscillations appear with a node at midspan? In Sect. 5.3.3 we will explain why a node appears at midspan.

It is one of the purposes of the present book also to venture satisfactory answers to questions **(Q1)–(Q2)–(Q3)**. In order to do so, we first need to survey all prior attempts to give answers: this will be done in the next section. Then we will introduce several mathematical models for suspension bridges and find the answers within the behavior of the solutions of the corresponding equations.

1.7 Partial Explanations of the Tacoma Narrows Bridge Collapse

1.7.1 Structural Failure

Leon Moisseiff (1873–1943), who was charged with the project, had an eye to economy and aesthetics, but he was not considered guilty for the TNB failure. For instance, Steinman-Watson [251] wrote that

> ... the span failure is not to be blamed on him; the entire profession shares in the responsibility. It is simply that the profession had neglected to combine, and apply in time, the knowledge of aerodynamics and of dynamic vibrations with its rapidly advancing knowledge of structural design.

And also the first conclusion of the Report [9] states that

> The Tacoma Narrows Bridge was well designed and built to resist safely all static forces, including wind, usually considered in the design of similar structures.

Moreover, the analysis of the Report [9, p. 59] indicate that

> ... neither faulty design, nor defective material or workmanship, contributed to such failure or to permanent local damage.

The reason of the Moisseiff discharge probably relies on forgotten similar collapses previously occurred, see Sect. 1.3. Let us mention that a couple of decades earlier, Mann [185, p. 84] concludes his bachelor thesis about the development of suspension bridges by writing

> The lack of rigidity combined with the inadequate allowance for stresses due to wind action has been the cause of the greater portion of the failures of this type of bridge.

Mann wrote a detailed list of all the collapses from the nineteenth century, including the ones reported in Sects. 1.2 and 1.3, and he was well aware that stiffening trusses were necessary. Why did the entire profession overlook these facts is unclear.

According to the above comments, no mistakes in the project were found and the attention has then turned to find design mistakes. From the New York Times [211, p. 5] we quote a comment by Andrew, chief engineer in charge of constructing the bridge, who claims that

> the collapse probably was due to the fact that flat, solid girders were used along one side of the span. These girders, he said, caught the wind like a kite and caused the bridge to sway.

A common belief is that this explanation is too simplistic and that the video of the collapse [253] does not show the TNB as a kite.

Then several people attempted to justify the collapse with a structural failure, as if some components might have reacted too weakly to the strong wind. Delatte [91, p. 31] suggests that

> A contributing factor may have been slippage of a band that retained the cables.

Then, by invoking [115, p. 226], he writes that

> on November 7 a cable band slipped out of place at mid-span, and the motions became asymmetrical, like an airplane banking in different directions. The twisting caused metal fatigue, and the hangers broke like paper clips that had been bent too often.

By referring to the recent monograph [241], Plaut-Davis [220] claim that

> The initiation of the disastrous torsional oscillations of the original Tacoma Narrows Bridge involved a sudden lateral asymmetry due to the loosening of a cable band at midspan.

They justify the subsequent collapse by analysing a suitable model. Also Malík [183, p. 3787] concludes his analysis of a particular model by claiming that

> One diagonal tie broke and the corresponding midspan cable band loosened.

However, none of these failures is unanimously accepted to be responsible of the TNB collapse. For instance, concerning the diagonal ties [190, p. 1548] writes that

> ... this explanation has not been proved yet and the effects of center diagonal stays may be questionable.

In Chap. VI of his monograph [234], Rocard attributes the collapse to a dynamic instability also visible in prior bridges, see Sect. 1.3. And making explicit comparisons with other bridges he views the structural failure as a consequence of a manifested instability: the TNB collapsed because its dynamic instability created torsional oscillations which, in turn, caused the structural failure. This is also clearly stated in the Report [9, p. 59]:

> ... the torsional shearing stresses in the concrete slab exceeded the ultimate strength and this explains the breaking down of the slab in that vicinity as one of the first failures.

On the other hand, according to [91, p. 30], one of the conclusions of the Report [9] was that

> The failure of the cable band on the north end, which was connected to the center ties, probably started the twisting motion of the bridge. The twisting motion caused high stresses throughout the bridge, which led to the failure of the suspenders and the collapse of the main span.

This kind of "domino effect" was not analysed further in the sequel and, a few years after the collapse, Steinman [250] wrote that the ties

> permitted - not caused - the catastrophic oscillations that wrecked the structure.

Steinman [249] claimed that the Report [9]

> leaves many questions unanswered. It does not tell what combinations of cross-sections produce aerodynamic instability, how aerodynamic instability can be reasonably predicted or readily tested, nor how it can be prevented.

His final observation is that

> It is more scientific to eliminate the cause than to build up the structure to resist the effect.

The same conclusion, from a mathematical point of view, was reached by McKenna [191, p. 2]:

> ... to remove the offending behaviour is not the same as mathematically understanding its cause.

As we have seen in Sect. 1.5, stiffening trusses are nowadays used to resist the effect of wind but Steinman claims that the cause of oscillations has not been eliminated. In order to eliminate the cause, one should revisit the collapses described in Sect. 1.3 which occurred at a time when suspension bridges did not have stiffening trusses resisting to the effect.

The main reason why a structural failure is rejected as a possible explanation of the origin of torsional oscillations, and therefore of the TNB collapse, is that the very same behavior was seen in several other bridges. At the Menai Straits Bridge *the movement of the undulatory wave was oblique*, Fig. 1.7 well shows torsional oscillations at the Brighton Chain Pier, the Wheeling Suspension Bridge *twisted and writhed*, the deck of the Matukituki Suspension Bridge was *lurching and twisting wildly*. Can it really be that for all these bridges there was some partial failure giving rise to torsional oscillations? More reasonable appears to consider a

structural failure, such as the loosening of a cable or the breaking of a diagonal tie, as the consequence and not the cause of torsional oscillations.

1.7.2 External Resonance

In an article appeared in the New York Times [212] a couple of days after the collapse, one may read

> Like all suspension bridges, that at Tacoma both heaved and swayed with a high wind. It takes only a tap to start a pendulum swinging. Time successive taps correctly and soon the pendulum swings with its maximum amplitude. So with the bridge. What physicists call resonance was established, with the result that the swaying and heaving exceeded the limits of safety.

Let us avoid obvious comments, who wrote these lines was certainly not a scientist.

According to [91, p. 31], the Federal Report [9] concluded that

> because of the TNB's extreme flexibility, narrowness, and lightness, the random force of the wind that day caused the torsional oscillations that destroyed the bridge. The Authors believed that wind-induced oscillations approached the natural frequencies of the structure, causing resonance (the process by which the frequency of an object matches its natural frequency, causing a dramatic increase in amplitude).

Most people believe that these explanations overlook the important question as to how wind, random in nature, could produce a precise periodic impulse. For instance, the mathematicians Lazer-McKenna [168, Sect. 1] point out that

> the phenomenon of linear resonance is very precise. Could it really be that such precise conditions existed in the middle of the Tacoma Narrows, in an extremely powerful storm?

Not only resonance is very precise but, if it occurs, the strength of the forcing term plays a minor role. To see this, consider the simple forced linear pendulum equation $y''(t) + y(t) = \varepsilon \cos t$ with $\varepsilon > 0$. Its solutions have the form $y(x) = a \cos t + b \sin t + \frac{\varepsilon}{2} t \sin t$ with a and b to be determined by the initial conditions; however, for any couple of initial conditions (that is, for any values of a and b) the principal part of the solution as $t \to \infty$ is given by $\frac{\varepsilon}{2} t \sin t$. Whence, the strength ε of the forcing term does not change qualitatively the solution while its frequency creates a resonance and determines the leading term of the solution. We have seen in Sect. 1.2 that even small periodic forcing terms (small when compared with a gale) may cause collapses provided their frequency coincides with a natural frequency of the structure. But this was not the case of the TNB where the forcing term was not periodic: Billah-Scanlan [47, p. 119] write that

> ... "gusts" and "gale" do not connote any well-defined periodicity.

The physicists Green-Unruh [136] mention that

> making the comparison to a forced harmonic oscillator requires that the wind generates a periodic force tuned to the natural frequency of the bridge.

Among engineers, Scanlan [238] discards the possibility of resonance while Billah-Scanlan [47] make a fool of physics textbooks who attempt to explain the TNB collapse with an aerodynamic resonance. Probably, the reason why the TNB collapse was attributed to resonance is hidden in history: some people tend to confuse the phenomena described in Sect. 1.2 with the TNB collapse. For instance, Braun [58, p. 83] claims that the TNB collapse was due to a resonance and that

> ... the phenomenon of resonance was also responsible for the collapse of the Broughton suspension bridge...

But we have seen that, as long as humans create the forcing term on the bridge, unconsciously their step tends to approach a natural frequency of the structure. And these accidents are fairly different from the TNB collapse: for the formers there was an extremely precise periodic forcing term which was similar to one of the eigenfunctions of the vibrating plate sustaining the bridges, while for the latter the forcing term was very disordered and could not create a resonance. Hence, mechanical resonance, intended as a perfect matching between the exterior wind and the parameters of the bridge, is not the culprit for the TNB collapse.

1.7.3 Vortices

Every oscillating structure has its own natural frequencies and resonance occurs if the excitation force acts periodically and with one of the natural frequencies. Due to the non-streamlined shape of the TNB, a possible candidate of the periodicity in the wind force was the vortex shedding, see e.g. [58, § 2.6.1]. These wakes are accompanied by alternating low-pressure vortices on the downwind side of the roadway, the von Kármán vortex street, see Fig. 1.19 in Sect. 1.7.6. As a consequence, the bridge would move towards the low-pressure zone, in an oscillating movement called vortex-induced vibration. If the frequency of vortex shedding matches the natural frequency of the bridge, then the structure will resonate and oscillations will become self-sustaining.

Von Kármán proposed that the motion seen on the day of the collapse was due to these vortices and that the von Kármán street wake reinforced the already present oscillations and caused the center span to violent twist until the bridge failure, see [91, p. 31]. But, according to Scanlan [238, p. 841],

> some of the writings of von Kármán leave a trail of confusion ... it can clearly be shown that the rhythm of the failure (torsion) mode has nothing to do with the natural rhythm of shed vortices following the Kármán vortex street pattern.

And, indeed, the calculated frequency of a vortex caused by a 68 km/h wind is 1 Hz, whereas the frequency of the torsional oscillations measured by Farquharson was 0.2 Hz, see [47, p. 120]. The conclusion in [47, p. 122] is that

> we see the flutter vortex trail as a consequence, not as a primary cause.

In fact, when a suspension bridge is attacked by wind its starts oscillating due to the vortex shedding, but soon afterwards the wind itself modifies its behavior following the oscillations of the bridge. A qualitative description of this phenomenon was given by Rocard [234, p. 135]:

> it is physically certain and confirmed by ordinary experience, although the effect is known only qualitatively, that a bridge vibrating with an appreciable amplitude completely imposes its own frequency on the vortices of its wake. It appears as if in some way the bridge itself discharges the vortices into the fluid with a constant phase relationship with its own oscillation.

This may remind the behavior of footbridges, see Sect. 1.2, where pedestrians fall spontaneously into step with the vibrations: for both kinds of bridges, external forces synchronise their effect and amplify the oscillations of the bridge. But Rocard [234, p. 142] also claims that

> it is unlikely that the vortices alone can create an effective coupled vibration if the independent natural frequencies of bending and of torsion are very different.

On a fairly simplified model, in Sect. 3.6 we will show that very different frequencies of bending and of torsion lead to more stable structures.

Also Green-Unruh [136, § III] believe that

> the von Kármán vortex street forms at a frequency determined by the geometry and the wind velocity. These vortices form independently of the motion and are not responsible for the catastrophic oscillations of the TNB.

Their own conclusion is similar, namely

> vortices are also produced as a result of the body's motion.

Only much later, in 2000, the vortex theory was partially readmitted by Larsen [166, p. 247] who writes

> the vortex street may cause limited torsion oscillations, but cannot be held responsible for divergent large-amplitude torsion oscillations.

And indeed, what remained obscure until that time was a deep understanding of how vortices may be responsible for the wind-excited twisting motion. Larsen [166, p. 245] claims that

> The key to the torsion instability mechanism is the formation and drift of large-scale vortices on the cross section. A discrete vortex simulation of the flow around a simplified model of the Tacoma Narrows section shape, in which the angle of attack changes stepwise from 0 to 10°, highlights the vortex dynamics involved.

Roughly speaking, it is claimed that the variation of the angle of attack creates an alternation of vortices characterised by the direction of rotation and the position above/below the roadway. These vortices are also due to the H-form of the cross

section and may either push up or pull down the endpoints of the cross section. The variation of the angles also generates extra energy that gives rise to higher amplitudes of torsional oscillations and the cross section oscillates in a self-sustaining motion. Design modifications, such as replacing the H-shaped section of the deck with an open girder, that would have rendered the original TNB more aerodynamically stable, are also suggested by Larsen. This explanation seems to have convinced the engineering community since [166] received the "Outstanding Paper Award" remitted each year to the author of a paper published in the issues of the IABSE Journal Structural Engineering International. But did the wind really change stepwise the angle of attack from 0° to 10°? Moreover, did this also happen during all the collapses described in Sect. 1.3?

The Report [9] does not clarify if the wind did really vary stepwise the angle of attack on November 7, 1940. Also recall that resonance is discarded precisely because nobody believes in "regular" winds. Moreover, the Report [9, p. 130] writes that

> It is very improbable that resonance with alternating vortices plays an important role in the oscillations of bridges.

And this statement is justified by

> ... there is no sharp correlation between wind velocity and oscillation frequency such as required in case of resonance with vortices whose frequency depends on the wind velocity ... there is no evidence for the formation of alternating vortices at a cross section similar to that used in the Tacoma Bridge...

The final conclusion of the Report [9, p. 131] is that

> ... it is more correct to say that the vortex formation and frequency is determined by the oscillation of the structure than that the oscillatory motion is induced by the vortex formation.

These statements raise some doubts on the work by Larsen [166]. More recently, McKenna [193] wrote that

> In Larsen [166], Figure 9 shows a graph of the simulated torsional response to one wind speed. The graph looks like a graph of $t \sin(\omega t)$. As we have seen, this behavior was never observed. The periodic torsional oscillations that lasted forty five minutes are never observed.

Skeptic comments on the Larsen work were also made by Green-Unruh [136] who write

> despite this success, this analysis is somewhat incomplete given the data available

and claim that

> the Larsen model does not adequately explain data at around 23 m/s,

which was the wind velocity the day of the TNB collapse. Green-Unruh pursue the Larsen explanation under three different aspects: they study how vortices drift near boundaries, how a vortex drifts near the trailing edge of the bridge, and the

production of vortices at the leading edge. The conclusion in [136] contains several criticisms on their own work; they write

> The detailed method through which the oscillatory behavior is established may require further details ... the range of wind speeds where the model is applicable has not been fully established. At the extreme high and low values, computational calculations become less reliable.

This is true in general: as long as a phenomenon is in a suitable range, any explanation is satisfactory. But was TNB behavior in a "reasonable range"?

1.7.4 Flutter

Flutter is a form of instability which can be seen in many objects and appears as an uncontrolled vibration; the simplest example are waving flags, if the air hits a flag with high velocity one sees a quivering within the flag. Rocard [234, p. 185] attributes to Bleich [49]

> ...to have pointed out the connection with the flutter speed of aircraft wings... He distinguishes clearly between flutter and the effect of the staggered vortices and expresses the opinion that two degrees of freedom (bending and torsion) at least are necessary for oscillations of this kind.

In [50, pp. 246–247] it is assumed that the bridge is subject to a natural steady state oscillating motion and the flutter speed is defined as follows.

> With increasing wind speed the external force necessary to maintain the motion at first increases and then decreases until a point is reached where the air forces alone sustain a constant amplitude of the oscillation. The corresponding velocity is called the critical velocity or flutter speed.

The flutter speed is then further characterised by noticing that

> ...below the critical velocity V_c an exciting force is necessary to maintain a steady-state motion; above the critical velocity the direction of the force must be reversed (damping force) to maintain the steady state motion. In absence of such a damping force the slightest increase of the velocity above V_c causes augmentation of the amplitude.

More credit to Bleich [49] is given in [241, p. 80] where one can read

> ...Bleich's work ... ultimately opened up a whole new field of study. Wind tunnel tests on thin plates suggested that higher wind velocities increased the frequency of vertical oscillation while decreasing that of torsional oscillation.

However, the conclusion is that

> ...Bleich's work could not be used to explain the Tacoma Narrows Bridge collapse.

The target of Bleich [50, p. 52] was

> to determine the relationship between the frequency and mode of motion and the corresponding "critical" or "resonant" wind velocity.

Bleich also suggests an implicit way to compute the flutter (or critical) speed, see [50, (7.28)]. Podolny [221, 15.89] comments these results by writing

> F. Bleich presented tables for calculation of flutter speed v_F for a given bridge, based on flat-plate airfoil flutter theory. These tables are applicable principally to trusses. But the tables are difficult to apply, and there is some uncertainty as to their range of validity.

Rocard [234, p. 101] writes that the main contribution of his own work is a

> ... precise method of calculating the critical speed of wind for any given suspension bridge.

He uses the parameters of the TNB and concludes that his computations lead to a critical speed of wind basically coinciding with the speed of the wind the day of the collapse, see [234, p. 158]. Let m be the mass of the unit length of the roadway (steel and concrete assembled within the same unit length) and let m_0 be the mass of air in a square parallelepiped erected above unit length; for common bridges, the ratio m/m_0 is around 50. Let 2ℓ be the width of the roadway and let r be the radius of gyration of the unit length in the roadway so that $r \approx \ell/\sqrt{2}$. Finally, let ω_v and ω_t denote, respectively, the natural vertical and torsional frequencies of the bridge: Rocard [234, p. 169] claims that for common bridges one has

$$\omega_t > \omega_v \tag{1.4}$$

and that if $\omega_t < \omega_v$ then the bridge would be stable under wind. Then, according to Rocard, the formula to compute the critical velocity V_c of the wind is

$$V_c^2 = \frac{2r^2\ell^2}{2r^2 + \ell^2} \frac{m}{m_0} (\omega_t^2 - \omega_v^2) \,. \tag{1.5}$$

With the parameters of the original TNB, (1.5) yields $V_c = 47$ mph (see [234, p. 178]) while the TNB collapsed under a wind having velocity $V = 42$ mph. There seems to be no continuous dependence in (1.5): the bridge is stable if $\omega_t < \omega_v$ and very unstable (with small V_c) if $\omega_t \approx \omega_v$ with $\omega_t > \omega_v$. We refer to Sect. 3.6 for an explanation of how the ratio between these two frequencies affects the stability of the bridge.

Formula (1.5) was later modified by Selberg [242] who obtains

$$V_c^2 = \frac{(3.71)^2}{2\sqrt{3}} \frac{m}{m_0} (\omega_t^2 - \omega_v^2) \,. \tag{1.6}$$

More recently, [189, (18)] suggests a larger coefficient for V_c, namely

$$V_c^2 = \frac{(3.81)^2}{2\sqrt{3}} \frac{m}{m_0} (\omega_t^2 - \omega_v^2) \,. \tag{1.7}$$

Finally, let us mention that different formulas were also suggested by Irvine [149, (4.91)] and by Como-Del Ferraro-Grimaldi [85, Sect. 8]. A mathematician

is naturally brought to raise the question: which is the correct formula for the flutter speed?

As far as we are aware, the Rocard formula (1.5) to compute the flutter speed was never used in later projects. A skeptic comment on how Rocard derived (1.5) comes from [282, p. 457]:

> His method, however, is not rigorous, and the logical inferences at some points are doubtful.

While referring explicitly to the work by Bleich and Rocard, Billah-Scanlan [47, p. 122] write that

> Another error accompanying many accounts has been the confusion of the phenomenon of bridge flutter with that of airplane wing flutter as though they were identical.

This was previously pointed out by Scanlan-Tomko [239, p. 1733]:

> ... the most striking differences between airfoil and bridge deck results is revealed by the flutter coefficients.

Moreover, Scanlan [238, p. 841] comments the work by Bleich by writing

> ... such an effort is doomed to failure because of the huge physical dissimilarity between a bluff bridge deck section and a streamlined airfoil.

Billah-Scanlan also emphasise that

> forced resonance and self-excitation are fundamentally different phenomena

and they claim that their work demonstrates that

> the ultimate failure of the bridge was in fact related to an aerodynamically induced condition of self-excitation or "negative damping" in a torsional degree of freedom.

The negative damping together with the torsional degree of freedom caused the torsional flutter so that, as the roadway rotated, the wind force acting on the surface changed, when the bridge rotated back the forces pushed the bridge in the opposite direction. They claim that this negative damping effect and increase in rotation lead up to the torsional oscillation that caused the collapse of the bridge. But Larsen [166, p. 244] writes that

> Billah and Scanlan ... fail to connect the vortex pattern to the shift of apparent section damping from positive to negative, which signifies the onset of torsional instability.

Scanlan-Tomko [239] do not mention neither Bleich nor Rocard, and attribute to Theodorsen [256] to have

> ... greatly influenced American flutter work...

They compute the flutter coefficients first with the so-called Theodorsen circulation function [256] and then experimentally: the comparison of these two computations shows a general good agreement with some discrepancies. Bleich [50, p. 248] comments the results by Theodorsen by emphasising that they are derived for small oscillations about the position of equilibrium, that

> ... they apply solely to the narrow zone of transition from stable to unstable motion...

and he then concludes that they are suitable to determine the critical wind speed. Also, Scanlan-Tomko [239, p. 1718] are mainly interested in small oscillations:

> While linearization of the aerodynamics of such models is still open to some criticism, it appears reasonable for small amplitudes of motion.

Nevertheless, the TNB collapsed because of **wide oscillations**, see [9].

The model in [239] was subsequently revisited by Billah-Scanlan [47] who, however, made no substantial progress. On [47, p. 121] they write that Scanlan-Tomko [239]

> ... demonstrated conclusively that the catastrophic mode of the old Tacoma Narrows bridge was a case of what they termed single-degree-of-freedom torsional flutter due to complex, separated flow.

But, more recently, McKenna [193] wrote that Billah-Scanlan [47]

> ... offered a mathematical model which is only valid for very small displacements and can only be verified in ideal wind tunnel experiments of "in torsion $0 \leq \alpha \leq \pm 3^o$". We are asked to believe that these "penetrating insights" explain the Tacoma Narrows oscillation. To us, the case is less than convincing.

With some badinage McKenna comments by writing that *apparently the authors were not familiar with the concept of absolute value* and then he continues by saying that [47]

> ... is a perfectly good explanation of something that was never observed, namely small torsional oscillations, and no explanation of what did occur, namely a large vertical oscillation with a double amplitude of five ft. and a frequency of 38 per min. followed by a change to the torsional.

And indeed, from the Report [9, p. 31] we learn that torsional oscillations were never recorded prior to the day of the TNB collapse, see also Sect. 1.7.6 for further details. Finally, McKenna wonders why

> ... if the explanation in [47] has any validity, why were small torsional oscillations never observed? After all, the bridge was known to have oscillated vertically in winds of 3 m.p.h., and remained motionless in winds of 35 m.p.h., (when according to [47], "divergent amplitudes" are reached). It is also worth noting that the bridge had survived winds of 48 m.p.h. without undergoing torsional oscillations, [9], page 28.

In fact, none of the above formulas (1.5)–(1.6)–(1.7) is usually employed to compute the flutter speed which is instead determined by fine experiments on prototypes in wind tunnels, see [84, Sect. 2.2.3]. Since wind tunnel tests are costly both in time and financial terms, it appears desirable to have a rigorous and unanimously shared formula for the computation of the flutter speed. But what we have seen so far in this section tells us that the major difficulty while studying flutter is that it is not just one but many phenomena. Scanlan [237, p. 194] writes that

> the term "flutter" is used broadly in the context of any oscillatory dynamic instabilities that typically exhibit divergent character with increasing wind velocity.

Como [84, Sect. 2.2.3] writes that (our translation):

> Flutter occurs when a resonance is established between non stationary aerodynamic forces, resulting from the movement of the structure, and the oscillating structure.

This sentence highlights the keywords **resonance** and **structure** and states that flutter should be evaluated in two steps: one should first determine the impact of the wind and the "resulting movement of the structure", then one should see if a "resonance is established". A few lines below, Como continues by writing (our translation):

> The most classical flutter is the one which occurs during combined vertical and torsional oscillations. In this case, the flutter condition is attained when the frequencies of the vertical and torsional oscillations, which vary for increasing wind speed, become equal and suitably out of phase at a given speed.

The main concern is then to determine in which way the wind speed varies the frequencies of vertical and torsional oscillations.

We conclude the present survey on flutter with a characterisation taken from [238, p. 840]:

> Classical flutter of the lifting-surface type occurs when an aerodynamically forced coalescence of frequencies occurs between two degrees of freedom.

Again, a resonance (coalescence of frequencies) seems to be somewhere hidden.

In this section we have seen that flutter is defined as a self-feeding and potentially destructive vibration where aerodynamic forces on an object couple with a natural mode of vibration of the structure to produce rapid periodic motion. Flutter may occur in any object within a strong fluid flow, under the conditions that a positive feedback occurs between the structure natural vibration and the aerodynamic forces. That is, the vibrational movement of the object increases an aerodynamic load, which in turn drives the object to move further. If the energy input by the aerodynamic excitation in a cycle is larger than that dissipated by the damping in the system, the amplitude of vibration will increase, resulting in self-exciting oscillations. This definition implicitly assumes the appearance of an external resonance or of a parametric resonance.

1.7.5 Parametric Resonance

A mathematical approach to study the instability of suspension bridges consists in the so-called parametric resonance which, as far as we are aware, was introduced by the Russian mathematicians Malkin-Krein-Yakubovich [159, 184, 281] around 1960. We refer to Sect. 3.2 for the application of this approach to a particular model. The parametric resonance method was adapted to the TNB model by Pittel-Yakubovich [218, 219], see also [282, Chap. VI] for the English translation and a more general setting. The conclusion on [282, p. 457] states that

> ... the most dangerous phenomenon for the stability of suspension bridges is a combination of parametric resonance.

Scanlan [238, p. 841] comments the attempts for an explanation to the TNB collapse by Yakubovich-Starzhinskii [282, Chap. VI] as follows:

> Others have added to the confusion. A recent mathematics text [282], for example, seeking an application for a developed theory of parametric resonance, attempts to explain the Tacoma Narrows failure through this phenomenon.

A simplified approach to parametric resonance may be found in the monograph by Irvine [149]. He models the cross section of the bridge section as a rod subject to the forces exerted at its endpoints by the two lateral hangers, see Sect. 4.1 for more details. This model has two degrees of freedom, the vertical displacement y of the barycenter of the rod and the torsional angle θ of the rod with respect to horizontal. Irvine [149, (4.78)–(4.79)] reaches the following dimensionless linear system of PDE's (to be compared with (4.1)):

$$I\theta_{tt}-\theta_{xx}-\gamma_1 V^2\theta+h(\theta)=0,\ y_{tt}-y_{xx}-\gamma_2 V^2\theta+h(y)=0 \quad (0<x<1,\ t>0) \tag{1.8}$$

where $h(w) := \lambda\int_0^1 w(x)dx$ for any $w \in L^1(0,1)$ and $\lambda > 0$, $I \in (\frac{1}{3},1)$, $\gamma_1 > 0$, $\gamma_2 > 0$ are physical constants depending on the structure, while $V \geq 0$ is the scalar speed of the wind. When $V = 0$ (absence of wind) the system (1.8) is uncoupled and the two equations describe free vibrations. Since $I < 1$ it is straightforward to verify that the frequency of θ is larger than the frequency of y, thereby confirming (1.4). When $V \neq 0$, the system (1.8) may be solved in two steps: one solves the first equation and finds θ, then one replaces θ in the second equation and finds y. This procedure raises some doubts on the reliableness of (1.8) since we have learned from Sect. 1.3 that vertical oscillations influence torsional oscillations and not viceversa. However, forgetting this crucial point, let us proceed further with the analysis of (1.8). For varying V the frequencies of θ and y in (1.8) also vary. For a certain critical value of V, the so-called **flutter speed**, the two frequencies coincide, giving rise to a resonance, the so-called **parametric resonance**, and to instability.

This sketchy description on a simplified model such as (1.8) well describes what is, nowadays, the most common procedure. In fact, a parametric resonance is fairly similar to an external resonance, which was discussed in Sect. 1.7.2. The difference is that the disordered action of the wind is regularised within vortices (as in (1.8)) and becomes more similar to a periodic forcing: one can then pretend that the frequency of this regularised action may match the natural frequency of the structure. However, we have already pointed out that the frequency of a vortex caused by a 68 km/h wind and the frequency of the oscillations at the TNB were fairly different, see [47, p. 120].

A further recent attempt of mathematical explanation of the TNB collapse is based on the self-oscillation phenomenon, as suggested by Jenkins [152].

We have seen several different keywords for a theoretical explanation of the TNB collapse: flutter, parametric resonance, self-oscillation. All these phenomena seem

to be somehow related. For instance, parametric resonance is shown to be connected with flutter, see [66, 140], while Jenkins [152, p. 178] writes first that

> In self-oscillating "aeroelastic flutter", including the motion of the bridge ... vortices are shed at the frequency of fluttering...

and then he writes

> ... parametric resonance resembles self-oscillation in that the growth of the amplitude of small oscillations is exponential in time, as long as there is some initial perturbation away from the unstable equilibrium...

Moreover, these three phenomena are all **linear phenomena** while we will see in next section that there is strong evidence for nonlinear behaviors of suspension bridges. For this reason, and for the existence of fairly divergent opinions, the history of possible explanations of the TNB failure seems far away from its end.

1.7.6 Partial Conclusions: Aerodynamic Effects

It is clear that in absence of wind or external sources a bridge remains still. A vertical load, such as a vehicle, bends the bridge and creates a bending energy. Less obvious is the way the wind inserts energy into the bridge: let us outline how this happens. When a fluid hits a bluff body its flow is modified and goes around the body. Behind the body, or a "hidden part" of the body, the flow creates vortices, see the sketch in Fig. 1.19. This is just a simplified explanation, further vortices and more complicated phenomena may appear. An event of probability zero is that the flow remains perfectly symmetric with respect to the obstacle. Whence, in general, asymmetric vortices appear: this asymmetry generates a forcing lift which starts the vertical oscillations of the body. Up to some minor details, this explanation is shared by the whole community and it has been studied with great precision in wind tunnel tests, see e.g. [166, 241].

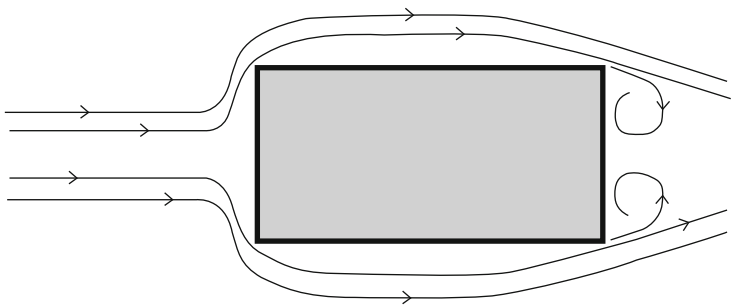

Fig. 1.19 Wind hitting the section of the roadway of a bridge

The questions **(Q1)–(Q2)–(Q3)** raised in Sect. 1.6 become quite natural immediately after that this aerodynamic effect started the vertical oscillations. The partial explanations discussed in the previous subsections are all based on further aerodynamic effects such as an external resonance (Sect. 1.7.2), the vortex shedding (Sect. 1.7.3), the flutter theory (Sect. 1.7.4), a parametric resonance (Sect. 1.7.5). All these phenomena may contribute to amplify the oscillations but, for several different reasons, none of them is unanimously recognized to be the origin of wide torsional oscillations. As an example, we quote several sentences from [190] about aerodynamic interferences between vertical and torsional oscillations at the TNB:

> ... the mystery of onset velocity of torsional flutter ... it can be supposed that the wind velocity increased till the torsional flutter region ... after this failure, there are two hypotheses...

The words *mystery*, *supposed*, *hypotheses*, suggest to afford the conclusion that

no aerodynamic effect seems to be able to give a complete answer to (Q1).

For both the model problems considered in [47] and [149] (see (1.8) for the latter), we may rephrase McKenna [193], as quoted in Sect. 1.7.4:

these models are a perfectly good explanation of something that was never observed in suspension bridges, namely small torsional oscillations, but do no explain what usually occurs, namely sudden wide oscillations.

This is confirmed by the Report [9, p. 31]:

> Prior to 10:00 A.M. on the day of the failure, there were no recorded instances of the oscillations being otherwise than the two cables in phase and with no torsional motions.

What was observed in suspension bridges may be summarised as follows.

$$\begin{aligned} \text{weak wind} &\to \text{small vertical oscillations} \twoheadrightarrow \text{no torsional oscillations;} \\ \text{moderate wind} &\to \text{medium vertical oscillations} \twoheadrightarrow \text{no torsional oscillations;} \\ \text{strong wind} &\to \text{large vertical oscillations} \twoheadrightarrow \text{large torsional oscillations.} \end{aligned} \tag{1.9}$$

The arrow $\to$ indicates an aerodynamic effect whereas the arrow $\twoheadrightarrow$ indicates a structural effect. Two facts appear evident from (1.9). The interaction between the wind and the structure is "almost linear": by this we mean that the amplitude of vertical oscillations is regularly increasing with respect to the strength of the wind. The interaction within the structure, from vertical to torsional oscillations, appears nonlinear and subject to a "sudden" phenomenon such as a resonance. As a consequence of these facts we may conclude the following:

- **The origin of torsional oscillations should be sought within the structure.**
- **Nonlinear structural models are unavoidable.**

Throughout this book we will try to convince the reader that the answers to **(Q1)–(Q2)–(Q3)** are hidden within the structure. The nonlinear structural behavior of a suspension bridge may give satisfactory answers to these questions.

1.8 Nonlinear Behavior of Suspension Bridges

Roughly speaking, one can say that chaos manifests itself as a disordered and unpredictable behavior of the solutions of a dynamical system. Jenkins [152, p. 185] writes that the chaotic behavior appears in pendulum-type equations where

> ... solutions may show sensitive dependence on initial conditions, making the precise behavior of the oscillator effectively unpredictable, even though it is governed by a deterministic equation.

With this characterisation, there is no doubt that chaos was somehow present in the dynamic described in Sects. 1.3 and 1.4. From [135, § 11.7] we recall a **General Principle of Classical Mechanics (GPCM):**

> neither linear differential equations nor systems of less than three first-order equations can exhibit chaos.

The (GPCM) states that any model aiming to describe the dynamics of suspension bridges should be **nonlinear** and involve at least **three** (mathematical) degrees of freedom. By "mathematical degrees of freedom" we mean here the order of a PDE, or the number of initial conditions for an ODE or a system of ODE's. A linear model obtained after linearisation of a nonlinear model makes sense for small deflections, for positions close to equilibrium. Lazer-McKenna [168, p. 550] write that

> a linear model is insufficient to explain the large oscillatory behavior that has been observed.

Hence, if somebody aims to afford an explanation of the TNB collapse, and how large oscillations may appear, he must necessarily use a nonlinear model.

A nonlinear effect is observable in pedestrian bridges, as the ones considered in Sect. 1.2. While studying the action of the negative damping due to pedestrians on the London Millennium Bridge, Macdonald [179, p. 1056] observes that

> above a certain critical number of pedestrians, this negative damping overcomes the positive structural damping, causing the onset of exponentially increasing vibrations.

Some doubts may arise about the precise meaning of "exponentially increasing vibrations" but, in any case, it describes a superlinear behavior which has also been observed in several further pedestrian bridges, see [114] and [285] from which we quote

> damping usually increases with increasing vibration magnitude due to engagement of additional damping mechanisms.

So, the oscillations are amplified by an observable superlinear effect.

This also occurs in suspension bridges: more the bridge is far from its equilibrium position, more the role of the restoring forces becomes relevant. Supported by analytical and experimental studies on the dynamic response of suspension bridges, Brownjohn [62] is able to show a strong nonlinear contribution of the cable/hanger effects. McKenna-Tuama [195] write

> ... we expect the bridge to behave like a stiff spring, with a restoring force that becomes somewhat superlinear.

It is well-known that traveling waves are a nonlinear phenomenon, they do not appear in fourth order linear equations. Cone [9, IX-1], chief engineer of the Golden Gate Bridge, observed some traveling waves during a windstorm on February 9, 1938:

> I also observed that the suspended structure of the Bridge was undulating vertically in a wavelike motion of considerable amplitude ... the wave motion appeared to be a running wave similar to that made by cracking a whip.

One may also have a look at the video on the Volgograd Bridge [270]: although some people believe it is fake, it well describes what is meant by traveling waves. The existence of traveling waves is another proof of the nonlinear behavior of bridges.

A further source of nonlinearity is the interaction between the structure and the air; we have seen in Sect. 1.7.3 that first the wind forces the bridge to oscillate but then the bridge imposes its own phase on the vortices; in this respect, Rocard [234, p. 141] writes

> The bridge excited by impulses due to the vortices is a nonlinear system ... One cause of non-linearity has already been described ... another much more important cause originates from interaction with the vortices.

Again, this describes a superlinear behavior of the forces with respect to the displacement.

Arena-Lacarbonara [17] use a nonlinear model for suspension bridges to describe its three-dimensional motions. They study the torsional divergence caused by the static part of the wind-induced forces and the onset of the static instability. They also study the dynamic bifurcation that occurs at the onset of flutter. The matching between theory and practice shows that their nonlinear model is much more powerful than previous linear models. In his monograph, Lacarbonara [160] studies the static and dynamic behavior of several structures and, in particular, of suspension bridges. In the introduction he writes

> Structures are very slender and flexible, and thus they respond nonlinearly to typical disturbances. The nonlinearities become an essential aspect of the structural behaviors under both static and dynamic excitation.

All these contributions enable us to conclude that it is by now well understood that suspension bridges behave nonlinearly and that nonlinearities are present everywhere in the structure. One can place into the hangers all the interactions of the roadway with the rest of the structure (including the sustaining cable and the

towers). The system consisting of the towers, the cable and the hangers is strongly elastic, and the forces behave in an elastic fashion. In this respect, the linear Hooke law of elasticity, discovered by the English scientist Robert Hooke in 1660, states that for small elongations of a spring from equilibrium, the restoring force of the spring is directly proportional to the elongation. This follows from the fact that, as a consequence of Taylor formula, any smooth function f can be written as $f(w) = f(0) + f'(0)w + o(w)$ when $w \to 0$. However, at relatively large values of the applied force, the deformation of any elastic material is often larger than expected on the basis of the linear law, thereby displaying a superlinear behavior. Whence, the usual form $f(w) = kw$, where w is the displacement from equilibrium and $k > 0$ depends on the elasticity of the spring, should be complemented with an additional superlinear term $\varphi(w)$ which becomes negligible for small displacements w. More precisely,

$$f(w) = kw + \varphi(w) \qquad \text{with} \qquad \lim_{w\to 0} \frac{\varphi(w)}{w} = 0\,. \tag{1.10}$$

The superlinear term φ may be arbitrarily small and should describe with more precision the elastic behavior of the spring when larger displacements w are involved. As we shall see, this apparently harmless and tiny nonlinear perturbation has devastative effects on the models and, moreover, it is amazingly useful to display self-excited oscillations as the ones visible in actual bridges. On the contrary, linear models prevent to view the real phenomena which occur in bridges, such as the sudden increase of the width of their oscillations and the switch to different ones. These conclusions are consistent with the (GPCM) stated above.

Which is the correct choice for the restoring force f due to the structure and transmitted by the hangers? Some springs resist to extensions but not to compressions. However, a remark by Brownjohn [62, p. 1364] implicitly claims that this choice is not adequate for suspension bridges:

> The hangers are critical elements in a suspension bridge and for large-amplitude motion their behaviour is not well modelled by either simple on/off stiffness or invariant connections.

This means that f should be active also across the equilibrium $w = 0$ so that

$$f \in \mathrm{Lip}_{loc}(\mathbb{R})\,, \quad f(w)\,w > 0 \quad \forall w \in \mathbb{R} \setminus \{0\}. \tag{1.11}$$

A natural choice seems to be

$$f(w) = kw + \varepsilon w^3 \qquad (\varepsilon > 0) \tag{1.12}$$

where $k > 0$ is the modulus of elasticity of the structure as transmitted by the springs. We will often use this form to introduce perturbations of nonlinear forces although we do not pretend it to be optimal. In fact, we will see that the qualitative

behavior of the solutions does not depend on the value of $\varepsilon > 0$ nor on more general superlinear perturbations $\varphi(w)$.

From [234, p. 186] we quote

> a bridge twice as wide will have exactly double the critical speed wind.

This simple remark shows that structural solutions may be planned in order to improve the stability of a bridge. More recently, some attempts to improve bridges performances can be found in [138] where, in particular, a careful analysis of the role played by the hangers is made. But much work has still to be done; Haberland-Hass-Starossek [138, p. 1624] assert that

> Research on the robustness of suspension bridges is at the very beginning.

We agree and we believe that a correct mathematical modeling would be of great help to improve the performances of suspension bridges through design factors. This is also one of the purposes of the next chapters.

Let us now summarise the contents of this chapter and how it will be linked to the subsequent chapters. We have seen that destructive torsional oscillations may appear in suspension bridges and, so far, there is no explanation for their appearance. Moreover, in this section we saw that the behavior of suspension bridges is nonlinear. The purpose of the next chapters is to derive nonlinear mathematical models able to explain the appearance of torsional oscillations.

In Chap. 2 we revisit the beam models which were initially used to describe the behavior of suspension bridges. Clearly, in such a model one cannot view torsional oscillations but, still, we can show that unexpected self-excited oscillations may also appear within this model provided some nonlinearity is present.

In Chap. 3, we consider a "fish-bone" model, namely a beam representing the midline of the roadway with orthogonal cross sections able to describe torsional oscillations; the Hill equation in its numerous versions enables us to give a detailed description of the origin of torsional instability.

In Chap. 4 we model a suspension bridge through several nonlinear coupled oscillators. This system has many mathematical degrees of freedom and represents a discrete version of a bridge. Classical mathematical tools, such as the Poincaré maps, enable us to give theoretical explanations of the observed torsional instability.

In Chap. 5 we explain why a suspension bridge is well described by a plate in nonlinear elasticity. The corresponding fourth order equations are derived after a careful analysis of the energies involved. As a compromise between a full quasilinear model and a linear one, we consider a semilinear model. Of particular interest appears the behavior of the eigenfunctions which describe the oscillating modes of the roadway. These plate models seem more reliable but they still need quantitative refinements.

In Chap. 6 we show how all these models enable us to give exhaustive answers to the questions **(Q1)–(Q2)–(Q3)** raised in Sect. 1.6. Hence these models allow to explain collapses from the past and, hopefully, may give some hints for future plans.

1.9 Bibliographical Notes

In his marvelous illustrated book Machinae Novae [265], Fausto Veranzio accompanied Figs. 1.2 and 1.3 with the descriptions in Fig. 1.20.

We quoted here the Italian version of the descriptions: in [265] one may also find the Latin version and the translation to French, Spanish, and German.

In 1808, Finley patented his system, see Fig. 1.4, and also published a description of the principles of the deck-stiffened suspension bridge [112]. We also refer to [210, p. 9] for the description of the patent. In Great Britain, Samuel Brown (1776–1852) was considered an early pioneer of suspension bridge design and construction. He is best known for the Union Bridge of 1820, the first vehicular suspension bridge in Britain. According to Bender [33],

> The invention of the suspension bridges by Sir Samuel Brown sprung from the sight of a spider's web hanging across the path of the inventor, observed on a morning's walk, when his mind was occupied with the idea of bridging the Tweed.

For an accurate description of early suspension bridges, prior to 1823, we refer to [210, Première Partie]. Figure 1.8 comes from a publication entitled *Papers Relating to the building of a Bridge over the Menai Strait, near Bangor Ferry*, published on 18 February 1819 by the United Kingdom House of Commons. For a detailed history of bridges collapses we refer to [50, Sect. 1.1], to [234, Chap. IV], to [84, 105, 139, 278], to the monographs [5, 153], and also to [148] for a complete database. We also refer to the beautiful book by Fernández Troyano [109] which contains an amazing number of pictures of bridges from all over the world.

The historical sources [10, 101, 225, 226, 255] may be downloaded from the web, the second paper by Provis [226] may also be found in [105, pp. 78–83]. The paper by Russell [235] is reproduced in [105, pp. 84–88]; in turn, the paper by Russell

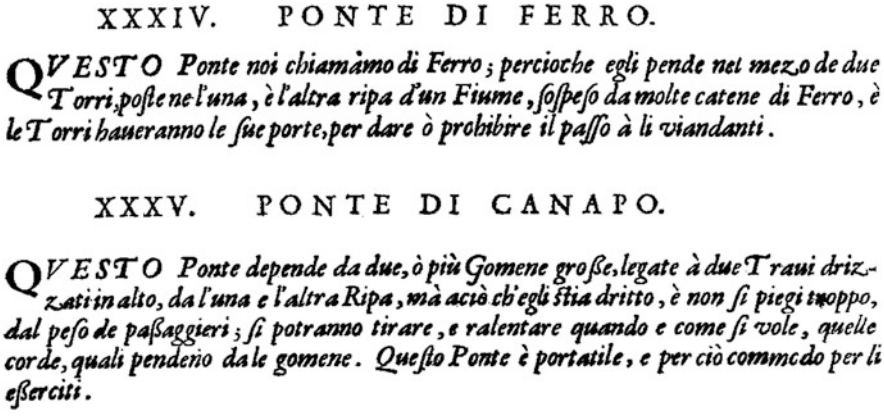

XXXIV. PONTE DI FERRO.

QVESTO Ponte noi chiamàmo di Ferro; percioche egli pende nel mezo de due Torri, poste ne l'una, è l'altra ripa d'un Fiume, sospeso da molte catene di Ferro, è le Torri haueranno le sue porte, per dare ò prohibire il passo à li viandanti.

XXXV. PONTE DI CANAPO.

QVESTO Ponte depende da due, ò più Gomene grosse, legate à due Trani drizzati in alto, da l'una e l'altra Ripa, mà acciò ch'egli stia dritto, è non si pieghi troppo, dal peso de passaggieri; si potranno tirare, e ralentare quando e come si vole, quelle corde, quali pendeno da le gomene. Questo Ponte è portatile, e per ciò commodo per li esserciti.

Fig. 1.20 Italian description of the Pons Ferreus and of the Pons Canabeus by Veranzio (1595) (Reproduced with permission from Fondazione Biblioteca di via Senato, Milano, Italy)

repeats word by word the description from the paper by Reid [230], see also [234]. Further details on the Brighton Chair Pier collapse may be found on [50, pp. 4–5]. Figure 1.10 is taken from [77].

As we already pointed out, the Chladni experiment [77] described in Sect. 1.3 raised the curiosity of Navier and other mathematicians. In 1809, the French Academy of Sciences promoted a competition in order to find some explanations to these experiments. Napoleon himself was very interested and he offered a golden medal of 1kg as a prize for an explanation. Marie-Sophie Germain took up the challenge and at the deadline of the competition she was the only candidate with a possible explanation. Lagrange was a member of the committee and found some mistakes in her arguments; therefore the committee rejected her work. Lagrange then helped Germain to correct the mistake and the prize was promoted a second time in 1813. But even this second prize was not attributed to her due to some further glitches in the proof. Only after the third attempt, in 1815, the tenacity of Germain received the deserved prize: the Chladni experiments finally had a theoretical explanation. The published work by Germain [131] should be considered the starting point of the theory of plates that we analyse in some detail in Chap. 5, see in particular Sect. 5.8 for more historical details. The book [131] is motivated by the Chladni experiment and the first lines of the introduction read

> Les phénomènes acoustiques, dont on doit la connaissance à M. Chladni, ont dirigé l'attention des géomètres vers la question des surfaces élastiques.

Most of the material in Sect. 1.4 comes from the Report [9], which contains also a copy of the letter by Farquharson [104], see [9, Appendix V]. Other material comes from the more recent monograph by Scott [241]. For the full description of the Tacoma collapse, including structural information, we refer to both [9, 241] and also to preliminary studies in [50, 105–107, 245, 269].

More details on the bridges described in Sect. 1.5 are available in the work by Farquharson [105, p. 15]. Rocard [234, p. 100] classifies some bridges as "stable" and some others as "unstable" according to some characteristic parameters (length of span, roadway width, sag of cables, etc.) but does not explain how he uses them in order to reach the conclusion; of course, the original TNB results as unstable. Similar pictures as those in Fig. 1.18 may be found in [276, p. 143] and in [160, Chap. 9].

Section 1.6 may be complemented with more questions and doubts. In the monograph by Akesson [5] one finds further attempts of explanations of more general collapses and some further questions. The Storebaelt East Bridge was built in 1998 in Denmark; it is the second largest suspension bridge in the world. During its construction several unexpected oscillations appeared and it was necessary to fix some additional anchorages on the bottom of the sea [89, p. 32]: this shows that new solutions are necessary to solve old problems and that unexpected oscillations still remain unexplained.

Section 1.7 is the extended version of the explanations given in [21]. Some complements to the description given in Sect. 1.7.6, namely more details on how the wind flow creates vortices, may be found in [227, Sect. 12.3]. Further evidence of the nonlinear behavior of suspension bridges may be found in [52, 121].

Chapter 2
One Dimensional Models

The first attempts to model suspension bridges were to view the roadway as a beam. Although this point of view rules out an important degree of freedom, the torsion, it appears to be a reasonable approximation since the width of the roadway is much smaller than its length. In this chapter we review classical modeling of beams and cables and of their interaction.

We analyse in detail the Melan equation and its variants by emphasising the role of the nonlinear nonlocal term which models the additional extension of the cable due to the live load. We discuss several different existing approximations of this term and we study the corresponding responses of the model equation. We also show that the problem is delicate from a theoretical point of view since it may admit multiple solutions.

Then we survey historical linear models from the twentieth century; these models take their origin from the Tacoma collapse and aim to justify its behavior. The role of nonlinearities is then studied in beam equations, both for ideal unbounded beams and for hinged beams. It turns out that they may generate sudden self-excited oscillations leading to blow up in unbounded beams, a phenomenon which is visible only because the equation is nonlinear and of higher (fourth) order. In the case of a hinged bounded beam we show that the (finite) number of oscillations increases with the nonlinearity.

Then we revisit the nonlinear behavior of the hangers and cables starting from the fundamental work by McKenna who first modeled, at the end of the 1980s, their possible slackening. We also discuss several subsequent nonlinear models which highlight interesting phenomena such as the multiplicity of solutions.

F. Gazzola, *Mathematical Models for Suspension Bridges*, MS&A 15,
DOI 10.1007/978-3-319-15434-3_2

2.1 From Navier to Melan

The celebrated report [210] by the French engineer and mathematician Claude-Louis Navier (1785–1836) published in 1823, see the cover in Fig. 2.1, has been for several decades the only mathematical treatise of suspension bridges.

Kawada [153, p. 97] describes the work by Navier as *a Bible for engineers for almost half a century*. It mainly deals with the static of cables and their interaction with towers: some second order ODE's are derived and solved. At that time, no stiffening trusses had yet appeared and the models suggested by Navier are oversimplified in several aspects. Moreover, no collapse had occurred and Navier treats first and with more accuracy the impact of vehicles [210, p. 134] rather than the impact of wind [210, p. 161]. Navier also describes the plan of the Menai Straits Bridge with great enthusiasm, see [210, p. vii]; as we have seen in Sect. 1.3 this bridge collapsed a few years later during a hurricane. But Navier was aware that wind could have caused serious troubles in suspension bridges; while describing the action of the wind, he writes [210, p. 161]:

> Les accidens qui résulteraient de cette action ne peuvent être appréciés et prévenus que d'après les lumières fournies par l'observation et l'expérience.

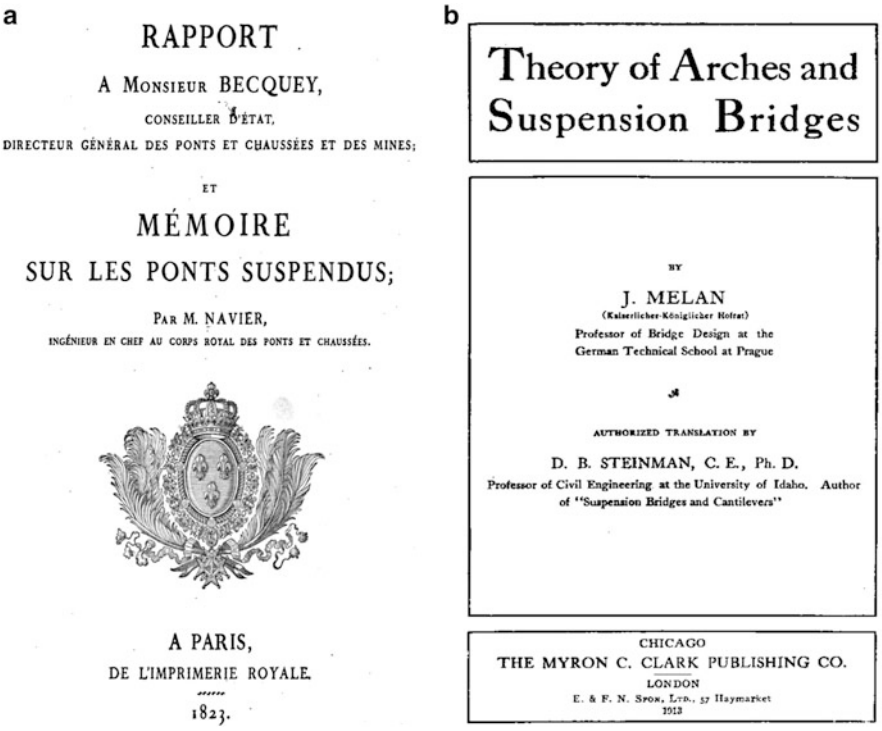

Fig. 2.1 Covers of the books by Navier [209] and Melan [199] (*Source*: (**a**) https://archive.org/details/theoryarchesand00melagoog; (**b**) https://archive.org/details/rapportamonsieu00navigoog)

In spite of a lack of prior history, the report by Navier appears as a masterpiece of amazing precision, including a part of applications intended to suggest how to plan some suspension bridges, see [210, Troisième Partie].

In the nineteenth century some further contributions deserve to be mentioned. The *Theory of structures*, contained in the monograph [229] by the Scottish engineer and physicist William John Macquorn Rankine (1820–1872), makes an analysis of the general principles governing chains, cords, ribs and arches; the part on *suspension bridge with sloping rods* [229, pp. 171–173] makes questionable assumptions and rough approximations. As far as we are aware, this contribution has not been applied to real bridges even if Rankine [229, p. 173] claims that

> The formulae of this Article are applicable to Mr. Dredge's suspension bridges, in which the suspending rods are inclined, and although not exactly parallel, are nearly so.

In a seminal paper [68] published in 1875, the Italian mathematician and engineer Carlo Alberto Castigliano (1847–1884) suggested a new theory for elastic systems close to equilibrium and proved a result known nowadays as the Castigliano Theorem; this theorem became the core of his main work [69], published in 1879, and allows to study the deflection of structures by strain energy method. His *Theorem of the derivatives of internal work of deformation* extended its application to the calculation of relative rotations and displacements between points in the structure and to the study of beams in flexure.

A milestone theoretical contribution to suspension bridges is certainly the monograph [199] by the Austrian engineer Joseph Melan (1854–1941), see again Fig. 2.1. This book was translated in English by the American engineer David Bernard Steinman (1886–1960) who, in the preface to his translation, writes

> The work has been enthusiastically received in Europe where it has already gone through three editions and the highest honors have been awarded the author.

In the book, Melan considers the bridges with

> all those forms of construction having the characteristic of transmitting oblique forces to the abutments even when the applied loads are vertical in direction.

Melan makes a detailed study of the static of cables and beams through a careful analysis of the different kinds of suspension bridges according to the number of spans, the stiffened or unstiffened structure, the effect of temperature. He repeatedly uses the Castigliano Theorem, in particular for the computation of deflection [199, p. 69]. It was Melan [199, p. 77] who first suggested a fourth order equation to describe suspension bridges; the equation reads

$$EI\, w''''(x) - (H + h)w''(x) - hy''(x) = p(x) \tag{2.1}$$

and will be widely discussed in the next sections to which we refer for the interpretation of the functions and parameters appearing in (2.1).

2.2 Linear and Quasilinear Beam Equations

A beam is a prismatical body with a resistance to bending and twisting. A beam is called a straight beam when the centers of gravity of all cross sections lie on a straight line, called the beam axis.

Assume that the x-axis of $\mathbb{R}^3$ coincides with the beam axis while the cross section is parallel to the yz-plane and it is symmetric with respect to the xz-plane. If $w(x)$ denotes the deviation in the z-direction from the horizontal equilibrium of the idealized one-dimensional beam at the point x, then the elastic energy stored in the beam due to the deformation consists of bending and stretching. Stretching occurs when the horizontal position of the beam is fixed at both endpoints and the beam increases its length. Assuming that the elastic force is proportional to the increase of length through the constant tension $T > 0$, the stretching energy for the beam in position w fixed at level 0 at the endpoints a and b is

$$\mathscr{T}_S(w) = T \int_a^b \left(\sqrt{1 + w'(x)^2} - 1 \right) dx. \tag{2.2}$$

Concerning the bending energy, several constants must be introduced. The Young modulus E is a measure of the stiffness of an elastic material and is defined as the ratio of the stress along the x-axis over the strain along the same axis: it is relatively small for very elastic materials such as rubber for which $E < 0.1\,\mathrm{GN/m^2}$, while for concrete $E \approx 30\,\mathrm{GN/m^2}$, for aluminium $E \approx 70\,\mathrm{GN/m^2}$, for copper $E \approx 117\,\mathrm{GN/m^2}$, for steel $E \approx 190\,\mathrm{GN/m^2}$. The moment of inertia I of the cross section of the beam is calculated with respect to the axis containing the barycenter: since the cross section is in the yz-plane and the deformation is in the z-direction, if the barycenter is at $y = z = 0$, then $I = \int z^2\, dydz$. The constant quantity EI is called the flexural rigidity of the beam. For a thin beam the energy stored by bending the beam is the square of the curvature times half the flexural rigidity:

$$\mathscr{T}_B(w) = \frac{EI}{2} \int_a^b \frac{w''(x)^2}{\left(1 + w'(x)^2\right)^3} \sqrt{1 + w'(x)^2}\, dx \tag{2.3}$$

where we highlighted the curvature and the arclength. Denote by $p = p(x)$ a load per unit length applied to the beam, then the total energy in the beam is given by

$$\frac{EI}{2} \int_a^b \frac{w''(x)^2}{\left(1 + w'(x)^2\right)^{5/2}}\, dx + T \int_a^b \left(\sqrt{1 + w'(x)^2} - 1 \right) dx - \int_a^b p(x) w(x)\, dx\,.$$

This energy function is not convex and it fails to be coercive in any reasonable functional space. Therefore, standard methods of calculus of variations do not apply. Formally, its critical points w satisfy the Euler–Lagrange equation

$$EI\left[\frac{w''(x)}{[1+w'(x)^2]^{5/2}}\right]''+\frac{5}{2}EI\left[\frac{w'(x)w''(x)^2}{[1+w'(x)^2]^{7/2}}\right]'-T\left[\frac{w'(x)}{\sqrt{1+w'(x)^2}}\right]'=p(x), \tag{2.4}$$

a fairly complicated quasilinear fourth order equation. And even if we drop the stretching energy ($T = 0$), the equation remains quite unpleasant:

$$EI\left[\frac{w''(x)}{[1+w'(x)^2]^{5/2}}\right]''+\frac{5}{2}EI\left[\frac{w'(x)w''(x)^2}{[1+w'(x)^2]^{7/2}}\right]'=p(x)\,.$$

We refer to [90] and references therein for some delicate results about this equation.

At this point, a possible way out is to linearise the equation. For

$$\text{small deformations } w \text{ of the beam} \tag{2.5}$$

we may use the asymptotic expansions of the involved formulas (as $w' \to 0$) so that $\mathscr{T}_S$ and $\mathscr{T}_B$ simplify as follows:

$$\mathscr{T}_S(w)=\frac{T}{2}\int_a^b w'(x)^2\,dx\,,\qquad \mathscr{T}_B(w)=\frac{EI}{2}\int_a^b w''(x)^2\,dx\,.$$

Therefore, if (2.5) holds then the total elastic energy may be approximated by

$$\mathscr{T}(w)=\int_a^b\left(\frac{EI}{2}w''(x)^2+\frac{T}{2}w'(x)^2-p(x)w(x)\right)dx. \tag{2.6}$$

The linear Euler–Lagrange equation that formally arises from (2.6) contains both second and fourth order terms and reads

$$EI\,w''''(x)-Tw''(x)=p(x)\,. \tag{2.7}$$

If the beam is moving in an elastic medium and if it can move freely at the endpoints, in case of zero tension there is no stretching component and we get

$$\mathscr{T}(w)=\int_a^b\left(\frac{EI}{2}w''(x)^2-p(x)w(x)\right)dx.$$

This leads to the Euler–Lagrange equation

$$EI\,w''''(x)=p(x)\,. \tag{2.8}$$

Fig. 2.2 A beam with left endpoint clamped and right endpoint hinged

The boundary conditions to be associated to these equations depend on the problem considered. If the beam is clamped at its endpoints then we impose the Dirichlet boundary conditions

$$w(a) = w'(a) = w(b) = w'(b) = 0\,. \tag{2.9}$$

If the beam is hinged at its endpoints then we impose the Navier boundary conditions

$$w(a) = w''(a) = w(b) = w''(b) = 0\,. \tag{2.10}$$

In Fig. 2.2 we represent both conditions (2.9) and (2.10).

These boundary conditions are variational and may be derived while minimising the energy functional in a suitable functional space. We say that $w \in H_0^2(a,b)$ (respectively, $w \in H^2 \cap H_0^1(a,b)$) is a weak solution of (2.7)–(2.9) [respectively, (2.7)–(2.10)] if

$$\int_a^b \left[EI\, w''(x)\varphi''(x) + w'(x)\varphi'(x)\right] dx = \int_a^b p(x)\varphi(x)\, dx$$

for all $\varphi \in H_0^2(a,b)$ (respectively, $\varphi \in H^2 \cap H_0^1(a,b)$). By the Lax–Milgram Theorem we infer

Theorem 2.1 *Assume that $p \in L^2(a,b)$. Then there exists a unique weak solution w of (2.7) [with one of the boundary conditions (2.9) or (2.10)] which is also the unique minimiser of the energy (2.6). If $p \in C^0[a,b]$ then $w \in C^4[a,b]$ is a classical solution of (2.7) and satisfies the boundary conditions (2.9) or (2.10).*

Whence, assumption (2.5) allows to linearise the equation and to study the problem with the classical tools of calculus of variations. However, it is not always possible to assume (2.5), in particular if one considers models where large oscillations appear. In this situation the linear equation does not reflect with sufficient accuracy the model. As a compromise between a rough approximation [leading to the linear equation (2.7)] and the full problem [leading to the quasilinear equation (2.4)] one may consider a semilinear equation, that is, an equation where the nonlinearities are concentrated in the zero order terms. This procedure is somehow justified in elasticity, see Sect. 5.1, and we will follow this trend in Sect. 2.6 below.

2.3 Deflection of Cables Under Vertical Loads

For several reasons, the sustaining cables have to be considered the main component of a suspension bridge. Not only they interact directly with the towers and the hangers, but also the stiffening trusses must be designed to take the compression induced by the cables. According to Podolny [221, Sect. 15.9],

> cables are one of the main components to inhibit the extension of suspension bridge spans.

The reason is that the weight of the cable grows more quickly than the weight of the roadway it supports; moreover, their dead load is superlinear with respect to the span length, see [221, Fig. 15.27].

In this section we derive the equation of the deflection of cables. We model the cable as a perfectly flexible string subject to vertical loads. If we assume that the string has no resistance to bending, as in the case of a rope, the only internal force is the tension $F = F(x)$ of the string which acts tangentially to the position of the curve representing the string. In Fig. 2.3 we sketch a picture of the string whose endpoints are A and B. The horizontal direction represents the abscissa x whereas the downwards axis represents the vertical displacement y. Denote by $\theta = \theta(x)$ the angle between the horizontal x-direction and the tangent to the curve so that

$$y'(x) = \tan\theta(x)\,. \tag{2.11}$$

Assume that the string is subject to a downwards vertical dead load $q(x)$. The horizontal component of the tension is constant, that is,

$$F(x)\cos\theta(x) \equiv H > 0\,. \tag{2.12}$$

At this point, two cases must be distinguished.

The load is distributed per horizontal unit. This is the situation which occurs when a beam is suspended to a cable as in Fig. 2.4. If we neglect the mass of the cable (dead load) then the load is distributed per horizontal unit. If we assume that spacing between hangers is small relative to the span, then the hangers can be considered as a

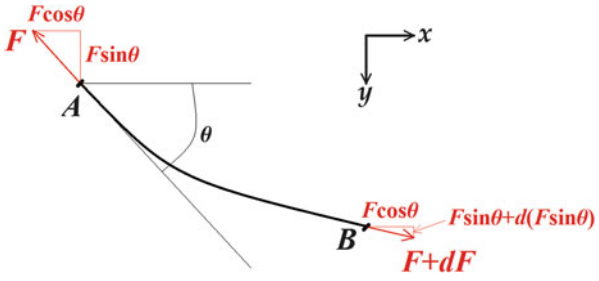

Fig. 2.3 Equilibrium of a string

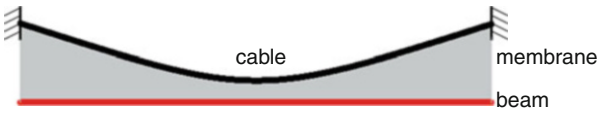

Fig. 2.4 Beam (*red*) sustained by a cable (*black*) through a membrane (*grey*)

continuous sheet or a membrane uniformly connecting the cable and the beam. This is a simplified sketch of what occurs in a suspension bridge, see Fig. 1, provided that the mass of the cable is neglected and that the roadway is sought as a beam. In this case, the vertical component of the tension has a variation given by

$$\frac{d}{dx}[F(x)\sin\theta(x)] = -q(x)$$

where we recall that the positive vertical axis is oriented downwards. In view of (2.12) we then obtain

$$H\frac{d}{dx}[\tan\theta(x)] = -q(x).$$

Moreover, by using (2.11), this equation yields

$$Hy''(x) = -q(x)\,. \tag{2.13}$$

If the left endpoint of the string is at the origin, $A(0,0)$, the other endpoint is at $B(x_0, y_0)$, and the load is constant, $q(x) \equiv q$, the solution of (2.13) is given by

$$y(x) = -\frac{q}{2H}x^2 + \left(\frac{y_0}{x_0} + \frac{q\,x_0}{2H}\right)x\,.$$

Hence, the cable takes the shape of a parabola (recall that y is positive downwards so that it has a $\cup$-shaped graph). The length L_c of the cable is then given by

$$L_c = L_c(x_0, y_0, q, H) = \int_0^{x_0} \sqrt{1 + y'(x)^2}\,dx\,. \tag{2.14}$$

If B is at the same height as A (as in suspension bridges, see Fig. 2.4), and if $L = x_0$ denotes the distance between the towers, then $B(L,0)$ and (2.13)–(2.14) yield

$$y(x) = \frac{q}{2H}\,x(L-x)\,, \qquad L_c = \frac{L}{2}\sqrt{1 + \frac{q^2L^2}{4H^2}} + \frac{H}{q}\log\left(\frac{qL}{2H} + \sqrt{1 + \frac{q^2L^2}{4H^2}}\right). \tag{2.15}$$

The load is distributed per unit length. This occurs when the cable is only subject to its own weight (dead load) or, at least, when its weight is the dominant part of the load. In this case, the vertical component of the tension has a variation given by

$$\frac{d}{dx}[F(x)\sin\theta(x)] = -q(x)\sqrt{1+y'(x)^2}$$

which, combined with (2.12), yields

$$H\frac{d}{dx}[\tan\theta(x)] = -q(x)\sqrt{1+y'(x)^2}\,.$$

In turn, by using (2.11), we obtain

$$Hy''(x) = -q(x)\sqrt{1+y'(x)^2}\,. \tag{2.16}$$

If the left endpoint of the string is at the origin, $A(0,0)$, the other endpoint is at $B(L,0)$, and the load is constant, $q(x) \equiv q$, the solution of (2.16) is given by

$$y(x) = \frac{H}{q}\left[\cosh\left(\frac{qL}{2H}\right) - \cosh\left(\frac{q}{2H}(2x-L)\right)\right]. \tag{2.17}$$

Hence, the cable takes the shape of a catenary (again, a $\cup$-shaped graph). The length L_c of the cable is given by (2.14) which, for (2.17), yields

$$L_c = \frac{2H}{q}\sinh\frac{qL}{2H}\,.$$

2.4 Suspension Bridges Modeled by Beams and Cables

The deflection theory models a suspension bridge as a combination of a string (the sustaining cable) and a beam (the roadway), see Fig. 2.5. The point O is the origin of the orthogonal coordinate system and positive displacements are oriented downwards. The point M has coordinates $M(0, L)$ where L is the distance between

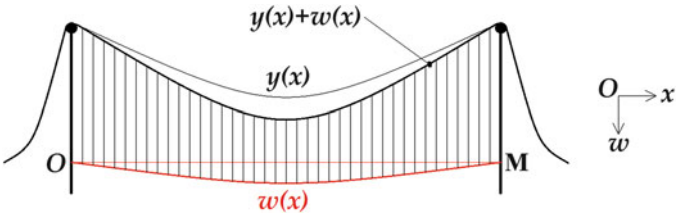

Fig. 2.5 Beam (*red*) sustained by a cable (*black*) through parallel hangers

the two towers. When the system is only subject to the action of dead loads, the cable is in position $y(x)$ while the unloaded beam is the segment connecting O and M. We assume that the cable is adjusted in such a way that it carries its own weight, the weight of the hangers and the dead weight of the roadway (beam) without producing a bending moment in the beam so that all additional deformations of the cable and the beam due to live loads are small, see (2.5). We have already underlined in Sect. 2.2 that assumption (2.5) is not always correct and therefore, in Sect. 2.6, we will also consider a nonlinear model. We assume that the cable is extensible, that is, it may increase its length due to both dead and live loads. We denote by:

L the length of the beam (the distance between the towers) and $x \in (0, L)$ the position on the beam;
q and $p = p(x)$ the dead and live loads per unit length applied to the beam;
$y = y(x)$ the downwards displacement of the cable from the horizontal line connecting the endpoints of the cable, due to the dead load q;
$w = w(x)$ the downwards displacement of the beam and, hence, the additional displacement of the cable due to the live load p;
H the horizontal tension in the cable, when subject to the dead load q only;
$h = h(w)$ the additional tension in the cable produced by the live load p.

The function w describes both the downwards displacements of the beam and the cable because

the elastic deformation of the hangers is neglected. (2.18)

This assumption is a traditional simplification of the model and appears justifiable as far as lower modes and weakly stiffened bridges are involved, see the results by Luco and Turmo [177]. However, since the flexibility of the hangers has a significant effect on the frequencies of the higher modes when the stiffness of the girder is important, see again [177] and previous work in [233, p. 123], in the nonlinear model we will remove this assumption.

Since the dead load q of the beam is constant, (2.13) yields

$$y''(x) = -\frac{q}{H}\,, \quad y'(x) = \frac{q}{H}\left(\frac{L}{2} - x\right) \qquad \forall x \in (0, L)\,. \tag{2.19}$$

We have here assumed that the endpoints of the cable are at the same altitude (which is here irrelevant), see again Fig. 2.5. Note that such altitude does not modify (2.19) in view of (2.18): it does not matter how large are the hangers since they are undeformable.

When a live load p is added, a certain amount p_1 of p is carried by the cable whereas the remaining part $p - p_1$ is carried by the bending stiffness of the beam. The horizontal tension of the cable is increased to $H + h(w)$ and the deflection w

is added to the displacement y. Hence, according to (2.13), the equation for this condition reads

$$(H + h(w))\Big(y''(x) + w''(x)\Big) = -q - p_1(x) \qquad \forall x \in (0, L)\,. \tag{2.20}$$

On the other hand, by (2.8) the equation for the displacement of the beam is

$$EI\, w''''(x) = p(x) - p_1(x) \qquad \forall x \in (0, L)\,. \tag{2.21}$$

Then, by combining (2.19)–(2.21) we obtain

$$EI\, w''''(x) - (H + h(w))\; w''(x) + \frac{q}{H}\, h(w) = p(x) \qquad \forall x \in (0, L), \tag{2.22}$$

which coincides with (2.1); the beam is assumed to be hinged at the endpoints which means that the boundary conditions read

$$w(0) = w(L) = w''(0) = w''(L) = 0\,. \tag{2.23}$$

We recall that (2.22) is obtained under assumption (2.18) and using repeatedly (2.5); in particular,

it is assumption (2.18) which allows the motions of the cable and of the beam to be treated within a single equation.

Even after all these approximations, (2.22) is by far nontrivial: it is a nonlinear integrodifferential equation of fourth order which we analyse in detail in next section. A further simplification is to consider h as a small constant (see e.g. [84, (4.10)]) and obtain the linear equation

$$EI\, w''''(x) - (H + h)\, w''(x) = p(x) - \frac{hq}{H} \qquad \forall x \in (0, L)$$

which can be integrated with classical methods. However, since the main concern of this book is precisely not to oversimplify (nor abuse with linearisations) we will not pursue this further and, in next section, we explain how to proceed with the computation of h. In classical engineering literature, (2.22) and its simplifications have been used for the computation of moments and shears for different kinds of suspension bridges, see [199, 248].

2.5 The Melan Equation

2.5.1 How to Compute the Additional Tension of the Cables

In this section we address the problem of the computation of the additional tension $h = h(w)$ in (2.22). Since the cable is extensible, it may be that $h(w) \neq 0$. We first recall that

$$\text{the sag-span ratio is always in the range } (\frac{1}{12}, \frac{1}{8}) \tag{2.24}$$

and, most frequently, it is around $1/10$, see e.g. [221, Sect. 15.17]. By using both (2.15) and (2.19), this means that

$$y\left(\frac{L}{2}\right) - y(0) = \frac{L}{10} \implies \frac{q}{H} = \frac{4}{5L} \implies y'(0) = 0.4\,. \tag{2.25}$$

The length L_c of the cable at rest is given by

$$L_c = \int_0^L \sqrt{1 + y'(x)^2}\, dx = \frac{L}{2}\sqrt{1 + \frac{L^2q^2}{4H^2}} + \frac{H}{q}\log\left(\frac{Lq}{2H} + \sqrt{1 + \frac{L^2q^2}{4H^2}}\right).$$

If we assume (2.25) then L_c may be written as a linear function of L:

$$L_c = \left(\frac{\sqrt{29}}{10} + \frac{5}{4}\log\frac{2+\sqrt{29}}{5}\right) L \approx 1.026\, L\,. \tag{2.26}$$

The increment ΔL_c of the length L_c due to the deformation w is

$$\Delta L_c = \Gamma(w) := \int_0^L \left(\sqrt{1 + [y'(x) + w'(x)]^2} - \sqrt{1 + y'(x)^2}\right) dx\,. \tag{2.27}$$

According to (2.19) and (2.27), the explicit value of $\Gamma(w)$ is

$$\Gamma(w) = \int_0^L \sqrt{1 + \left[w'(x) + \frac{q}{H}\left(\frac{L}{2} - x\right)\right]^2}\, dx - L_c\,. \tag{2.28}$$

Finally, if A denotes the cross-sectional area of the cable and E denotes the modulus of elasticity of the material, then the additional tension in the cable produced by the live load p is given by

$$h = \frac{EA}{L_c}\,\Delta L_c\,, \qquad h(w) = \frac{EA}{L_c}\,\Gamma(w)\,. \tag{2.29}$$

In literature, there are at least three different ways to approximate $\Gamma(w)$. Let us analyse them in detail.

2.5.1.1 First Approximation

Recall the asymptotic expansion, valid for any $\rho \neq 0$,

$$\sqrt{1+(\rho+\varepsilon)^2} - \sqrt{1+\rho^2} \sim \frac{\varepsilon\rho}{\sqrt{1+\rho^2}} \quad \text{as } \varepsilon \to 0\,. \tag{2.30}$$

By applying it to (2.28) one obtains

$$\Delta L_c \approx \int_0^L \frac{y'(x)w'(x)}{\sqrt{1+y'(x)^2}}\,dx. \tag{2.31}$$

While introducing the model in Fig. 2.5, Biot and von Kármán [48, p. 277] warn the reader by writing

> whereas the deflection of the beam may be considered small, the deflection of the string, i.e., the deviation of its shape from a straight line, has to be considered as of finite magnitude.

However, after reaching (2.31), Biot-von Kármán [48, (5.14)] decide to *neglect* $y'(x)^2$ *in comparison with unity* and write

$$\Gamma(w) \approx \Gamma_1(w) = \int_0^L y'(x)w'(x)\,dx = -\int_0^L w(x)y''(x)\,dx = \frac{q}{H}\int_0^L w(x)\,dx$$

where the integration by parts takes into account that $w(0) = w(L) = 0$ and, for the second equality, one uses (2.19). We denote by Γ_1 the approximated quantity obtained in [48]. A first approximation of $\Gamma(w)$ is then

$$\Gamma_1(w) = \frac{q}{H}\int_0^L w(x)\,dx\,. \tag{2.32}$$

Assuming that $y'(x)$ is small means that the cable is almost horizontal, which seems quite far from the truth, see (2.24). This is a mistake while deriving (2.32): it was already present in the Report [9, VI-5] and also appears in more recent literature, see [280, (17)] and [85, (1)].

In order to quantify the error of this approximation, we notice that (2.25) yields

$$\sqrt{1+y'(0)^2} \approx 1.077$$

yielding an error of 7.7 % if we approximate with unity. The same error occurs at the other endpoint ($x = L$). Using again (2.25), a similar computation leads to

$$\sqrt{1 + y'(\tfrac{L}{4})^2} \approx 1.02$$

yielding an error of 2 %, while it is clear that there is no error at all at the vertex of the parabola $x = L/2$. In some particular situations one may also have a sag-span ratio of $1/8$, see (2.24), in which case $y'(0) = 1/2$ and $\sqrt{1 + y'(0)^2} \approx 1.12$, yielding an error of 12 %. In any case, this approximation appears too rude.

2.5.1.2 Second Approximation

After reaching (2.27), Timoshenko [257] (see also [261, Chap. 11]) multiplies and divides the integrand by its conjugate expression and obtains

$$\Gamma(w) = \int_0^L \frac{2w'(x)y'(x) + w'(x)^2}{\sqrt{1 + [y'(x) + w'(x)]^2} + \sqrt{1 + y'(x)^2}}\, dx\,.$$

Then he neglects the derivatives and approximates the denominator with 2:

$$\Gamma(w) \approx \int_0^L \left(w'(x)y'(x) + \frac{w'(x)^2}{2} \right) dx\,.$$

With an integration by parts and taking into account both $w(0) = w(L) = 0$ and (2.19) we obtain

$$\Gamma_2(w) = \frac{q}{H} \int_0^L w(x)\, dx + \int_0^L \frac{w'(x)^2}{2}\, dx\,. \tag{2.33}$$

With a further integration by parts one may also obtain (see [261, (11.16)])

$$\Gamma_2(w) = \frac{q}{H} \int_0^L w(x)\, dx - \frac{1}{2} \int_0^L w(x)w''(x)\, dx$$

but we prefer to stick to (2.33) since it does not involve the second derivative of w. Note that also Γ_2 is obtained by neglecting y' which, as already underlined, is not small compared to unity, especially near the endpoints $x = 0$ and $x = L$.

2.5.1.3 Third Approximation

Without neglecting y', an integration by parts and the conditions $w(0) = w(L) = 0$ transform (2.31) into

$$\Delta L_c \approx -\int_0^L \frac{y''(x)w(x)}{(1+y'(x)^2)^{3/2}}\,dx.$$

Hence, invoking (2.19), a third approximation of Γ is

$$\Gamma_3(w) = \frac{q}{H}\int_0^L \frac{w(x)}{\left[1+\frac{q^2}{H^2}\left(x-\frac{L}{2}\right)^2\right]^{3/2}}\,dx\,. \tag{2.34}$$

In order to obtain (2.34), one uses the asymptotic expansion (2.30) which holds for any $\rho \neq 0$ and for $|\varepsilon| \ll |\rho|$. But, in our case, from (2.19) we have that $\rho = y'(x)$ and hence $\rho = 0$ if $x = \frac{L}{2}$. More generally, since y is given and w depends on the load p, $|w'(x)|$ may not be small when compared to $|y'(x)|$. So, a second mistake is that (2.30) is not correct for any $x \in (0, L)$. Nevertheless, if the live load $p = p(x)$ is assumed to be symmetric with respect to $x = \frac{L}{2}$ (the center of the beam) also the displacement w will have such symmetry and then $|w'(x)|$ will indeed be small with respect to $|y'(x)|$ for all x; in particular, $w'(\frac{L}{2}) = y'(\frac{L}{2}) = 0$. Hence, this approximation appears reasonable only if the live load p is "almost" symmetric.

Quite curiously, the approximations yielding Γ_1 and Γ_3 are based on two opposite wrong arguments: basically, one follows by assuming that $|y'|$ is too small, the other follows by assuming that $|y'|$ is too large. Note that Γ_2 equals Γ_1 plus an additional positive term and that Γ_3 has a smaller integrand when compared to Γ_1; therefore,

$$\Gamma_3(w) < \Gamma_1(w) < \Gamma_2(w) \qquad \forall w\,.$$

Here and in the next sections we compare (2.28)–(2.32)–(2.33)–(2.34) and we show that there may be large discrepancies. We estimate the difference between the Γ_i's for some given vertical displacements w. To this end, we notice that it is likely to expect that the maximum vertical displacement of the beam is around $1/100$ of the length of the span; if the bridge is 1 km long, the maximum amplitude of the vertical oscillation should be expected of at most 10 m. Whence, a reasonable assumption is that

$$w\left(\frac{L}{2}\right) = \frac{L}{100}\,. \tag{2.35}$$

We now compute the Γ_i's on three different configurations of the beam.

2.5.1.4 Parabolic Shape

Assume that the displacement w has the shape of a parabola,

$$w(x) = \delta x(L - x) \qquad (\delta > 0), \tag{2.36}$$

although this does not represent a hinged beam since it fails to satisfy the conditions $w''(0) = w''(L) = 0$. However, this simple case allows by hand computations and gives a qualitative idea of the differences between Γ and its approximations Γ_i $(i = 1, 2, 3)$. For the configuration (2.36), the constraint (2.35) implies that

$$\delta = \frac{1}{25\,L}\,. \tag{2.37}$$

The computations in [124] show that if w is as in (2.36) and we assume both (2.25) and (2.37), then

$$\Gamma_1(w) \approx \Gamma(w)\,, \qquad \Gamma_2(w) \approx 1.05\,\Gamma(w)\,, \qquad \Gamma_3(w) \approx 0.96\,\Gamma(w)\,.$$

But, as already mentioned, (2.36) does not represent a hinged beam. So, let us consider a realistic beam.

2.5.1.5 Simplest Symmetric Beam Shape

The simplest shape for a hinged beam is the fourth order polynomial

$$w(x) = \delta x(x^3 - 2Lx^2 + L^3) \qquad (\delta > 0)\,; \tag{2.38}$$

this function will also serve to build a counterexample in Sect. 2.5.2. In this case, if we assume again (2.35), we obtain

$$\delta = \frac{4}{125\,L^3}\,.$$

The computations in [124] show that

$$\Gamma_1(w) \approx \Gamma_2(w) \approx \Gamma(w) \approx 1.05\,\Gamma_3(w)\,.$$

2.5.1.6 Asymmetric Beams

We assume here that there is some load concentrated on the interval $(0, \ell)$ for some $\ell \in (0, \frac{L}{2})$ (the case $\ell > \frac{L}{2}$ being specular) and that the corresponding deformation

w has the shape of the piecewise affine function

$$w(x) = \sigma x \ \text{ if } x \in (0, \ell)\,, \qquad w(x) = \frac{\sigma \ell}{L - \ell}(L - x) \ \text{ if } x \in (\ell, L) \tag{2.39}$$

so that $w(\ell) = \sigma \ell$. A reasonable value of σ satisfies the rule in (2.35), that is,

$$\sigma \ell = w(\ell) = \frac{\ell}{50} \implies \sigma = \frac{1}{50}\,.$$

Then the computations in [124] show that

$$\frac{\Gamma_1(w)}{\Gamma(w)} \to 1.054\,, \quad \frac{\Gamma_2(w)}{\Gamma(w)} \to 1.08\,, \quad \frac{\Gamma_3(w)}{\Gamma(w)} \to 1.015 \quad \text{as } \ell \to 0\,,$$

yielding approximate errors of 5.4 %, 8 %, 1.5 % respectively. Moreover,

$$\frac{\Gamma(w)}{\Gamma_1(w)} \to 1.008\,, \quad \frac{\Gamma(w)}{\Gamma_2(w)} \to 0.96\,, \quad \frac{\Gamma(w)}{\Gamma_3(w)} \to 1.047 \quad \text{as } \ell \to \frac{L}{2}\,,$$

yielding approximate errors of 0.8 %, 4 %, 4.7 % respectively.

2.5.2 *Existence and Uniqueness Results*

In this section we simply denote the L^p-norms by

$$\|v\|_p := \|v\|_{L^p(0,L)} \qquad \forall\, p \in [1, \infty]\,, \quad \forall\, v \in L^p(0, L)\,.$$

Our purpose is to state the existence of at least a solution of (2.22) and (2.23). For simplicity, we drop some constants and consider the problem

$$\begin{cases} w''''(x) - (a + h(w))\ w''(x) + b\, h(w) = p(x) \ \text{ for } x \in (0, L) \\ w(0) = w(L) = w''(0) = w''(L) = 0 \end{cases} \tag{2.40}$$

where $a, b > 0$ and $h(w)$ is a nonlocal term, of indefinite sign, satisfying

$$\exists c > 0\,, \qquad |h(u)| \le c\|u\|_1 \quad \forall u \in H_0^1(0, L)\,. \tag{2.41}$$

Note that assumption (2.41) is satisfied when h is defined by

$$h(w) = \frac{EA}{L_c}\,\Gamma_i(w) \qquad (i = 1, 3)\,,$$

see (2.29), with Γ_1 and Γ_3 defined in (2.32) and (2.34). In both these cases, one can take $c = \frac{EA}{L_c}\frac{q}{H}$.

The first results yields the existence of a solution of (2.40) provided that L and p are sufficiently small.

Theorem 2.2 *Let $a, b > 0$ and let $h : H_0^1(0, L) \to \mathbb{R}$ be a continuous functional such that there exists $c > 0$ satisfying (2.41). Assume that $L^5 < \pi^3/bc$. Then for all $p \in L^1(0, L)$ satisfying*

$$\|p\|_1 \leq \frac{a(\pi^3 - bc\, L^5)}{c\, L^4}$$

there exists at least one solution $w \in W^{4,1}(0, L) \cap H_0^1(0, L)$ of (2.40) which satisfies the estimate

$$\|w\|_\infty \leq \frac{L^3}{\pi^3 - bc\, L^5}\, \|p\|_1 .$$

Theorem 2.2 does not apply to Γ since the corresponding functional h in (2.29) fails to satisfy (2.41). So, we now state a different result which allows to include Γ.

Consider again (2.40) with $a, b > 0$ and $h(w)$ being a nonlocal term, of indefinite sign, satisfying

$$\exists c > 0\,, \qquad |h(u)| \leq c\|u'\|_1 \quad \forall u \in H_0^1(0, L)\,. \tag{2.42}$$

Note that assumption (2.42) is satisfied when h is defined by (2.29), with Γ defined in (2.28). Indeed, from the simple inequality

$$\sqrt{1 + (\gamma + s)^2} - \sqrt{1 + \gamma^2} \leq |s| \qquad \forall \gamma \in \mathbb{R}\,, \quad \forall s \in \mathbb{R}\,,$$

we infer that

$$|\Gamma(w)| \leq \int_0^L \left| \sqrt{1 + [y'(x) + w'(x)]^2} - \sqrt{1 + y'(x)^2} \right| dx \leq \int_0^L |w'(x)|\, dx$$

and therefore one can take $c = 1$ in (2.42). Then we have

Theorem 2.3 *Let $a, b > 0$ and let $h : H_0^1(0, L) \to \mathbb{R}$ be a continuous functional such that there exists $c > 0$ satisfying (2.42). Assume that $L^4 < 1/bc$. Then for all $p \in L^1(0, L)$ satisfying*

$$\|p\|_1 \leq \frac{a(1 - bc\, L^4)}{c\, L^3}$$

there exists at least one solution $w \in W^{4,1}(0,L) \cap H_0^1(0,L)$ *of* (2.40) *which satisfies the estimate*

$$\|w'\|_\infty \le \frac{L^2}{1 - bc\,L^4}\,\|p\|_1\,.$$

Remark 2.4 Neither Theorem 2.2 nor Theorem 2.3 cover the case where h is defined through Γ_2 since

$$|\Gamma_2(w)| \le c\|w\|_1 + \frac{\|w'\|_2^2}{2} \qquad \forall w \in H_0^1(0,L)$$

and therefore Γ_2 has quadratic growth. However, using some a priori bounds for the linearised equation, one may estimate the quadratic term $\|w'\|_2^2$ with a linear term $\|w'\|_2$ and, consequently, obtain a result in the spirit of Theorems 2.2 and 2.3 also when h is defined through Γ_2.

So far, we merely stated existence results for small solutions of (2.40). We now state an existence and uniqueness result (for small solutions) which, however, has the disadvantage of some tedious and painful assumptions. We first assume that

$$h(0) = 0,\ \exists c > 0, \quad |h(u) - h(v)| \le c\|u'' - v''\|_2 \quad \forall u, v \in H^2 \cap H_0^1(0,L). \tag{2.43}$$

When h is defined by (2.29), the condition (2.43) is satisfied for Γ, Γ_1 and Γ_3.

Let us state the following existence and uniqueness result for small solutions of (2.40) which, again, holds when both L and p are sufficiently small.

Theorem 2.5 *Let* $a, b > 0$ *and let* $h : H_0^1(0,L) \to \mathbb{R}$ *be a continuous functional such that there exists* $c > 0$ *satisfying* (2.43)*. Assume that*

$$L < \min\left\{ \frac{1}{(bc)^2}\,,\ \frac{\pi}{(bc)^{2/5}} \right\}\,. \tag{2.44}$$

Then for all $p \in L^1(0,L)$ *satisfying*

$$\|p\|_1 < \min\left\{ \left(\frac{\pi}{L}\right)^{3/2} \frac{(\pi^{5/2} - bc\,L^{5/2})(1 - bc\sqrt{L})}{c(\pi^{5/2} - bc\,L^{5/2} + bc\pi\,L^{7/2})}\,,\ \frac{a(\pi^{5/2} - bc\,L^{5/2})}{\pi c\,L^{5/2}} \right\} \tag{2.45}$$

there exists a unique solution $w \in W^{4,1}(0,L) \cap H_0^1(0,L)$ *of* (2.40) *satisfying*

$$\|w''\|_2 \le \frac{\pi\,L^{5/2}}{\pi^{5/2} - bc\,L^{5/2}}\,\|p\|_1\,. \tag{2.46}$$

Note that the smallness of L assumed in (2.44) ensures that the right hand side of (2.45) is positive. Clearly, which is the maximum to be considered in (2.44) depends on whether $bc \lesseqgtr 1$. We also emphasise that Theorem 2.5 only states the **existence and uniqueness of a small solution** satisfying (2.46) but it does not clarify if there exist additional large solutions violating (2.46). And, indeed, as the following counterexample shows, **there may exist additional large solutions**.

Remark 2.6 For a given $L > \sqrt{12}$ consider the functional

$$h(w) = \int_0^L w''(x)\,dx \qquad \forall w \in H^2(0,L) \cap H_0^1(0,L)$$

so that (2.43) is satisfied with $c = \sqrt{L}$. Fix $\delta > 0$ and consider the problem

$$\begin{cases} w''''(x) - \big(2\delta L^3 + \varepsilon + h(w)\big)\, w''(x) + \frac{12}{L^3} h(w) = p_\varepsilon(x) \text{ for } x \in (0,L) \\ w(0) = w(L) = w''(0) = w''(L) = 0 \end{cases} \tag{2.47}$$

where $p_\varepsilon(x) = 12\delta\varepsilon(Lx - x^2)$ and $\varepsilon > 0$ will be fixed later. Equation (2.47) is as (2.40) with

$$a = 2\delta\, L^3 + \varepsilon\,, \qquad b = \frac{12}{L^3}\,, \qquad c = \sqrt{L}\,, \qquad p(x) = p_\varepsilon(x)\,.$$

Whence,

$$\frac{1}{(bc)^2} = \frac{L^5}{144}\,, \qquad \frac{\pi}{(bc)^{2/5}} = \frac{\pi\, L}{12^{2/5}}\,.$$

Since we assumed $L > \sqrt{12}$ and since $12^{2/5} < \pi$, the condition (2.44) is satisfied. Now we choose $\varepsilon > 0$ sufficiently small so that p_ε satisfies the bound (2.45). Then all the assumptions of Theorem 2.5 are fulfilled and there exists a unique solution w of (2.47) satisfying (2.46).

Note that the function $w_\delta(x) = \delta x(x^3 - 2Lx^2 + L^3)$, already considered in (2.38), solves (2.47). However, if $\varepsilon > 0$ is sufficiently small, it fails to satisfy (2.46) and therefore w_δ is not the small solution found in Theorem 2.5. This shows that, besides a small solution, also a large solution may exist.

We conclude this section with a simple calculus statement which will be repeatedly used while implementing the numerical procedures in the next sections.

Proposition 2.7 *Let* $\alpha > 0$ *and* $f \in L^1(0, L)$. *The unique solution* $u \in W^{4,1}(0, L) \cap H_0^1(0, L)$ *of the problem*

$$u''''(x) - \alpha^2 u''(x) = f(x) \quad \text{in } (0, L)\,, \quad u(0) = u(L) = u''(0) = u''(L) = 0 \tag{2.48}$$

is given by

$$u(x) = \frac{x}{\alpha^2 L} \int_0^L (L - t) f(t)\, dt - \frac{\sinh(\alpha x)}{\alpha^3 \sinh(\alpha L)} \int_0^L \sinh[\alpha(L - t)]\, f(t)\, dt + \int_0^x \left[\frac{t - x}{\alpha^2} + \frac{\sinh[\alpha(x - t)]}{\alpha^3} \right] f(t)\, dt\,.$$

Note that the assumption $\alpha^2 > 0$ in Proposition 2.7 is crucial since otherwise the equation (2.48) changes type: instead of hyperbolic functions one has trigonometric functions with possible resonance problems.

2.5.3 Numerical Implementations with a Stable Fixed Point

In this section and the following one we apply an iterative procedure in order to numerically determine a solution of (2.40). We inductively construct sequences $\{w_n\}$ of approximating solutions and it turns out that an excellent estimator of the rate of approximation is the corresponding numerical sequence $\{h(w_n)\}$. As we shall see, depending on the parameters involved, the fixed points of our iterative method may be both stable or unstable. In this section we deal with stable cases whereas in Sect. 2.5.4, which involves an actual bridge, we deal with an unstable case.

We drop here the constant EA/L_c so that $h(w) = \Gamma(w)$, we fix constants $a, b, c > 0$ and a load p, and consider the equations

$$a\, w''''(x) - (b + h(w))\, w''(x) + c\, h(w) = p(x) \qquad \forall x \in (0, L)\,, \tag{2.49}$$

complemented with the boundary conditions (2.23). We define a map $\Lambda : \mathbb{R} \to \mathbb{R}$ as follows. For any $\Theta \in \mathbb{R}$ we denote by W_Θ the unique solution w of the equation

$$a\, w''''(x) - (b + \Theta)\, w''(x) + c\, \Theta = p(x) \qquad \forall x \in (0, L)\,,$$

satisfying (2.23). The solution of this equation may be obtained by using Proposition 2.7. Then we put

$$\Lambda(\Theta) := h(W_\Theta)\,. \tag{2.50}$$

Clearly, W_Θ is a solution of (2.49)–(2.23) if and only if Θ is a fixed point for Λ, that is, $h(W_\Theta) = \Lambda(\Theta) = \Theta$.

If $\Lambda(\Theta) \neq \Theta$ we try to find a fixed point for Λ by an iterative procedure. We fix some $\Theta_0 \in \mathbb{R}$ (for instance, $\Theta_0 = 0$) and define a sequence $\Theta_n := \Lambda(\Theta_{n-1})$ for all $n \geq 1$. This defines a discrete dynamical system which, under suitable conditions, may force the sequence to converge to a fixed point $\overline{\Theta}$ of Λ. For the equations considered in this section, this procedure works out perfectly.

In Tables 2.1, 2.2, 2.3, 2.4, 2.5, and 2.6 we report some of our numerical results; we always started with $\Theta_0 = 0$. For each table we emphasise the values of the parameters involved in (2.49). Since $\overline{\Theta}$ turned out to be small, we magnify $\Lambda(\Theta_n)$ by some powers of 10.

In all the above results it appears that the sequence $\{\Lambda(\Theta_n)\}$ is not monotonic but the two subsequences of odd and even iterations appear, respectively, decreasing and increasing. Since they converge to the same limit, this means that

$$\Lambda(\Theta_{2k}) < \Lambda(\Theta_{2k+2}) < \overline{\Theta} < \Lambda(\Theta_{2k+1}) < \Lambda(\Theta_{2k-1}) \qquad \forall k \geq 1\,. \tag{2.51}$$

Table 2.1 Case $L = 2$, $a = b = c = 1$, $p(x) \equiv 1$

n	1	2	3	4	5	6	7	8
$100\,\Lambda(\Theta_n)$	9.55239	8.1815	8.37021	8.34408	8.3477	8.3472	8.34727	8.34726

Table 2.2 Case $L = 2$, $a = b = c = 1$, $p(x) = 0$ in $(0, 1)$ and $p(x) = 10$ in $(1, 2)$

n	1	2	3	4	5	6	7	8
$10\,\Lambda(\Theta_n)$	8.04928	4.80539	5.90186	5.50443	5.6451	5.59488	5.61276	5.60638

Table 2.3 Case $L = 2$, $a = b = c = 1$, $p(x) = 0$ in $(0, 3/2)$ and $p(x) = 20$ in $(3/2, 2)$

n	1	2	3	4	5	6	7	8
$10\,\Lambda(\Theta_n)$	3.93699	2.84652	3.1149	3.04668	3.06388	3.05954	3.06064	3.06036

Table 2.4 Case $L = 2$, $a = b = c = 1$, $p(x) = 10e^{-10(x-1)^2}$

n	1	2	3	4	5	6	7	8
$10\,\Lambda(\Theta_n)$	6.19365	3.96853	4.65526	4.4316	4.50324	4.48017	4.48758	4.4852

Table 2.5 Case $L = 2$, $a = 10$, $b = c = 1$, $p(x) \equiv 1$

n	1	2	3	4
$100\,\Lambda(\Theta_n)$	1.02565	1.01427	1.01439	1.01439

Table 2.6 Case $L = 2$, $a = b = 1$, $c = 10$, $p(x) \equiv 1$

n	1	2	3	4	5	6	7	8
$100\,\Lambda(\Theta_n)$	9.55239	0.3214	9.16847	0.60499	8.83393	0.858085	8.5387	1.08607

This readily gives an approximation of $\overline{\Theta}$ and, in turn, of the solution $\overline{w}$ of (2.49). As should be expected, the convergence is slower for larger values of c: in the very last experiment we found $100\,\Lambda(\Theta_{126}) < 4.3$ and $100\,\Lambda(\Theta_{127}) > 4.7$.

In all these cases this procedure worked out, which means that the fixed point $\overline{\Theta}$ is stable and that the discrete dynamical system behaves as in Fig. 2.6. The map $\Theta \mapsto \Lambda(\Theta)$ is decreasing and its slope is larger than -1 in a neighborhood of $\overline{\Theta}$.

We also used this procedure in order to estimate the responses of the different forms of $h = \Gamma_i$. We fix the parameters involved in (2.49) and we perform the iterative procedure for each one of the Γ_i $(i = 1, 2, 3)$ and $\Gamma_0 = \Gamma$. We define again $\Lambda_i(\Theta)$ $(i = 0, 1, 2, 3)$ as in (2.50). After some iterations we have an approximation of

$$\overline{\Theta}_i := \lim_{n\to\infty} \Lambda_i(\Theta_n)\,.$$

Then, we obtain a limit equation (2.49) having the form

$$a\,w''''(x) - \left(b + \overline{\Theta}_i\right) w''(x) + c\,\overline{\Theta}_i = p(x) \qquad \forall x \in (0, L)\,,\ (i = 0, 1, 2, 3)\,.$$

By integrating these linear equations with the boundary conditions (2.23) we obtain the different solutions. In Tables 2.7 and 2.8 we quote our numerical results for the different values of $\overline{\Theta}_i$.

In all these experiments we found the same qualitative behavior represented in Fig. 2.6: the sequence $\{\Lambda_i(\Theta_n)\}$ is not monotonic, it satisfies (2.51), and it converges to a fixed point for Λ_i. As we shall see in next section, this is not the case for different values of the parameters.

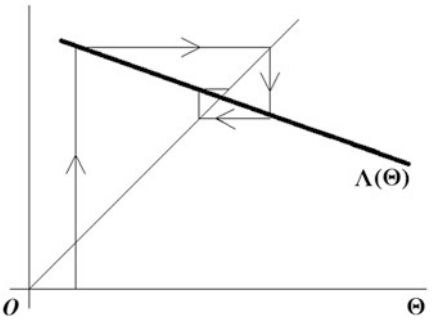

Fig. 2.6 The stable fixed point for the map $\Theta \mapsto \Lambda(\Theta)$ defined by (2.50)

Table 2.7 Case $L = 2$, $a = c = 1$, $b = 10$, $p(x) \equiv 1$

$100\,\overline{\Theta}_0$	$100\,\overline{\Theta}_1$	$100\,\overline{\Theta}_2$	$100\,\overline{\Theta}_3$
2.15633	2.07143	2.26845	1.98463

Table 2.8 Case $L = 2$, $a = c = 1$, $b = 10$, $p(x) = 0$ in $(0, 3/2)$ and $p(x) = 20$ in $(3/2, 2)$

$100\,\overline{\Theta}_0$	$100\,\overline{\Theta}_1$	$100\,\overline{\Theta}_2$	$100\,\overline{\Theta}_3$
7.7621	6.19506	8.47472	5.91363

2.5.4 Numerics with an Unstable Fixed Point for an Actual Bridge

We consider here a possible actual bridge and we fix the parameters in (2.22) following Wollmann [280]. The stiffness EI is known to be $EI = 57 \cdot 10^6\,\mathrm{kN}\cdot\mathrm{m}^2$ whereas $EA = 36 \cdot 10^8\,\mathrm{kN}$. Wollmann considers a bridge with main span of length $L = 460\,\mathrm{m}$ and he assumes (2.25) so that

$$\frac{q}{H} = 1.739 \cdot 10^{-3}\,\mathrm{m}^{-1}\,, \qquad q = 170\,\mathrm{kN/m}\,, \qquad H = 97.75 \cdot 10^3\,\mathrm{kN}\,.$$

By (2.26) we find $L_c = 472\,\mathrm{m}$, while from (2.29) we infer

$$h(w) = (7.627 \cdot 10^6\,\mathrm{kN/m})\,\Gamma_i(w)$$

where the $\Gamma_i(w)$ are measured in meters; we will consider $i = 0, 1, 2, 3$ with $\Gamma_0 = \Gamma$ as in (2.28) and the remaining Γ_i as in (2.32)–(2.34).

We first take as live load a vehicle, a **coach** of length 10 m having a weight density of 10 kN/m, that is

$$p(x) = 10\,\chi_{(d,d+10)}\,\mathrm{kN/m} \qquad 0 < d < 230\,,$$

where $\chi_{(d,d+10)}$ denotes the characteristic function of the interval $(d, d+10)$. Then, after dropping the unity measure kN/m and dividing by 10, (2.22) reads

$$57 \cdot 10^5\, w''''(x) - \Big(9775 + 7.627 \cdot 10^5\,\Gamma_i(w)\Big)\, w''(x) + 1326\,\Gamma_i(w) = \chi_{(d,d+10)} \tag{2.52}$$

for $x \in (0, 460)$, where the solution w is computed in meters. For numerical reasons, it is better to rescale (2.52): we put

$$w(x) = v\left(\frac{x}{230}\right) = v(s)\,. \tag{2.53}$$

Let us compute the different values of Γ_i after this change. We have

$$\begin{aligned}
\Gamma_0(w) &= \int_0^{460} \sqrt{1 + [w'(x) + 1.739 \cdot 10^{-3}\,(230 - x)]^2}\,dx - 1.026 \cdot 460 \\
&= 230\left[\int_0^2 \sqrt{1 + [4.35 \cdot 10^{-3}\,v'(s) + 0.4\,(1-s)]^2}\,ds - 2.052\right] =: \Upsilon_0(v)\,; \\
\Gamma_1(w) &= 1.739 \cdot 10^{-3} \int_0^{460} w(x)\,dx = 0.4 \int_0^2 v(s)\,ds =: \Upsilon_1(v)\,;
\end{aligned}$$

$$\Gamma_2(w) = 0.4 \int_0^2 v(s)\,ds + 2.17 \cdot 10^{-3} \int_0^2 v'(s)^2\,ds =: \Upsilon_2(v)\,;$$

$$\Gamma_3(w) = 1.739 \cdot 10^{-3} \int_0^{460} \frac{w(x)\,dx}{[1 + 3.02 \cdot 10^{-6}\,(x-230)^2]^{3/2}}$$
$$= 0.4 \int_0^2 \frac{v(s)\,ds}{[1 + 0.16(s-1)^2]^{3/2}} =: \Upsilon_3(v)\,.$$

After the change (2.53) and division by $\frac{57\cdot 10^5}{230^4}$, Eq. (2.52) becomes

$$v''''(s) - \Big(90.72 + 7078\,\Upsilon_i(v)\Big)v''(s) + 650999\,\Upsilon_i(v) = 491\,\psi_d(s) \quad \forall s \in (0,2) \tag{2.54}$$

where ψ_d is the characteristic function of the interval $(\frac{d}{230}, \frac{d+10}{230})$. We try to proceed as in Sect. 2.5.3. We fix some $\Theta > 0$ and we solve Eq. (2.54) by replacing $\Upsilon_i(v)$ with Θ:

$$v''''(s) - \alpha^2\,v''(s) = f(s) \qquad \forall s \in (0,2) \tag{2.55}$$

where $\alpha^2 := 90.72 + 7078\,\Theta$ and $f(s) := 491\,\psi_d(s) - 650999\,\Theta$. By Proposition 2.7, this linear equation, complemented with hinged boundary conditions, admits a unique solution V_Θ given by

$$V_\Theta(s) = 491\,\Psi_{d,\Theta}(s) + \left(\frac{491(455-d)}{10580} - 650999\Theta\right)\frac{s}{\alpha^2}$$
$$+ \frac{650999\Theta}{2\,\alpha^2}\,s^2 + \frac{650999\Theta}{\alpha^4}\Big(1 - \cosh(\alpha s)\Big)$$
$$+ \left[650999\Theta\Big(\cosh(2\alpha) - 1\Big) - 982\sinh\frac{\alpha}{46}\sinh\frac{\alpha(455-d)}{230}\right]\frac{\sinh(\alpha s)}{\alpha^4\sinh(2\alpha)}$$

where

$$\Psi_{d,\Theta}(s) = \begin{cases} 0 & \text{if } 0 \le s \le \frac{d}{230} \\ \frac{1}{\alpha^4}\left(\cosh[\alpha(s - \frac{d}{230})] - 1\right) - \frac{(s-\frac{d}{230})^2}{2\,\alpha^2} & \text{if } \frac{d}{230} < s < \frac{d+10}{230} \\ \frac{2}{\alpha^4}\sinh\frac{\alpha}{46}\sinh\left(\alpha\left(s - \frac{d+5}{230}\right)\right) + \frac{1}{46\,\alpha^2}\left(\frac{d+5}{115} - 2s\right) & \text{if } \frac{d+10}{230} \le s \le 2\,. \end{cases}$$

We then compute $\Upsilon_i(V_\Theta)$ according to the above formulas and we put

$$\Lambda_i(\Theta) = \Upsilon_i(V_\Theta)\,. \tag{2.56}$$

Again, this defines a sequence $\Theta_n = \Lambda_i(\Theta_{n-1})$. However, for the values in (2.54), this sequence appears to diverge and to be quite unstable: contrary to the experiments in Sect. 2.5.3, see (2.51), we have here that $\Lambda_i(\Theta_{2k}) \to +\infty$ and

$\Lambda_i(\Theta_{2k+1}) \to -\infty$ as $k \to \infty$. This behavior describes an unstable fixed point, as represented in Fig. 2.7. Here, the slope of $\Theta \mapsto \Lambda_i(\Theta)$ is smaller than -1. In fact, our experiments show that it is very negative, possibly $-\infty$.

In order to apply Proposition 2.7 one needs $90.72 + 7078\,\Theta_n > 0$ since otherwise the equation changes type. These difficulties suggest to proceed differently. We fix $\Theta_0 = 0$ and, for any $k \geq 0$, if $\Theta_{2k+1} = \Lambda_i(\Theta_{2k}) > \Theta_{2k}$ (resp. $\Theta_{2k+1} < \Theta_{2k}$) we take some $\Theta_{2k+2} \in (\Theta_{2k}, \Theta_{2k+1})$ (resp. $\Theta_{2k+2} \in (\Theta_{2k+1}, \Theta_{2k})$). With this procedure we obtained a bounded sequence such that $(\Theta_{2k+1} - \Theta_{2k}) \to 0$ as $k \to \infty$, that is,

$$\exists\, \overline{\Theta}_i = \lim_{n\to\infty} \Theta_n \qquad (i = 0, 1, 2, 3) \tag{2.57}$$

where the index i identifies the Υ_i used to construct the sequence, see (2.56).

We numerically computed these limits for different values of d, see Table 2.9 where we only report the first digits of $\overline{\Theta}_i$: the results turned out to be very sensitive to modifications of these values up to four more digits and our numerical procedure stopped precisely when Θ_{2k} and Θ_{2k+1} had the first seven nonzero digits coinciding.

It appears that the best approximation of $\overline{\Theta}_0$ is $\overline{\Theta}_2$ if $d = 0, 50, 100$ (asymmetric load) whereas it is $\overline{\Theta}_3$ if $d = 225$ (symmetric load). The most frequently used approximation in literature is $\overline{\Theta}_1$ and it is never the best one. The corresponding

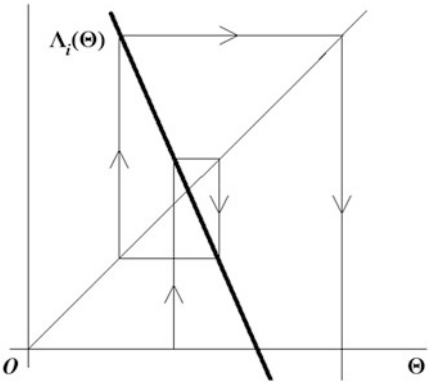

Fig. 2.7 The unstable fixed point for the map $\Theta \mapsto \Lambda_i(\Theta)$ defined by (2.56)

Table 2.9 Approximate value of the optimal constants $\overline{\Theta}_i$ in (2.57), case of a single coach

d	0	50	100	225
$\overline{\Theta}_0$	$1.131 \cdot 10^{-6}$	$1.021 \cdot 10^{-5}$	$1.74 \cdot 10^{-5}$	$2.509 \cdot 10^{-5}$
$\overline{\Theta}_1$	$9.842 \cdot 10^{-7}$	$1.016 \cdot 10^{-5}$	$1.729 \cdot 10^{-5}$	$2.477 \cdot 10^{-5}$
$\overline{\Theta}_2$	$9.843 \cdot 10^{-7}$	$1.017 \cdot 10^{-5}$	$1.73 \cdot 10^{-5}$	$2.477 \cdot 10^{-5}$
$\overline{\Theta}_3$	$9.672 \cdot 10^{-7}$	$1.005 \cdot 10^{-5}$	$1.723 \cdot 10^{-5}$	$2.492 \cdot 10^{-5}$

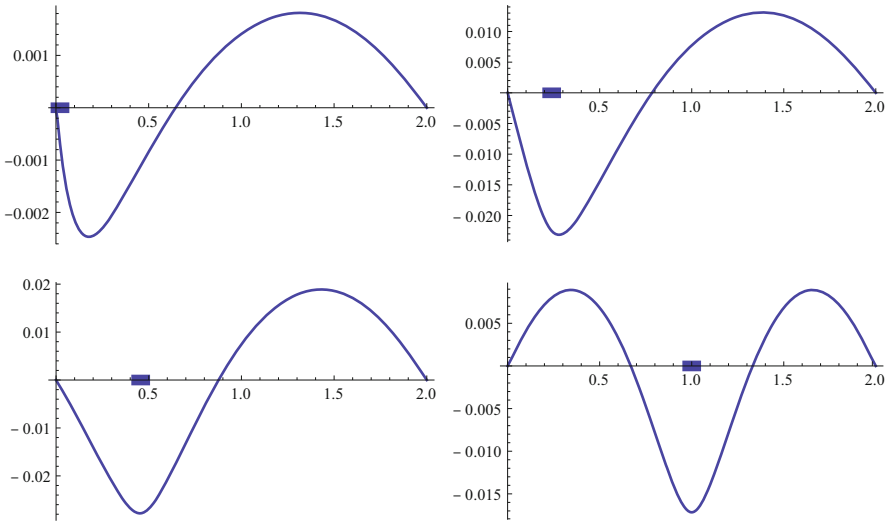

Fig. 2.8 Plots of the solutions of (2.54) for $i = 0$ and $d = 0,\ 50,\ 100,\ 225$ (from *left* to *right* and *top* to *bottom*)

solutions of (2.54), which we denote by v_i, satisfy the linear equation

$$v_i''''(s) - \left(90.72 + 7078\,\overline{\Theta}_i\right) v_i''(s) + 650999\,\overline{\Theta}_i = 491\,\psi_d(s) \qquad \forall s \in (0,2)$$

and can be explicitly computed by means of Proposition 2.7. In Fig. 2.8 we plot the solutions of (2.54) for $i = 0$ and for the different positions of the coach, represented in thick black: the vertical scale is very small.

Instead of giving the analytic form of the v_i, we plot the differences between these solutions. Since $\overline{\Theta}_1 \approx \overline{\Theta}_2$ in all the above experiments, we also found that $v_1 \approx v_2$. Therefore, in Fig. 2.9 we only plot the functions $v_2 - v_0$ and $v_3 - v_0$.

We now take as live load a **freight train** of length 230 m having a weight density of 20 kN/m, that is

$$p(x) = 20\,\chi_{(d,d+230)}\,\text{kN/m} \qquad 0 < d < 230$$

where $\chi_{(d,d+230)}$ is the characteristic function of the interval $(d, d + 230)$. We consider both the cases where the train occupies the first half of the span ($d = 0$) and the case where the train is in the middle of the span ($d = 115$). With the same scaling as above, instead of (2.54) we obtain

$$v''''(s) - \left(90.72 + 7078\,\Upsilon_i(v)\right) v''(s) + 650999\,\Upsilon_i(v) = 982\,\psi_\delta(s) \qquad \forall s \in (0,2) \tag{2.58}$$

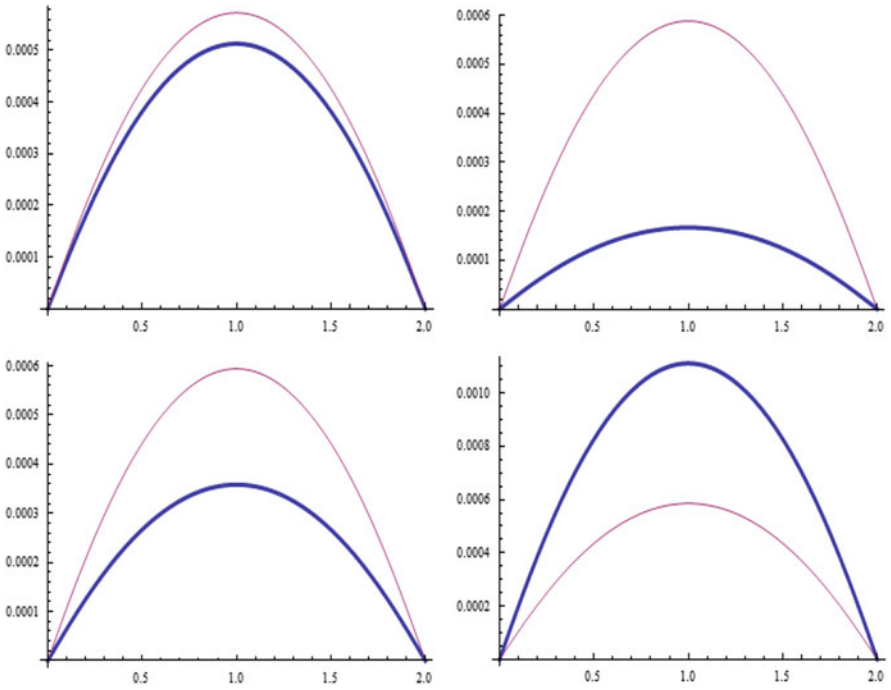

Fig. 2.9 Plots of the functions $v_2 - v_0$ (*thick*) and $v_3 - v_0$ (*thin*) for $d = 0,\ 50,\ 100,\ 250$ (from *left* to *right* and *top* to *bottom*)

where ψ_δ is the characteristic function of $(\delta, 1+\delta)$ with $\delta = 0$ or $\delta = \frac{1}{2}$. We solve Eq. (2.58) by replacing $\Upsilon_i(v)$ with Θ, that is, we consider again (2.55) where

$$\alpha^2 := 90.72 + 7078\,\Theta\,, \qquad f(s) := 491\,\psi_\delta(s) - 650999\,\Theta\,.$$

By Proposition 2.7, this linear equation, complemented with hinged boundary conditions, admits a unique solution V_Θ given by

$$\begin{aligned} V_\Theta(s) = {} & 982\,\Psi_{\delta,\Theta}(s) + \left(\frac{491(3-2\delta)}{2} - 650999\Theta\right)\frac{s}{\alpha^2} \\ & + \frac{650999\Theta}{2\,\alpha^2}\,s^2 + \frac{650999\Theta}{\alpha^4}\Big(1 - \cosh(\alpha s)\Big) \\ & + \left[650999\Theta\Big(\cosh(2\alpha) - 1\Big) - 1964\sinh\frac{\alpha}{2}\sinh\frac{\alpha(3-2\delta)}{2}\right]\frac{\sinh(\alpha s)}{\alpha^4\sinh(2\alpha)} \end{aligned}$$

where

$$\Psi_{\delta,\Theta}(s) = \begin{cases} 0 & \text{if } 0 \le s \le \delta \\ \frac{1}{\alpha^4}\left(\cosh[\alpha(s-\delta)] - 1\right) - \frac{(s-\delta)^2}{2\alpha^2} & \text{if } \delta < s < \delta + 1 \\ \frac{2}{\alpha^4} \sinh\frac{\alpha}{2} \sinh\frac{\alpha(2s-2\delta-1)}{2} + \frac{1+2\delta-2s}{2\alpha^2} & \text{if } \delta + 1 \le s \le 2\,. \end{cases}$$

We then define again Λ_i as in (2.56) and we find that it has an unstable fixed point, that is, the behavior of the sequence Θ_n is well described by Fig. 2.7. With the same previously described algorithm, we are again able to construct a converging sequence and we denote again by $\overline{\Theta}_i$ its limit, see (2.57), where the index i identifies which of the Υ_i's is used to construct the sequence, see (2.56). We numerically computed these limits for $d = 0$ (train in the first half of the span) and $d = 115$ (train in the middle of the span), see Table 2.10 where we only report the first digits of $\overline{\Theta}_i$: again, the results turned out to be very sensitive to modifications of these values up to four more digits and our numerical procedure stopped when Θ_{2k} and Θ_{2k+1} had the first seven nonzero digits coinciding.

Again, the best approximation of $\overline{\Theta}_0$ is $\overline{\Theta}_2$ if $d = 0$ (asymmetric load) whereas it is $\overline{\Theta}_3$ if $d = 115$ (symmetric load). And, again, $\overline{\Theta}_1$ is never the best one. The corresponding solutions of (2.58), which we denote by v_i, satisfy the linear equation

$$v_i''''(s) - \left(90.72 + 7078\,\overline{\Theta}_i\right) v_i''(s) + 650999\,\overline{\Theta}_i = 982\,\psi_\delta(s) \qquad \forall s \in (0,2)$$

and can be explicitly computed by means of Proposition 2.7. In Fig. 2.10 we plot the solution of (2.58) for $i = 0$ and for the two positions of the train, represented in thick black. Again, the vertical scale is very small.

Table 2.10 Approximate value of the optimal constants $\overline{\Theta}_i$ in (2.57), case of a whole train

d	0	115
$\overline{\Theta}_0$	$7.582 \cdot 10^{-4}$	$1.047 \cdot 10^{-3}$
$\overline{\Theta}_1$	$7.538 \cdot 10^{-4}$	$1.042 \cdot 10^{-3}$
$\overline{\Theta}_2$	$7.582 \cdot 10^{-4}$	$1.044 \cdot 10^{-3}$
$\overline{\Theta}_3$	$7.538 \cdot 10^{-4}$	$1.046 \cdot 10^{-3}$

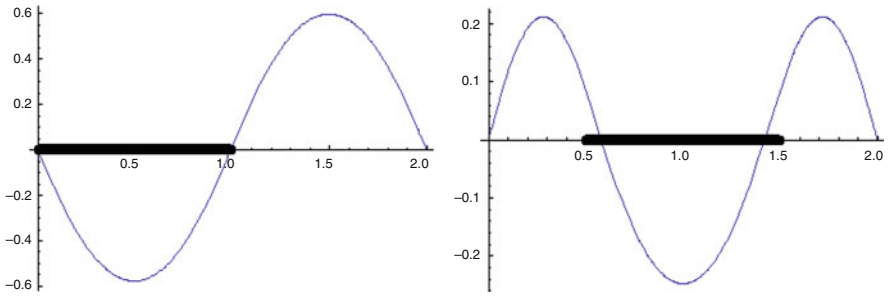

Fig. 2.10 Plots of the solutions of (2.58) for $i = 0$ and $d = 0,\ 115$ (from *left* to *right*)

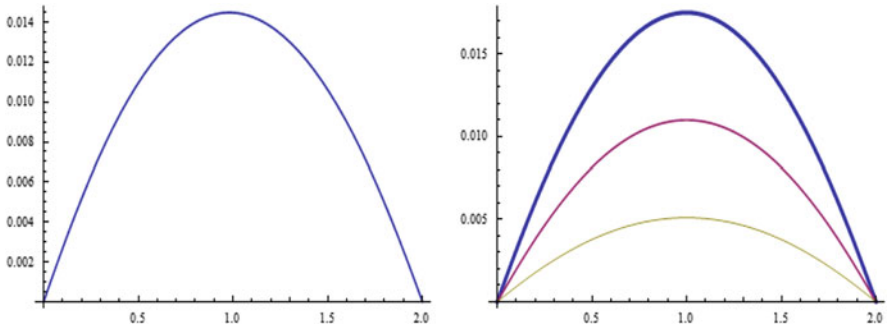

Fig. 2.11 *Left* plot of the function $v_1 - v_0$ for $d = 0$; *Right* plots of the functions $v_1 - v_0$ (*thick*), $v_2 - v_0$ (*intermediate*), $v_3 - v_0$ (*thin*) for $d = 115$

In Fig. 2.11 we plot the differences between the solutions of (2.58) for different i. When $d = 0$ we have $\overline{\Theta}_1 \approx \overline{\Theta}_3$ and $\overline{\Theta}_2 \approx \overline{\Theta}_0$: whence, we only plot the function $v_1 - v_0$ since $v_3 - v_0$ is almost identical and $v_2 - v_0$ is almost 0. When $d = 115$ we plot the differences $v_i - v_0$ ($i = 1, 2, 3$) which show how the v_i's are ordered. By scaling, similar pictures can be obtained for the original solutions w_i of (2.52) after undoing the change of variables (2.53).

2.6 Self-excited Oscillations in Semilinear Beam Equations

2.6.1 A Model with Superlinear Springs

Assume that a beam, possibly unbounded, is subject to the restoring forces of a large number of nonlinear two-sided springs as in Fig. 2.12.

If the beam has finite length, it is intended to model the roadway of a suspension bridge and the springs model the hangers. Assume that, besides the nonlinear restoring force $g = g(w)$ due to the springs [taken as in (1.12)], there is a uniform downwards load $P(x) \equiv P$ acting on the beam, for instance, its weight per unit length. Then, the same arguments which lead to (2.7) yield the semilinear equation

$$EI\, w''''(x) - Tw''(x) = P - (kw(x) + \varepsilon w(x)^3) \qquad (x > 0) \tag{2.59}$$

where EI is the flexural rigidity and $T \geq 0$ is the constant tension which is usually small compared with the flexural rigidity; therefore, we assume that

$$0 \leq T < 2\sqrt{k\, EI}\,. \tag{2.60}$$

This assumption gives the "right behavior" to the solutions of the linear version of (2.59), see (2.62) below. Take g as in (1.12) and consider first the case where

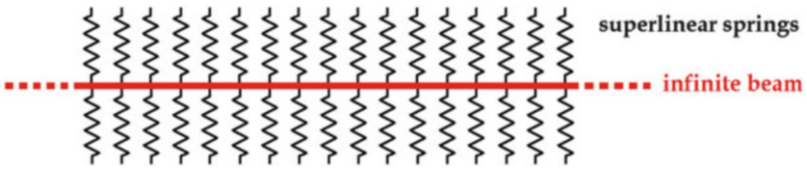

Fig. 2.12 Beam subject to two-sided restoring springs

$\varepsilon = 0$. Then (2.59) reads

$$EI\, w''''(x) - Tw''(x) + kw(x) = P\,. \tag{2.61}$$

If (2.60) is satisfied then the solutions of (2.61) have the form

$$\begin{aligned} w(x) = a\cosh\left[x\sqrt{\tfrac{2\sqrt{kEI}+T}{4EI}}\right]\cos\left[x\sqrt{\tfrac{2\sqrt{kEI}-T}{4EI}}\right] + b\cosh\left[x\sqrt{\tfrac{2\sqrt{kEI}+T}{4EI}}\right]\sin\left[x\sqrt{\tfrac{2\sqrt{kEI}-T}{4EI}}\right] \\ + c\sinh\left[x\sqrt{\tfrac{2\sqrt{kEI}+T}{4EI}}\right]\cos\left[x\sqrt{\tfrac{2\sqrt{kEI}-T}{4EI}}\right] + d\sinh\left[x\sqrt{\tfrac{2\sqrt{kEI}+T}{4EI}}\right]\sin\left[x\sqrt{\tfrac{2\sqrt{kEI}-T}{4EI}}\right] + \frac{P}{k} \end{aligned} \tag{2.62}$$

with the coefficients a, b, c, d depending on the boundary or initial conditions.

Consider now g as in (1.12) with $\varepsilon > 0$. If $T > 0$, after the changes of variables

$$x \mapsto x\sqrt{\frac{T}{EI}}\,, \quad \gamma = \frac{k\,EI}{T^2} > \frac{1}{4}\,, \quad \delta = \frac{\varepsilon\, EI}{T^2}\,, \quad Q = \frac{P\,EI}{T^2}\,,$$

Eq. (2.59) becomes

$$w''''(x) - w''(x) + \gamma w(x) + \delta w(x)^3 = Q\,. \tag{2.63}$$

In the pictures of Fig. 2.13, we plot the solutions w_δ of the initial value problem

$$w_\delta''''(x) - w_\delta''(x) + w_\delta(x) + \delta w_\delta(x)^3 = 1, \quad w_\delta(0) = w_\delta'(0) = w_\delta''(0) = w_\delta'''(0) = 0, \tag{2.64}$$

for $\delta = 0$ (linear case), $\delta = 0.01$, $\delta = 0.02$. Close to $x = 0$, say for $x \in [0, 4.5]$, the solutions are almost identical. Then, the larger is δ, the earlier an oscillation starts. For $\delta = 0.02$ the solution numerically appears to blow up for $x \approx 7.1$.

The purpose of the next sections is to explain these behaviors and to study the difference between the solutions of (2.61) and (2.63). We will show that the presence of $\delta > 0$ creates a phenomenon of self-excited oscillations which increases immeasurably the vibrations of the beam.

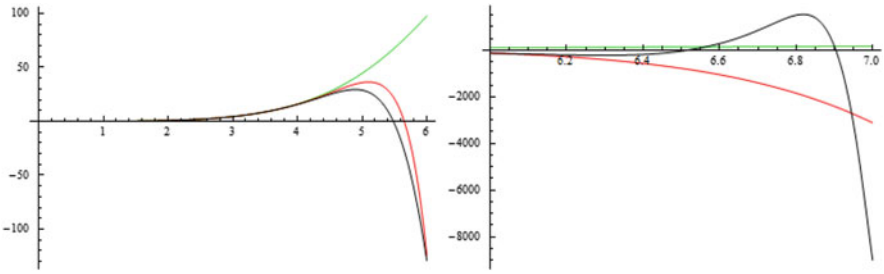

Fig. 2.13 Solutions of (2.64) when $\delta = 0$ (*green*), $\delta = 0.01$ (*red*), $\delta = 0.02$ (*black*)

2.6.2 Unbounded Beams and Self-excited Oscillations

An unbounded beam allows to emphasise the natural behavior of a free beam with no constraints such as the boundary conditions (clamped or hinged beams). In this section we show that nonlinear springs may produce self-excited oscillations in an ideal unbounded beam.

For the reader convenience, we recall the "minimal" assumption (1.11) on f:

$$f \in \mathrm{Lip}_{loc}(\mathbb{R}), \qquad f(w)\, w > 0 \quad \forall w \in \mathbb{R} \setminus \{0\}. \tag{2.65}$$

Then, for any $T \in \mathbb{R}$, we consider the ordinary differential equation

$$w''''(x) - Tw''(x) + f(w(x)) = 0 \qquad (x \in \mathbb{R}). \tag{2.66}$$

We wish to emphasise some properties of the solutions of (2.66). The first statement describes how nonlinear springs may cause a fracture within the infinite beam.

Theorem 2.8 *Let $T \in \mathbb{R}$ and assume that f satisfies* (2.65).

(*i*) *If a local solution w of* (2.66) *blows up at some finite $R \in \mathbb{R}$, then*

$$\liminf_{x \to R} w(x) = -\infty \qquad \text{and} \qquad \limsup_{x \to R} w(x) = +\infty. \tag{2.67}$$

(*ii*) *If f also satisfies*

$$\limsup_{w \to +\infty} \frac{f(w)}{w} < +\infty \qquad \text{or} \qquad \limsup_{w \to -\infty} \frac{f(w)}{w} < +\infty, \tag{2.68}$$

then any local solution of (2.66) *exists for all $x \in \mathbb{R}$.*

If both the conditions in (2.68) are satisfied then global existence follows from the classical theory of ODE's. But (2.68) merely requires that f is "one-sided at most linear" so that statement (ii) is far from being trivial and, as shown in [126], it does not hold for differential equations of order at most 3; this is related to the (GPCM), see Sect. 1.8. Theorem 2.8(i) states that, under the sole assumption (2.65), the only way that finite space blow up can occur is with "wide and thinning oscillations" of the solution w; again, in [126] it is shown that this kind of blow up is a phenomenon typical of (at least) fourth order problems such as (2.66) since it does not occur in similar lower order equations. Note that assumption (2.68) includes, in particular, the cases where f is either concave or convex.

Theorem 2.8 does not tell if (2.67) indeed occurs. Under some restriction on T and f, it may be complemented with the following statement.

Theorem 2.9 *Let $T \geq 0$ and assume that*

$$f(w) = \alpha|w|^{q-1}w + \beta|w|^{p-1}w \qquad (p > q \geq 1,\ \alpha \geq 0,\ \beta > 0)\,. \tag{2.69}$$

Assume that $w = w(x)$ is a local solution of (2.66) in a neighborhood of $x = 0$ which satisfies

$$w'(0)w''(0) - w(0)w'''(0) + Tw(0)w'(0) > 0\,. \tag{2.70}$$

Then, w blows up in finite time for $x > 0$, that is, there exists $R < +\infty$ such that (2.67) holds. Therefore, there exists an increasing sequence $\{z_j\}_{j\in\mathbb{N}}$ such that:

(i) $z_j \nearrow R$ *as* $j \to \infty$.
(ii) $w(z_j) = 0$ *and w has constant sign in (z_j, z_{j+1}) for all $j \in \mathbb{N}$.*

Furthermore, in each interval (z_j, z_{j+1}) where $w(x) > 0$ the following facts occur:

(iii) $0 < w'(z_j) < -w'(z_{j+1})$ *and there exists a unique $m_j \in (z_j, z_{j+1})$ such that $w'(m_j) = 0$.*
(iv) $w''(z_{j+1}) < 0 < w''(z_j)$, *there exists a unique $r_j \in (z_j, z_{j+1})$ where w'' changes sign, and $r_j < m_j$.*

Similar facts as (iii)–(iv) (with obvious changes) occur in intervals (z_j, z_{j+1}) where $w(x) < 0$. Finally, with the notations of (iii),

(v) $|w(m_j)| \to +\infty$ *monotonically as* $j \to \infty$.
(vi) *There exist $\kappa_1, \kappa_2 > 0$ (depending only on α, β, p, q) such that*

$$m_{j+1} - m_j \leq \frac{\kappa_1}{|w(m_j)|^{(p-1)/4}}\,, \qquad z_{j+1} - z_j \geq \frac{\kappa_2}{|w(m_j)|^{(p-1)/4}} \qquad \forall\, j\,. \tag{2.71}$$

A particular example of function f satisfying (2.69) is (1.12) for any $k, \varepsilon > 0$, so any tiny nonlinear perturbation of a linear force yields the result. But much more general nonlinearities are allowed, see [125]. In particular, statements (i)–(iv) of Theorem 2.9 still hold if f is increasing and satisfies the regularity conditions

$$f \in \mathrm{Lip}_{\mathrm{loc}}(\mathbb{R}) \cap C^1(\mathbb{R} \setminus \{0\}) \tag{2.72}$$

and the growth conditions

$$\begin{aligned} \exists c, \delta, \tau > 0, \text{ s.t. } & w f(w) \geq c|w|^{2+\delta} \ \forall w \in \mathbb{R}, \\ & w f(w) \geq cF(w) \ \forall |w| \geq \tau, \end{aligned} \tag{2.73}$$

$$\exists \lambda \in (0,1), \ \exists \alpha > 0, \quad \text{s.t.} \quad \liminf_{w \to \pm\infty} \frac{F(\lambda w)}{F(w)^\alpha} > 0 \tag{2.74}$$

where $F(w) := \int_0^w f(s)\, ds$ is an antiderivative of f. Clearly, f in (2.69) satisfies these conditions. A further example is obtained by taking $f(w) = \sinh w$: in particular, $f(w)$ is allowed to grow exponentially fast as $w \to +\infty$. These general forms of f show that the self-excited blow up described by Theorem 2.9, see (2.67), is a very general phenomenon appearing for a wide class of nonlinear restoring forces f.

Let us now explain how this result may be applied to a beam modeling a suspension bridge. Let $w = w(x)$ denote the vertical displacement of the beam in position x. If the beam is subject to both a nonlinear (increasing) restoring force $g = g(w)$ due to the hangers and to a uniform downwards load $P(x) \equiv P$, we have seen that the corresponding equation is (2.59). Let $W_P > 0$ be the unique solution of $g(W_P) = P$. Put $f(w) := g(w + W_P) - P$ so that f is also increasing and $f(0) = 0$. Translate $w(x) - W_P \mapsto w(x)$, then w solves the equation

$$EI\, w''''(x) - Tw''(x) + f(w(x)) = 0 \qquad (x \in \mathbb{R})$$

which coincides with (2.66), up to the division by EI. Then Theorem 2.9 ensures (finite-in-space) fracture of the beam, provided f satisfies (2.72)–(2.74).

Back to the simple form (2.69), in [128] one finds numerical evidence that, when all the other parameters remain fixed, the map $w''(0) \mapsto R(w''(0))$ is strictly increasing, whereas the maps $p \mapsto R(p)$, $\alpha \mapsto R(\alpha)$, $w(0) \mapsto R(w(0))$, $T \mapsto R(T)$ are strictly decreasing. The oscillations of the solutions of (2.66) cannot be prevented since they arise suddenly for large x after a "long apparent calm". In Fig. 2.14, we display the plot of a solution of (2.66). It can be observed that the solution has oscillations with increasing amplitude and rapidly decreasing "nonlinear frequency"; numerically, the blow up seems to occur at $x = 8.164$. Even

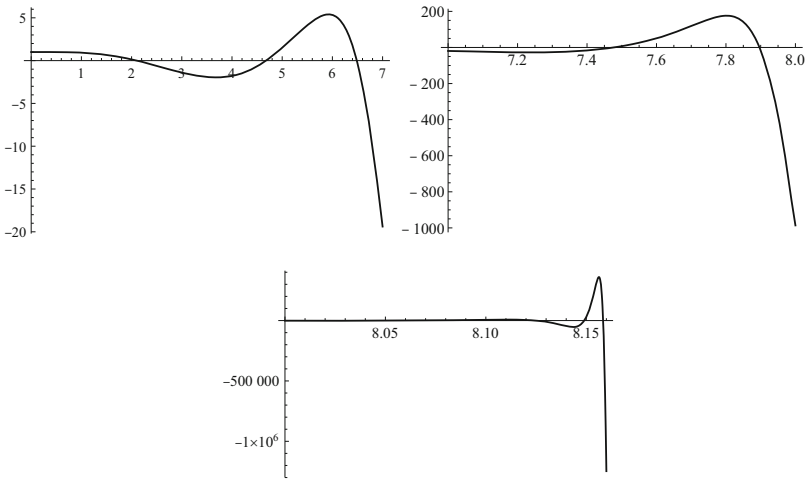

Fig. 2.14 Solution of (2.66) for $T = 3$, $[w(0), w'(0), w''(0), w'''(0)] = [1, 0, 0, 0]$, $f(w) = w + w^3$. The three intervals are $x \in [0, 7]$, $x \in [7, 8]$, $x \in [8, 8.16]$ (from *left* to *right*)

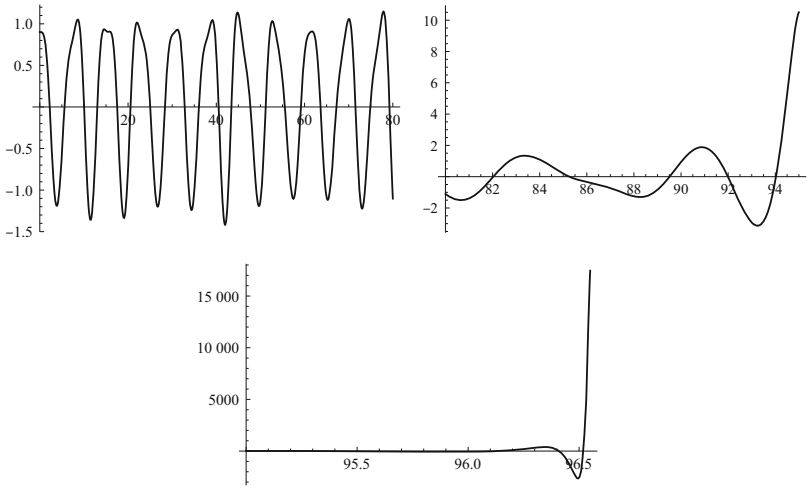

Fig. 2.15 Solution of (2.66) for $T = 3.6$, $[w(0), w'(0), w''(0), w'''(0)] = [0.9, 0, 0, 0]$, $f(w) = w + w^3$. The three intervals are $x \in [0, 80]$, $x \in [80, 95]$, $x \in [95, 96.55]$ (from *left* to *right*)

more impressive appears the plot in Fig. 2.15. Here the solution has "almost regular" oscillations between -1 and $+1$ for $x \in [0, 80]$. Then the amplitude of oscillations nearly doubles in the interval $[80, 93]$ and, suddenly, it violently amplifies after $x = 96.5$ until the blow up which seems to occur only slightly later at $x = 96.59$.

This sudden and violent self-excited blow up is quite alarming regardless of the physical model considered. In (free) beams and bridges it leads to a fracture.

2.6.3 Hinged Beams Subject to Nonlinear Elastic Forces

In the previous section we saw that an unbounded beam subject to superlinear restoring forces has a natural tendency to vibrate with self-excited oscillations, leading to fracture. It is then reasonable to expect that a similar behavior, although less accentuated, might be visible in beams of finite length and, for instance, hinged at the endpoints. This is the purpose of the present section.

Consider a hinged beam, of finite length $2R$, subject to the restoring forces of a large number of nonlinear two-sided springs as in Fig. 2.16.

Assume that, besides the nonlinear restoring force g due to the springs there is a downwards distributed load $P = P(x)$ acting on the beam. The vertical deformation w of the beam is then governed by the semilinear equation (2.59), which we rewrite here in a bounded interval,

$$EI\, w''''(x) - Tw''(x) = P(x) - g(w(x)) \qquad (-R < x < R) \tag{2.75}$$

complemented with the hinged boundary conditions

$$w(\pm R) = w''(\pm R) = 0\,. \tag{2.76}$$

To begin we just assume that $g \in C^0(\mathbb{R})$ is increasing. Then it is quite standard to prove that (2.75) is well-posed, it suffices to set up a suitable variational formulation. Let us briefly sketch what is meant by weak solution and under which assumptions it exists and is unique. Consider the second order Sobolev space $H^2 \cap H_0^1(-R, R)$ and let $H^*(-R, R)$ denote its dual space. The space $H^2 \cap H_0^1(-R, R)$ is a Hilbert space when endowed with the scalar product

$$(u, v) = \int_{-R}^{R} u''(x)v''(x)\,dx \qquad \forall u, v \in H^2 \cap H_0^1(-R, R)\,.$$

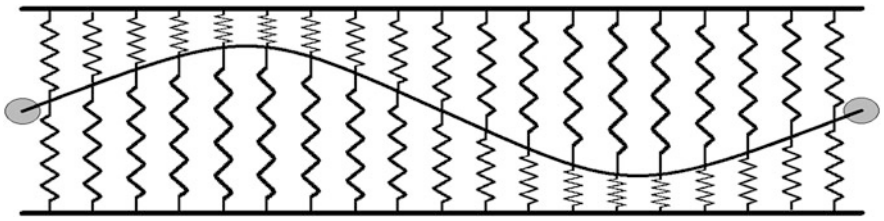

Fig. 2.16 A hinged beam subject to two-sided restoring springs

For $P \in H^*(-R, R)$ we call $w \in H^2 \cap H_0^1(-R, R)$ a weak solution of (2.75) and (2.76) if

$$\int_{-R}^{R} \Big(EIw''(x)v''(x) + Tw'(x)v'(x) + g(w(x))v(x) \Big) dx = \langle P, v \rangle \tag{2.77}$$

for all $v \in H^2 \cap H_0^1(-R, R)$, where $\langle \cdot, \cdot \rangle$ denotes the duality between $H^*(-R, R)$ and $H^2 \cap H_0^1(-R, R)$. Since $H^2 \cap H_0^1(-R, R) \subset C^1[-R, R]$, the integral $\int g(w)v$ makes sense. Weak solutions of (2.75) and (2.76), as defined in (2.77), are critical points of the energy functional

$$J(u) = \int_{-R}^{R} \left(\frac{EI}{2} u''(x)^2 + \frac{T}{2} u'(x)^2 + G(u(x)) \right) dx - \langle p, u \rangle \quad \forall u \in H^2 \cap H_0^1(-R, R)$$

where $G(s) = \int_0^s g(\sigma) d\sigma$. Since g is increasing, $G \in C^1(\mathbb{R})$ is a convex function. Hence, the functional J consists in the sum of two quadratic (convex) terms, of an additional convex term containing G, and of a linear term. Therefore, J is convex and since it is continuous and coercive in $H^2 \cap H_0^1(-R, R)$ it admits a unique critical point, its absolute minimum, which is a weak solution w of (2.77). If we additionally assume that $P \in C^0[-R, R]$ (in particular, if P is constant) then the weak solution w belongs to $C^4[-R, R]$ and it is a classical solution of (2.75) and (2.76). Let us summarise these facts in the following

Theorem 2.10 *Assume that g is increasing and (2.60). Then for all $P \in H^*(-R, R)$ there exists a unique $w \in H^2 \cap H_0^1(-R, R)$ satisfying (2.77). If $p \in C^0[-R, R]$ then $w \in C^4[-R, R]$ and w is a classical solution of (2.75) and (2.76).*

We now consider nonlinearities g as in (1.12) with $\varepsilon > 0$. In view of the general results in [125, 128], we expect different nonlinearities to generate the same qualitative behavior of solutions. To simplify further the task, we restrict our attention to the case of a constant load $P(x) \equiv P$. Then we obtain (2.59) on the interval $(-R, R)$. After the changes of variables

$$x \mapsto x \sqrt[4]{\tfrac{k}{4EI}}, \quad \tau = \frac{T}{2\sqrt{k\,EI}}, \quad \delta = \frac{4\varepsilon}{k}, \quad P \mapsto \frac{4}{k} P, \quad L = R \sqrt[4]{\tfrac{k}{4EI}},$$

the equation becomes

$$w''''(x) - 4\tau w''(x) + 4w(x) + \delta w(x)^3 = P \qquad (-L < x < L) \tag{2.78}$$

with $\tau < 1$ in view of (2.60). The boundary conditions (2.76) simply become

$$w(\pm L) = w''(\pm L) = 0\,. \tag{2.79}$$

We wish to compare the behavior of the solution of (2.78) and (2.79) with the solution of the corresponding linear problem. If $\varepsilon = 0$ then $g(w) = kw$ and the springs obey the classical linear Hooke law. Then $\delta = 0$ and Eq. (2.78) becomes

$$w''''(x) - 4\tau w''(x) + 4w(x) = P \qquad (-L < x < L)\,. \tag{2.80}$$

The solution of (2.80) satisfying (2.79) is even for all $L > 0$ so that the general solution of (2.80)–(2.79) reads

$$w(x) = a\cosh\left[x\sqrt{1+\tau}\right]\cos\left[x\sqrt{1-\tau}\right] + b\sinh\left[x\sqrt{1+\tau}\right]\sin\left[x\sqrt{1-\tau}\right] + \frac{P}{4}$$

with a and b to be determined in dependence of L. For our convenience we restrict the possible values of L by requiring that

$$\frac{a}{\sqrt{1+\tau}} = \frac{b}{\sqrt{1-\tau}} =: \gamma \tag{2.81}$$

in such a way that the solution of (2.80)–(2.79) reads

$$w(x) = \gamma\left[\sqrt{1+\tau}\cosh\left[x\sqrt{1+\tau}\right]\cos\left[x\sqrt{1-\tau}\right] + \sqrt{1-\tau}\sinh\left[x\sqrt{1+\tau}\right]\sin\left[x\sqrt{1-\tau}\right]\right] + \frac{P}{4}.$$

By differentiating we find $w'(x) = 2\gamma\sinh\left[x\sqrt{1+\tau}\right]\cos\left[x\sqrt{1-\tau}\right]$ and it is therefore quite simple to compute the number of critical points of w. Restricting to the half-line $x \geq 0$, we see that $w'(x) = 0$ if and only if

$$x = x_0 := 0 \qquad \text{or} \qquad x = x_j := \frac{(2j-1)\,\pi}{2\sqrt{1-\tau}} \qquad (j \in \mathbb{N},\ j \geq 1)\,. \tag{2.82}$$

A further differentiation yields

$$w''(x) = 2\gamma\left[\sqrt{1+\tau}\cosh\left[x\sqrt{1+\tau}\right]\cos\left[x\sqrt{1-\tau}\right] - \sqrt{1-\tau}\sinh\left[x\sqrt{1+\tau}\right]\sin\left[x\sqrt{1-\tau}\right]\right].$$

By imposing the second boundary condition in (2.79) we find

$$\tan\left[L\sqrt{1-\tau}\right] = \sqrt{\frac{1+\tau}{1-\tau}}\coth\left[L\sqrt{1+\tau}\right] \tag{2.83}$$

and it is clear that

$$\forall m \in \mathbb{N}\ (m \geq 1) \quad \exists!\, L_m \in \left(\frac{(m-1)\,\pi}{\sqrt{1-\tau}}, \frac{(2m-1)\,\pi}{2\sqrt{1-\tau}} \right) \text{ s.t. } L_m \text{ satisfies (2.83).} \tag{2.84}$$

We refer to Fig. 2.17, where $\Lambda_m = \frac{(2m-1)\,\pi}{2\sqrt{1-\tau}}$, for the qualitative description of the position of L_m as defined in (2.84). In fact, since the right hand side of (2.83) is larger than 1, we know that $L_m > \frac{(4m-3)\,\pi}{4\sqrt{1-\tau}}$. Once L_m is fixed we compute $\gamma = \gamma_m$ by imposing the first boundary condition in (2.79) and by using (2.84):

$$\gamma_m = -\frac{P}{8\sqrt{1+\tau}\,\cosh\left[L_m\sqrt{1+\tau}\right]\cos\left[L_m\sqrt{1-\tau}\right]}. \tag{2.85}$$

Since L_m satisfies (2.84) we have $\gamma_m < 0$.

Let us summarise the above results in the following statement.

Theorem 2.11 *Assume that $L = L_m$ and $\gamma = \gamma_m$ for some $m \in \mathbb{N}$ $(m \geq 1)$, where L_m is defined in (2.84) and γ_m is defined in (2.85). Then the function*

$$w_m(x) = \gamma_m \Big[\sqrt{1+\tau}\cosh[x\sqrt{1+\tau}]\cos[x\sqrt{1-\tau}] + \sqrt{1-\tau}\sinh[x\sqrt{1+\tau}]\sin[x\sqrt{1-\tau}] \Big] + \frac{P}{4}$$

solves the problem

$$w_m''''(x) - 4\tau w_m''(x) + 4w_m(x) = P \quad \forall x \in (-L_m, L_m),$$
$$w_m(\pm L_m) = w_m''(\pm L_m) = 0.$$

Therefore, w_m admits $2m-1$ critical points given by x_0 and $\pm x_j$ for $j = 1, \ldots, m-1$, see (2.82); in particular, w_1 only admits the unique critical point $x_0 = 0$.

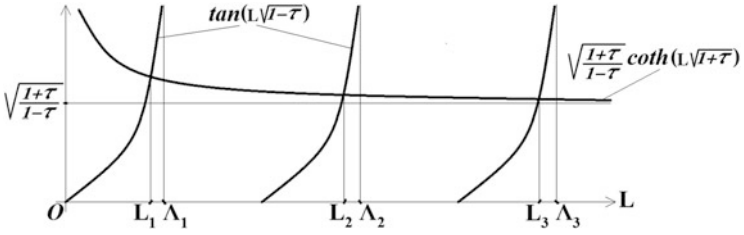

Fig. 2.17 Positions of L_m as defined in (2.84)

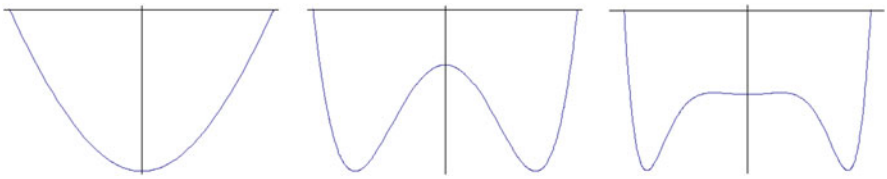

Fig. 2.18 Graphs of w_1, w_2, w_3, as defined in Theorem 2.11

Theorem 2.11 counts the number of critical points of w_m. Recalling that the vertical axis is oriented downwards, the unique constant solution of (2.80) is given by

$$\tilde{w}(x) \equiv \frac{P}{4}\,. \tag{2.86}$$

Roughly speaking, we can say that the "target" of w_m, who aims to minimise the energy of the beam, is to approach as much as possible the equilibrium position $\tilde{w}$. In Fig. 2.18 we plot the qualitative graphs of w_1, w_2, w_3. One sees that the first beam is not large enough to allow w_1 to reach $P/4$. On the other hand, the second beam is large enough and w_2 goes beyond $P/4$ in order to get close to it after the first maximum point. Finally, the third beam tends to hide the oscillations of w_3 around $P/4$; after the first maximum, w_3 just slightly oscillates around $P/4$ and w_3 appears almost constant in the central part of the beam. The same phenomenon becomes more and more evident as m increases, that is, as the length of the beam increases.

As a complement to Theorem 2.11 we add two information on the qualitative behavior of w_m. First, we distinguish between maxima and minima points; we have

$$\forall m \in \mathbb{N}\,, \quad m \geq 1 \qquad (-1)^{m+j} w_m''(x_j) > 0 \qquad \forall\, j = 0, \ldots, m-1\,.$$

Then, we formalise the tendency to flatten in the center of the beam as follows

$$\text{the map } \{0, \ldots, m-1\} \to \mathbb{R}_+ \text{ defined by } j \mapsto \left| w_m(x_j) - \frac{P}{4} \right| \text{ is strictly increasing.}$$

Due to the linear nature of (2.80), it is clear that the number of critical points of w_m does not depend on P. Moreover, we have linked τ to L_m through (2.84). Therefore, the number of critical points of the solution w_m of (2.80)–(2.79) (for $L = L_m$) merely depends on m. Theorem 2.11 states that it equals $2m - 1$.

We now compute numerically the number of critical points of the solution of (2.78) and (2.79) and we compare it with $2m - 1$; for the nonlinear problem, the number of critical points depends both on P and δ. In the nonlinear case $\delta \neq 0$ we do not have explicit solutions of (2.78) and (2.79) and we cannot proceed theoretically in order to find the number of critical points of the corresponding solutions. Let

us notice that, by the Cardano formula, the unique constant solution of (2.78) is given by

$$\overline{w}(x) \equiv W(\delta, P) \coloneqq \frac{3 \cdot 4^{1/3} \cdot P}{[3P\sqrt{3\delta} + \sqrt{27P^2\delta + 256}]^{2/3} + 4^{4/3} + [3P\sqrt{3\delta} - \sqrt{27P^2\delta + 256}]^{2/3}} \tag{2.87}$$

which coincides with (2.86) when $\delta = 0$.

Assume again that, for a given $\tau \in (0, 1)$, the length of the beam is given by (2.84) for some $m \in \mathbb{N}$ ($m \geq 1$). We are interested in finding the number of critical points of the solution of (2.78) and (2.79) when $L = L_m$ and τ satisfies (2.84): by symmetry, we may restrict our attention to the interval $[0, L_m)$. This number also depends both on the load P and on the nonlinear coefficient δ; let us denote it by

$$Z(L_m, P, \delta) := \text{number of critical points of the solution of (2.78) and (2.79) in } [0, L_m).$$

Note that $Z(L_m, P, 0) = m$ for all P. By putting $w(x) = \alpha z(x)$, one sees that

$$Z(L_m, P, \delta) = Z\left(L_m, \frac{P}{\alpha}, \delta\alpha^2\right) \qquad \forall \alpha > 0 \tag{2.88}$$

which states that the number of critical points does not vary if we decrease the nonlinearity and we increase the load (or viceversa) following a suitable rule.

In order to compute $Z(L_m, P, \delta)$ we proceeded numerically by using the `bvptwp` code, whose MATLAB version was published in [67]. It is an optimised high-quality code and we refer to [129] for the details of how it has been implemented for the problem under study. We first tested this code on the linear case $\delta = 0$: to rule out possible roundoff errors we studied the oscillations the function $z(x) = w(x) - P/4$ so that, instead of (2.80), we dealt with the problem

$$z'''' - 4\tau z'' + 4z = 0\,, \qquad z(\pm L) = -\frac{P}{4}\,, \quad z''(\pm L) = 0\,. \tag{2.89}$$

The numerical critical values that we found exhibited a very good accordance with the analytical ones as they had more than seven correct digits. For the nonlinear equation we introduced the variable $z(x) = w(x) - W(\delta, P)$ where $W(\delta, P)$ is defined in (2.87). Then, instead of (2.78) and (2.79), we considered the problem

$$\begin{cases} z'''' - 4\tau z'' + \left(4 + 3W(\delta, P)^2\right) z + 3\delta W(\delta, P) z^2 + \delta z^3 = 0 \\ z(\pm L) = -W(\delta, P)\,, \quad z''(\pm L) = 0\,. \end{cases} \tag{2.90}$$

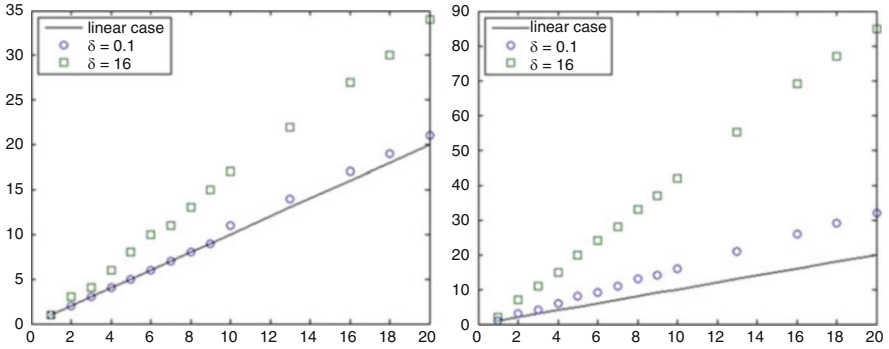

Fig. 2.19 The maps $m \mapsto Z(L_m, 10, \delta)$ for $\delta = 0,\ 0.1,\ 16$ when $\tau = 0.1$ (*left*) and $\tau = 0.9$ (*right*)

In all our experiments we found $Z(L_m, P, \delta) \geq m$ for all $\delta > 0$, that is,

the number of critical points of the solution of the nonlinear equation is larger than the number of critical points of the solution of the linear equation

and, consequently, the last maximum, which is the absolute maximum, is closer to the right end of the integration interval. In order to check this behavior, we considered some different values of δ and τ whereas we always assumed $P = 10$ in view of (2.88). In Fig. 2.19 we quote the plots of the map $Z(L_m, P, \delta)$ for different values of its arguments. It appears that the gap $Z(L_m, P, \delta) - m$ increases with τ.

We also introduce the two numbers

$$M_l := \max\{|z(x)|;\ z'(x) = 0,\ z \text{ solves } (2.89)\},$$
$$M_{nl} := \max\{|z(x)|;\ z'(x) = 0,\ z \text{ solves } (2.90)\}$$

which represent the maximum deviation of critical points with respect to the equilibrium positions (2.86) and (2.87): we found that the deviation from equilibrium decreases for increasing tension τ.

Moreover, the numerical results obtained in [129] suggest that

the map $\delta \mapsto Z(L_m, P, \delta)$ is increasing;

the map $P \mapsto Z(L_m, P, \delta)$ is increasing;

the map $\tau \mapsto Z(L_m, P, \delta)$ is increasing;

the maps $\tau \mapsto M_l$ and $\tau \mapsto M_{nl}$ are decreasing.

Recalling the meaning of the parameters, we may conclude that a stronger nonlinearity of the restoring force, an increasing load, an increasing tension of the sustaining cable, all contribute to increase the number of vibrations within the beam. Moreover, the map $m \mapsto Z(L_m, P, \delta) - m$ is increasing; since m somehow measures

the length of the beam, as $m \to \infty$ we obtain the limit situation of an infinite number of oscillations, as shown in detail in Sect. 2.6.2.

2.7 The Birth of Aerodynamics

2.7.1 From Melan Until the Wake of Tacoma

The first reference of the bibliography in the book by Melan [199] is the contribution by Navier [210], whereas the last one is a contribution by Moisseiff, the chief engineer of the TNB project. For this and other reasons, the book by Melan should be considered as the connection between the first theoretical attempts to model suspension bridges and the Tacoma collapse. Rocard [234, p. 184] writes

> Before the accident of the Tacoma Bridge - 7th November 1940 - no mention could be found in literature of any work analysing the effect of wind on suspension bridges.

After the Tacoma collapse, the engineering community felt the necessity to introduce the time variable in mathematical models and equations in order to attempt explanations of what had occurred. In the Federal Report, Rannie [9, Appendix VI] considers inextensible cables and derives the linearised Melan equation [9, (10), VI-15] with the mistake explained in Sect. 2.5.1: he considers the wrong form (2.32) so that the inextensibility assumption reduces to $\int_0^L w(x)\,dx = 0$. He then makes an analysis of both symmetric and asymmetric modes, aiming to compare the theoretical results with the behavior of the TNB. His conclusion is that

> The agreement of the theoretical results with the observations of frequencies and modes on both prototype and model is remarkably good.

But then he defines this agreement *rather surprising* since *the observations were not obtained very accurately*, see [9, VI-19,20]. It is hard to say if his results are reliable: the formulas are obtained by neglecting many terms and Rannie himself admits that they are not accurate. In any case, his work fails to give an answer to the questions **(Q1)–(Q2)–(Q3)** raised in Sect. 1.6.

Further important contributions are the works by Smith and Vincent [245], which was written precisely *with special reference to the Tacoma Narrows Bridge*, and the analysis of vibrations in suspension bridges by Bleich et al. [50] which was published in the same year (1950) and appears more detailed. The downwards vertical displacement u of the beam, seen again as the space interval $x \in (0, L)$, depends on the time $t > 0$ as well, $u = u(x, t)$. The fundamental rule of the classical dynamics states that the acceleration of the mass at any instant has the opposite direction to u; this yields the following partial differential equation:

$$m\,u_{tt} + \delta\,u_t + EI\,u_{xxxx} - (H + h(u))\,u_{xx} + \frac{q}{H}\,h(u) = p\,, \qquad x \in (0, L)\,,\ t > 0\,, \tag{2.91}$$

where m denotes the mass per unit length, $\delta > 0$ is a damping parameter, $q = mg$ is the weight (dead load) and $p = p(x,t)$ is the live load per unit length applied to the beam; also the live load p depends on time, modeling either a variable wind, or rain, or the dynamic load of vehicles crossing the bridge. All the other parameters are as in Sect. 2.4. The beam is assumed to be hinged at its endpoints:

$$u(0,t) = u(L,t) = u_{xx}(0,t) = u_{xx}(L,t) = 0 \quad \forall t > 0\,. \tag{2.92}$$

The solutions of (2.91) and (2.92) are determined by the initial conditions. An undamped ($\delta = 0$), simplified (and incomplete) version of (2.91) first appears in [50, (2.6)]: the term $h(u)u_{xx}$ is dropped because it is considered quadratically small and $h(u)$ is computed in an incorrect way, see Sect. 2.5.1. The live load is taken periodic in time and in the form $p(x,t) = p(x)\sin(\omega t)$ where $\omega > 0$ is the frequency. Also the function u is then periodic in time, that is,

$$u(x,t) = w(x)\sin(\omega t).$$

Here $w = w(x)$ denotes the maximum values of the deflection at any point. Since Eq. (2.91) is linearised by dropping the term $h(u)u_{xx}$, after deleting the term $\sin(\omega t)$ one finds that w satisfies the equation (see [50, (2.7)])

$$EI\, w''''(x) - H\, w''(x) - m\omega^2\, w(x) + \frac{q}{H}h(w) = p(x) \qquad \forall x \in (0,L)$$

which is just the Melan equation (2.22) with the nonlinear term dropped and with the additional term due to the acceleration. Unfortunately, there is no justification for the assumption that p and u are periodic in time. On the contrary, the events described in Sects. 1.3 and 1.4 allowed to conclude (1.1). Moreover, the recorded oscillations at the TNB had a fairly variable frequency, see [9, pp. 21–27]. In particular, from [9, p. 118], we quote

> The observations of the Tacoma Bridge oscillations ... show that in most cases one definite mode prevailed over a certain length of time. However, the modes frequently changed.

Summarising, in [50, 245] Eq. (2.91) is oversimplified and only (unjustified) periodic solutions are sought. The spirit of these works is well explained at [50, p. 23]:

> ...the degree of nonlinearity of the system, taken as a whole, is so small for small amplitudes of vibration that it may be neglected with only negligible error.

It is obviously true that small amplitudes may be well described by linear theory but the amplitudes visible on the collapses described in Sects. 1.3 and 1.4 cannot be classified as small. Therefore, linear models fail to give an answer to the questions **(Q1)–(Q2)–(Q3)** raised in Sect. 1.6.

The main purpose of Bleich et al. [50] is to provide a systematic method (called the energy method) for the treatment of free vibrations in order to analyse the modes of oscillation, the frequencies, and the energy storage capacity of the suspension

bridge structures. This method, which is none other than a variational method, allows to study the dependence of the performances of a bridge with respect to its structural parameters such as the mass, the lengths of the span and of the cable, the flexibility of the materials. For these reasons, the contribution of [50] appears interesting and innovative but, as far as we are aware, it has never been used for practical purposes. We believe that it could be extremely useful to repeat its analysis on more reliable models by following a couple of fundamental suggestions which we now emphasise.

The first suggestion is already mentioned at [50, p. 52]: one of the phases of the research on suspension bridges aims to determine

> the relationship between the frequency and mode of motion and the corresponding "critical" or "resonant" wind velocity. In general, each mode of motion is generated at a particular wind velocity which appears to be either in resonance or in subharmonic resonance with the natural frequency of the structure for that particular mode.

From these sentences we understand that [50] had the intuition that there is no absolute critical wind velocity which, instead, depends on the oscillating mode. There is also an explicit reference to an external resonance with wind, a phenomenon which was described in Sect. 1.2 and subsequently ruled out in Sect. 1.7.2. However, up to replacing the external resonance with an internal resonance and the critical speed with a critical energy, we believe that this is the correct way to study the instability of a suspension bridge. We refer to Sect. 6.1 for our own conclusions, after having analysed several different models.

The second suggestion is to simplify the task: [50, p. 23] observes that

> ... out of the infinite number of possible modes of motion in which a suspension bridge might vibrate, we are interested only in a few, to wit: the ones having the smaller numbers of loops or half waves.

There is a deep physical reason why only low modes should be considered: higher modes require large bending energy. This is well explained in [245, p. 11]:

> The higher modes with their shorter waves involve sharper curvature in the truss and, therefore, greater bending moment at a given amplitude and accordingly reflect the influence of the truss stiffness to a greater degree than do the lower modes.

The suggestion to restrict attention to lower modes mathematically corresponds to project an infinite dimensional phase space on a finite dimensional subspace, a technique which should be attributed to Galerkin [119]. We will use this technique for the nonlinear models studied in Chaps. 3 and 5.

Summarising, we feel that it would be interesting to revisit [50] with the just mentioned suggestions. One should introduce more reliable nonlinear models and focus the attention on the structural behavior. And this target may be reached by analysing a finite number of modes through a Galerkin procedure, see Chaps. 3 and 5.

A quite accurate analysis of (2.91) was also performed by Rocard [234] who first considers several particular cases (linearised, undamped, unforced) and then he ends up with (2.91): he makes estimates of how much is lost by linearising and by

neglecting terms. Assuming that the load p is periodic in time, he seeks solutions of (2.91) which are periodic both in space and time; we have already observed that this should not be the target, see (1.1). Rocard makes a clear distinction between symmetric and asymmetric spatial modes. Subsequently, he introduces a similar equation for torsional oscillations and on [234, p. 122] he writes:

> If the bridge is excited only in bending, no torsional motion can arise, and vice versa. Mathematically this is shown by the fact that the bending variable does not appear in the torsional equation and that the torsion variable not in the bending equation.

We believe that this is incorrect and that it is precisely a coupling between vibrating modes which is responsible of the torsional instability of suspension bridges. In Chap. 3 we explain what we mean by "coupling" in a specific model; further examples will be given in Chaps. 4 and 5. Rocard [234, p. 130] essentially feels that the torsional oscillations cannot be predicted:

> If a horizontal wind impinges on a horizontal bridge, the force acts vertically and excites vertical bending vibrations. As moreover there is no reason why the resultant force should have its point of application at the centre of the profile ... the wind will also excite torsional vibrations.

Assuming that vertical and torsional oscillations are governed by *uncoupled linear* equations of the kind of (2.91), each one having its own natural frequency, he then claims that only the aerodynamic forces may synchronize vertical and torsional modes, see [234, p. 142]. This claim is absolutely reasonable but, in our opinion, it is incomplete. In view of (1.2) we believe that the equations are **nonlinear and coupled**, two properties which yield variable frequencies also if we neglect aerodynamic forces. In fact, there may exist some unstable situation where the two nonlinear equations are perfectly synchronized and yield periodic solutions, see Chap. 4 and, in particular, Fig. 4.5. But precisely because this solution is unstable, it has no physical relevance. As a conclusion about the bending and twisting of the roadway, Rocard [234, p. 142] writes

> ... the two modes will appear coupled by the aerodynamic forces

while we also believe that the **two modes will be coupled provided enough energy is present within the structure**. This is one of the main contribution of this monograph: it shows that the starting spark for instability has to be sought inside the structure, in particular by measuring the internal energy, see the next three chapters, and that aerodynamic forces play a major role only after the instability appears, see Sect. 3.7. All this will be made precise in the concluding Sect. 6.1.

While commenting some of the made assumptions, Rocard [234, pp. 140–141] recognizes that theory and reality are fairly different:

> ... the author knows of no accident inflicted on a suspension bridge by this type of action. ... The authors knows of no suspension bridge fractured by the action of vortices during a pure oscillation in a single mode...

Summarising, although Rocard makes several hardly verifiable assumptions and seeks periodic solutions, from his work we learn that a kind of internal

resonance between different oscillations may occur in the structure. We will follow some of his suggestions by modifying several fundamental parts. First of all, the problems are nonlinear and this yields a strong coupling between vertical and torsional oscillations. Second fact, nonlinear systems have variable frequencies also in absence of an external forcing; this means that the resonance may also occur independently of the source (wind) which can then be assumed to be non-periodic. Finally, these arguments show that instead of a critical wind speed one could seek a critical energy; and, of course, one should define rigorously this energy and determine an effective way how to compute it. We will do all this work starting from the one dimensional model considered in Chap. 3, then on the model involving coupled oscillators considered in Chap. 4, and finally on the plate model in Chap. 5.

2.7.2 More Recent Models and the Sin of Mathematics

The mathematical contributions which followed the TNB collapse leave several nagging doubts. The models are derived by approximating factors, by linearising equations, by neglecting higher order terms. Are the so obtained equations reliable? Do these equations give satisfactory responses? More doubts are added by the authors themselves. In the Federal Report, Rannie [9, VI-1] writes

> In order to make the problem tractable, the equations may be linearized ... neglecting second and higher order terms.

And we know that linearisation may lead to incorrect problems, see for instance Sect. 2.5.1. Smith and Vincent [245, p. 9] admit that

> The formulas developed here, like most others used in engineering, are not precise. The engineer starts with certain more or less valid assumptions, makes a series of approximations of varying degree, and attempts to develop equations that will predict with fair precision the performance of the designed structure.

Unfortunately, the gap between models and reality has not been filled even in recent years; Podolny [221, 15.61] writes that

> Much of the literature on classical suspension-bridge theory deals with the effects of minor terms neglected in the assumptions of deflection theory.

Let us also recall that assumption (2.18) and, consequently, Eq. (2.22) are not realistic, the hangers play a major role both directly with their extension and indirectly by transmitting to the roadway the actions of towers and cables. In this respect, Robinson and West [233, p. 26] claim that

> The nonlinear response of the bridge is a result of the changes of cable geometry.

Hence, at least for a first approximation, the nonlinear behavior of a suspension bridge may be concentrated into the action of the hangers. Lazer and McKenna [168, p. 559] believe that (2.22)

> ... is clearly inappropriate when considering the large scale oscillations in which the stays are known to alternately loosen and tighten.

In Sects. 2.8.1 and 2.8.2 we give further details on this deep remark and we describe alternative models.

Let $u(x,t)$ and $\theta(x,t)$ denote respectively the vertical and torsional components of the oscillation of the bridge, then the following linearised equations of the elastic combined vertical-torsional oscillation motion are used in [85, (1)–(2)]:

$$\begin{cases} m\,u_{tt} + EI\,u_{xxxx} - H\,u_{xx} + \dfrac{q^2}{H^2}\,\dfrac{EA}{L_c}\displaystyle\int_0^L u(z,t)\,dz = f(x,t) \\ I_0\,\theta_{tt} + C_1\,\theta_{xxxx} - (C_2 + H\ell^2)\,\theta_{xx} + \dfrac{\ell^2 q^2}{H^2}\,\dfrac{EA}{L_c}\displaystyle\int_0^L \theta(z,t)\,dz = g(x,t) \\ x \in (0,L)\,,\ t > 0, \end{cases} \tag{2.93}$$

where m, EI, q, H are as in (2.91), EA is as in (2.29), C_1 and C_2 are respectively the warping and torsional stiffness of the girder, I_0 the polar moment of inertia of the girder section, L is the roadway length and 2ℓ is the roadway width, L_c is the length of the cable as given by (2.14), $f(x,t)$ and $g(x,t)$ are the lift and the moment per unit girder length of the external forces. The system (2.93) is an improved version of (2.1), showing that the Melan equation is considered a good model for small oscillations in suspension bridges. But when large oscillations are involved, linearisation should be avoided. The linearisation here consists in dropping the term $h(u)u_{xx}$.

All the just described doubts are strengthened by the impossibility for the models considered to give an answer to the questions **(Q1)–(Q2)–(Q3)** raised in Sect. 1.6. In turn, the models appear inadequate because they fail to fulfil the (GPCM), in particular they fail to be nonlinear. One should then choose a compromise between realistic and tractable models. However, for suspension bridges, this was not the initial strategy since several tools of nonlinear analysis were not yet developed. For long time nonlinear mathematical problems have been considered intractable due to their difficulty; whence, it is mathematics with its difficulties which should be considered guilty for the lack of reliable models. However, in recent years some progress has been made and one may try to take advantage of modern tools from nonlinear analysis.

2.8 McKenna and the Awakening of Nonlinearity

Any model aiming to describe the behavior of suspension bridges must satisfy three main requirements. First, it should be physically correct and reproduce, at least qualitatively, the phenomena of actual bridges; we already underlined that in order to

be as close as possible to reality, one should avoid excessive linearisations. Second, it must be well-posed and theoretically tractable; this requirement needs a correct mathematical setting and rigorous theoretical proofs. The third requirement is the possibility to use the information obtained theoretically into practical measures for engineering projects. In this section we mainly deal with the second requirement.

The demand for more reliable models from the engineers dates of about half a century ago, see e.g. [233]; the discrepancy between theory and practice and the appearance of computers lead the scientific community to start tackling nonlinear models. From [233, p. 15] we quote

> Actually, some linear theories serve a simple introduction to some of the essential problems of the stiffened suspension bridge. Nevertheless, all major modern bridges are such that linear theories are unacceptable.

Mathematicians have not shown an interest in suspension bridges until recent years. It was McKenna in 1987, followed by several other mathematicians, who started to introduce nonlinear models and to study them from a theoretical point of view.

2.8.1 Beam Suspended by Possibly Slackening Hangers

Consider a beam which is hanged to a fixed upper base by means of a large number of nonlinear springs as in Fig. 2.20.

The springs model the hangers which tend to return the beam to equilibrium if stretched but exert no restoring force if compressed. If we denote by u the downwards displacement of the beam, the restoring force due to the hangers is then described by ku^+ where $k > 0$ denotes the elastic constant and $u^+ = \max\{u, 0\}$ is the positive part of u. This nonlinearity describes the possible slackening of the hangers which was observed by Farquharson [9, V-12] during the TNB collapse:

> one of the four suspenders in its group was permanently slack.

Let m denote the mass of the beam per unit length and let EI denote the flexural rigidity of the beam. By modeling the beam with the segment $x \in (0, \pi)$ and by arguing as for (2.8) and (2.91), one finds that the displacement $u = u(x, t)$ solves the equation

$$m\, u_{tt} + EI\, u_{xxxx} + ku^+ = f(x, t)\,, \qquad x \in (0, \pi)\,, \quad t > 0\,, \tag{2.94}$$

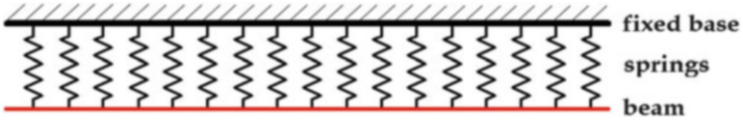

Fig. 2.20 Beam hanged with springs

where f represents the forcing term acting on the beam (both dead and live loads), including its own weight per unit length, the wind, the traffic loads, or other external sources. We assume that the beam is hinged so that to (2.94) we associate the boundary conditions

$$u(0,t) = u(\pi,t) = u_{xx}(0,t) = u_{xx}(\pi,t) = 0 \qquad \forall t > 0\,. \tag{2.95}$$

We restrict our attention to functions $\psi : [0,\pi] \times \mathbb{R}_+ \to \mathbb{R}$ satisfying

$$\begin{cases} x - \text{symmetry: } \psi(\frac{\pi}{2} + x, t) = \psi(\frac{\pi}{2} - x, t) \ \forall |x| \le \frac{\pi}{2}\,, \ \forall t \ge 0 \\ t - \text{symmetry: } \psi(x, \frac{\pi}{2} + t) = \psi(x, \frac{\pi}{2} - t) \ \forall |t| \le \frac{\pi}{2}\,, \ \forall x \in [0,\pi] \\ t - \text{periodicity: } \psi(x, t + \pi) = \psi(x,t) \qquad \forall t \ge 0\,, \ \forall x \in [0,\pi]\,. \end{cases} \tag{2.96}$$

Let us introduce the spaces

$$H = \left\{ \psi : [0,\pi] \times \mathbb{R}_+ \to \mathbb{R};\ \psi \text{ satisfies (2.96) and } \int_0^\pi \int_0^\pi \psi(x,t)^2 dx dt < +\infty \right\}\,,$$

$$D = \{\psi \in H \cap C^\infty([0,\pi] \times \mathbb{R}_+);\ \psi(0,t) = \psi(\pi,t) = \psi_{xx}(0,t) = \psi_{xx}(\pi,t) = 0 \ \forall t > 0\}\,.$$

We consider a particular form for the forcing term f, we take $f(x,t) = q + h(x,t)$ where $q > 0$ denotes the dead load (the constant weight per unit length) and $h \in H$. For simplicity we normalise the constants so that (2.94) becomes

$$u_{tt} + u_{xxxx} + k u^+ = 1 + \varepsilon h(x,t)\,, \qquad x \in (0,\pi)\,, \quad t > 0\,, \tag{2.97}$$

where the coefficient ε emphasises the fact that only small live loads will be considered. We say that $u = u(x,t)$ is a weak solution of (2.97)–(2.95) if $u \in H$ and

$$\int_0^\pi \int_0^\pi (\phi_{tt} + \phi_{xxxx}) u \, dx dt = \int_0^\pi \int_0^\pi (1 + \varepsilon h - k u^+) \phi \, dx dt \qquad \forall \phi \in D\,.$$

Some integrations by parts show that any smooth weak solution is also a strong solution of (2.97) satisfying the boundary conditions (2.95). The following multiplicity result is due to McKenna and Walter [196]:

Theorem 2.12 *Assume that* $3 < k < 15$. *For all* $h \in H$ *there exists* $\varepsilon_h > 0$ *such that if* $|\varepsilon| < \varepsilon_h$ *then the problem* (2.97)–(2.95) *admits at least two weak solutions.*

We discuss Theorem 2.12 with an explicit example. By [196, Lemma 5] we know that for all $k > 0$ there exists a unique solution y_k of the boundary value problem

$$y_k''''(x) + k y_k(x)^+ = 1\,, \qquad x \in (0,\pi)\,, \quad y_k(0) = y_k(\pi) = y_k''(0) = y_k''(\pi) = 0;$$

moreover, y_k is positive and symmetric with respect to $x = \frac{\pi}{2}$ and satisfies $y_k'(0) = -y_k'(\pi) > 0$. In particular,

$$y_4(x) = \frac{1}{4} + \frac{\cos(x)\sinh(x - \pi/2)}{4\,\sinh(\pi/2)}\,.$$

Some computations show that, for any $0 < k < 15$, the problem

$$u_{tt} + u_{xxxx} + ku^+ = 1 + \varepsilon \sin(x)\cos(4t)\,, \qquad x \in (0,\pi)\,, \quad t > 0\,, \tag{2.98}$$

with boundary conditions (2.95), admits the solution

$$\overline{u}(x,t) = y_k(x) + \frac{\varepsilon}{k - 15}\sin(x)\cos(4t) \tag{2.99}$$

which is positive provided ε is sufficiently small; for instance, when $k = 4$ one has $\overline{u}(x,t) > 0$ in $(0,\pi) \times (0,+\infty)$ if and only if $|\varepsilon| < \frac{11}{4}$. Thanks to the usual contraction mapping principle one sees that if $0 < k < 3$ then (2.98)–(2.95) admits a unique solution in H, which is necessarily $\overline{u}$ in (2.99). But if $3 < k < 15$, then Theorem 2.12 states that there exists at least another solution which is sign-changing.

Which periodic solution appears depends on the energy within the structure, that is, on the initial conditions on u at $t = 0$. A positive solution for ε small is physically obvious: small oscillatory forces give rise to small oscillations about the (positive) equilibrium position generated by the uniform load. Theorem 2.12 states that, if $3 < k < 15$ then there also exists a (less obvious) solution which changes sign. Hence, if the elastic constant k is sufficiently large, there exists a sign-changing periodic solution, which appears because Eq. (2.98) operates in its nonlinear regime (when u changes sign). According to [168, p. 555], this shows that

> strengthening a bridge can lead to its destruction.

For all these reasons, and also because it is the first rigorous mathematical result on a model for suspension bridges, Theorem 2.12 deserves a deep attention. But, possibly, it may be improved. Firstly, we have already discussed why periodic solutions are misleading, see (1.1). Secondly, the model described by Fig. 2.20 appears too far from an actual suspension bridge: no damping, no flexible cables, no towers, etc. However, if this simplified model displays a neat phenomenon one should expect a similar phenomenon to appear also in more sophisticated models.

The multiplicity statement in Theorem 2.12 may be improved. In fact, if $3 < k < 15$ the problem (2.97)–(2.95) admits at least three weak solutions, see [78]. Moreover, if $15 < k < 15 + \gamma$ with $\gamma > 0$ sufficiently small, then (2.97)–(2.95) admits at least four weak solutions, see [143]. These results are related to the so-called "crossing of eigenvalues"; further multiplicity results for (2.97) are obtained in [98] which also shows that multiple solutions exist because of the absence of a damping term. Last but not least, let us mention multiplicity results by Drábek and

Nečesal [97] for arbitrarily large periodic solutions; these depend on the periods considered and create somehow an external resonance phenomenon.

Attempting to reproduce the nonlinear phenomenon of traveling waves, see Sect. 1.8, one is led to consider the equation in (2.94) on the whole real line by dropping the conditions (2.95) at the endpoints. In such infinite beam, the (finite) energy of the beam plays the role of the live load; so, one can restrict the attention to a conservative system and consider different energy levels. By dropping the contribution of the live load, we obtain the equation ($q > 0$ is the dead load)

$$m\,u_{tt} + EI\,u_{xxxx} + ku^+ = q\,, \qquad x \in \mathbb{R}\,, \quad t > 0\,. \tag{2.100}$$

This ideal beam is at equilibrium for $u(x,t) \equiv q/k$. A traveling wave for (2.100) is a solution of the form $u(x,t) = w(x - ct)$ where $c > 0$ is the speed of propagation of the wave. Chen and McKenna [75] and Lazer and McKenna [169] proved the following statement:

Theorem 2.13 *The nonlinear beam Eq. (2.100) has traveling waves solutions. As $c \to 0$, the amplitude of traveling waves tends to $+\infty$.*

The range of possible speed velocities c depends on all the parameters involved: m, EI, k and q. Theorem 2.13 confirms the nonlinear nature of (2.100) and also states that traveling waves change sign, that is, they go again in the region where (2.100) displays a nonlinear behavior. To push the beam in such region requires a lot of energy and this explains why traveling waves and slacken hangers have been observed only in violent storms.

A first possible variant of (2.94) consists in adding a term representing the structural damping. The new equation reads

$$m\,u_{tt} + EI\,u_{xxxx} + \delta u_t + ku^+ = q + h(x,t)\,, \qquad x \in (0,\pi)\,, \quad t > 0\,, \tag{2.101}$$

where q represents the weight (dead load) whereas $h(x,t)$ is a live load; $\delta > 0$ is the damping coefficient. After division by EI and the changes of variables

$$u(x,t) \to u\left(x, \sqrt{\tfrac{EI}{m}}t\right), \quad \frac{h\left(x, \sqrt{\frac{m}{EI}}t\right)}{EI} \to \varepsilon h(x,t), \quad \frac{\delta}{\sqrt{m\,EI}} \to \delta, \quad \frac{k}{EI} \to k, \quad \frac{q}{EI} \to q,$$

the equation may be rewritten as

$$u_{tt} + u_{xxxx} + \delta u_t + ku^+ = q + \varepsilon h(x,t)\,, \qquad x \in (0,\pi)\,, \quad t > 0\,. \tag{2.102}$$

Fonda et al. [113] found large amplitude subharmonic solutions of (2.101) with hinged boundary conditions by assuming that the forcing term is periodic; subharmonic means here periodic solutions whose period is an integer multiple of the period of the forcing term h. Their conclusion [113, p. 138] is that their results

> ... should at least produce the suspicion that the oscillation could have been of a nonlinear nature.

Consider again a hinged beam so that u satisfies (2.95). We now drop the symmetry assumption (2.96) and consider the more general spaces

$$H = \left\{ \psi : [0,\pi] \times \mathbb{R}_+ \to \mathbb{R};\ \psi(x,\cdot) \text{ is } \pi\text{-periodic},\ \int_0^\pi \int_0^\pi \psi(x,t)^2 dxdt < +\infty \right\},$$

$$D = \{ \psi \in H \cap C^\infty([0,\pi] \times \mathbb{R}_+);\ \psi(0,t) = \psi(\pi,t) = \psi_{xx}(0,t) = \psi_{xx}(\pi,t) = 0\ \forall t > 0 \}.$$

We say that $u \in L^2\big((0,\pi)^2\big)$ is a weak solution of (2.102)–(2.95) if

$$\int_0^\pi \int_0^\pi (\phi_{tt} + \phi_{xxxx} - \delta\phi_t) u\, dxdt = \int_0^\pi \int_0^\pi (q + \varepsilon h - k u^+)\phi\, dxdt \qquad \forall \phi \in D.$$

The following result is due to Berkovits et al. [45]:

Theorem 2.14 *Assume $\delta > 0$. For all $h \in H$ there exists $\varepsilon_h > 0$ such that if $|\varepsilon| < \varepsilon_h$ then the problem (2.102)–(2.95) admits a unique weak solution.*

Some remarks are in order. Theorems 2.12 and 2.14 show a striking difference between the undamped and the damped equation: multiplicity against uniqueness of periodic solutions. Although the equations considered are of hyperbolic type, some regularity for the solutions is available and one may find strong solutions. Finally, let us mention that any period $T > 0$ in time can replace $T = \pi$ in the statements.

2.8.2 A Cable-Beam System with Possibly Slackening Hangers

In the previous section, we considered the case where a beam is sustained, through nonlinear hangers, to a fixed base as in Fig. 2.20. We consider here the case where the fixed base is replaced by an extensible cable, see the model represented in Fig. 2.5 where the sustaining cable may increase its length if forced by a load. Since time is introduced, we denote now by $u = u(x,t)$ and $v = v(x,t)$, respectively, the downwards displacements of the beam and the cable. The same arguments developed so far lead to the system

$$\begin{cases} m_c\, v_{tt} - H\, v_{xx} + \delta_c v_t - k(u-v)^+ = q_c + f_c(x,t) & x \in (0,\pi),\ t > 0, \\ m_b\, u_{tt} + EI\, u_{xxxx} + \delta_b u_t + k(u-v)^+ = q_b + f_b(x,t) & x \in (0,\pi),\ t > 0, \end{cases} \tag{2.103}$$

where v and u are the displacements of, respectively, the cable and the beam, both measured in the downwards direction. The cable is assumed to be fixed at its endpoints whereas the beam is hinged; this leads to the boundary conditions

$$v(0,t) = v(\pi,t) = u(0,t) = u(\pi,t) = u_{xx}(0,t) = u_{xx}(\pi,t) = 0 \qquad \forall t > 0. \tag{2.104}$$

The constants appearing in (2.103) have the following meaning:

m_c and m_b are the masses per unit length of, respectively, the cable and the beam;
$q_c = m_c g$ and $q_b = m_b g$ are the weights per unit length of, respectively, the cable and the beam;
H is the horizontal component of the tension of the cable, see (2.12);
EI is the flexural rigidity of the beam;
δ_c and δ_b are the structural damping of, respectively, the cable and the beam;
$k > 0$ is the elastic Hooke constant of the hangers.

The positive part $(u - v)^+$ describes again the fact that the hangers exert a restoring force only under extension while if compressed they slacken. This is a crucial difference with the classical systems in [50, 234] described in Sect. 2.7.1, where the hangers were treated as inextensible rods, incapable of either extension or compression. Numerical results lead Lazer and McKenna [168, p. 561] to the following explanation of oscillations in bridges in violent storms:

> First, the gusts of wind would act as a random large buffeting force on the cable superstructure, causing the towers and cable to go into a high frequency periodic motion (much as what happens when a guitar string is struck randomly). Then ... nonlinear coupling would take place, and the bridge would go into a low frequency motion.

This is the reason why the live load f_c plays a major role, the action of the wind starts by moving the cables. Let us also mention that somehow surprising numerical results by Humphreys and Shammas [146] (see also [113, 144, 145]) show that if a nonlinear mechanical model of a suspension bridge is subject to a low-frequency periodic force, it may give different responses, some of them having high-frequency components.

In literature both periodic solutions and solutions of the Cauchy problem

$$v(x,0) = v_0(x),\ v_t(x,0) = v_1(x),\ u(x,0) = u_0(x),\ u_t(x,0) = u_1(x), \qquad \forall x \in (0,\pi) \tag{2.105}$$

have been considered. Similar to problem (2.100), also well-posedness of (2.103) was proved. We summarise some results in the following informal statement.

Proposition 2.15

(*i*) *If $\delta_c = \delta_b = 0$, if $k > 0$ lies in a suitable range and if $f_c(x,\cdot)$ and $f_b(x,\cdot)$ are periodic and sufficiently small, then there exists at least two t-periodic solutions (u, v) of (2.103) and (2.104).*

(*ii*) *If $\delta_c, \delta_b > 0$, if $m_c \ll m_b$ and if $f_c(x,\cdot)$ and $f_b(x,\cdot)$ are periodic and sufficiently small, then there exists a unique t-periodic solution (u, v) of (2.103) and (2.104).*

(*iii*) *For any f_c and f_b (not necessarily periodic) there exists a unique solution (u, v) of (2.103)–(2.104)–(2.105).*

We refer to Sect. 2.9 for the references to the precise statements.

We conclude this section by emphasising that (2.103) is considered also in the engineering community, see e.g. [175] where the interactions between moving vehicle loads and vertical seismic excitations are studied in a suspension bridge.

Since the Tacoma Bridge collapse was mainly due to a wide torsional motion of the bridge, see [253], the bridge cannot be considered as a one dimensional beam. If some model aims to display the instability of bridges, it should necessarily take into account more degrees of freedom than just a beam. In fact, to be exhaustive one should consider vertical oscillations y of the roadway, its torsional angle θ, and coupling with the two sustaining cables u and v. This model was suggested by Matas and Očenášek [187] who consider the hangers as linear springs and obtain a system of four equations; three of them are second order wave-type equations, the last one is again a fourth order equation such as

$$m\, y_{tt} + k\, y_{xxxx} + \delta\, y_t + E_1(y - u - \ell \sin\theta) + E_2(y - v + \ell \sin\theta) = W(x) + f(x,t)\,;$$

we refer to (SB_4) in [99] for an interpretation of the parameters involved.

2.8.3 Stretching Energy in a Compressed Beam

In 1744, Euler [102] gave a mathematical description of the action of an axial thrust on a uniform elastic beam and he reduced this problem to a description of the solutions of the following quasilinear boundary value problem

$$u''(x) + Pu(x)\Big(1 + u'(x)^2\Big)^{3/2} = 0\,, \quad u(0) = u(1) = 0\,.$$

Euler found that the beam deflects out of its plane which means, in modern language, that the beam is subject to buckling: if $P > 0$ is large enough this problem also admits nontrivial solutions.

Woinowsky-Krieger [279] modified the classical beam theory by Bernoulli–Euler assuming a nonlinear dependence of the axial strain on the deformation gradient, by taking into account the midplane stretching of the roadway due to its elongation. For simplicity, we consider again a beam modeled by the segment $x \in (0,\pi)$. The resulting nonlinear beam equation reads

$$m\, u_{tt} + EI\, u_{xxxx} + \Big[\gamma - M\, \|u_x\|^2_{L^2(0,\pi)}\Big] u_{xx} = f \quad x \in (0,\pi)\ t > 0\,, \tag{2.106}$$

where the term $M\, \|u_x\|^2_{L^2(0,\pi)} = M \int_0^\pi u_x(x,t)^2 dx$ takes into account the geometric nonlinearity of the beam due to its stretching and $\gamma > 0$ is the axial force acting at the endpoints of the beam; we have a positive γ because the beam is compressed (see e.g. the Deer Isle Bridge in Fig. 1.14) while a negative γ would mean that the beam is stretched. The constant $M > 0$ depends on the elasticity of the material composing the beam. Here $f = f(x,t)$ is an external load.

More recently, Bochicchio et al. [52–54] connected the beam, as described by Eq. (2.106), with a moving cable through hangers, thereby generalising (2.103). The equations now read

$$\begin{cases} m_c v_{tt} - H v_{xx} + \delta_c v_t - k(u-v)^+ = q_c + f_c(x,t) \qquad x \in (0,\pi),\ t>0, \\ m_b u_{tt} + EI u_{xxxx} + \delta_b u_t + \left[\gamma - M\|u_x\|^2_{L^2(0,\pi)}\right] u_{xx} + k(u-v)^+ = q_b + f_b(x,t), \end{cases} \tag{2.107}$$

where the constants have the same meaning as in (2.103) and (2.106). This system is complemented with the boundary and initial conditions (2.104) and (2.105). Well-posedness of this problem is known:

Proposition 2.16 *For any f_c and f_b there exists a unique solution (u,v) of* (2.107)–(2.104)–(2.105).

The first step to understand the dynamics of the model described by (2.107) is to study its stationary solutions. By dropping all the loads and by normalising the constants, we are led to the following system of ODE's:

$$\begin{cases} u''''(x) + \left[\gamma - \frac{2}{\pi}\|u'\|^2_{L^2(0,\pi)}\right] u''(x) + k\big(u(x)-v(x)\big)^+ = 0 \quad x \in (0,\pi) \\ -v''(x) - k\big(u(x)-v(x)\big)^+ = 0 \quad x \in (0,\pi)\,, \end{cases} \tag{2.108}$$

complemented with the boundary conditions

$$v(0) = v(\pi) = u(0) = u(\pi) = u''(0) = u''(\pi) = 0\,. \tag{2.109}$$

Bochicchio et al. [53] proved the following statement.

Theorem 2.17 *If $\gamma < 1$ then $(u,v) = (0,0)$ is the unique solution of* (2.108) *and* (2.109).

If $\gamma > 1$ then (2.108) *and* (2.109) *also admits the solution $u(x) = -\sqrt{\gamma-1}\sin(x)$, $v(x) = 0$.*

If $\gamma > \frac{1+2k}{1+k}$ then (2.108) *and* (2.109) *also admits the solution*

$$u(x) = \sqrt{\gamma - \frac{1+2k}{1+k}}\,\sin(x)\,, \quad v(x) = \frac{k}{1+k}\sqrt{\gamma - \frac{1+2k}{1+k}}\,\sin(x)\,.$$

The trivial solution $(u,v) = (0,0)$ corresponds to the position at rest and exists for any $\gamma > 0$. For large enough γ, that is $\gamma > 1$, there is a buckling effect and Theorem 2.17 states that there exists also an additional equilibrium position where the beam is displaced upwards ($u < 0$) while the cable is at rest ($v = 0$); in this case the hangers are slacken because $u - v < 0$ and $(u-v)^+ = 0$. If we increase further

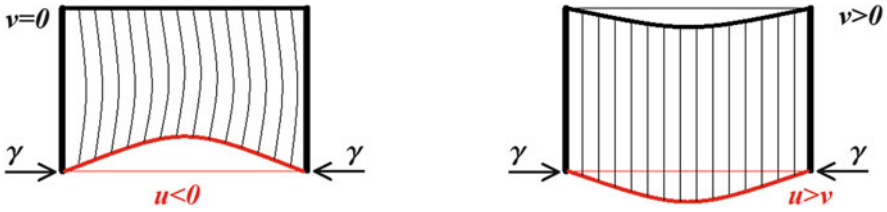

Fig. 2.21 Slacken hangers (*left*) and hangers in tension (*right*), as described in Theorem 2.17

γ, that is $\gamma > 1 + \frac{k}{1+k}$, there is another equilibrium position where the hangers are in tension since $u - v > 0$. These two situations are described in Fig. 2.21.

By recalling the meaning of γ, we conclude that if the beam is weakly compressed at the endpoints then there exists only the trivial equilibrium position, while if the beam is strongly compressed there exist two additional equilibrium positions, one with slack hangers and the other with hangers in tension.

2.9 Bibliographical Notes

The study of the deflection of cables goes back to the Swiss mathematician Jacques Bernoulli (1654–1705). All the material from Sects. 2.2–2.4 is by now classical and may be found in several sources; here we followed [199, Sect. 3], [48, Chap. VII], [84, Sect. 4] and [123, Sect. 1.1.1]. Not enough credit is given in literature to Melan [199] for his contribution and for his fundamental equation (2.1). It was Steinman who took care of the translation to English of the book by Melan; but then, in his subsequent monograph he quotes [199] as "Melan–Steinman", see [248, Footnote p. 19]. Moreover, [9, 48, 234, 245] and several subsequent papers make no mention of [199].

The necessity of having exact parameters of catenaries modeling cables is known since the very beginning of the history of suspension bridges, see [133]. For a modern modeling of elastic cables and an accurate technical description of different kinds of cables, the interested reader may have a look at the monograph by Lacarbonara [160, Chap. III] and at the contribution by Podolny [221].

The Young modulus is named after the British scientist Thomas Young (1773–1829). However, the concept was developed in 1727 by the Swiss mathematician Leonhard Euler (1707–1783), and the first experiments that used the concept of Young modulus in its current form were performed in 1782 by the Italian scientist Giordano Riccati (1709–1790), predating Young work by 25 years, see *The Rational Mechanics of Flexible or Elastic Bodies, 1638–1788: Introduction to Leonhardi Euleri Opera Omnia, Volumes X and XI*.

The problem of computing the additional tension (2.28), see Sect. 2.5.1, was also initially studied by Melan [199] (see also [48]) who suggested (2.32). The alternative form (2.33) is taken from [124], while Timoshenko [261, (11.16)]

suggested (2.34). All the material in Sect. 2.5 is an extended version of a paper by Gazzola et al. [124] where one can find the proofs of Theorems 2.2, 2.3, and 2.5.

In its full complete form, (2.91) was essentially suggested by Rocard [234]; he first considers the linearised equation, then he adds the nonlinear term, the source and the damping term. All the rest of the material from Sect. 2.7 is taken from [50, 234, 239, 245]. The Report [245] studies in detail the effect of the torsional rigidity of towers and the energy of vibrations in dependence of the modes of vertical oscillations; this is done for several different structures (flexible bridges, bridges with stiffening trusses, bridges with torsional rigidity).

Both Bleich [50, (7.16)] and Rocard [234, p. 167] exhibit coupled linear equations to describe vertical and torsional oscillations. In this case, it is well-known that a suitable change of unknowns (a diagonalisation procedure) will decouple the equations. Moreover, solutions of linear equations cannot display self-excited oscillations.

With few variants, Eq. (2.91) seems nowadays to be well-accepted among engineers, see e.g. [84, Sect. VII.4]; moreover, quite similar equations are derived to describe related phenomena in cable-stayed bridges [63, (1)] and in arch bridges traversed by high-speed trains [161, (14)–(15)].

Abdel-Ghaffar [1] makes use of variational principles to obtain the combined equations of a suspension bridge motion in a fairly general nonlinear form although he starts with the "usual" linearisation $\sin\theta \simeq \theta$, see [1, (1)]. The effect of coupled vertical-torsional oscillations as well as cross-distortional of the stiffening structure is clarified by separating them into four different kinds of displacements: the vertical displacement v, the torsional angle θ, the cross section distortional angle ψ, the warping displacement u which can be expressed in terms of θ and ψ. After making such huge effort (with an unjustified initial linearisation), Abdel-Ghaffar simplifies the problem by neglecting the cross section deformation, the shear deformation and rotatory inertia; he obtains a coupled nonlinear vertical-torsional system of two equations in the two unknowns functions v and θ. These equations are finally linearised further, by neglecting terms considered small when compared with the initial tension H. Then the coupling effect disappears and Eq. (2.93) are recovered, see [1, (34)–(35)].

Section 2.6.3 contains results by Gazzola and Pavani [129] where one can also find several tables with detailed numerical results. The material in Sect. 2.7 is taken from [50, 234, 245]. The copyright for *the wake of Tacoma* has to be attributed to Scott [241].

As we have seen in Sect. 2.7, after the pioneering equation (2.1) by Melan [199] and the TNB collapse the attention of engineers has turned to improving performances of bridges through design factors or how to solve structural problems, rather than improving the mathematical models. Only modeling modern footbridges has attracted some interest from a theoretical point of view. As already mentioned, pedestrian bridges are extremely flexible and display elastic behaviors similar to suspension bridges, although the oscillations are of different kind. In [55] a simple 1D model was proposed in order to describe the crowd-flow phenomena occurring when pedestrians walk on a flexible footbridge.

Equation (2.66) arises in several contexts. With no hope of being exhaustive, let us mention some related models. When $T > 0$ (2.66) is known as the extended Fisher–Kolmogorov equation, whereas when $T < 0$ it is referred to as Swift–Hohenberg equation, see [216]. For $f(w) = w - w^2$, (2.66) arises in the dynamic phase-space analogy of a nonlinearly supported elastic strut [147]. In [7] the existence of even homoclinics to $w \equiv 0$ was proved whenever $T \geq 0$. When $f(w) = w^3 - w$, (2.110) serves as a model of pattern formation in many physical, chemical or biological systems, see [56, 57] and references therein. The slightly different nonlinearity $f(w) = w - w^3 + w^5$ was used in [217] in order to investigate localisation and spreading of deformation of a strut confined by an elastic foundation. After a change of variables, (2.66) with $T = \frac{n^2-4n+8}{2} > 0$ and $f(w) = \frac{n^2(n-4)^2}{16} w + |w|^{8/(n-4)} w$ appears in the study of radial entire solutions of critical biharmonic equations in $\mathbb{R}^n$ ($n \geq 5$), see [122]. Last but not least, we mention the book by Peletier and Troy [216] where one can find more physical models, a survey of existing results, and further references.

The model described in Fig. 2.12 is taken from [121]. Theorem 2.8 is due to Berchio et al. [35]; in this paper, one may find more qualitative properties of the solutions of (2.110). Theorem 2.9 is due to Gazzola and Pavani [128]. This theorem has been recently extended to the case $-2 < T < 0$, see [228]: in this case, T does not represent the tension but $-T > 0$ may be seen as the squared velocity of traveling waves for the general equation (2.111), see (2.110). The numerical results and the material in Sect. 2.6 are taken from [35, 125–128] where one can find further properties of the solutions of (2.110), different nonlinearities f, more detailed description of how the blow up occurs. In particular, since the term $|w''(x)|$ measures the vertical acceleration whereas $|w(x)|$ measures the vertical displacement, [128, Theorem 3] states that the vertical acceleration has a higher rate of blow up when compared with the vertical displacement. The generalised assumptions (2.72)–(2.73)–(2.74) are due to Gazzola and Karageorgis [125]. Figures 2.14 and 2.15 are taken from [121]. We refer again to [126–128] for further plots. We also refer to [125, 126, 128] for numerical results and plots of solutions of (2.66) with nonlinearities $f = f(w)$ having different growths as $w \to \pm\infty$. In such case, the solution still blows up according to (2.67) but, although its "limsup" and "liminf" are respectively $+\infty$ and $-\infty$, the divergence occurs at different rates.

The story of the book [50] is quite sad since two of the authors (McCullough and Bleich) passed away during its preparation. This book appears to be the first reference for a systematic theoretical treatise of vibrations in suspension bridges. It certainly appears more of theoretical than of practical interest since engineers usually refer to it for the models but not for the quantitative analysis.

A further source to derive the equation of vertical oscillations in suspension bridges is [234, Chap. IV] where all the details are explained. The author, the French physicist Yves-André Rocard (1903–1992), also helped to develop the atomic bomb for France after the end of the second world war.

The beam equation (2.94) was suggested by Lazer and McKenna [167], Theorem 2.12 and the subsequent comments are due to McKenna and Walter [196]. For stability results of large solutions of (2.98)–(2.95) we refer to [134]. For the study of periodic solutions of (2.98) with free boundary conditions (floating beam) we refer to [201, 202]. The first traveling waves for (2.100) were obtained by McKenna and Walter [197] by sticking together the solutions in the two regimes when the hangers exert a restoring force and when they are slacken. The first part of Theorem 2.13 is due to Chen and McKenna, see [75, Theorem 2.7], the behavior as $c \to 0$ is due to Lazer and McKenna [169, Theorem 2]. Slightly more general nonlinearities are considered in [75, Theorem 2.9]: they also study the stability of traveling waves and they numerically show that not only some of them are extremely stable but also that when two such waves collide, they interact nonlinearly and then emerge intact. Multiplicity results for traveling waves were obtained in [73]: multiplicity means here not merely traveling waves which are translations of each other but which are substantially different. After some normalisation, by seeking traveling waves of (2.100) of the kind $u(x,t) = 1 + w(x - ct)$, McKenna and Walter [197] reach the following ODE

$$w''''(\tau) + c^2 w''(\tau) + f(w(\tau)) = 0 \qquad (x - ct = \tau \in \mathbb{R}) \tag{2.110}$$

where $f(w) = (w+1)^+ - 1$. Subsequently, in order to maintain the same behavior but with a smooth nonlinearity, Chen and McKenna [75] suggest to consider (2.110) with $f(w) = e^w - 1$. Note that both these nonlinearities satisfy (2.65) and that (2.110) resembles to (2.66) with a different sign for the coefficient of w''; we recall that Theorem 2.8 holds for any coefficient multiplying w''. We also notice that (2.100) is a special case of the more general semilinear fourth order wave equation

$$u_{tt} + u_{xxxx} + f(u) = 0\,, \qquad x \in \mathbb{R}\,, \quad t > 0\,, \tag{2.111}$$

where the natural assumptions on f are (2.65) plus further conditions, according to the model considered. Traveling waves of (2.111) solve (2.110). For $f(u) = (u+1)^+ - 1$ and its variants, Benci and Fortunato [32] proved the existence of special solutions of (2.110) deduced by solitons of the beam equation (2.111) while we refer to [59] for a computer assisted proof of the existence of multiple traveling waves. Recent results in [228] show that there exist no traveling waves of (2.111) if f is as in (2.69), see also [110] for an alternative proof. The blow-up profile for (2.66) has been studied in [87].

The rigorous statements and proofs of the results contained in Proposition 2.15 may be found in the following references: statement (*i*) is taken from [95, Theorem 2.2] where some technical restrictions on the parameters are made and the same symmetries as Theorem 2.12 are assumed, statement (*ii*) is taken from [100, Theorem 4.2], while statement (*iii*) is quite standard, see [4, Theorem 4.6] where the initial data (2.105) satisfy $u_0 \in H^2 \cap H_0^1(0,\pi)$, $v_0 \in H_0^1(0,\pi)$, $u_1, v_1 \in L^2(0,\pi)$. We also refer to [99] for a condensed survey of results and for further references.

Equation (2.106) was suggested by Woinowsky-Krieger [279]; the nonlinear problem of the free vibrations of a bar with hinged ends is reduced to a nonlinear ordinary differential equation which is solved with the aid of elliptic functions. A table then gives numerical values of frequencies versus amplitude of vibration. Complemented with the initial and hinged boundary conditions (2.104) and (2.105), Eq. (2.106) has then been intensively studied by Dickey [93, 94] and Ball [27, 28].

The beam equation (2.106) with an additional restoring force ku^+, as in (2.97) was introduced in [51] where well-posedness was also established, see [51, Proposition 2.1]. Since this models the case where the sustaining cable is fixed, we skipped directly to the more reliable model (2.107); here the coupling term is just $k(u-v)^+$ and we refer to [54] for more general coupling terms involving also the derivatives u_t and v_t. The proof of Proposition 2.16 is somehow standard and may be obtained with the Galerkin method, see [52, Proposition 2.3] and [53, Proposition 4.1]. Theorem 2.17 is due to Bochicchio et al. [53, Theorem 3.2].

Chapter 3
A Fish-Bone Beam Model

In the previous chapter we saw beam models for the main span of a bridge, within different equations and different coupling with the sustaining cable. However, modeling the roadway of a suspension bridge as a beam prevents to highlight the most dangerous oscillations in bridges, the torsional oscillations which are considered responsible for the TNB collapse. If one wishes to give an answer to question **(Q1)** raised in Sect. 1.6, the bridge cannot be seen as a simple one dimensional beam.

In this chapter we study a fish-bone beam model which also allows to describe torsional oscillations. We give both theoretical and numerical explanations of the structural mechanism which creates a sudden appearance of torsional oscillations. The main theoretical tools are suitable Hill equations and related stability criteria. We study a mechanically isolated system and we show that its conserved internal energy may transfer from vertical oscillating modes to torsional modes. This happens when enough energy is present within the structure. We name flutter energy the critical energy threshold where this transfer may occur. The conclusion is that if the internal energy exceeds the flutter energy then torsional oscillations suddenly appear and this mechanism is purely structural, with no aerodynamic effect. Since the energy is strictly related to the width of the amplitudes, torsional oscillations arise only when vertical oscillations are sufficiently large. A simplified analysis explains which torsional mode captures the energy of the active vertical mode.

We also analyse the effect of aerodynamic forces: the theoretical and numerical results suggest that the aerodynamic forces do not create torsional instability but they play a destructive role only after that the structural instability is manifested.

F. Gazzola, *Mathematical Models for Suspension Bridges*, MS&A 15,
DOI 10.1007/978-3-319-15434-3_3

3.1 A Beam Showing Torsional Oscillations

Consider a suspension bridge whose main span has length L and width 2ℓ, let $y = y(x,t)$ denote the vertical deflection of the bridge axis and let $\theta = \theta(x,t)$ be the angle of torsion of the cross-section. In Fig. 3.1 we sketch the model that we call **fish-bone**. The grey part is the roadway, the two extremal black cross sections are fixed and the plate is hinged there. The red line contains the barycenters of the cross sections and is the line where y is computed. The green orthogonal lines are virtual cross sections that can rotate around their barycenter and the angle of rotation with respect to the horizontal position is denoted by θ.

The kinetic energy of a rotating object is $\frac{1}{2} I \dot{\theta}^2$ where I is the moment of inertia and $\dot{\theta}$ is the angular velocity. The moment of inertia of a rod of length 2ℓ about the perpendicular axis through its center is given by $\frac{1}{3} m \ell^2$ where m is the mass of the rod. Hence,

$$\begin{aligned} &\text{the kinetic energy of a rod having mass } m \text{ and half-length } \ell, \\ &\text{rotating about its center with angular velocity } \dot{\theta}, \text{ is given by } \tfrac{m}{6} \ell^2 \dot{\theta}^2 . \end{aligned} \tag{3.1}$$

In this chapter we consider systems of PDE's based on this model. We will see that linear equations do not allow to explain the possible appearance of torsional oscillations while nonlinear equations do. In particular, the results obtained will enable us to give an answer to the main question **(Q1)** raised in Sect. 1.6: when enough energy is present within the model, a sudden transition between vertical and torsional oscillations may occur. The reason is a kind of internal resonance which gives rise to an instability. The target is then to estimate the energy threshold of instability: we will give both theoretical and numerical bounds. We will also explain the criterion which determines the torsional mode which will capture the energy of the system.

A linearised fish-bone model has been previously studied with other tools such as parametric resonance. Hence, in next section we start by recalling its story.

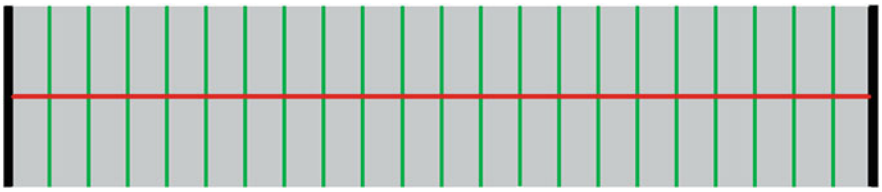

Fig. 3.1 The fish-bone model

3.2 Parametric Resonance in a Linearised Model

Pittel-Yakubovich [219] suggest, as differential equations for the vertical-torsional oscillations of the bridge modeled by the just described fish-bone, the system

$$\begin{cases} my_{tt} - \rho I y_{xxtt} + EIy_{xxxx} - Hy_{xx} + \frac{W}{2}\,(x(L-x)\theta)_{xx} = 0 & x \in (0,L),\ t > 0 \\ \frac{m\ell^2}{3}\theta_{tt} - \gamma_1\theta_{xxtt} + \frac{W}{2}x(L-x)y_{xx} + \gamma_2\theta_{xxxx} - \mu\theta_{xx} - W\ell\theta = 0 & x \in (0,L),\ t > 0 \\ y(0,t) = y(L,t) = y_{xx}(0,t) = y_{xx}(L,t) = 0 & t > 0 \\ \theta(0,t) = \theta(L,t) = \theta_{xx}(0,t) = \theta_{xx}(L,t) = 0 & t > 0\,, \end{cases} \tag{3.2}$$

where L is the length of the roadway while 2ℓ is its width, m is the mass per unit length in the x-direction, ρ is the density of the material, I is the moment of inertia of the cross-section, EI is the flexural rigidity, H is the tension of the cables, W is the uniformly distributed horizontal wind load, γ_1 and γ_2 are two geometric parameters of the cross section, $\mu = GJ + H\ell^2$ (with $G =$ shear modulus, $J =$ moment of inertia of the pure torsion). All these constants are positive.

An interesting approach to study the instability of this model consists in the so-called parametric resonance. In Sect. 1.7.5 we saw a simple application of this approach. In the present situation, one puts $U^T = (y, \theta)$ so that U is a column vector and system (3.2) may be written as

$$\frac{d^2}{dt^2}(MU) + AU = 0 \qquad (A = A_0 + WA_1) \tag{3.3}$$

where

$$MU = \begin{pmatrix} my - \rho I y_{xx} \\ \frac{m\ell^2}{3}\theta - \gamma_1\theta_{xx} \end{pmatrix}, \quad A_0U = \begin{pmatrix} EIy_{xxxx} - Hy_{xx} \\ \gamma_2\theta_{xxxx} - \mu\theta_{xx} \end{pmatrix}, \quad A_1U = \begin{pmatrix} \frac{1}{2}\,(x(L-x)\theta)_{xx} \\ \frac{1}{2}x(L-x)y_{xx} - \ell\theta \end{pmatrix}.$$

Several integrations by parts show that, for all $U, V \in C^4[0,L]$ satisfying the boundary conditions in (3.2), we have

$$(MU,V)_{L^2(0,L)} = \int_0^L MU \cdot V = (MV,U)_{L^2(0,L)}\,, \quad (A_0U,V)_{L^2(0,L)} = (A_0V,U)_{L^2(0,L)}\,,$$
$$(MU,U)_{L^2(0,L)} \geq c_1\|U\|^2_{H^1(0,L)}\,, \quad (A_0U,U)_{L^2(0,L)} \geq c_2\|U\|^2_{H^2(0,L)}\,,$$

for some $c_1, c_2 > 0$. Whence, M and A_1 are symmetric positive operators. The theory of self-adjoint differential operators then tells us that (3.3) is stable if and only if all the eigenvalues of A are positive. Since $U \equiv 0$ solves (3.3), stability means here that this trivial solution is stable, that is, that any solution of (3.3) is globally bounded. This is certainly true if $W = 0$ because A_0 is positive definite. The important parameter is then

$$\overline{W} := \min\{W > 0;\ \text{the least eigenvalue of } A \text{ is } 0\}\,.$$

It can be shown that system (3.3) is stable if $0 \leq W < \overline{W}$ and unstable if $W \geq \overline{W}$. Unfortunately, $\overline{W}$ is not easily determined in dependence of the parameters in the system and one is led to find lower bounds. We refer to [282, Sect. IV.1.1] for some possible lower bounds. The doubts about this approach are the usual ones: is a linear model sufficiently accurate? what are the correct assumptions on the wind?

3.3 A Nonlinear Version

3.3.1 Well Posedness

In this section we introduce some nonlinearities in the fish-bone model (3.2). At the same time, we neglect some terms, in particular the mixed derivatives. We also drop damping and forcing: the former because its only effect is to diminish the amplitudes of the oscillations, the latter because the frequency of the external force may give rise to unexpected responses [144–146]. From [233, p. 26] we learn that the nonlinear behavior of a suspension bridge is mainly due to the changes of the cables geometry. Since the cables are connected to the fish-bone beam through the hangers, the nonlinearity should explicitly appear in the restoring force due to the hangers, both because they are extensible springs not obeying the Hooke law and because they transmit the nonlinear behavior of the cables. The latter cause was suggested by Bartoli-Spinelli [30, p. 180] who, in their model, assume that

> The nonlinear behavior of the two springs has been evaluated thinking the cables as the only cause of this nonlinearity.

We consider the system

$$\begin{cases} m y_{tt} + EI y_{xxxx} + f(y + \ell \sin\theta) + f(y - \ell \sin\theta) = 0 & 0 < x < L \quad t > 0 \\ \frac{m\ell^2}{3}\theta_{tt} - \mu\ell^2\theta_{xx} + \ell\cos\theta\,(f(y + \ell\sin\theta) - f(y - \ell\sin\theta)) = 0 & 0 < x < L \quad t > 0, \end{cases} \tag{3.4}$$

where $\mu > 0$ is a constant depending on the shear modulus and the moment of inertia of the pure torsion, $EI > 0$ is the flexural rigidity of the beam (both as in (3.2)) while f represents the restoring action of the prestressed hangers and also includes the action of gravity. We have not yet simplified by ℓ the second equation in (3.4) in order to emphasise all the terms.

To (3.4) we associate the following boundary-initial conditions:

$$y(0,t) = y_{xx}(0,t) = y(L,t) = y_{xx}(L,t) = \theta(0,t) = \theta(L,t) = 0 \qquad t \geq 0 \tag{3.5}$$

$$y(x,0) = \eta_0(x),\ y_t(x,0) = \eta_1(x),\ \theta(x,0) = \theta_0(x),\ \theta_t(x,0) = \theta_1(x) \quad 0 < x < L. \tag{3.6}$$

The first four boundary conditions in (3.5) model a beam hinged at its endpoints whereas the last two boundary conditions model the fixed cross sections between towers.

It is not our purpose to give the precise quantitative behavior of the model under consideration. Therefore, we make several simplifications which do not modify the qualitative behavior of the nonlinear system (3.4). First of all, up to scaling we may assume that $L = \pi$; this will simplify the Fourier series expansion. Then we take $EI = 3\mu = 1$ although these parameters may be fairly different in actual bridges. Moreover, we are not interested in describing accurately the behavior of the bridge under large torsional oscillations. Instead, we are willing to describe how small torsional oscillations may suddenly become larger ones. And if θ is small (and only in this case), then the approximations $\sin\theta \cong \theta$ and $\cos\theta \cong 1$ are legitimate; these approximations will be fully justified in Sect. 3.3.2. Then we set $z := \ell\theta$ and this cancels the dependence of (3.4) on the width ℓ; to recover the dependence on ℓ, note that $\theta = \frac{z}{\ell}$ so that

smaller ℓ yield larger θ, that is, less stability. (3.7)

Finally, note that the change of variable $t \mapsto \sqrt{m}t$ results in a positive or negative delay in the occurrence of any (possibly catastrophic) phenomenon; whence, we may take $m = 1$. After all these changes, (3.4) becomes

$$\begin{cases} y_{tt} + y_{xxxx} + f(y+z) + f(y-z) = 0 \ (0 < x < \pi,\ t > 0) \\ z_{tt} - z_{xx} + 3f(y+z) - 3f(y-z) = 0 \quad (0 < x < \pi,\ t > 0)\,. \end{cases} \tag{3.8}$$

The boundary-initial conditions (3.5)–(3.6) may be rewritten as

$$y(0,t) = y_{xx}(0,t) = y(\pi,t) = y_{xx}(\pi,t) = z(0,t) = z(\pi,t) = 0 \quad t \geq 0 \tag{3.9}$$

$$y(x,0) = \eta_0(x),\ y_t(x,0) = \eta_1(x),\ z(x,0) = \zeta_0(x),\ z_t(x,0) = \zeta_1(x) \quad 0 < x < \pi \tag{3.10}$$

where $\zeta_0(x) := \ell\theta_0(x)$ and $\zeta_1(x) := \ell\theta_1(x)$. If $f(0) = 0$ and f is nondecreasing, as in the physical situation, then

$$F(s) := \int_0^s f(\tau)\,d\tau > 0 \tag{3.11}$$

is a convex function. Therefore, the convex and coercive functional (here $' = \frac{d}{dx}$)

$$J(y,z) = \frac{\|y''\|_2^2}{2} + \frac{\|z'\|_2^2}{6} + \int_0^\pi [F(y+z) + F(y-z)]\,dx$$
$$\forall\, y \in H^2 \cap H_0^1(0,\pi), \qquad \forall\, z \in H_0^1(0,\pi)$$

admits a unique critical point, which is the absolute minimum and coincides with $(y, z) = (0, 0)$; in this section $\|\cdot\|_2$ denotes the $L^2(0,\pi)$-norm. Hence, (3.8) admits a unique stationary solution (equilibrium) given by $y = z = 0$ and corresponding to the initial conditions $\eta_0 = \eta_1 = \zeta_0 = \zeta_1 = 0$.

We say that the functions

$$y \in C^0(\mathbb{R}_+; H^2 \cap H_0^1(0,\pi)) \cap C^1(\mathbb{R}_+; L^2(0,\pi)) \cap C^2(\mathbb{R}_+; H^*(0,\pi))$$
$$z \in C^0(\mathbb{R}_+; H_0^1(0,\pi)) \cap C^1(\mathbb{R}_+; L^2(0,\pi)) \cap C^2(\mathbb{R}_+; H^{-1}(0,\pi))$$

are solutions of (3.8)–(3.9)–(3.10) if they satisfy the initial conditions (3.10) and

$$\langle y_{tt}, \varphi\rangle_{H^*} + (y_{xx}, \varphi'') + (f(y-z) + f(y+z), \varphi) = 0 \quad \forall\, \varphi \in H^2 \cap H_0^1(0,\pi)\,, \forall t > 0\,,$$
$$\langle z_{tt}, \psi\rangle_{H^{-1}} + (z_x, \psi') + 3(f(y+z) - f(y-z), \psi) = 0 \quad \forall\, \psi \in H_0^1(0,\pi)\,, \forall t > 0\,,$$

where $\langle\cdot,\cdot\rangle_{H^{-1}}$ and $\langle\cdot,\cdot\rangle_{H^*}$ are the duality pairings in $H^{-1} = (H_0^1(0,\pi))'$ and $H^* = (H^2 \cap H_0^1(0,\pi))'$ while $(\cdot,\cdot)$ denotes the scalar product in $L^2(0,\pi)$. From [36] we know that the problem is well-posed.

Theorem 3.1 *Let $\eta_0 \in H^2 \cap H_0^1(0,\pi)$, $\zeta_0 \in H_0^1(0,\pi)$, $\eta_1, \zeta_1 \in L^2(0,\pi)$. Assume that $f \in \mathrm{Lip}_{loc}(\mathbb{R})$ is nondecreasing, with $f(0) = 0$, and $|f(s)| \le C(1 + |s|^p)$ for every $s \in \mathbb{R} \setminus \{0\}$ and for some $p \ge 1$. Then there exists a unique solution (y, z) of (3.8)–(3.9)–(3.10).*

The main concern is then to establish if the solution is torsionally stable in the following sense: do small initial torsional data give rise to small torsional behavior? In Sect. 3.4 we answer to this question through a finite dimensional approximation of the dynamical system.

3.3.2 Dropping the Trigonometric Functions

Since we are willing to describe how small torsional oscillations may suddenly become larger ones, we can use the following approximations:

$$\sin\theta \cong \theta \quad \text{and} \quad \cos\theta \cong 1\,. \tag{3.12}$$

This statement requires a rigorous justification. It is known from the Report [9, p. 59] that the torsional angle of the Tacoma Narrows Bridge prior to its collapse grew up until 45°. On the other hand, Scanlan-Tomko [239, p. 1723] judge that the torsional angle can be considered harmless provided that it remains smaller than 3°.

In radians this means that

$$\text{the torsional angle may grow up until } \frac{\pi}{4} \text{ and remains harmless until } \frac{\pi}{60}\,. \tag{3.13}$$

By the Taylor expansion with the Lagrange remainder term, we know that

$$\sin\varepsilon = \sum_{k=0}^{n}(-1)^k\frac{\varepsilon^{2k+1}}{(2k+1)!} + (-1)^{2n+3}\cos(\varepsilon_\sigma)\frac{\varepsilon^{2n+3}}{(2n+3)!} := P(\varepsilon,n) + \Gamma_s(\varepsilon,n)$$

for all $\varepsilon \in \mathbb{R}$, where $|\varepsilon_\sigma| < |\varepsilon|$ while P and Γ_s represent, respectively, the approximating polynomial and the approximating error. We have that

$$P\left(\frac{\pi}{60},0\right) = \frac{\pi}{60}\,, \quad P\left(\frac{\pi}{60},1\right) = \frac{\pi}{60} - \frac{\pi^3}{1296}\cdot 10^{-3}\,,$$
$$P\left(\frac{\pi}{4},0\right) = \frac{\pi}{4}\,, \quad P\left(\frac{\pi}{4},1\right) = \frac{\pi}{4} - \frac{\pi^3}{384}\,,$$

while we know that

$$\sin\frac{\pi}{60} \approx 0.0523\,, \quad \sin\frac{\pi}{4} = \frac{1}{\sqrt{2}}\,.$$

Then the relative error $R_s(\varepsilon,n) := |\frac{\sin\varepsilon - P(\varepsilon,n)}{\sin\varepsilon}|$ (or percentage error) is given by

$$R_s\left(\frac{\pi}{60},0\right) \approx 4.6\cdot 10^{-4}\,, \quad R_s\left(\frac{\pi}{60},1\right) \approx 6.3\cdot 10^{-8}\,,$$
$$R_s\left(\frac{\pi}{4},0\right) \approx 0.11\,, \quad R_s\left(\frac{\pi}{4},1\right) \approx 3.5\cdot 10^{-3}\,.$$

Similarly, we proceed with the cosine function. The Taylor expansion yields

$$\cos\varepsilon = \sum_{k=0}^{n}(-1)^k\frac{\varepsilon^{2k}}{(2k)!} + (-1)^{2n+2}\sin(\varepsilon_\sigma)\frac{\varepsilon^{2n+2}}{(2n+2)!} := Q(\varepsilon,n) + \Gamma_c(\varepsilon,n)$$

for all $\varepsilon \in \mathbb{R}$. We have that

$$Q\left(\frac{\pi}{60},0\right) = 1\,, \quad Q\left(\frac{\pi}{60},1\right) = 1 - \frac{\pi^2}{7200}\,, \quad Q\left(\frac{\pi}{4},0\right) = 1\,, \quad Q\left(\frac{\pi}{4},1\right) = 1 - \frac{\pi^2}{32}\,,$$

while we also know that

$$\cos\frac{\pi}{60} \approx 0.999\,, \quad \cos\frac{\pi}{4} = \frac{1}{\sqrt{2}}\,.$$

Then the relative error $R_c(\varepsilon, n) := |\frac{\cos\varepsilon - P(\varepsilon,n)}{\cos\varepsilon}|$ is given by

$$R_c\left(\frac{\pi}{60}, 0\right) \approx 1.4 \cdot 10^{-3}\,, \quad R_c\left(\frac{\pi}{60}, 1\right) \approx 3.1 \cdot 10^{-7}\,,$$
$$R_c\left(\frac{\pi}{4}, 0\right) \approx 0.41\,, \quad R_c\left(\frac{\pi}{4}, 1\right) \approx 2.2 \cdot 10^{-2}\,.$$

The above results enable us to draw the following conclusions.

Proposition 3.2

- *If the model allows torsional angles up to $\frac{\pi}{4}$, then the approximation (3.12) is incorrect, yielding large relative errors (41 % for the cosine and 11 % for the sine); a second order approximation still yields fairly large relative errors (2.2 % for the cosine and 0.4 % for the sine).*
- *If the model allows torsional angles up to $\frac{\pi}{60}$, the approximation (3.12) is quite accurate, yielding small relative errors (0.14 % for the cosine and less than 0.05 % for the sine); a second order approximation does not improve significantly the precision of the model.*

Since the purpose of our numerical results is to consider small torsional data, of the order of 10^{-4}, and since our purpose is merely to detect when the torsional angle θ increases of two orders of magnitude, thereby reaching at most $10^{-2} \ll \frac{\pi}{60}$, we can make use of the approximation (3.12). We emphasise that our results do not aim to describe the behavior of the bridge when the torsional angle becomes large, they just aim to describe how a small torsional angle ceases to be small.

Proposition 3.2 allows us to implement the approximation suggested by (3.12); we set $z := \ell\theta$ so that (3.4) becomes (3.8). In (3.8) the dependence on the width ℓ is somehow hidden and we already pointed out that, in fact, smaller ℓ yield less stability, see (3.7).

3.3.3 Choosing the Nonlinearity

We consider a specific nonlinearity f satisfying the assumptions of Theorem 3.1. Since our purpose is merely to describe the qualitative phenomenon, the choice of the nonlinearity is not of fundamental importance; it is shown in [22] that several different nonlinearities yield the same qualitative behavior for the solutions. Augusti-Sepe [25] (see also [24]) view the restoring force at the endpoints of a cross-section of the roadway as composed by two connected springs, the top one

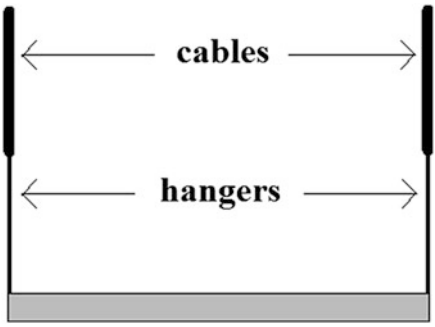

Fig. 3.2 The system cables-hangers modeled with two connected springs

representing the action of the sustaining cable and the bottom one (connected with the roadway) representing the hangers, see Fig. 3.2. The action of the hangers is almost linear since they have only small elongations, see [177]. The action of the cables is considered by Bartoli-Spinelli [30, p. 180] the main cause of the nonlinearity of the restoring force: following [240], they suggest [30, (15)] quadratic and cubic perturbations of a linear behavior. Here we simply take

$$f(s) = s + \gamma s^3 \quad \text{for } \gamma > 0\,, \tag{3.14}$$

which allows to simplify several computations. Let us also mention that Plaut-Davis [220, Sect. 3.5] make the same choice and that this nonlinearity appears in several elasticity contexts, see e.g. [150, (1)].

The parameter γ measures how far is f from a linear function. When f is as in (3.14), the system (3.8) becomes

$$\begin{cases} y_{tt} + y_{xxxx} + 2y(1 + \gamma y^2 + 3\gamma z^2) = 0 & (0 < x < \pi,\ t > 0) \\ z_{tt} - z_{xx} + 6z(1 + 3\gamma y^2 + \gamma z^2) = 0 & (0 < x < \pi,\ t > 0)\,. \end{cases} \tag{3.15}$$

To (3.15) we associate some initial conditions which determine the conserved energy of the system, that is,

$$E_\gamma = \frac{\|y_t(t)\|_2^2}{2} + \frac{\|z_t(t)\|_2^2}{6} + \frac{\|y_{xx}(t)\|_2^2}{2} + \frac{\|z_x(t)\|_2^2}{6} + \int_0^\pi \left(y(x,t)^2 + z(x,t)^2 + 3\gamma z(x,t)^2 y(x,t)^2 + \gamma \frac{y(x,t)^4}{2} + \gamma \frac{z(x,t)^4}{2} \right) dx\,.$$

Let (y_γ, z_γ) be the solution of (3.15) with some initial conditions. If we put $(\overline{y}, \overline{z}) = \sqrt{\gamma}\,(y_\gamma, y_\gamma)$, then $(\overline{y}, \overline{z})$ solves system (3.15) when $\gamma = 1$. Accordingly, the conserved energy is modified:

Proposition 3.3 *Let $\gamma > 0$. The conserved energy of (3.15) satisfies $E_\gamma = E_1/\gamma$, where E_1 is the conserved energy of (3.15) when $\gamma = 1$. Moreover, the widest vertical amplitude $\|y_\gamma\|_\infty$ satisfies $\|y_\gamma\|_\infty = \|\overline{y}\|_\infty/\sqrt{\gamma}$.*

The proof of Proposition 3.3 follows by rescaling. Proposition 3.3 enables us to restrict our attention to the case $\gamma = 1$, that is,

$$f(s) = s + s^3 . \tag{3.16}$$

In this case (3.8) reduces to

$$\begin{cases} y_{tt} + y_{xxxx} + 2y(1 + y^2 + 3z^2) = 0 \ (0 < x < \pi,\ t \geq 0) \\ z_{tt} - z_{xx} + 6z(1 + 3y^2 + z^2) = 0 \quad (0 < x < \pi,\ t \geq 0) . \end{cases} \tag{3.17}$$

Moreover, the conserved energy is given by

$$\begin{aligned} E = & \frac{\|y_t(t)\|_2^2}{2} + \frac{\|z_t(t)\|_2^2}{6} + \frac{\|y_{xx}(t)\|_2^2}{2} + \frac{\|z_x(t)\|_2^2}{6} \\ & + \int_0^\pi \left[\frac{y(x,t)^4}{2} + \frac{z(x,t)^4}{2} + 3z(x,t)^2 y(x,t)^2 + y(x,t)^2 + z(x,t)^2 \right] dx . \end{aligned} \tag{3.18}$$

We aim to determine energy thresholds for torsional stability of vertical modes (still to be rigorously defined), see Sect. 3.4.2. From Proposition 3.3 we see that $\gamma \mapsto E_\gamma$ and $\gamma \mapsto \|y_\gamma\|_\infty$ are decreasing with respect to γ and both tend to 0 if $\gamma \to \infty$, whereas they tend to ∞ if $\gamma \to 0$. This shows that the nonlinearity plays against stability:

more nonlinearity yields more instability and almost linear elastic behaviors are extremely stable.

3.4 Finite Dimensional Torsional Stability

3.4.1 Why Can We Neglect High Torsional Modes?

Our finite dimensional analysis is performed on the low modes. This procedure is widely accepted in classical engineering literature, see the comments by Bleich-McCullough-Rosecrans-Vincent [50, p. 23] and Smith-Vincent [245, p. 11] reported in Sect. 2.7.1. In order to restrict the study to low modes, we project the infinite dimensional phase space on a finite dimensional subspace, following the original technique by Galerkin [119].

Consider the solution (y, z) of (3.17)–(3.9)–(3.10), as given by Theorem 3.1, and let us expand it in Fourier series with respect to x:

$$y(x,t) = \sum_{j=1}^{\infty} y_j(t) \sin(jx) , \quad z(x,t) = \sum_{j=1}^{\infty} z_j(t) \sin(jx) , \tag{3.19}$$

where the functions y_j and z_j are the unknowns. Denote by z^m the projection of z on the space spanned by $\{\sin(x), \ldots, \sin(mx)\}$ and by w^m the projection of z on the

infinite dimensional space spanned by $\{\sin((m+1)x), \sin((m+2)x)\ldots\}$:

$$z(x,t) = z^m(x,t) + w^m(x,t)\,,$$

$$z^m(x,t) = \sum_{j=1}^{m} z_j(t)\sin(jx)\,, \quad w^m(x,t) = \sum_{j=m+1}^{\infty} z_j(t)\sin(jx)\,. \tag{3.20}$$

In [36] the following sufficient smallness condition for w^m is obtained.

Theorem 3.4 *Let $\omega > 0$, let (y,z) be a solution of (3.17)–(3.9)–(3.10) having energy $E > 0$ and let (3.20) be the decomposition of z. Then $\|w^m\|_\infty < \omega$ provided that at least one of the following inequalities holds*

$$\pi\,\omega^4\,(m+1)^2\left[\pi(m^2+2m+7)^2+36E\right]-36\,\pi^2\,E^2\,(m+1)^4-9\omega^8 \geq 0 \tag{3.21}$$

$$E^3 + \frac{\pi}{2}\,E^2 - \frac{3\,\omega^4}{4}\,E - \frac{3\,\omega^8}{32\,\pi} - \frac{\pi\,\omega^4}{3} \leq 0\,. \tag{3.22}$$

The choice of ω depends both on ℓ (through the substitution $z = \ell\theta$) and on the harmless criterion (3.13), see Sect. 3.3.2. Nevertheless, since the purpose here is merely to give a qualitative description of the phenomena and of the corresponding procedures, we will not quantify its value.

The two inequalities (3.21) and (3.22) have a completely different meaning. The condition (3.22) is somehow obvious and uninteresting: it states that if the total energy E is sufficiently small then all the torsional components are small. In Table 3.1 we give some numerical bounds for E in dependence of the maximum allowed amplitude ω. It appears that the energy E needs to be very small.

On the contrary, the condition (3.21) is much more useful: it gives an upper bound on the modes to be checked. High torsional modes remain small provided that they are above a threshold which depends on the energy E and on the maximum allowed amplitude ω. In Tables 3.2 and 3.3 we give some numerical bounds on the modes m in dependence of the energy E, when ω is fixed.

Table 3.1 Upper bound for E in dependence of ω

ω	0.2	0.1	0.05	0.01
E	$3.3\cdot10^{-2}$	$8.2\cdot10^{-3}$	$2\cdot10^{-3}$	$8.2\cdot10^{-5}$

Table 3.2 Upper bound for m in dependence of E when $\omega = 0.1$

E	1	0.5	0.4	0.3	0.2	0.1	0.05
m	598	298	238	178	118	58	28

Table 3.3 Upper bound for m in dependence of E when $\omega = 0.2$

E	1	0.5	0.4	0.3	0.2	0.1	0.05
m	148	73	58	43	28	13	5

It turns out that the map $E \mapsto m$ appears to be almost linear: in fact, we have

$$m \approx \frac{6E}{\omega^2} - 2\,.$$

This approximation is reliable for small ω: it follows by dropping the term $9\omega^8$ in (3.21), by dividing by $(m+1)^2$, and by solving the remaining second order algebraic inequality with respect to m.

With the very same procedure we may rule out high vertical modes where, possibly, (3.22) becomes more useful. We have here focused our attention only on the torsional modes because they are more dangerous for the safety of the bridge.

3.4.2 *Stability of the Low Modes*

Let us fix some energy $E > 0$. After having ruled out high modes (say, larger than m) through Theorem 3.4, we focus our attention on the lowest m modes, $j \le m$. The proof of Theorem 3.1 in [36] is constructive: it ensures that finite sums such as

$$y^m(x,t) = \sum_{j=1}^{m} y_j(t)\sin(jx)\,, \quad z^m(x,t) = \sum_{j=1}^{m} z_j(t)\sin(jx) \tag{3.23}$$

approximate the solution (3.19) of (3.17) as $m \to \infty$. The time-dependent Fourier coefficients y_j and z_j $(j = 1,\dots,m)$ are solutions of the system

$$\begin{cases} \ddot{y}_j(t) + j^4 y_j(t) + \frac{4}{\pi}\int_0^\pi y^m(x,t)(1+y^m(x,t)^2+3z^m(x,t)^2)\sin(jx)\,dx = 0 \\ \ddot{z}_j(t) + j^2 z_j(t) + \frac{12}{\pi}\int_0^\pi z^m(x,t)(1+3y^m(x,t)^2+z^m(x,t)^2)\sin(jx)\,dx = 0. \end{cases} \tag{3.24}$$

The proof of Theorem 3.1 in [36] then ensures that y^m and z^m converge (as $m \to \infty$) to the unique solution of (3.17). We call (3.24) the **approximated m-mode system** and, for simplicity, we put $(Y,Z) = (y_1,\dots,y_m,z_1,\dots,z_m) \in \mathbb{R}^{2m}$. To (3.24) we associate the initial conditions

$$Y(0) = Y_0\,, \quad \dot{Y}(0) = Y_1\,, \quad Z(0) = Z_0\,, \quad \dot{Z}(0) = Z_1\,, \tag{3.25}$$

where the components of the vector $Y_0 \in \mathbb{R}^m$ are the Fourier coefficients of the projection of $y(0)$ onto the finite dimensional space spanned by $\{\sin(jx)\}_{j=1}^m$; similarly for Y_1, Z_0, Z_1. In the sequel, we denote by

$$\{e_j\}_{j=1}^m \quad \text{the canonical basis of} \quad \mathbb{R}^m\,.$$

The conserved total energy of (3.24), to be compared with (3.18), is given by

$$E := \frac{|\dot{Y}|^2}{2} + \frac{|\dot{Z}|^2}{6} + \frac{1}{2}\sum_{j=1}^{m} j^4 y_j^2 + \frac{1}{6}\sum_{j=1}^{m} j^2 z_j^2 \tag{3.26}$$

$$+\frac{2}{\pi}\int_0^\pi \left[\frac{y^m(x,t)^4}{2} + \frac{z^m(x,t)^4}{2} + 3y^m(x,t)^2 z^m(x,t)^2 + y^m(x,t)^2 + z^m(x,t)^2\right] dx.$$

Note that (3.26) implies the boundedness of each of the y_j, $\dot{y}_j$, z_j, $\dot{z}_j$. Once (3.24) is solved, the functions y^m and z^m in (3.23) provide finite dimensional approximations of the solutions (3.19) of (3.17). In view of Theorem 3.4, this approximation is reliable since higher modes have small components.

Let us describe rigorously what we mean by vertical mode of (3.24).

Definition 3.5 (Vertical Mode) Let $m \geq 1$ and $1 \leq k \leq m$; let $\mathbb{R}^2 \ni (\alpha, \beta) \neq (0,0)$. We say that Y_k is the k-th vertical mode at energy $E_k(\alpha, \beta)$ if $(Y_k, 0) \in \mathbb{R}^{2m}$ is the solution of (3.24) with initial conditions (3.25) satisfying

$$Y(0) = \alpha e_k\,, \quad \dot{Y}(0) = \beta e_k\,, \quad Z(0) = \dot{Z}(0) = 0 \in \mathbb{R}^m\,. \tag{3.27}$$

Next, we state a calculus lemma which is needed to compute the integrals in (3.24) and to determine the coefficients of all the terms in the system.

Lemma 3.6 *For all $k \in \mathbb{N}$ we have*

$$c_{k,k,k} = \frac{8}{\pi}\int_0^\pi \sin^4(kx)\,dx = 3\,.$$

For all $l, k \in \mathbb{N}$ $(l \neq k)$ we have

$$c_{l,k,k} = \frac{8}{\pi}\int_0^\pi \sin^3(kx)\sin(lx)\,dx = \begin{cases} -1 & \text{if } l = 3k \\ 0 & \text{if } l \neq 3k\,. \end{cases}$$

For all $l, k \in \mathbb{N}$ $(l \neq k)$ we have

$$c_{l,l,k} = \frac{8}{\pi}\int_0^\pi \sin^2(kx)\sin^2(lx)\,dx = 2\,.$$

For all $l, j, k \in \mathbb{N}$ (all different and $l < j$) we have

$$c_{l,j,k} = \frac{8}{\pi}\int_0^\pi \sin^2(kx)\sin(jx)\sin(lx)\,dx = \begin{cases} 1 & \text{if } j + l = 2k \\ -1 & \text{if } j - l = 2k \\ 0 & \text{if } j \pm l \neq 2k\,. \end{cases}$$

By (3.26) and Lemma 3.6 the conserved energy of (3.24)–(3.27) is given by

$$E_k(\alpha,\beta) := \frac{\beta^2}{2} + (k^4+2)\frac{\alpha^2}{2} + \frac{3}{8}\alpha^4\,. \tag{3.28}$$

The initial conditions in (3.27) determine the constant value of the energy $E_k(\alpha,\beta)$. Different couples of data (α,β) in (3.27) may yield the same energy; in particular, for all $(\alpha,\beta)\in\mathbb{R}^2$ there exists a unique $\mu>0$ such that

$$E_k(\mu,0) = E_k(\alpha,\beta)\ :$$

μ is the **amplitude of the initial oscillation of the k-th vertical mode**.

The standard procedure to deduce the stability of $(Y_k,0)$ consists in studying the behavior of the perturbed vector $(Y-Y_k,Z)$ where (Y,Z) solves (3.24), see [266, Chap. 5]. This leads to linearise the system (3.24) around $(Y_k,0)$ and, subsequently, to apply the Floquet theory for differential equations with periodic coefficients, at least for $m=1,2$. The torsional components ξ_j of the linearisation of system (3.24) around $(Y_k,0)$ satisfy

$$\ddot{\Xi} + P_k(t)\Xi = 0\,, \tag{3.29}$$

where $\Xi=(\xi_1,\dots,\xi_m)$ and $P_k(t)$ is a $m\times m$ matrix depending on Y_k.

Definition 3.7 (Torsional Stability) We say that the k-th vertical mode Y_k at energy $E_k(\alpha,\beta)$ (that is, the solution of (3.24)–(3.27)) is torsionally stable if the trivial solution of (3.29) is stable.

In Sect. 3.6.2 we give numerical evidence that this definition is well suited to characterise the torsional stability, see Remark 3.15. In the two following subsections we state the (theoretical and numerical) stability results when $m=1$ and $m=2$. The cases where $m\geq 3$ are more involved because Y may spread on more components; this will be discussed in Sect. 3.5. The results lead to the conclusion that

if the energy $E_k(\alpha,\beta)$ in (3.28) is small enough then small initial torsional oscillations remain small for all time $t>0$, whereas if $E_k(\alpha,\beta)$ is large (that is, the vertical oscillations are initially large) then small torsional oscillations suddenly become wider.

Therefore, a crucial role is played by the amount of energy inside the system (3.17). In the next sections we analyse the energy, both theoretically and numerically, within (3.24) when $m=1$ and $m=2$. For the theoretical estimates of the critical energy we make use of a stability criterion by Zhukovskii [284] applied to suitable Hill equations [141]. For the numerical estimates, we choose "small" data Z_0 and Z_1 in (3.25) and, to evaluate the stability of the k-th vertical mode

of (3.24), we consider data Y_0 and Y_1 concentrated on the k-th component of the canonical basis of $\mathbb{R}^m$. More precisely, we take

$$Y_0 = \mu e_k\,, \qquad Y_1 = 0 \in \mathbb{R}^m\,, \qquad |Z_0| \le |\mu| \cdot 10^{-4}\,, \qquad |Z_1| \le |\mu| \cdot 10^{-4}\,. \tag{3.30}$$

Then the initial (constant) energy (3.26) is approximately $E \approx (k^4+2)\frac{\mu^2}{2} + \frac{3}{8}\mu^4$ and the remaining (small) part of the initial energy is the torsional energy of Z_0 and Z_1 plus some coupling energy. We also found that different initial data, with $Y_1 \neq 0$, give the same behavior provided the initial energy is the same.

3.4.3 The Approximated 1-Mode System

When $m = 1$, the approximated 1-mode solutions (3.23) have the form

$$y^1(x,t) = y_1(t)\sin x\,, \qquad z^1(x,t) = z_1(t)\sin x\,.$$

By Lemma 3.6, the approximated 1-system (3.24) reads

$$\begin{cases} \ddot{y}_1 + 3y_1 + \frac{3}{2}y_1^3 + \frac{9}{2}y_1 z_1^2 = 0 \\ \ddot{z}_1 + 7z_1 + \frac{9}{2}z_1^3 + \frac{27}{2}z_1 y_1^2 = 0\,, \end{cases} \tag{3.31}$$

with some initial conditions

$$y_1(0) = \eta_0\,,\ \dot{y}_1(0) = \eta_1\,,\ z_1(0) = \zeta_0\,,\ \dot{z}_1(0) = \zeta_1\,. \tag{3.32}$$

In this case $Y_1 = \overline{y}$, where $\overline{y}$ is the unique (periodic) solution of

$$\ddot{y} + 3y + \frac{3}{2}y^3 = 0\,, \qquad y(0) = \alpha\,,\ \dot{y}(0) = \beta\,; \tag{3.33}$$

this problem admits the conserved quantity

$$E = \frac{\dot{y}^2}{2} + \frac{3}{2}y^2 + \frac{3}{8}y^4 \equiv \frac{\beta^2}{2} + \frac{3}{2}\alpha^2 + \frac{3}{8}\alpha^4\,. \tag{3.34}$$

For any $E > 0$, define

$$\Lambda_\pm(E) := 2\sqrt{1 + \frac{2}{3}E} \pm 2.$$

The following result is proved in [36]:

Theorem 3.8 *For any $\alpha, \beta \in \mathbb{R}$ problem (3.33) admits a unique solution $\overline{y}$ which is periodic of period*

$$T(E) = \frac{8}{\sqrt{3}} \int_0^1 \frac{ds}{\sqrt{(\Lambda_+(E) + \Lambda_-(E)s^2)(1-s^2)}}\,. \tag{3.35}$$

In particular, the map $E \mapsto T(E)$ is strictly decreasing and $\lim_{E\to 0} T(E) = 2\pi/\sqrt{3}$.

Therefore, in the 1-mode system, (3.29) reduces to the following Hill equation:

$$\ddot{\xi} + a(t)\xi = 0 \quad \text{with} \quad a(t) = 7 + \frac{27}{2}\overline{y}(t)^2\,, \tag{3.36}$$

The following result holds (see again [36] for the proof):

Theorem 3.9 *The first vertical mode $Y_1 = \overline{y}$ at energy $E_1(\alpha, \beta)$ (that is, the solution of (3.33)) is torsionally stable provided that the two following (equivalent) inequalities hold*

$$\|\overline{y}\|_\infty \le \sqrt{\frac{10}{21}} \approx 0.69 \qquad \textit{and} \qquad E_1 \le \frac{235}{294} \approx 0.799\,.$$

The first vertical mode is represented in the top picture of Fig. 1.18. As already remarked, since it deals with the linear equation (3.29), Definition 3.7 is the usual one. Nevertheless, the stability results obtained in [213] for suitable nonlinear Hill equations suggest that different equivalent definitions can be stated, possibly not involving a linearisation process. As far as we are aware, there is no general theory for nonlinear systems of any number of equations but it is reasonable to expect that results similar to [213] might hold. This is why, in our numerical experiments, we consider system (3.31) without any linearisation. The below numerical results suggest that the threshold of instability is larger than the one in Theorem 3.9. Clearly, they only give a "local stability" information (for finite time), but the observed phenomenon is very precise and the thresholds of torsional instability are determined with high accuracy. The pictures in Fig. 3.3 display the plots of the solutions of (3.31) with initial data

$$y_1(0) = \|y_1\|_\infty = 10^4 z_1(0)\,, \quad \dot{y}_1(0) = \dot{z}_1(0) = 0 \tag{3.37}$$

for different values of $\|y_1\|_\infty$. The green plot is y_1 and the black plot is z_1. For $\|y_1\|_\infty = 1.45$ no wide torsion appears, which means that the solution $(y_1, 0)$ is torsionally stable. For $\|y_1\|_\infty = 1.47$ we see a sudden increase of the torsional oscillation around $t \approx 50$. Therefore, the stability threshold for the vertical amplitude of oscillation lies in the interval $[1.45, 1.47]$. Finer experiments show that the threshold is $\|y_1\|_\infty \approx 1.46$, corresponding to a critical energy of about $E \approx 4.9$: these values should be compared with the statement of Theorem 3.9. When the

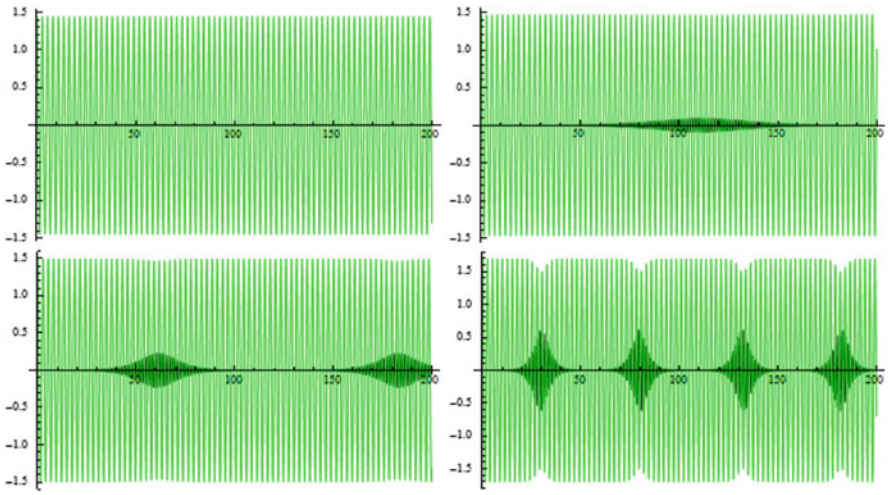

Fig. 3.3 On the interval $t \in [0, 200]$, plot of the solutions y_1 (*green*) and z_1 (*black*) of (3.31)–(3.37) for $\|y_1\|_\infty = 1.45,\ 1.47,\ 1.5,\ 1.7$ (from *left* to *right* and *top* to *bottom*)

amplitude is increased further, for $\|y_1\|_\infty = 1.5$ and $\|y_1\|_\infty = 1.7$, the appearance of wide torsional oscillations is anticipated (earlier in time) and amplified (larger in magnitude). This phenomenon continues to increase for increasing $\|y_1\|_\infty$. We then tried different initial data with $\dot{y}_1(0) \neq 0$; as expected, the sudden appearance of torsional oscillations always occurs at the energy level $E \approx 4.9$, no matter of how it is initially distributed between the kinetic and potential energies of y_1. Whence, we have seen that the "true" (numerical) thresholds are larger than the ones obtained in Theorem 3.9.

For suspension bridges in absence of wind, it is well-known that the torsional frequency is always greater than its vertical counterpart, see (1.4). We wish to emphasise this fact in our fish-bone model. We slightly modify the parameters involved: instead of $EI = 3\mu = 1$, we take $EI = \mu = 1$ and (3.31) is then replaced by

$$\begin{cases} \ddot{y}_1 + 3y_1 + \frac{3}{2}y_1^3 + \frac{9}{2}y_1 z_1^2 = 0 \\ \ddot{z}_1 + 9z_1 + \frac{9}{2}z_1^3 + \frac{27}{2}z_1 y_1^2 = 0\,. \end{cases} \tag{3.38}$$

Then the following result from [36] holds:

Theorem 3.10 *Let (y_1, z_1) be a nontrivial solution of (3.38). Let $t_1 < t_2$ be two consecutive critical points of $y_1(t)$. Then there exists $\tau \in (t_1, t_2)$ such that $z_1(\tau) = 0$.*

Theorem 3.8 states that the frequency of a nonlinear oscillator depends on the amplitude of oscillations. Theorem 3.10 also shows that the nonlinear frequency of z_1 is always larger than the frequency of y_1, thereby confirming experimental

observations, see (1.4). Further evidence of this fact comes from [149, p. 178] from which we quote

> ... in the absence of wind the torsional frequency was always greater than its vertical counterpart.

The results discussed in this section complement Theorem 3.10 as follows:

if the nonlinear frequency of z_1 reaches a multiple of the frequency of y_1 then an internal resonance is created and this yields a possible transfer of energy from y_1 to z_1.

3.4.4 The Approximated 2-Modes System

Let us fix $m = 2$ in (3.23) and (3.24) and put

$$y^2(x,t) = y_1(t)\sin x + y_2(t)\sin(2x)\,, \qquad z^2(x,t) = z_1(t)\sin x + z_2(t)\sin(2x)\,.$$

Then, after integration over $(0,\pi)$ and using Lemma 3.6, we see that y_j and z_j satisfy the approximated 2-system

$$\begin{cases} \ddot{y}_1 + 3y_1 + \dfrac{9}{2}y_1z_1^2 + 3y_1z_2^2 + 3y_1y_2^2 + \dfrac{3}{2}y_1^3 + 6z_1z_2y_2 = 0 \\ \ddot{y}_2 + 18y_2 + \dfrac{9}{2}y_2z_2^2 + 3y_2z_1^2 + 3y_2y_1^2 + \dfrac{3}{2}y_2^3 + 6z_1z_2y_1 = 0 \\ \ddot{z}_1 + 7z_1 + \dfrac{27}{2}z_1y_1^2 + 9z_1y_2^2 + 9z_1z_2^2 + \dfrac{9}{2}z_1^3 + 18y_1y_2z_2 = 0 \\ \ddot{z}_2 + 10z_2 + \dfrac{27}{2}z_2y_2^2 + 9z_2y_1^2 + 9z_2z_1^2 + \dfrac{9}{2}z_2^3 + 18y_1y_2z_1 = 0\,, \end{cases} \tag{3.39}$$

while the energy becomes

$$\begin{aligned} E = {} & \frac{1}{2}(\dot{y}_1^2 + \dot{y}_2^2) + \frac{1}{6}(\dot{z}_1^2 + \dot{z}_2^2) + \frac{3}{2}y_1^2 + 9y_2^2 + \frac{7}{6}z_1^2 + \frac{5}{3}z_2^2 + 6y_1y_2z_1z_2 \\ & + \frac{9}{4}(y_1^2z_1^2 + y_2^2z_2^2) + \frac{3}{2}(y_1^2y_2^2 + y_1^2z_2^2 + y_2^2z_1^2 + z_1^2z_2^2) + \frac{3}{8}(y_1^4 + y_2^4 + z_1^4 + z_2^4)\,. \end{aligned}$$

Since our purpose is to emphasise perturbations of linear equations, it is more convenient to rewrite the two last equations in (3.39) as

$$\begin{cases} \ddot{z}_1 + \left(7 + \dfrac{27}{2}y_1^2 + 9y_2^2 + 9z_2^2\right)z_1 + \dfrac{9}{2}z_1^3 = -18y_1y_2z_2 \\ \ddot{z}_2 + \left(10 + \dfrac{27}{2}y_2^2 + 9y_1^2 + 9z_1^2\right)z_2 + \dfrac{9}{2}z_2^3 = -18y_1y_2z_1\,. \end{cases} \tag{3.40}$$

In this case we have $Y_j = \overline{y}_j e_j$ $(j = 1, 2)$, where $\overline{y}_j$ is the unique solution of

$$\ddot{y}_j(t) + (j^4 + 2)y_j(t) + \frac{3}{2}y_j(t)^3 = 0\,, \quad y_j(0) = \alpha\,, \quad \dot{y}_j(0) = \beta\,;$$

this problem admits the conserved energy

$$E_j = \frac{\dot{y}(t)^2}{2} + (j^4+2)\frac{y(t)^2}{2} + \frac{3y(t)^4}{8} = \frac{\beta^2}{2} + (j^4+2)\frac{\alpha^2}{2} + \frac{3}{8}\alpha^4 \geq 0\,. \tag{3.41}$$

Then (3.29) becomes the following system of uncoupled Hill equations:

$$\begin{cases} \ddot{\xi}_1(t) + a_{1,j}(t)\xi_1(t) = 0 \\ \ddot{\xi}_2(t) + a_{2,j}(t)\xi_2(t) = 0 \end{cases} \qquad (j = 1, 2) \tag{3.42}$$

where $a_{i,j}(t) = i^2 + 6 + 9\alpha_{i,j}\overline{y}_j(t)^2$, $\alpha_{i,j} = 1$ if $i \neq j$ and $\alpha_{i,i} = \frac{3}{2}$.

The following result taken from [36] holds:

Theorem 3.11 *The first vertical mode $Y_1 = (\overline{y}_1, 0)$ of (3.39) at energy E_1 is torsionally stable provided that*

$$\|\overline{y}_1\|_\infty \leq \frac{1}{\sqrt{3}} \approx 0.577 \iff E_1 \leq \frac{13}{24} \approx 0.542\,. \tag{3.43}$$

The second vertical mode $Y_2 = (0, \overline{y}_2)$ of (3.39) at energy E_2 is torsionally stable provided that

$$\|\overline{y}_2\|_\infty \leq \sqrt{\frac{32}{51}} \approx 0.792 \iff E_2 \leq \frac{5024}{867} \approx 5.795\,.$$

The second vertical mode is represented in the middle picture of Fig. 1.18. Again, Theorem 3.11 merely gives a sufficient condition for the torsional stability and, numerically, the thresholds seem to be larger. Once more, numerics only shows local stability but the observed phenomena are very precise and hence they appear reliable. Here the situation is slightly more complicated because two modes (four equations) are involved. Therefore, we proceed differently.

We start by studying the stability of the first vertical mode. The pictures in Fig. 3.4 display the plots of the torsional components (z_1, z_2) of the solutions of (3.39) with initial data

$$\begin{aligned} y_1(0) &= \|y_1\|_\infty = 10^4 y_2(0) = 10^4 z_1(0) = 10^4 z_2(0), \\ \dot{y}_1(0) &= \dot{y}_2(0) = \dot{z}_1(0) = \dot{z}_2(0) = 0 \end{aligned} \tag{3.44}$$

for different values of $\|y_1\|_\infty$. The green plot is z_1 and the black plot is z_2. Recalling that the initial torsional amplitudes are of the order of 10^{-4} we can see that, for

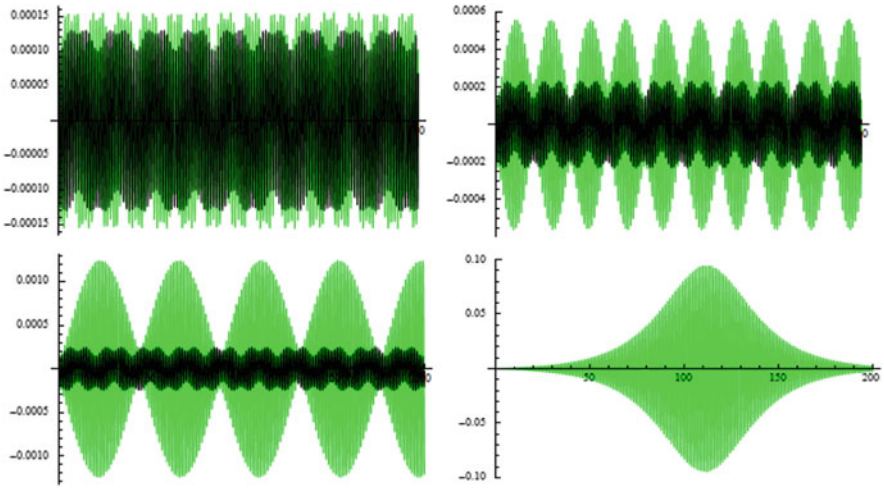

Fig. 3.4 On the interval $t \in [0, 200]$, plot of the torsional components z_1 (*green*) and z_2 (*black*) of (3.39)–(3.44) for $\|y_1\|_\infty = 1,\ 1.4,\ 1.45,\ 1.47$ (from *left* to *right* and *top* to *bottom*)

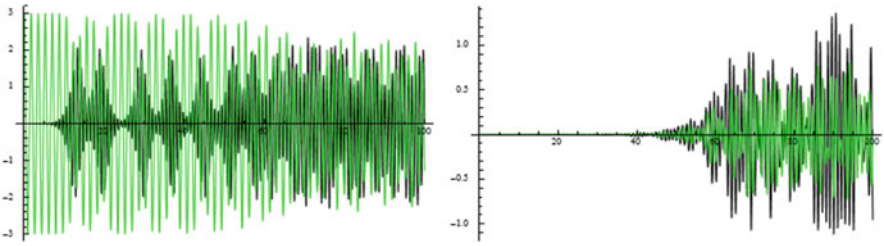

Fig. 3.5 On the interval $t \in [0, 100]$, plot of the solution of (3.39)–(3.44) for $\|y_1\|_\infty = 3$. *Left* green=y_1, black=z_1; *Right* green=y_2, black=z_2

$\|y_1\|_\infty = 1$, both torsional components remain small, although z_1 is slightly larger than z_2. By increasing the y_1 amplitude, $\|y_1\|_\infty = 1.4$ and $\|y_1\|_\infty = 1.45$, we see that z_1 and z_2 still remain small but now z_1 is significantly larger than z_2 and displays bumps. When $\|y_1\|_\infty = 1.47$, z_1 has become so large that z_2, which is still of the order of 10^{-4}, is no longer visible in the fourth plot of Fig. 3.4. The threshold for the appearance of $z_1 \gg z_2$ is again $\|y_1\|_\infty \approx 1.46$, see Sect. 3.4.3. Therefore, it seems that the stability of the first vertical mode does not transfer energy on the second modes; but, as we now show, this is not true.

We increased further the initial datum up to $\|y_1\|_\infty = 3$. In Fig. 3.5 we display the plot of all the components (y_1, y_2, z_1, z_2) of the corresponding solution of (3.39)–(3.44). One can see that some energy is also transferred to both the vertical and torsional second modes, although this occurs with some delay (in the second picture, the green oscillation is hidden but it is almost as wide as the black oscillation).

Concerning the stability of the second vertical mode, we just quickly describe our numerical results. The loss of stability appeared for $\|y_2\|_\infty \approx 0.945$ corresponding to $E \approx 8.33$; in this case, Theorem 3.11 gives a fairly good sufficient condition. For $\|y_2\|_\infty \leq 0.94$, both z_1 and z_2 (and also y_1) remain small and of the same magnitude, with the amplitude of oscillations of z_1 being almost constant while the amplitude of oscillations of z_2 being variable. For $\|y_2\|_\infty \geq 0.945$, z_2 suddenly displays the bumps seen in the above pictures. Finally, for $\|y_2\|_\infty \geq 1.08$, also y_1 and z_1 display sudden wide oscillations which, however, appear delayed in time when compared with z_2.

From Figs. 3.3, 3.4, and 3.5 it appears that there is some energy transfer from vertical to torsional oscillations and that the energy transfer occurs after some waiting time. This may be seen as a special case of the Wagner effect [275] discovered by the Austrian scientist Herbert Alois Wagner (1900–1982). This effect was originally seen in the aerodynamic action of the wind on the airfoil of an aircraft: if the incidence of a wing changes suddenly, the new lifting force resulting from the change in incidence is not set up instantaneously. In our model, even if the amount of energy E is large enough to generate instability, the energy transfer does not occur instantaneously, it takes some time $T = T(E) > 0$.

3.5 The Flutter Energy

In this section we explain how all the theoretical and numerical results obtained in the previous sections may be used to define the **flutter energy**. Consider the original system (3.8) which, for the sake of clarity, we rewrite here:

$$\begin{cases} y_{tt} + y_{xxxx} + f(y+z) + f(y-z) = 0 \ (0 < x < \pi,\ t > 0) \\ z_{tt} - z_{xx} + 3f(y+z) - 3f(y-z) = 0 \quad (0 < x < \pi,\ t > 0)\,. \end{cases} \tag{3.45}$$

The system (3.45) is conservative and its constant energy is given by

$$E = \int_0^\pi \Big(\frac{y_t(x,t)^2}{2} + \frac{z_t(x,t)^2}{6} + \frac{y_{xx}(x,t)^2}{2} + \frac{z_x(x,t)^2}{6} + F\big(y(x,t)+z(x,t)\big) + F\big(y(x,t)-z(x,t)\big)\Big)\, dx\,.$$

In order to analyse the torsional stability of the k-th vertical mode (for some $k \in \mathbb{N}$) one should take the initial data

$$y(x,0) = \alpha \sin(kx)\,, \quad y_t(x,0) = \beta \sin(kx)\,, \quad z(x,0) = z_t(x,0) = 0\,. \tag{3.46}$$

By Theorem 3.1, we know that (3.45)–(3.46) (under the boundary conditions (3.9)) admits a unique solution. Since it has the form (3.19), one has to determine the

(infinitely many) unknowns $y_j(t)$ and $z_j(t)$ ($j \in \mathbb{N}$). It is straightforward to verify that the unique solution is given by

$$\overline{y}_k(x,t) = \sum_{j=1}^{\infty} y_j(t)\sin(jx)\,, \quad z(x,t) = 0\,, \tag{3.47}$$

that is, it has no torsional part z while the vertical part y is to be determined and has infinitely many nontrivial components y_j. Our purpose is to study the torsional stability of $\overline{y}_k$ and the criterion described in Sect. 3.4.1, see in particular Theorem 3.4, enables us to fix the number m of torsional modes to be examined. This leads to the approximated m-mode system (3.24) and to define the k-th vertical mode as in Definition 3.5.

In order to improve the precision of the response, one should consider approximated m-modes systems for large values of m. But if $m \geq 3$, (3.24) with initial conditions (3.27) has solutions $(Y, 0)$ with more than one nontrivial component within the vector Y. Then the study of the stability of the k-th vertical mode ($1 \leq k \leq m$) cannot be reduced to that of a single Hill equation as in the cases $m = 1$ and $m = 2$: one obtains, instead, a system of coupled equations. We underline that the "critical number" $m = 3$ is due to the particular nonlinearity f chosen in (3.14): different nonlinearities may yield coupled equations also for $m = 1, 2$ or, maybe, uncoupled equations also for some $m \geq 3$.

Although the theoretical analysis of the approximated m-modes systems appears more involved, we could however perform several numerical experiments and confirm the conclusions stated in Sect. 3.4.2 also for $m \geq 3$. The initial conditions (3.27) determine the constant energy (3.28) which, in turn, determines the amplitude of the initial oscillation of the k-th vertical mode.

Then we perturb the initial conditions in (3.27) and we characterise the torsional stability of Y_k according to Definition 3.7. Finally we may introduce the fundamental notion of flutter energy.

Definition 3.12 (Flutter Energy) We call flutter energy of the k-th vertical mode Y_k of the approximated m-mode system (3.24) the positive number $\overline{E}_k$ being the supremum of the energies $E_k(\alpha, \beta)$ such that the vertical mode Y_k at any energy $E < E_k(\alpha, \beta)$ is torsionally stable.

In fact, the flutter energy corresponds to a maximal amplitude of the initial oscillation of the k-th vertical mode. The exact value of the flutter energy of each mode seems out of reach. However, the finite dimensional reductions performed in the previous sections (both theoretical and numerical) yield approximations of the flutter energy: this is what we call flutter energy of the k-th vertical mode of the approximated m-mode system. In the next section we explain how to proceed theoretically on a simplified model in order to compute this energy threshold.

3.6 Which Residual Mode Captures the Energy of the Dominant Mode?

3.6.1 Stability for Low Energy

Consider the general second order Hamiltonian system ($i = 1, \dots, n$)

$$\ddot{y_i} + \lambda_i^2 y_i + U_{y_i}(Y) = 0\,, \qquad Y = (y_1, \dots, y_n) \in \mathbb{R}^n \tag{3.48}$$

for some $n \geq 2$, $\lambda_i > 0$ and some potential $U \in C^1(\mathbb{R}^n, \mathbb{R})$. In the previous sections we studied the evolution of the solutions of (3.48) satisfying the initial conditions

$$y_1(0) = \alpha\,,\ \dot{y}_1(0) = \beta\,, \qquad \sum_{i=2}^{n}(|y_i(0)| + |\dot{y}_i(0)|) \ll |\alpha| + |\beta| \tag{3.49}$$

for some $\alpha, \beta \in \mathbb{R}$. Due to these uneven boundary conditions, we call y_1 the **dominant mode** and y_i (for $i = 2, \dots, n$) the **residual modes**. In a bridge model, the dominant mode is a vertical oscillation whereas residual modes are torsional oscillations. Our main purpose is to establish if there is some energy transfer from the dominant mode towards the residual modes, that is, if the residual modes of the unique solution $Y = Y(t)$ of (3.48)–(3.49) grow up suddenly for some time $t > 0$. We saw that this is false if $|\alpha| + |\beta|$ is sufficiently small whereas it may become true if $|\alpha| + |\beta|$ is sufficiently large.

A natural question which arises is the following: which residual mode first captures the energy of y_1? Moreover, which is the criterion governing the transfer of energy? The relevance of these questions relies on the possibility to understand which kind of oscillating mode will first appear in the bridge when enough energy is inside the structure. In particular, this could enable designers to prevent the appearance of the destructive torsional oscillations. It is our purpose here to give a sound answer to these questions by considering a particular second order Hamiltonian system. This will give a qualitative explanation of what happens in more general systems.

We choose a potential U in such a way that the associated linearised problem (3.29) becomes a system of Mathieu equations [188]. The advantage of the Mathieu equations on the more general Hill equations is that much more precise information is known on the behavior of the stability regions. Using this fact, we give here a detailed explanation of how the stability is lost for the dominant mode and which residual mode will first capture its energy.

We consider (3.48) with $n = 3$; for our convenience we denote by (y, z_1, z_2) the unknowns instead of (y_1, y_2, y_3) and by $\mu, \lambda_1, \lambda_2$ the frequencies instead of $\lambda_1, \lambda_2, \lambda_3$. Finally, we choose as potential

$$U(y, z_1, z_2) = \frac{y^2 z_1^2 + y^2 z_2^2 + z_1^2 z_2^2}{2}\,; \tag{3.50}$$

note that U is perfectly symmetric with respect to the three variables and therefore U will not be responsible for the selection of the residual mode z_i capturing the energy of y. More general potentials U are discussed in Section 3.6.3. With the potential in (3.50), the system (3.48) with initial conditions becomes

$$\begin{cases} \ddot{y} + \mu^2 y + (z_1^2 + z_2^2)y = 0 & y(0) = \alpha,\ \dot{y}(0) = \beta \\ \ddot{z}_1 + \lambda_1^2 z_1 + (y^2 + z_2^2)z_1 = 0 & z_1(0) = z_1^0,\ \dot{z}_1(0) = z_1^1 \\ \ddot{z}_2 + \lambda_2^2 z_2 + (y^2 + z_1^2)z_2 = 0 & z_2(0) = z_2^0,\ \dot{z}_2(0) = z_2^1 . \end{cases} \tag{3.51}$$

The Hamiltonian system (3.51) has a conserved energy given by

$$E = \frac{1}{2}\Big(\dot{y}^2 + \dot{z}_1^2 + \dot{z}_2^2 + \mu^2 y^2 + \lambda_1^2 z_1^2 + \lambda_2^2 z_2^2 + y^2 z_1^2 + y^2 z_2^2 + z_1^2 z_2^2\Big) .$$

If in (3.51) we take $(\alpha, \beta) \neq (0, 0)$ and $z_1(0) = \dot{z}_1(0) = z_2(0) = \dot{z}_2(0) = 0$, then its unique solution satisfies $z_1 \equiv z_2 \equiv 0$, while y solves $\ddot{y} + \mu^2 y = 0$. Up to a time translation, we may reduce to the initial conditions $y(0) = x_0$ and $\dot{y}(0) = 0$: then the unique solution of (3.51) is given by $(y, z_1, z_2) = (x_0 \cos(\mu t), 0, 0)$. By linearising the (z_1, z_2)-equations in (3.51) around this solution we obtain the following couple of Mathieu equations

$$\ddot{\xi}_1 + \big(\lambda_1^2 + x_0^2 \cos^2(\mu t)\big)\,\xi_1 = 0 , \quad \ddot{\xi}_2 + \big(\lambda_2^2 + x_0^2 \cos^2(\mu t)\big)\,\xi_2 = 0 . \tag{3.52}$$

The system (3.52) takes the place of (3.29). Then, by mimicking Definition 3.7, we characterise the stability of the dominant mode.

Definition 3.13 We say that the dominant mode $y(t) = x_0 \cos(\mu t)$ of (3.51) is stable if the trivial solution $(\xi_1, \xi_2) = (0, 0)$ of (3.52) is stable. If one of the two Mathieu equations (3.52) has unstable trivial solution, we say that the corresponding residual mode captures the energy of the dominant mode.

The following stability result was proved in [38].

Theorem 3.14 *For any $\mu, \lambda_1, \lambda_2 > 0$ there exists $\overline{x_0} = \overline{x_0}(\mu, \lambda_1, \lambda_2) > 0$ such that the dominant mode $y(t) = x_0 \cos(\mu t)$ of (3.51) is stable for all $0 < x_0 < \overline{x_0}$.*

Since the proof of Theorem 3.14 is constructive and it gives an effective way to compute $\overline{x_0}$, we briefly outline it. From [198] we recall that the canonical form of the Mathieu equation is

$$\ddot{w} + (a + 2q \cos(2t))\, w = 0 \tag{3.53}$$

and therefore we first rewrite (3.52) as

$$\ddot{\xi}_1 + \left(\lambda_1^2 + \frac{x_0^2}{2} + \frac{x_0^2}{2}\cos(2\mu t)\right)\xi_1 = 0 , \quad \ddot{\xi}_2 + \left(\lambda_2^2 + \frac{x_0^2}{2} + \frac{x_0^2}{2}\cos(2\mu t)\right)\xi_2 = 0$$

and then, after a time scaling, we obtain

$$\ddot{\xi}_1+\left(\frac{2\lambda_1^2+x_0^2}{2\mu^2}+\frac{x_0^2}{4\mu^2}\cos(2t)\right)\xi_1=0,\quad \ddot{\xi}_2+\left(\frac{2\lambda_2^2+x_0^2}{2\mu^2}+\frac{x_0^2}{4\mu^2}\cos(2t)\right)\xi_2=0. \tag{3.54}$$

After comparison with (3.53) we see that in this case we have

$$a_i=\frac{2\lambda_i^2+x_0^2}{2\mu^2}\quad\text{and}\quad q_i=q=\frac{x_0^2}{4\mu^2}\quad\text{for } i=1,2\,, \tag{3.55}$$

that is, $a_i=2q+\lambda_i^2/\mu^2$. In the (q,a)-plane, the instability lines for (3.53) emanate from the points $(n^2,0)$, with $n\in\mathbb{N}$, see [198, fig.8A]. We reproduce the Mathieu stability diagram in the left picture of Fig. 3.6. The white (resp. grey) regions correspond to couples (q,a) for which the trivial solution of the equation (3.53) is stable (resp. unstable). In the right picture of Fig. 3.6 (which has a different scale), the green segments represent the lines (3.55). They start from the a-vertical axis at level λ_i^2/μ^2 and they all have slope 2. Therefore, starting from $x_0=0$ ($q=0$) there is an initial segment which lies in the stability (white) region. One should follow these lines by increasing x_0 until an instability (red) curve is reached. The abscissa of the intersection point is

$$q=\frac{x_0^2}{4\mu^2}\approx\frac{E}{2\mu^4}\,. \tag{3.56}$$

This gives both the stability bound for the amplitude x_0 and the flutter energy E.

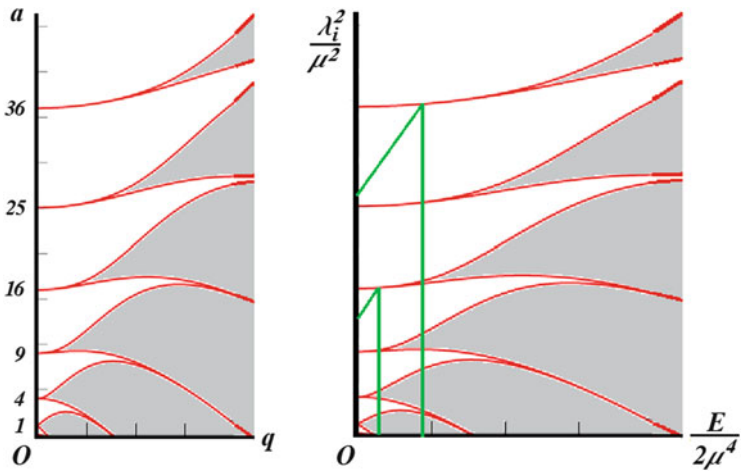

Fig. 3.6 The Mathieu diagram (*left*); How to compute the energy threshold (*right*)

3.6.2 Numerical Computation of the Flutter Energy

We numerically studied (3.51) by taking $\mu^2 = 1$, $\lambda_1^2 = 0.9$, $\lambda_2^2 = 0.1$, that is

$$\begin{cases} \ddot{y} + y + (z_1^2 + z_2^2)y = 0 & y(0) = x_0,\ \dot{y}(0) = 0 \\ \ddot{z}_1 + 0.1 \cdot z_1 + (y^2 + z_2^2)z_1 = 0 & z_1(0) = 10^{-3}x_0,\ \dot{z}_1(0) = 0 \\ \ddot{z}_2 + 0.9 \cdot z_2 + (y^2 + z_1^2)z_2 = 0 & z_2(0) = 10^{-3}x_0,\ \dot{z}_2(0) = 0\,. \end{cases} \tag{3.57}$$

The conserved energy of (3.57) is given by

$$E = \frac{\dot{y}^2}{2} + \frac{\dot{z}_1^2}{2} + \frac{\dot{z}_2^2}{2} + \frac{1}{2}y^2 + \frac{1}{20}z_1^2 + \frac{9}{20}z_2^2 + \frac{y^2z_1^2 + y^2z_2^2 + z_1^2z_2^2}{2} \approx \frac{x_0^2}{2}\,. \tag{3.58}$$

By using Mathematica, we could plot the graphs of the solution of (3.57) on the interval of time $t \in [0, 400]$ for varying x_0 and, therefore, varying energy E. We varied x_0 from $x_0 = 0.1$ to $x_0 = 3$ with step 0.1; we obtained plots of the residual modes z_1 and z_2 and we could see which of the two modes (if any!) captured the energy of the dominant mode y. We also plotted the graph of y which is somehow less interesting since for small $t > 0$ it essentially looks like $y(t) \approx x_0 \cos(\mu t)$ and is too large to allow to see the variations of the residual modes z_i. Since both the z_i start with amplitude of oscillations of the order of 10^{-3} (or even 10^{-4} for small x_0), we could detect their instability when their oscillations increased in amplitude of at least one order of magnitude. In order not to plot too many pictures, we describe the obtained results with 15 graphs from $x_0 = 0.2$ to $x_0 = 3$ with step 0.2. All the graphs are put side to side in Fig. 3.9 and are complemented with comments.

It is apparent that for $x_0 = 0.2$ both the residual modes remain small, nearly as their initial amplitude. It is however already visible that z_2 (black) has somehow regular cycles of variable amplitude. For $x_0 = 0.4$ we only see z_2 which grows up to $\approx 0.16 \gg z_2(0)$ while z_1 is not visible because it remains of the order of $z_1(0)$; this picture shows that z_2 has captured some of the energy of y whose amplitude has decreased as in Fig. 3.3. The same phenomenon is accentuated for $x_0 = 0.6$ where it appears earlier in time and z_2 grows up until ≈ 0.43.

An explanation of how the instability arises and a careful analysis of the transition may be performed as follows. By using the functions

`MathieuCharacteristicA[1,x]` and `MathieuCharacteristicB[1,x]`,

with the help of Mathematica we reproduce the Mathieu diagram in a neighborhood of $(q, a) = (0, 1)$ and, on the same graph, we plot the straight lines given by (3.55):

$$(\ell_1) \quad a = 0.1 + 2q \qquad \text{and} \qquad (\ell_2) \quad a = 0.9 + 2q\,.$$

The obtained picture on the interval $q \in [0, 1/4]$ is represented in Fig. 3.7. Starting from $q = 0$ (that is, $x_0 = 0$ by (3.56)), the line (ℓ_2) is the first one

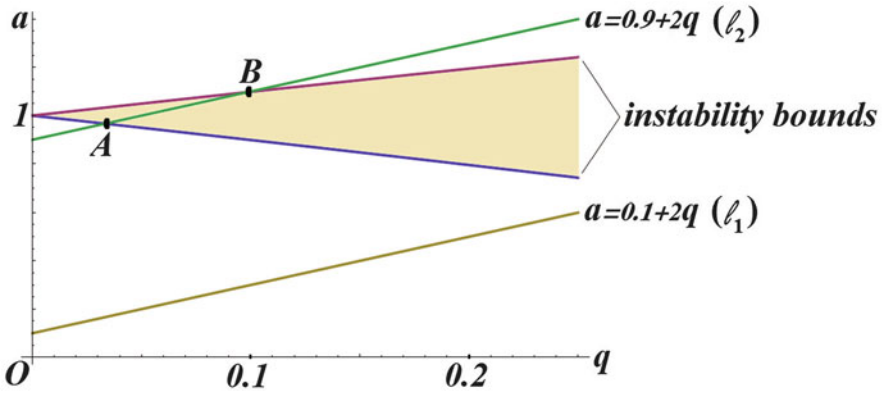

Fig. 3.7 Intersections between the stability regions and the parametric lines (local view)

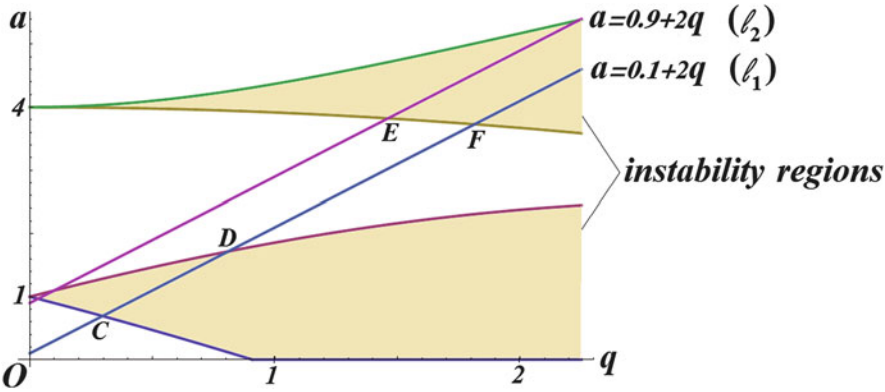

Fig. 3.8 Intersections between the stability regions and the parametric lines (global view)

which exits the (white) stability region. This happens at the point A which, again computed with Mathematica, has the abscissa $q \approx 0.033$ and therefore, in view of (3.55), $x_0 \approx 0.36$. At this amplitude of oscillation of y, the residual mode z_2 starts capturing its energy. Fig. 3.9 confirms that the transition occurs for $0.2 < x_0 < 0.4$. By (3.58) the flutter energy is $E \approx 0.066$. In the next two pictures ($x_0 \in \{0.8, 1\}$) we see that none between z_1 and z_2 captures the energy of y, they essentially remain of the same order of magnitude as the initial data. This means that the line (ℓ_1) has not yet entered in the instability region of the Mathieu diagram while (ℓ_2) has exited. Looking again at Fig. 3.7, we see that the latter fact occurs at the point B, which corresponds to $q \approx 0.099$ and therefore to $x_0 \approx 0.63$. At this amplitude of oscillation of y, the residual mode z_2 stops capturing its energy. The graphs in Fig. 3.9 confirm that the transition occurs for $0.6 < x_0 < 0.8$. In order to see when (ℓ_1) enters into the instability region we need to take a larger view of the Mathieu diagram, see Fig. 3.8. In this picture we represent the diagram for $q \in [0, 9/4]$ since

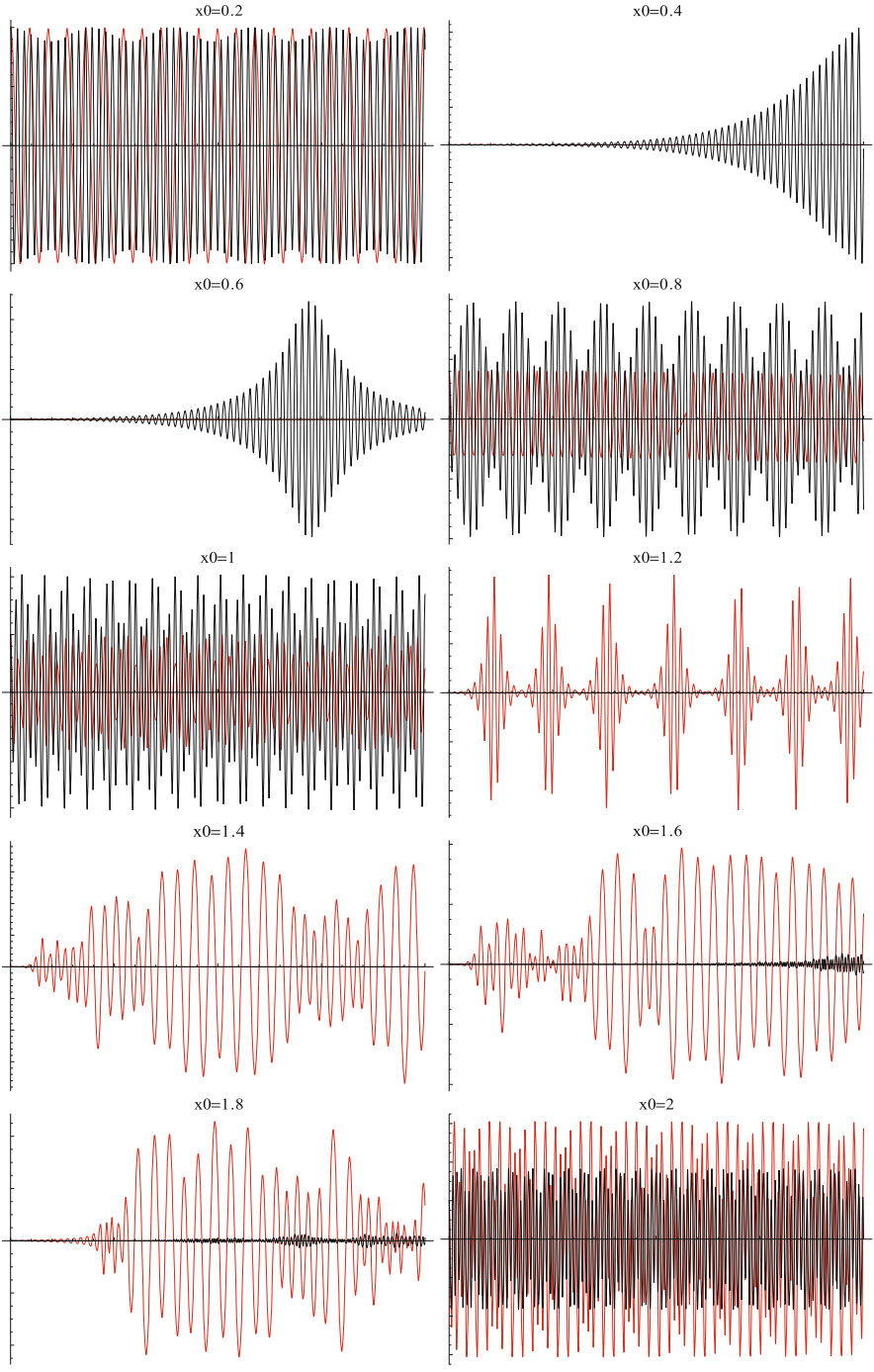

Fig. 3.9 (continued)

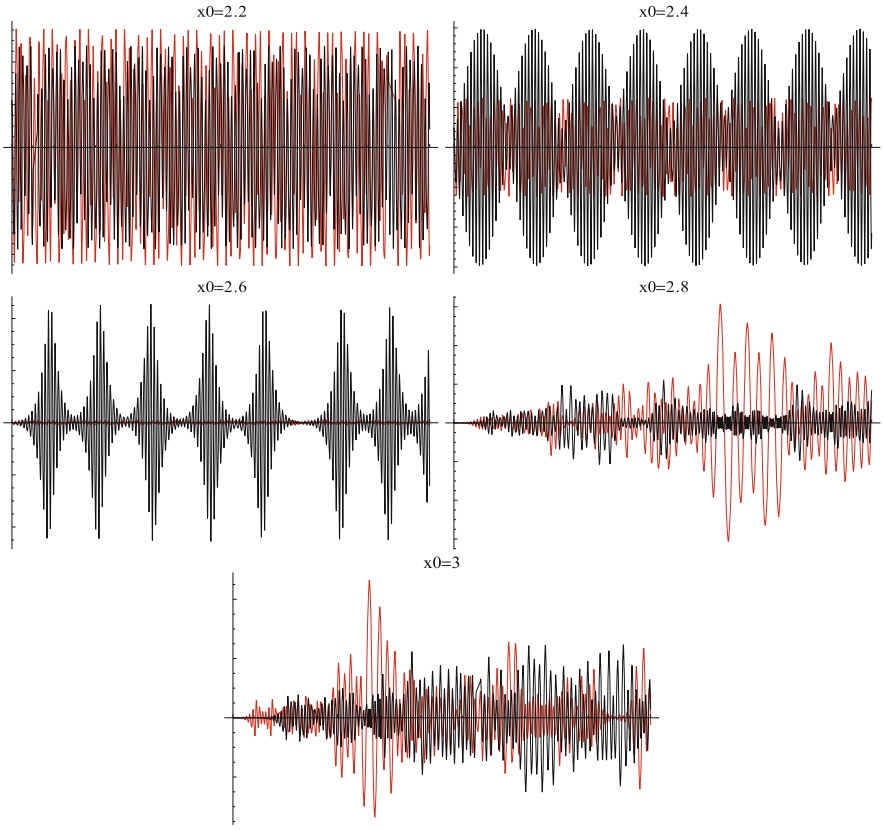

Fig. 3.9 Plots of z_1 (*red*) and z_2 (*black*) for x_0 from 0.2 to 3 with step 0.2

$q = 9/4$ corresponds to $x_0 = 3$; moreover, we do not place again the points A and B in order to have a more readable picture. The point where (ℓ_1) enters the instability region is C, see Fig. 3.8: numerically, it corresponds to $q \approx 0.3$ and to $x_0 \approx 1.1$. This explains why in Fig. 3.9, case $x_0 = 1.2$, we see that z_1 enlarges and captures the energy of the dominant mode y.

By increasing further x_0, namely for $x_0 \in \{1.4, 1.6, 1.8\}$, we learn from Fig. 3.9 that z_1 may become even larger than x_0, that is, of the initial amplitude of the dominant mode. From the energy conservation we infer that this can happen only if y is almost 0 when $|z_1|$ reaches its maximum. This shows that there has been a change of the frequencies and that the period of z_1 is essentially a multiple (possibly the same) of the period of y. For $x_0 \in \{1.6, 1.8\}$ we also see that z_2 increases its amplitude after some (long) interval of time. We believe that this happens because z_2 captures some energy from z_1; this would mean that the linearised problem has changed and that different straight lines should be drawn on the Mathieu diagram. Therefore, this does not mean that (ℓ_2) has reached the point E in Fig. 3.8.

If $x_0 \in \{2, 2.2\}$ we see that no residual mode is capturing the energy of the dominant mode, both z_1 and z_2 have an amplitude of oscillation of the order of 10^{-3}. This means that the line (ℓ_1) has crossed the point D which, numerically, is seen to occur for $q \approx 0.81$ and to $x_0 \approx 1.8$. This fact is confirmed by a finer experiment performed for $x_0 = 1.81$: in this case, the picture looks like that for $x_0 = 2$. If $x_0 = 2.4$, we see that z_2 starts to become larger, which means that the line (ℓ_2) is approaching the point E in Fig. 3.8. And, indeed, we numerically found that the abscissa of E is $q \approx 1.46$ which corresponds to $x_0 \approx 2.42$.

For $x_0 = 2.6$ the line (ℓ_2) is beyond E and has entered in the second instability region, a fact which is clearly displayed in the related picture in Fig. 3.9. The point F in Fig. 3.8 is the point where also (ℓ_1) enters in the second instability region: its abscissa is $q = 1.81$ corresponding to $x_0 \approx 2.69$. And indeed, the plots for $x_0 \in \{2.8, 3\}$ show a chaotic behavior where both the residual modes capture the energy of the dominant mode.

The just described numerical results enable us to give a precise answer to the question raised in the title of Section 3.6 relatively to the particular second order Hamiltonian system (3.57).

The residual mode which captures the energy of the dominant mode depends on its amplitude of oscillation or, equivalently, on the amount of energy present within (3.57).

The response is summarised in Table 3.4 where RMCE means **residual mode capturing the energy** and x_0 varies in the interval $[0, 3]$.

Table 3.4 Residual modes capturing the energy of the dominant mode

$x_0 \in$	$[0, 0.36)$	$(0.36, 0.63)$	$(0.63, 1.1)$	$(1.1, 1.8)$	$(1.8, 2.42)$	$(2.42, 2.69)$	$(2.69, 3]$
RMCE	None	z_2	None	z_1	None	z_2	Both

We performed further experiments which confirmed the just illustrated precise pattern. The lines (ℓ_1) and (ℓ_2) intersect alternatively the stability/instability regions giving rise to one of the above pictures. From these experiments we may draw the following conclusions.

- Which residual mode captures the energy of the dominant mode depends on the ratios λ_i/μ: these ratios determine the point of the a-axis in the Mathieu diagram where the straight lines (3.55) start at zero energy.
- The flutter energy is $\mu^2 x_0^2/2$, see (3.56): one can use Fig. 3.6 to compute it.

Remark 3.15 The numerical results in the present section are extremely precise and perfectly match the behavior illustrated in Figs. 3.7 and 3.8. We also refer to [38] for more related results. This confirms that Definitions 3.7 and 3.13 are suitable to describe the torsional instability.

3.6.3 More General Nonlinearities

If we replace (3.50) with

$$U(y,z_1,z_2)=\frac{\alpha y^2z_1^2+\beta y^2z_2^2+z_1^2z_2^2}{2}\qquad \alpha,\beta>0\,,$$

then (3.54) becomes

$$\ddot{\xi}_1+\left(\lambda_1^2+\frac{\alpha x_0^2}{2}+\frac{\alpha x_0^2}{2}\cos(2\mu t)\right)\xi_1=0,\quad \ddot{\xi}_2+\left(\lambda_2^2+\frac{\beta x_0^2}{2}+\frac{\beta x_0^2}{2}\cos(2\mu t)\right)\xi_2=0,$$

so that we still obtain two Mathieu equations but with (3.55) replaced by

$$a_1=\frac{2\lambda_i^2+\alpha x_0^2}{2\mu^2}\quad\text{and}\quad q_1=\frac{\alpha x_0^2}{4\mu^2}\,,\quad a_2=\frac{2\lambda_i^2+\beta x_0^2}{2\mu^2}\quad\text{and}\quad q_2=\frac{\beta x_0^2}{4\mu^2}\,.$$

In both cases we have $a_i=\frac{\lambda_i^2}{\mu^2}+2q_i$, that is, we obtain a different parametrisation of the same lines. In terms of the stability analysis the size of α and β may be exploited to increase or decrease the energy threshold for the stability of the corresponding equation.

If we consider a potential $U=U(y,z_1,z_2)$ satisfying

$$U_{z_1z_1}(y,0,0)=U_{z_2z_2}(y,0,0)=0\qquad\forall y\in\mathbb{R}\tag{3.59}$$

then the linearised problem (3.54) simply becomes

$$\ddot{\xi}_1+\lambda_1^2\xi_1=0\,,\quad \ddot{\xi}_2+\lambda_2^2\xi_2=0\tag{3.60}$$

and is therefore independent of y and of its amplitude of oscillation. As an example, consider the potential

$$U(y,z_1,z_2)=\frac{y^4z_1^4+y^4z_2^4+z_1^4z_2^4}{4}$$

so that (3.51) becomes (for some small ε)

$$\begin{cases}\ddot{y}+\mu^2y+(z_1^4+z_2^4)y^3=0 & y(0)=x_0,\ \dot{y}(0)=0\\ \ddot{z}_1+\lambda_1^2z_1+(y^4+z_2^4)z_1^3=0 & z_1(0)=\varepsilon x_0,\ \dot{z}_1(0)=0\\ \ddot{z}_2+\lambda_2^2z_2+(y^4+z_1^4)z_2^3=0 & z_2(0)=\varepsilon x_0,\ \dot{z}_2(0)=0\,.\end{cases}\tag{3.61}$$

In this case, the parametric equations (3.55) make no sense and the corresponding (green) lines in Fig. 3.6 are horizontal: we call this case **degenerate**. We have tried some numerical experiments but we could not formulate a precise rule for instability. Let us describe some of the results we obtained.

- If $\mu = \lambda_1 = 1$, $\lambda_2 = 2$ and $\varepsilon = 10^{-3}$, the system was extremely unstable. The residual mode z_1 started capturing the energy of y even for small values of x_0. With some fine experiments we could detect instability already for $x_0 = 0.5$, but we suspect the system to be unstable since the very beginning. Completely similar results were obtained for other choices of $\lambda_2 > \lambda_1 = \mu$. And also the case $\lambda_2 = \lambda_1 = \mu$ gave similar response with the addition (of course!) that both z_1 and z_2 captured the energy of y.
- If $\mu = 1$, $\lambda_1 = \sqrt{2}$, $\lambda_2 = 2$, $x_0 = 1$ and $\varepsilon = 0.5$ (a large ε compared with 10^{-3} in (3.57)!) we found that the dominant mode y captured some small amount of energy from the residual mode z_2. Therefore, it is not true that the energy always moves from the dominant to a residual mode, also the dominant mode can capture the energy and become "more dominant". This seems to be related to the "end of the black bumps" displayed in many plots, see e.g. Fig. 3.3.
- If $\mu = 1$, $\lambda_1 = \sqrt{2}$, $\lambda_2 = 2$ and $\varepsilon = 10^{-3}$, we could see some energy going from y to z_2 only for $x_0 \geq 10$. Therefore, the system turned out to be very stable. We suspect that, again, the ratios λ_i/μ play a major role.

Instead of a simple linearisation of (3.61), yielding the constant coefficient system (3.60), one could also try something slightly different. First solve (3.61) with $\varepsilon = 0$ and obtain the solution $(y, z_1, z_2) = (x_0 \cos(\mu t), 0, 0)$. Then replace this solution into the z_i-equations of (3.61) to obtain the system

$$\begin{cases} \ddot{\xi}_1 + \lambda_1^2 \xi_1 + x_0^4 \cos^4(\mu t)\, \xi_1^3 = 0 \\ \ddot{\xi}_2 + \lambda_2^2 \xi_2 + x_0^4 \cos^4(\mu t)\, \xi_2^3 = 0\,. \end{cases} \tag{3.62}$$

This system appears somehow intermediate between the original problem (3.61) and its linearisation (3.60). However, as a consequence of a result by Ortega [213], also the trivial solution of (3.62) is stable and no additional information is obtained from this procedure.

What we have seen in this section suggests that degenerate problems such as (3.61) are either extremely unstable (manifesting instability for very small energies) or extremely stable with instability appearing only for very large energies. This alternative depends on the ratios λ_i/μ. It is also clear that (3.61) cannot remain stable for any energy since (3.62) fails to take into account both the interactions between the residual modes and the perturbations of the periodic solution $y(t) = x_0 \cos(\mu t)$: these are fairly small but for large energies they do play some role.

Summarising, the degenerate case, where (3.59) holds and the linearised problem (3.60) does not depend on the energy nor on the amplitude of the dominant mode, behaves quite differently and a neat pattern as the one described in Sect. 3.6.2 is not available.

Finally, we point out that if U does not have a polynomial behavior, then more general Hill equations appear. The parametric lines (3.55) may be significantly different as well as the stability/instability diagram, see [60, 61]. Whence, a precise stability analysis becomes more difficult although the underlying phenomena remain the same.

3.6.4 Mechanical Interpretation and Structural Remedies

Although obtained in a fairly simplified model, the results in the previous sections enable us to relate the stability of a suspension bridge with its vertical and torsional frequencies. In suspension bridges the dominant mode is vertical whereas the residual modes are torsional. Therefore, in (3.51) y represents vertical oscillations and the z_i represent the torsional oscillations.

In this section we aim to justify from a mechanical point of view the numerical results described in the previous sections and some further results found in [38]. Let us first summarise the main phenomena observed.

(I) As long as the two couples of parameters (q, a_i) of (3.55) lie in the (white) stability region of the Mathieu diagram, see Figs. 3.7 and 3.8, the solution $(\bar{y}, 0, 0) = (x_0 \cos(\mu t), 0, 0)$ of system (3.51) is stable, see Definition 3.13.
(II) When a couple (q, a) lies in an instability region and is sufficiently far from the stability region, then the corresponding residual modes become fairly large.
(III) When the couple (q, a) lies in an instability region but is close to the stability region, our numerical results could not detect a neat instability.

The most intriguing result is certainly (III). In order to better understand it, we performed some numerical experiments on the classical linear Mathieu equation (3.53). To obtain two independent solutions, in all our experiments we plotted the two solutions with initial data $(w(0), \dot{w}(0)) \in \{(1, 0); (0, 1)\}$. We analysed in particular the two first instability regions. From [267] we know that (q, a) lies in the first or second instability region for small enough q if, respectively,

$$1-q+O(q^2)<a<1+q+O(q^2) \text{ or } 4-\frac{1}{12}q^2+O(q^4)<a<4+\frac{5}{12}q^2+O(q^4).$$

Therefore, we considered couples such as $(q, a) = (q, 1)$ and $(q, a) = (q, 4)$ for $q > 0$ sufficiently small and we could observe the following facts.

(IV) In all the experiments the solutions of (3.53) were unbounded (thereby confirming instability).
(V) For very small q the solutions became large only after a long interval of time.
(VI) For larger values of q the solutions became large much earlier in time.
(VII) For the same $q > 0$ the instability was stronger when $a = 1$ than when $a = 4$.

The observation (VII) appears strictly related to (II) and (III) and enables us to conclude that

if the couple (q, a) lies in the instability region of the Mathieu diagram, then the instability of the trivial solution of (3.53) increases with the distance of the couple (q, a) from the stability regions.

But the model system (3.51) is nonlinear and all its solutions are bounded in view of the energy conservation. Whence, we cannot expect that its solutions start increasing in amplitude as for (3.53). Roughly speaking,

when the residual mode exhibits a tendency to grow up, the energy conservation bounces it back and decreases its amplitude.

We can however expect that the residual modes start growing up earlier in time and wider in amplitude if the parameters are farther from the stability region. This is precisely what we saw in our experiments, see [38]. In particular, when the parametric lines (3.55) reach and intersect a thin instability region (one of the cusps close to some $a = n^2$ with $n \geq 2$), the parameters are so close to the stability region that the energy inhibits the residual modes to capture a significant amount of energy. From the physical point of view, the instability which occurs when the lines (3.55) cross a thin cusp is irrelevant, both because it has low probability to occur and because, even if it occurs, the residual mode remains fairly small. In turn, from the mechanical point of view, we know that small torsional oscillations are harmless and the bridge would remain safe, see (3.13). Summarising, we conclude that

when the parametric lines (3.55) cross a thin instability region, only small torsional oscillations appear and the bridge basically remains stable.

From the Mathieu diagram and from the asymptotic behavior of the separating lines (see again [267]) we learn that the instability regions become more narrow as $a = n^2$ increases. Let us recall that for common bridges one has $\lambda_i > \mu$, see (1.4): since the parametric lines (3.55) take their origin when $a = \lambda_i^2/\mu^2 > 1$ (see the right picture in Fig. 3.6), it would be desirable that $\lambda_i \gg \mu$. This readily gives a structural remedy to improve the torsional stability of a bridge:

the torsional stability of a suspension bridge depends on the ratios between the torsional frequencies and the vertical frequencies; the larger they are, more stable is the bridge.

Therefore, our results suggest that bridges should be planned in such a way that these ratios become very large.

For a different model, obtained with several linearisations and simplifications (including the one discussed in Sect. 2.5.1), Malík [182, Criterion S] claims that the stability of a bridge modeled by (3.4) depends on how close are the eigenvalues of

the linearised (and decoupled) beam and torsional equations. He studies decoupled equations because on [183, p. 3775] he states that at the TNB

. . .during the violent oscillations the hangers did not loosen. . .

But from the video [253] and from the testimony of Farquharson [9, V-12] we know that during the TNB collapse *one of the four suspenders in its group was permanently slack*. And, as discussed in Sect. 2.8, slackening of the hangers is one of the main sources of nonlinearity and, in turn, of the coupling between the cables and the roadway. Therefore, this coupling should also appear between vertical and torsional equations. We also claim that the behavior of the eigenvalues (frequencies) plays a major role in the torsional stability but our arguments are completely different. Theorem 3.10 shows that the intrinsic nonlinearity of the coupling term generates "variable in time spectra" which may lead to a resonance: we believe that

a structural nonlinearity is responsible for the internal resonance which is the starting spark for torsional instability when the internal energy reaches the flutter energy.

This is confirmed by the results in this chapter, in particular in the present Sect. 3.6.

3.7 The Role of Aerodynamic Forces

3.7.1 Numerical Results

Even in absence of wind, an aerodynamic force is exerted on the bridge by the surrounding air in which the structure is immersed: it is due to the relative motion between the bridge and the air. Pugsley [227, Sect. 12.7] assumes that the aerodynamic forces depend linearly on the cross-derivatives and functions, see also [239] and (4.5) in the next chapter. In this section we investigate the effects of the aerodynamic forces on the 1-mode system (3.31).

We first consider the case where only the cross-derivatives are involved. This leads to the following modified system:

$$\begin{cases} \ddot{y}_1 + 3y_1 + \frac{3}{2}y_1^3 + \frac{9}{2}y_1 z_1^2 + \delta \dot{z}_1 = 0 \\ \ddot{z}_1 + 7z_1 + \frac{9}{2}z_1^3 + \frac{27}{2}z_1 y_1^2 + \delta \dot{y}_1 = 0 \end{cases} \tag{3.63}$$

with $\delta > 0$. As in (3.37), we take the initial conditions

$$y_1(0) = \sigma = 10^4 z_1(0)\,, \quad \dot{y}_1(0) = \dot{z}_1(0) = 0 \tag{3.64}$$

for different values of σ and we wish to highlight the differences, if any, between (3.31) and (3.63). For (3.63) we have no energy conservation; however, let

us consider the (variable) energy function

$$E(t) = \frac{\dot{y}_1^2}{2} + \frac{\dot{z}_1^2}{6} + \frac{3}{2}y_1^2 + \frac{7}{6}z_1^2 + \frac{9}{4}y_1^2 z_1^2 + \frac{3}{8}(y_1^4 + z_1^4)\,. \tag{3.65}$$

We first take $\sigma = 1.47$ and we modify the aerodynamic parameter δ. In Figs. 3.10 and 3.11 we plot both the behavior of the solutions (first line) and the behavior of the energy $E(t)$ (second line), for increasing values of δ.

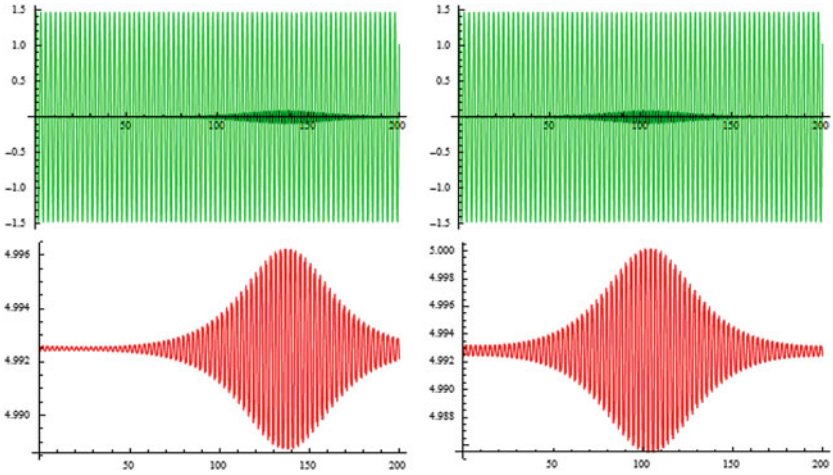

Fig. 3.10 On the interval $t \in [0, 200]$, plot of the solutions y_1 (*green*) and z_1 (*black*) of (3.63)–(3.64) for $\sigma = 1.47$ and $\delta = 0.01,\ 0.02$ (from *left* to *right* on the first line). On the second line (*red*), the energy $E = E(t)$ defined in (3.65)

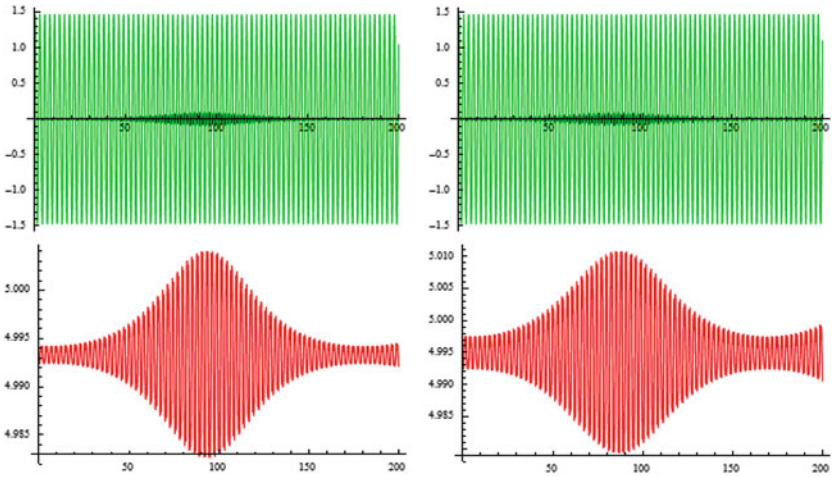

Fig. 3.11 On the interval $t \in [0, 200]$, plot of the solutions y_1 (*green*) and z_1 (*black*) of (3.63)–(3.64) for $\sigma = 1.47$ and $\delta = 0.03,\ 0.05$ (from *left* to *right* on the first line). On the second line (*red*), the energy $E = E(t)$ defined in (3.65)

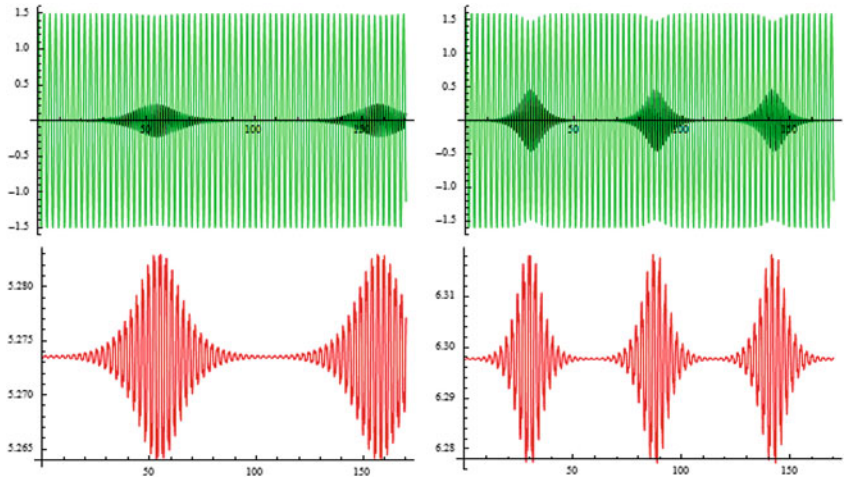

Fig. 3.12 On the interval $t \in [0, 170]$, plot of the solutions y_1 (*green*) and z_1 (*black*) of (3.63)–(3.64) for $\delta = 0.01$ and $\sigma = 1.5,\ 1.6$ (from *left* to *right* on the first line). On the second line (*red*), the energy $E = E(t)$ defined in (3.65)

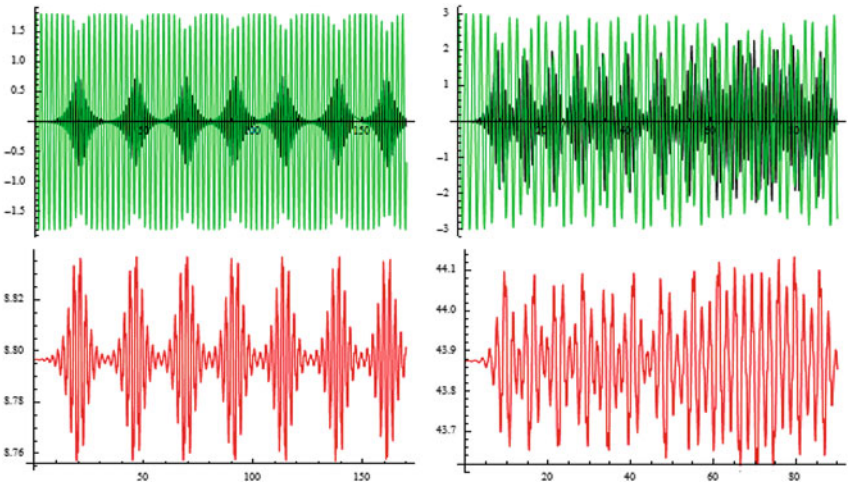

Fig. 3.13 On the interval $t \in [0, 170]$, plot of the solutions y_1 (*green*) and z_1 (*black*) of (3.63)–(3.64) for $\delta = 0.01$ and $\sigma = 1.8,\ 3$ (from *left* to *right* on the first line). On the second line (*red*), the energy $E = E(t)$ defined in (3.65)

The first lines in Figs. 3.10 and 3.11 should be compared with the second picture in Fig. 3.3 (case $\delta = 0$). We note that, as the aerodynamic parameter increases, the transfer of energy is anticipated but it is not amplified. Quite surprisingly, on the second line we see that the energy $E(t)$ remains almost constant except in the interval of time where the transfer of energy occurs: for increasing aerodynamic parameters δ we observe increasing variations in the energy behavior.

Then we maintain fixed $\delta = 0.01$ and we increase the initial energy, that is, the initial amplitude of oscillation. In Figs. 3.12 and 3.13 we plot both the behavior

of the solutions (first line) and the behavior of the energy $E(t)$ (second line), for increasing values of σ. It turns out that all the phenomena are anticipated (in time) and amplified (in width) and reach a quite chaotic behavior for $\sigma = 3$ where we had to stop the numerical integration at $t = 90$. Finally, let us mention that below the flutter energy the aerodynamic forces did not vary the initial energy of (3.63).

Let us now consider the case where also the cross-terms of order 0 are involved. Then, instead of (3.63) we obtain the system

$$\begin{cases} \ddot{y}_1 + 3y_1 + \frac{3}{2}y_1^3 + \frac{9}{2}y_1 z_1^2 + \delta(\dot{z}_1 + z_1) = 0 \\ \ddot{z}_1 + 7z_1 + \frac{9}{2}z_1^3 + \frac{27}{2}z_1 y_1^2 + 3\delta(\dot{y}_1 + y_1) = 0 \end{cases} \tag{3.66}$$

where the coefficient 3 in the second equation comes from the variation of the energy

$$E(t) = \frac{\dot{y}_1^2}{2} + \frac{\dot{z}_1^2}{6} + \frac{3}{2}y_1^2 + \frac{7}{6}z_1^2 + \frac{9}{4}y_1^2 z_1^2 + \frac{3}{8}(y_1^4 + z_1^4) + \delta y_1 z_1 \,. \tag{3.67}$$

Also for (3.66) we do not have energy conservation but this function E better approximates the internal energy. It may be questionable whether to include the last term $\delta y_1 z_1$ into E since this term depends on the aerodynamic coefficient δ. However, the behavior of E which we now analyse does not depend on the presence of this term. We take again as initial conditions

$$y_1(0) = \sigma = 10^4 z_1(0)\,, \quad \dot{y}_1(0) = \dot{z}_1(0) = 0 \tag{3.68}$$

with $\sigma \geq 1.47$ so that we are above the flutter energy, see Sect. 3.4.3. In Fig. 3.14 we plot both the behavior of the solution (left picture) and the behavior of the energy $E(t)$ (right picture) of (3.66)–(3.68).

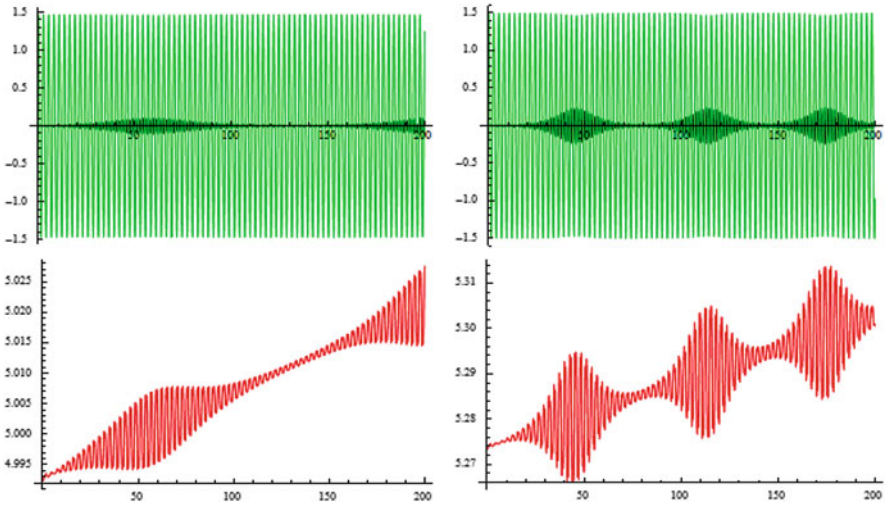

Fig. 3.14 On the interval $t \in [0, 200]$, plot of the solutions y_1 (*green*) and z_1 (*black*) of (3.66)–(3.68) for $\delta = 0.01$ and $\sigma = 1.47,\ 1.5$ (from *left* to *right* on the first line). On the second line (*red*), the energy $E = E(t)$ defined in (3.67)

It is quite visible that the instability is further anticipated but now also the amplitude is enlarged. Moreover, the energy increases also in absence of torsional instability: this variation is due to the cross-derivatives since all the other terms appear in the energy (3.67). The very same behavior is obtained for the internal energy, namely the energy (3.67) without the last term $\delta y_1 z_1$. We also remark that the energy E fails to follow a regular pattern only in presence of instability. We only quote these numerical results because all the other experiments gave completely similar responses. In particular, the dependence on δ described by Figs. 3.10 and 3.11 continues also for negative δ: the sign of δ tells whether the action of the aerodynamic force is a friction or an input of energy (self-excitation).

3.7.2 The Pattern Creating Oscillations in Suspension Bridges

As pointed out by Irvine [149, p. 176], the numerical approach is probably the most appropriate to analyse a model which also involves aerodynamic forces. The reason is that a satisfactory stability theory for systems such as (3.63) and (3.66) is not available. Nevertheless, some theoretical conclusions can be drawn also for these systems near the pure vertical mode $\bar{y}$. Here "pure" means that no interactions with the surrounding are admitted and only the structural behavior of the bridge is considered. Let us explain how the results for the isolated system (3.31) may be extended to (3.63); one can then proceed similarly for (3.66).

For system (3.31), two steps were necessary to define the torsional stability of the unique (periodic) solution $\bar{y}$ of (3.33) (the pure mode):

(i) We linearise the torsional equation of the system (3.31) around $(\bar{y}, 0)$, see (3.36).
(ii) We apply Definition 3.7, that is, we say that the pure vertical mode $\bar{y}$ at energy $E(\alpha, \beta)$ is torsionally stable if the trivial solution of (3.36) is stable.

We underline that the system (3.31) is isolated and that (3.36) is unforced. In this situation, the above steps (i)–(ii) are equivalent to:

(I) In the torsional equation of the system (3.31) we drop all the z_1-terms of order greater than or equal to one and we replace y_1 with $\bar{y}$.
(II) We say that the pure vertical mode $\bar{y}$ at energy $E(\alpha, \beta)$ is torsionally stable if all the solutions of (3.36) are globally bounded.

If we replace (3.31) with the system (3.63), then (i)–(ii) make no sense while (I)–(II) do. A linearisation as in (i) would exclude the aerodynamic forces, while acting as in (I) preserves them and gives rise to the forced Hill equation

$$\ddot{\xi} + a(t)\xi = f(t) \quad \text{with} \quad a(t) = 7 + \frac{27}{2}\overline{y}(t)^2 \text{ and } f(t) = -\delta\dot{\bar{y}}(t)\,, \tag{3.69}$$

where $\bar{y}$ is the unique periodic solution of (3.33). Needless to say, f and a have the same period. The definition (ii) is inapplicable to (3.69) since $\xi \equiv 0$ is not a solution, while (II) is a verifiable property for (3.69). This is the general definition of stability that we adopt for the vertical mode $\bar{y}$. With this definition the following statement holds.

Theorem 3.16 *Let $\overline{y}$ be the pure vertical mode at energy $E(\alpha, \beta)$, that is, the solution of (3.33). Then $\bar{y}$ is torsionally stable for (3.31) if and only if it is torsionally stable for (3.63).*

By applying Theorems 3.9 and 3.16 we infer that the energy threshold for the stability of (3.63) is at least $\frac{235}{294}$. Furthermore, in agreement with the numerical results described in Sect. 3.7.1, Theorem 3.16 shows that

the flutter energy does not depend on the strength of aerodynamic forces; in particular, an isolated system has the same flutter energy.

The elementary numerical results in Sect. 3.7.1 raise many natural questions and suggest to study further the impact of aerodynamic forces. However, they also suggest that

the onset of torsional instability is of structural nature, the aerodynamic forces excite the energy only after that the structural torsional instability has appeared.

This is confirmed by further numerical results: if we delete the nonlinearity, then the coupling between the two equations in (3.63) or in (3.66) is of purely aerodynamic nature and the resulting (linear) system does not display an energy transfer. Therefore, the torsional instability has a structural origin although the whole phenomenon governing the oscillations appears to be more complicated, especially if we also consider the action of the wind. As we saw in Sect. 1.7.6, when the wind hits the bridge, vortices are created. The vortices generate aerodynamic forces which increase the internal energy of the structure. When the amount of energy reaches the flutter energy, a structural instability appears: this is the onset of torsional oscillations. At this stage the aerodynamic forces excite the internal energy irregularly giving rise to further self-excited oscillations.

The full energy-oscillation mechanism is described above through a very simplified model which certainly needs to be significantly improved. But, at least qualitatively, we believe that the mechanism generating oscillations in a suspension bridge is the following:

1. The impact of the wind with the structure creates vortices.
2. Vortices create a lift which starts vertical oscillations of the bridge.
3. When vertical oscillations are sufficiently large, torsional oscillations may appear.
4. The onset of torsional instability is of structural nature.
5. The aerodynamic forces excite the energy after that the structural torsional instability has appeared.
6. The flutter energy is independent of the strength of aerodynamic forces.

3.8 Brief History of the Hill and the Mathieu Equations

The Hill equation (1) is due to the American astronomer and mathematician George William Hill (1838–1914) and was systematically studied since the paper [141], which is the reprinted version of an original manuscript first published at Cambridge (US) in 1877. Roughly speaking, Hill viewed the motion of the moon as a harmonic oscillator in a periodic gravitational field. In the Preface we stated that the Hill equation plays a crucial role in the stability analysis of suspension bridges. Let us rewrite it here:

$$\ddot{y}(t) + a(t)y(t) = 0 \tag{3.70}$$

where $a(t)$ is a periodic coefficient. It is not difficult to exhibit examples where the solutions of (3.70) are unbounded. For instance, the equation

$$\ddot{y}(t) - \frac{2(1+\cos t)}{2+\sin t}\, y(t) = 0$$

admits the family of unbounded solutions $y(t) = c\, e^t (2+\sin t)$ for any $c \neq 0$. The main issue concerning the Hill equation (3.70) is precisely to determine whether all its solutions are globally bounded. Since (3.70) is a linear equation, it suffices to consider solutions corresponding to linearly independent initial conditions such as

$$(y(0), \dot{y}(0)) \in \Big\{(1,0);(0,1)\Big\}.$$

Moreover, the linear feature of (3.70) yields the following equivalence

any solution of (3.70) is bounded $\Longleftrightarrow$ the solution $y \equiv 0$ of (3.70) is stable.

Starting from the celebrated result by the Russian mathematician Aleksandr Michajlovič Lyapunov [178] (1857–1918), there have been a large amount of studies to find sufficient conditions for the stability of the solution $y \equiv 0$ of (3.70), see [64, 72, 76, 180, 282, 284] and references therein. In recent years the attention has turned to the stability of nonlinear versions of (3.70). For instance, Ortega [213] considers equations of the form

$$\ddot{y}(t) + a(t)y(t) + c(t)y(t)^{2n+1} = 0 \tag{3.71}$$

where a, c are periodic coefficients having the same period and $n \in \mathbb{N}$; he proves that if c does not change sign then the trivial solution of (3.71) is stable provided that the trivial solution of (3.70) is stable. This shows a connection between the original Hill equation (3.70) and its nonlinear variants. By [213] we know that the stability of the trivial solution of (3.36) implies the stability of the trivial solution of

$$\ddot{\xi} + a(t)\xi + \frac{9}{2}\xi^3 = 0 \quad \text{with} \quad a(t) = 7 + \frac{27}{2}\overline{y}(t)^2$$

which coincides with the second equation in the system (3.31).

For some stability criteria of the trivial solution of a system of linear differential equations with periodic coefficients we refer to [247]. In the case of a nonlinear system such as (3.31) the stability analysis is much more complicated: as far as we are aware there are only few stability results for nonlinear *first order planar systems*. This is why we focused our attention to the initial conditions $z_1(0) = \dot{z}_1(0) = 0$; this reduces the system (3.31) to the autonomous equation which admits a periodic solution. In turn, a suitable transformation of this periodic solution becomes the coefficient of the linearised equation (3.36). And the just seen connection between (3.71) and (3.70) seems to justify our approach.

The Mathieu equations [188] are a particular case of the Hill equations and were introduced much earlier by the French mathematician Émile Léonard Mathieu (1835–1890) when analysing the motion of elliptical membranes. The Mathieu equations are (3.70) with $a(t) = a + 2q\cos(2t)$, see (3.53) and precise stability criteria are known according to the values of a and q, see e.g. [267]. However, also the Mathieu functions are difficult to employ, *mainly because of the impossibility of analytically representing them in a simple and handy way*, see e.g. [116, 244].

3.9 Bibliographical Notes

The material from Sect. 3.2 is taken from [282]. A forced and damped version of (3.4) was studied by Moore [205] with

$$f(s) = k\left[\left(s + \frac{mg}{2k}\right)^+ - \frac{mg}{2k}\right], \tag{3.72}$$

a nonlinearity which models hangers behaving as linear springs of elastic constant $k > 0$ if stretched but exert no restoring force if compressed; here g is gravity. This nonlinearity describes the possible slackening of the hangers (occurring for $s \leq -\frac{mg}{2k}$). But Moore considers the case where the hangers do not slacken: then f becomes linear, $f(s) = ks$, and the two equations in (3.4) decouple. In this situation there is obviously no interaction between vertical and torsional oscillations. A general nonlinear f was introduced in (3.4) by Holubová-Matas [142] who were able to prove well-posedness for a forced-damped version of (3.4). The copyright of the name *fish-bone model* should be attributed to Berchio-Gazzola [36].

Up to replacing the wind speed with the internal energy, the conclusion in (3.7) is in line with [234, p. 186], as recalled in Sect. 1.8: *a bridge twice as wide will have exactly double the critical speed wind*. Theorem 3.1 is proved by Berchio-Gazzola [36] by using a Galerkin method. This method allows to estimate the stability threshold for (3.8) with the stability of the trivial solution of the linear differential equation (3.36); in this respect, the criterion by Zhukovskii [284] is applied.

All the discussions and the numerical results reported in Sects. 3.3 and 3.4 are taken from [36]. The definition of flutter energy and the material in Sect. 3.5 are

new and in line with similar definitions in Chaps. 4 and 5. The detailed example of Sect. 3.6 is taken from a paper by Berchio-Gazzola-Zanini [38] where one can also find hints on how to extend the results to more general Hamiltonian systems, possibly leading to Hill equations. The material from Sect. 3.7 comes from the paper by Berchio-Gazzola [37].

Chapter 4
Models with Interacting Oscillators

In this chapter we model a suspension bridge through a number of coupled oscillators. This generates second order Hamiltonian systems which can be tackled with ODE methods. We first analyse a single cross section of the bridge and we model it as a nonlinear double oscillator able to describe both vertical and torsional oscillations. By means of a suitable Poincaré map we show that its conserved internal energy may transfer from the vertical oscillation of the barycenter to the torsional oscillation of the cross section. This happens when enough energy is present in the system, as for the fish-bone model considered in Chap. 3. We name again flutter energy the critical energy threshold where this transfer may occur.

Then we model the whole bridge by connecting several double oscillators, each one representing a cross section of the bridge. The conclusion is the same, if the internal energy exceeds the flutter energy then torsional oscillations suddenly appear. We also give some hints on the extension of this phenomenon to damped and forced systems. Several numerical results, also available on the web [20], show that this model well reproduces the sudden appearance of torsional oscillations and the behavior seen during the TNB collapse [253].

4.1 Coupled Oscillators Modeling the Cross Section of a Bridge

In this section we introduce a nonlinear model for the dynamics of a cross section of a suspension bridge. This model enables us to explain (in Sect. 4.2) what is the starting spark for torsional oscillations when purely vertical oscillations of the roadway are visible. The same phenomenon will be shown to appear in more sophisticated models in the subsequent sections of this chapter.

Consider a rod of mass m and length 2ℓ, subject to the forces exerted by two lateral nonlinear springs C_1 and C_2, see Fig. 4.1: θ is the angle of deflection of

F. Gazzola, *Mathematical Models for Suspension Bridges*, MS&A 15,
DOI 10.1007/978-3-319-15434-3_4

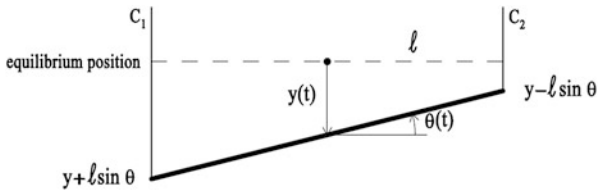

Fig. 4.1 Vertical and torsional displacements of a rod

the rod from horizontal and y is the downwards displacement from equilibrium of the barycenter. Following the construction technique described in the Preface, the hangers are prestressed and the equilibrium position of the barycenter is $y = 0$, while $y > 0$ corresponds to a downwards displacement. Whence, the forces, which are denoted by $f(y + \ell \sin\theta)$ and $f(y - \ell \sin\theta)$, take into account the gravity. This means that for a displacement $s = 0$ the elastic force $f(s)$ exerted by the spring balances the gravity, so that the endpoint of the rod is at an equilibrium; hence $f(0) = 0$.

By taking into account (3.1), the energy conservation law for this model leads to the following system

$$\begin{cases} \frac{m\ell^2}{3}\,\ddot{\theta} = \ell\cos\theta\,\Big(f(y-\ell\sin\theta) - f(y+\ell\sin\theta)\Big)\,, \\ m\,\ddot{y} = -\Big(f(y-\ell\sin\theta) + f(y+\ell\sin\theta)\Big)\,. \end{cases} \tag{4.1}$$

By adding some damping and forcing, (4.1) becomes

$$\begin{cases} \frac{m\ell^2}{3}\,\ddot{\theta} + \delta_\theta\dot{\theta} = \ell\cos\theta\,\Big(f(y-\ell\sin\theta) - f(y+\ell\sin\theta)\Big) + \phi(t)\,, \\ m\,\ddot{y} + \delta_y\dot{y} = -\Big(f(y-\ell\sin\theta) + f(y+\ell\sin\theta)\Big) + \psi(t)\,. \end{cases} \tag{4.2}$$

This system may be considerably simplified after linearisation. First one takes $f(s) = ks$ in order to model the hanger as a linear spring with Hooke constant $k > 0$. Then one approximates

$$\sin\theta \approx \theta\,, \quad \cos\theta \approx 1\ : \tag{4.3}$$

we refer to Sect. 3.3.2 for a discussion of the validity of (4.3). After these linearisations, the unforced version of (4.2) reads

$$\begin{cases} \frac{m}{3}\,\ddot{\theta} + \delta'_\theta\dot{\theta} + 2k\theta = 0\,, \\ m\,\ddot{y} + \delta_y\dot{y} + 2ky = 0\,, \end{cases} \tag{4.4}$$

where $\delta'_\theta = \delta_\theta/\ell^2$. We observe that the equations are linear, decoupled, and that the width 2ℓ enters marginally into (4.4). In view of the (GPCM), of (1.2), of the

dependence of the stability on the roadway width (see Sect. 1.8), the system (4.4) appears unable to describe the behavior of bridges.

Thanks to the linearisation (4.3), Scanlan-Tomko [239] obtain the following equations satisfied by the torsional angle θ:

$$I\,[\ddot{\theta}(t) + 2\zeta_\theta \omega_\theta \dot{\theta}(t) + \omega_\theta^2 \theta(t)] = A\dot{\theta}(t) + B\theta(t)\,, \tag{4.5}$$

where I, ζ_θ, ω_θ are, respectively, associated inertia, damping ratio, and natural frequency. The r.h.s. of (4.5) represents the aerodynamic force (see Sect. 3.7) which is postulated to depend linearly on both $\dot{\theta}$ and θ with $A, B > 0$ depending on the structural parameters of the bridge. Since (4.5) is equivalent to a two-variables first order linear system, it fails to fulfill both the requirements of the (GPCM). Hence, (4.5) is not suitable to fully describe the disordered behavior of a bridge. And indeed, elementary calculus at a sophomore level shows that, for suitable A and B, the solutions of (4.5) are positive exponentials times trigonometric functions which do not exhibit a sudden appearance of self-excited oscillations, they merely blow up in infinite time. In this chapter we will try to convince the reader that a structural instability generates a sudden excitation of the torsional mode and, once the torsional mode is activated, (4.5) may explain how aerodynamic forces lead to the TNB collapse.

In fact, Scanlan-Tomko [239, p. 1735] are well aware that the equations should be nonlinear:

> In the course of testing many small phenomena were observed which exhibited the approach of nonlinear regimes.

Still, they claim that the linear equation (4.5) explains the large torsional oscillations that caused the TNB collapse, while they also write [239, p. 1723] that, in their experiments,

> It was necessary to permit only small amplitudes of oscillations to occur, (e.g., in torsion $0 \le \alpha \le \pm 3^\circ$)...

It is known from the Report [9, p. 59] that the torsion grew up until 45°, thereby displaying a huge discrepancy with the linear model. The approximation (4.3) is correct only for small θ, see Sect. 3.3.2 for a detailed discussion. For $\theta = \frac{\pi}{4}$, as occurred during the TNB collapse, the relative error of such approximations is fairly large, see Proposition 3.2:

$$\theta = \frac{\pi}{4} \implies \frac{1-\cos\theta}{\cos\theta} = \sqrt{2} - 1 > 0.41\,, \quad \frac{\theta - \sin\theta}{\sin\theta} = \frac{\pi\sqrt{2}}{4} - 1 > 0.11\,,$$

which yield errors of more than 41 % and 11 % respectively. The same approximation was used by Smith-Vincent [245, p. 32] and by Abdel-Ghaffar [1, (1)]; McKenna [193] comments this choice by writing

> In [1], the author claims to use variational methods "to obtain the coupled equations of motion in their most general and nonlinear form." The results are not reassuring. The first

> step in the derivation is to put $\sin\alpha = \alpha$ and $\cos\alpha = 1$, where α is the angle of torsional oscillation.

That linearisation yields wrong models was earlier noticed by McKenna [191, p. 4] who comments (4.5) by writing

> This is the point at which the discussion of torsional oscillation starts in the engineering literature.

He claims that the problem is in fact nonlinear and that (4.5) is obtained after the incorrect linearisation (4.3). McKenna concludes by noticing that

> Even in recent engineering literature ... this same mistake is reproduced.

The numerical results obtained in [191] show that even if no slackening of hangers occurs, the nonlinearities introduced by the trigonometric functions in (4.2) are sufficient to explain the large amplitudes seen during the TNB collapse; in the purely linear model (4.4) the oscillation dies in finite time.

Our own opinion is that (4.3) is indeed incorrect if one wishes to study wide oscillations like the ones at the TNB. No model based on (4.3) may give precise answers nor correct quantitative responses in presence of wide torsional oscillations. The linearisation (4.3) may be however used for a qualitative study of small oscillations and their instability. This is precisely what was done in Chap. 3.

The other source of nonlinearity, also yielding a coupling in (4.2), is the restoring force f. It should not be taken linear since the hangers behave nonlinearly. Lazer-McKenna [168, (28)] take

$$f(s) = (s+1)^+ - 1\,, \tag{4.6}$$

in agreement with the model discussed in Sect. 2.8.1, see also (3.72). This choice of f describes hangers having elastic constant $k = 1$ (the coefficient of $(s+1)^+$) which tend to return the endpoint of the rod to equilibrium if stretched but exert no restoring force if compressed. The hanger is not at rest due to gravity and the distance from the equilibrium position to the unloaded position is also taken equal to 1 (this is expressed by the term 1 in $(s+1)^+$). Finally, the -1 in (4.6) is the normalisation of the half weight $mg/2$, see again (3.72); in the second equation in (4.2), the coupling term simply becomes

$$f(y - \ell\sin\theta) + f(y + \ell\sin\theta) = (1 + y - \ell\sin\theta)^+ + (1 + y + \ell\sin\theta)^+ - 2\,.$$

With such a choice for f, first numerical results about (4.2) were obtained by Jacover-McKenna [151] who showed that, depending on the initial conditions, a given periodic forcing term can generate either one of the following three kinds of solutions: small oscillations about equilibrium, large vertical oscillations about equilibrium, large torsional oscillations about equilibrium.

The numerical results for (4.2) obtained in [191] were able to show a sudden development of large torsional oscillations as soon as the hangers lose tension, that is, as soon as the restoring force behaves nonlinearly: when purely vertical

oscillations are large enough to slacken the hangers and the system (4.2) is subjected to torsional periodic forcing ϕ, the system becomes violently unstable in its torsional component. Further numerical results by Doole-Hogan [96] and McKenna-Tuama [195] show that a purely vertical periodic forcing in (4.2) (that is, $\phi = 0$ and $\psi \neq 0$) may create a torsional response: *high frequency vertical forcing can result in a periodic motion that is predominantly torsional*. They also considered different nonlinear restoring forces, in particular

$$f(s) = \frac{k}{a}(e^{ax} - 1) \tag{4.7}$$

where $k > 0$ is the elastic constant of the hangers and $a = k/mg$. Not only f in (4.7) is a smooth version of (4.6), but also it describes a **nonlinear behavior of the hangers starting from equilibrium**. The function f in (4.7) obeys the fundamental rule (1.10) and also the usual constraint (2.65). It is of course physically unreasonable to expect an exponential behavior of $f(s)$ when $s \to \infty$ but this behavior becomes visible only for large s which are outside the range considered in [195]. McKenna-Moore [194] studied the bifurcation and stability properties of periodic solutions of (4.2) both for (4.6) and (4.7).

As far as we are aware, these were the first results able to display a rapid transition from a vertical motion to a torsional motion. For this reason, we believe that the model system (4.2) is quite reliable. However, we also believe that it should be tackled from a different point of view. The forcing term ψ is taken periodic and the instability strongly depends on its frequency. As we repeatedly said, one of the purposes of this monograph is to show that the forcing term only plays a secondary role; this is the purpose of the present chapter.

The just described results are purely numerical. This lead McKenna [192, Problem 7.4] to raise the following question:

> Can one employ the tools of nonlinear analysis to say anything further about this coupled system, either in terms of stability or multiplicity?

As we shall see in next section, nonlinear analysis may be employed to determine the stability. We also extend the same arguments to a refined model for suspension bridges that considers many cross sections and not just one as in (4.2).

4.2 Energy Transfer and Poincaré Maps

In order better model the cross section of a suspension bridge, we slightly modify the model considered in the previous section by introducing two further fixed rods and an elastic membrane. The moving rod is linked to the two fixed rods through the membrane as in Fig. 4.2 where the view is now from above. The membrane has a linear elastic constant $K > 0$ and models the roadway connecting the moving cross section with the two fixed cross sections between the towers. For simplicity we take

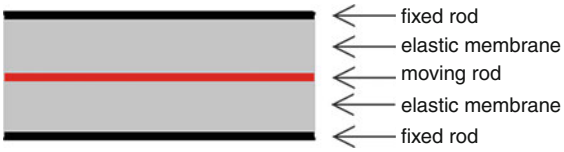

Fig. 4.2 Model with one moving and two fixed rods, linked by a membrane

$m = \ell = 1$ and we also fix $K = 1$. Since we wish to emphasise the existence of a flutter energy, we strip the model by dropping both forcing and damping and we consider an isolated system. This procedure was also followed by Irvine [149, p. 176] who comments his own approach to a model similar to (4.2) by writing:

> In this formulation any damping of structural and aerodynamic origin has been ignored... We could include aerodynamic damping which is perhaps the most important of the omitted terms. However, this refinement, although frequently of significance, yields a messy flutter determinant that requires a numerical solution.

If we put

$$F(s) = \int_0^s f(\sigma)d\sigma \quad \text{and} \quad U(\theta, y) = F(y + \sin\theta) + F(y - \sin\theta) + y^2 + \theta^2$$

and we recall (3.1), then the Newton equation for this system reads

$$\frac{1}{3}\ddot{\theta} + U_\theta(\theta, y) = 0\,, \qquad \ddot{y} + U_y(\theta, y) = 0\,. \tag{4.8}$$

When compared with (4.1), the two additional linear terms y and θ model the interaction of the moving rod with the fixed rods through the elastic membrane. The energy, invariant under the flow of (4.8), is given by

$$E = \frac{\dot{\theta}^2}{6} + \frac{\dot{y}^2}{2} + U(\theta, y)\,. \tag{4.9}$$

If f were linear, then (4.8) would decouple and the y and θ oscillators would not interact. But the strong evidence of the nonlinear behavior of suspension bridges, see Sect. 1.8, suggests a different choice. In particular, we follow both the suggestion by Brownjohn [62, p. 1364] recalled in Sect. 2.6.1 to avoid simple on/off restoring forces and the particular form considered in [30, (15)]: we take

$$f(s) = s + s^2 + s^3 \quad \text{and then} \quad F(s) = \frac{s^2}{2} + \frac{s^3}{3} + \frac{s^4}{4}\,. \tag{4.10}$$

This choice reproduces the linear Hooke law for small displacements, that is when $s \to 0$, with the elasticity constant taken equal to 1. The function f is convex at the origin, that is $f''(0) > 0$, which means that the hangers behave differently under tension and compression and, in particular, that the restoring force is more relevant for large displacements from equilibrium. Last but not least, a further reason for

the choice of f in (4.10) is that it represents the simplest nonlinear perturbation, via Taylor formula, of a linear phenomenon: the nonlinearity is also due to the sustaining cable, see [30, p. 180]. The same idea was used in the famous Fermi-Pasta-Ulam experiment [108] and, more recently, in engineering literature, see e.g. [220, Sect. 3.5]. In any case, this choice satisfies the minimal requirements of being an asymmetric perturbation of a linear force but it is not necessarily expected to yield accurate quantitative information. Numerical experiments in [22] show that the qualitative behavior of the system is not affected by the specific choice of the nonlinearity.

To (4.8) we associate the initial conditions

$$(\dot\theta, \dot y, \theta, y)(0) = (\theta^1, y^1, \theta^0, y^0) \quad \text{with} \quad 0 < |\theta^0| + |\theta^1| < 10^{-4}(|y^0| + |y^1|)\,. \tag{4.11}$$

Hence, at $t = 0$ the torsional oscillations θ are negligible with respect to the vertical oscillations y and the energy E in (4.9) is initially concentrated on the y-oscillator. Figure 4.3 displays the graph of the solutions of (4.8)–(4.11) for $(y^0, y^1) = (0, 2.8)$, $(y^0, y^1) = (0, 3)$, and $(y^0, y^1) = (0, 3.2)$ corresponding to energies $E = 3.92$, $E = 4.5$, and $E = 5.12$. It appears that tiny torsional oscillations θ suddenly become wider oscillations. The delay in the appearance of torsional oscillations may be seen as a Wagner-type effect, see Chap. 3. This phenomenon may be observed for any initial data, provided the energy (4.9) is sufficiently large: it disappears for $E \lessapprox 3.56$ which seems to be a **critical energy threshold** which we will call **flutter energy**. The increase of the torsional oscillations θ occurs simultaneously to a decrease of the vertical oscillations y. This means that there is an **energy transfer**

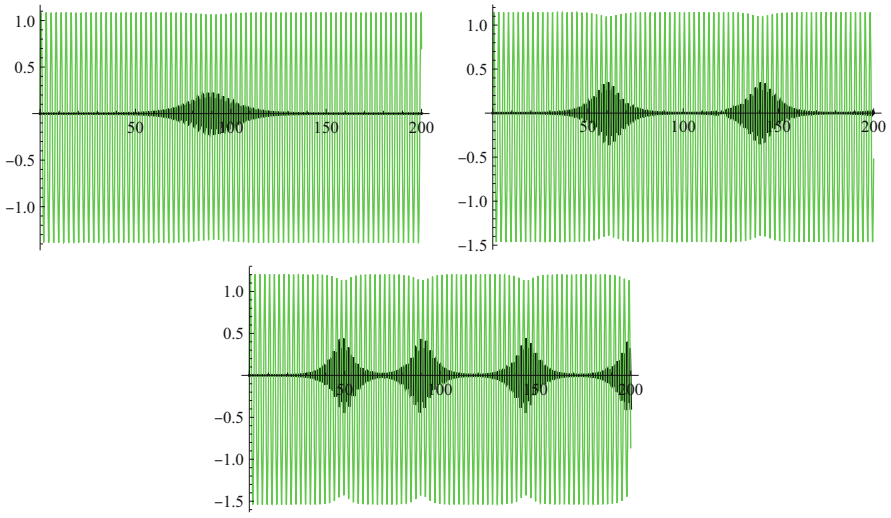

Fig. 4.3 Solutions of (4.8)–(4.11): y (*green*) and θ (*black*)

between the y-oscillator and the θ-oscillator. In order to make this fact more precise, we rewrite the energy (4.9) as

$$E = E^y + E^\theta + E^{y\theta}$$

where

$$E^y = \frac{\dot{y}^2}{2} + 2y^2 + \frac{2}{3}y^3 + \frac{y^4}{2}\,,\quad E^\theta = \frac{\dot{\theta}^2}{6} + \theta^2 + \sin^2\theta + \frac{\sin^4\theta}{2} \tag{4.12}$$

are the energies of the vertical and torsional oscillator when f is as in (4.10), while $E^{y\theta} = 2y\sin^2\theta + 3y^2\sin^2\theta$ is the coupling energy. Dropping the latter, in Fig. 4.4 we plot the energies E^y and E^θ of the solutions (y, θ) of (4.8)–(4.11) plotted in Fig. 4.4. It appears that there is an energy transfer from the y-oscillator to the θ-oscillator. Although the total energy E is conserved, the energy E^y suddenly decreases while the energy E^θ suddenly increases.

In order to insert these results within a theoretical framework and to compute the flutter energy, we study the solutions of system (4.8) from a different point of view. For simplicity, we take again $m = \ell = 1$ and (4.10). Since the energy E in (4.9) is a constant of motion, for any $E_0 > 0$ the three-dimensional submanifold $E(\dot{\theta}, \dot{y}, \theta, y) = E_0$ of the phase space $\mathbb{R}^4$ is flow-invariant, that is, the motion is confined to this three-dimensional energy surface. We study a two-dimensional

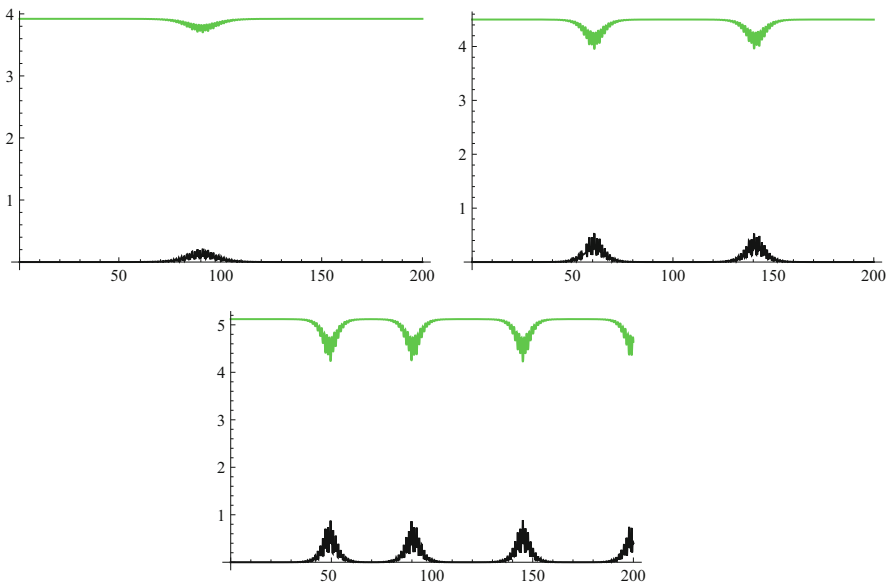

Fig. 4.4 Energies for solutions of (4.8)–(4.11): E^y (*green*) and E^θ (*black*)

section of this surface, the so-called Poincaré section, see Sect. 4.7 for the definition and full details of its construction.

First observe that also

$$\text{the plane } \theta = \dot{\theta} = 0 \text{ is flow-invariant;} \tag{4.13}$$

in particular, for all $y^1 \in \mathbb{R}$, the initial data

$$(\dot{\theta}, \dot{y}, \theta, y)(0) = (0, y^1, 0, 0) \tag{4.14}$$

yields a periodic solution of system (4.8) whose constant energy is given by $E = (y^1)^2/2$. We wish to study the stability of this solution under small $(\dot{\theta}, \theta)$-perturbations of the initial data (4.14).

Fix $E_0 > 0$, let $E^\theta = E^\theta(\dot{\theta}, \theta)$ be as in (4.12), and let

$$\mathscr{U}_{E_0} := \left\{(\theta^1, \theta^0) \in \mathbb{R}^2;\ E^\theta(\theta^1, \theta^0) < E_0\right\} .$$

For all $(\theta^1, \theta^0) \in \mathscr{U}_{E_0}$ define

$$y^1 = y^1(E_0, \theta^1, \theta^0) := \sqrt{2[E_0 - E^\theta(\theta^1, \theta^0)]} > 0 ,$$

namely the unique positive value of y^1 that satisfies $E(\theta^1, y^1, \theta^0, 0) = E_0$. Then there exists a first $T = T(\theta^1, \theta^0) > 0$ such that the solution of (4.8) with initial data

$$(\dot{\theta}, \dot{y}, \theta, y)(0) = (\theta^1, y^1(E_0, \theta^1, \theta^0), \theta^0, 0) \tag{4.15}$$

satisfies $y(T) = 0$ and $\dot{y}(T) > 0$. The Poincaré map $P_{E_0} : \mathscr{U}_{E_0} \to \mathbb{R}^2$ is defined by

$$P_{E_0}(\theta^1, \theta^0) := (\dot{\theta}(T), \theta(T)) \tag{4.16}$$

where $(\theta(t), y(t))$ is the solution of (4.8)–(4.15). Note that, for such solution, one has $E = E_0$. In view of (4.13), the origin $(0, 0) \in \mathscr{U}_{E_0}$ is a fixed point for the map P_{E_0} for any $E_0 > 0$. In Fig. 4.5 we represent, in the plane $(\dot{\theta}, \theta)$, some iterates of the map P_{E_0} for system (4.8) with different initial data $(\dot{\theta}, \theta)(0)$ close to $(0, 0)$. From left to right and top to bottom, the energies considered are $E_0 = 3.4$, $E_0 = 3.5$, $E_0 = 3.6$, and $E_0 = 3.8$.

A change of behavior between $E_0 = 3.5$ and $E_0 = 3.6$ appears neatly, so that the flutter energy of (4.8) satisfies $3.5 < \overline{E} < 3.6$. Finer experiments yield $\overline{E} \approx 3.56$. Stable fixed points are plotted in red and unstable fixed points in green. The pictures in Fig. 4.5 show that if $E < \overline{E}$, then any initial condition with small $(\dot{\theta}, \theta)(0)$ leads to solutions with small $(\dot{\theta}, \theta)(t)$ for all t, while if $E > \overline{E}$, any initial condition with small $(\dot{\theta}, \theta)(0)$ leads to large values of $(\dot{\theta}, \theta)(t)$ for some t. Hence, if $E_0 < \overline{E}$ then the origin is a stable fixed point of P_{E_0}, whereas if $E_0 > \overline{E}$ then the origin is unstable, that is, the system undergoes a bifurcation at $E_0 = \overline{E}$. The stability of the

origin can be determined by the eigenvalues λ_1 and λ_2 of the Jacobian $JP_{E_0}(0,0)$ of P_{E_0} at $(0,0)$. Since the system (4.8) is conservative, $JP_{E_0}(0,0)$ has determinant equal to 1 and one of the following cases holds:

(i) $|\lambda_1| = |\lambda_2| = 1$ and $\lambda_2 = \overline{\lambda_1}$, in which case $(0,0)$ is stable for P_{E_0}.
(ii) $\lambda_1, \lambda_2 \in \mathbb{R}$ and $0 < |\lambda_1| < 1 < |\lambda_2|$, in which case $(0,0)$ is unstable for P_{E_0}.

Since the eigenvalues depend continuously on E_0, the bifurcation, i.e. the loss of stability, may only occur when $\lambda_1 = \lambda_2 = 1$ or $\lambda_1 = \lambda_2 = -1$. In the former case the Jacobian of $P_{E_0} - I$ at $(0,0)$ is not invertible, therefore the fixed point is not guaranteed to be locally unique, and indeed two new stable fixed points are created: this kind of bifurcation is called *pitchfork*. In the latter case the Jacobian of $P_{E_0} - I$ at $(0,0)$ is invertible, but the Jacobian of $P_{E_0}^2 - I$ is not; then, by the implicit function theorem the fixed point is locally unique, but periodic points of period 2 are not, and indeed two such points are created at the bifurcation: this kind of bifurcation is called *period doubling*.

The experiments displayed in Fig. 4.5 show that the bifurcation generates two new stable fixed points (red color), therefore we have a pitchfork bifurcation. Since at the bifurcation point both eigenvalues of the Jacobian of P_{E_0} at $(0,0)$ are equal to 1, then $P_{\overline{E}}(\theta^1, \theta^0) = (\theta^1, \theta^0) + o(\theta^1, \theta^0)$, so that small initial data (θ^1, θ^0) yield solutions $\theta(t)$ of (4.8) close to a periodic solution having the same period of $y(t)$. This is what we call an **internal resonance**. In our experiments we observe that, as E_0 increases from 0, the eigenvalues λ_1 and λ_2 move on the unit circle of the complex plane and meet at the point $(1,0)$ when $E_0 = \overline{E}$. When $E_0 > \overline{E}$ the eigenvalues move along the real line in opposite directions and the two new stable (red) fixed points represent periodic solutions $\theta(t)$ having the same period of $y(t)$.

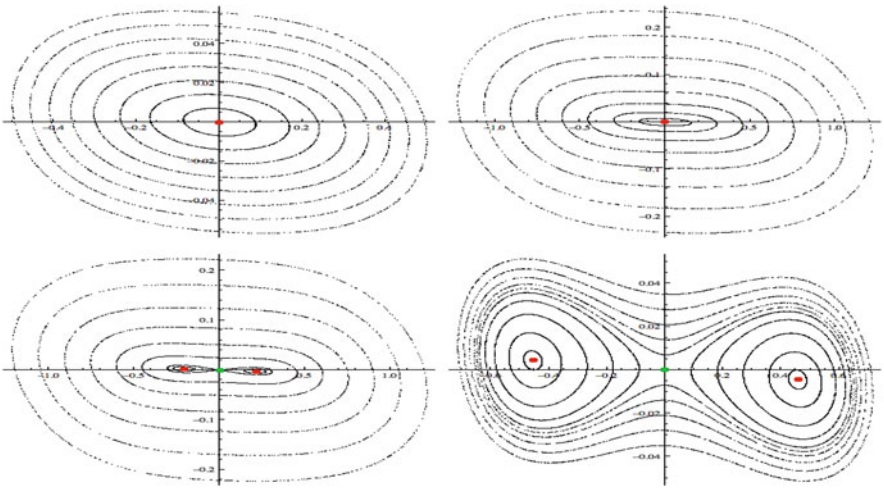

Fig. 4.5 The Poincaré map for (4.8) for different values of the energy E_0

In the case of a period doubling bifurcation we would have $P_{\overline{E}}(\theta^1, \theta^0) = -(\theta^1, \theta^0) + o(\theta^1, \theta^0)$, so that small initial data (θ^1, θ^0) would yield solutions $\theta(t)$ to (4.8) being close to a periodic solution having period equal to the double of the period of $y(t)$. This is another kind of **internal resonance**, which does not happen in the experiment that we describe here, but can be observed with other nonlinearities, e.g. with $f(s) = s + s^2$. If $E_0 > \overline{E}$, then P_{E_0} has two periodic points of period 2, corresponding to periodic solutions $\theta(t)$ having the double of the period of $y(t)$.

Summarising, a necessary condition for a bifurcation to occur is a resonance between the oscillators; in absence of resonance the double oscillator is torsionally stable and small initial torsional data remain small for all time. What we have just explained leads us to the following definition and criterion:

Definition 4.1 (Torsional Stability) We say that the system (4.8) is torsionally stable at energy $E_0 > 0$ if the origin $(0, 0) \in \mathbb{R}^2$ is stable for the Poincaré map P_{E_0}. Otherwise, we say that the system is torsionally unstable.

Criterion 4.2 *Let $\lambda_1 = \lambda_1(E_0)$ and $\lambda_2 = \lambda_2(E_0)$ be the complex eigenvalues of the Jacobian of the Poincaré map P_{E_0} at the origin $(0, 0) \in \mathbb{R}^2$. Then $\lambda_1\lambda_2 = 1$ and two cases may occur:*

(S) *If $|\lambda_1| = |\lambda_2| = 1$ and $\lambda_2 = \overline{\lambda_1}$, then the system (4.8) is torsionally stable.*
(U) *If $\lambda_1, \lambda_2 \in \mathbb{R}$ and $0 < |\lambda_1| < 1 < |\lambda_2|$, then the system (4.8) is torsionally unstable.*

We have observed above that equal eigenvalues yield a resonance between the oscillators, which may occur only at particular values of the energy. When the energy is smaller than such value, the system is in the stable regime, while when the energy is larger the system is in the unstable regime. In principle it may happen that also at higher energies the system undergoes another bifurcation and the origin becomes again stable: this is related to the behavior of the stability regions as illustrated in Sect. 3.6. Hence, we have shown that there exists $\overline{E} > 0$ such that the system (4.8) is stable (case (S)) whenever $0 < E < \overline{E}$ whereas the system (4.8) is unstable (case (U)) whenever $\overline{E} < E < \overline{E} + \delta$ for some $\delta > 0$.

Definition 4.3 (Flutter Energy) We call

$$\overline{E} := \inf \left\{ E_0 > 0;\ \max\{|\lambda_1(E_0)|, |\lambda_2(E_0)|\} > 1 \right\}$$

the flutter energy of (4.8).

What we have seen in this section enables us to conclude that

the bifurcation is caused by a resonance between the nonlinear oscillators and generates torsional instability.

Moreover, the Poincaré maps show that

the onset of torsional instability is generated by internal resonances.

This simple description is possible because we are dealing with a 2×2 system as (4.8). In Sect. 4.4 we provide a suitable generalisation of these results to a full bridge model. Before doing this we show a strict connection between the Poincaré maps and the Hill equation.

4.3 A Link Between the Poincaré Maps and the Hill Equations

The instability results for the fish-bone model considered in Chap. 3 are obtained thanks to the analysis of some Hill equations. For the model considered in the previous section (and in all the present chapter), the instability is uncovered thanks to the analysis of some Poincaré maps. The purpose of this section is to emphasise a connection between the Poincaré maps and the Hill equations in the study of the stability of suspension bridges.

In his introduction to the mathematical works by Hill, Poincaré [222] starts by describing general results and on [222, p. x] he writes

> Mais j'ai hâte d'arriver à son oeuvre capitale, à celle où s'est dévoilée toute l'originalité de son esprit, à sa théorie de la Lune.

Poincaré spends several pages to describe the importance of the Hill equation and on [222, p. xviii] he ends the presentation by writing that, among his discoveries,

> ... celle qui fera son nom immortel, c'est sa théorie de la Lune.

Finally, he was well aware that the Moon theory was not the only application of the Hill equation, his last comment on the equation reads

> ... quand elles s'étendront à un domaine plus vaste, on ne devra pas oublier que c'est à M. Hill que nous devons un instrument si précieux.

Hence, Poincaré had clearly in mind that the very same equation could be used to describe many further natural phenomena. In fact, also the Poincaré maps are nowadays used to study the stability of many different models. We are sure that both Poincaré and Hill would be extremely happy to see that their work applies as well to the stability of suspension bridges.

We show here that there is a direct link between these two approaches for models of suspension bridges. In particular, we complement the numerical results of Sect. 4.2 with a theoretical estimate of an "approximated" flutter energy. We first linearise (4.8) by using (4.3) so that, for f as in (4.10) we obtain the system

$$\begin{cases} \ddot{y} + 4y + 2y^2 + 2\theta^2 + 2y^3 + 6y\theta^2 = 0 \\ \ddot{\theta} + 12\theta + 12y\theta + 6\theta^3 + 18y^2\theta = 0\,. \end{cases} \tag{4.17}$$

With the initial conditions $\theta(0) = \dot{\theta}(0) = 0$ the system (4.17) has the solution $(y, \theta) = (\psi, 0)$, where ψ is the periodic solution of the autonomous equation

$$\ddot{\psi} + 4\psi + 2\psi^2 + 2\psi^3 = 0\,, \qquad \psi(0) = \alpha\,,\ \dot{\psi}(0) = \beta\,, \tag{4.18}$$

for some $\alpha, \beta \in \mathbb{R}$. A result similar to Theorem 3.8 holds, including an "explicit" formula replacing (3.35) and allowing to compute the period $T = T(E)$ in dependence of the energy (and hence of the initial data α and β). By arguing as for (3.29) we reach the following Hill equation

$$\ddot{\xi} + a(t)\xi = 0 \quad \text{with} \quad a(t) = 12 + 12\psi(t) + 18\psi(t)^2\,. \tag{4.19}$$

We then say that the solution of (4.18) is torsionally stable if the trivial solution of (4.19) is stable. Finally, one gets a statement similar to Theorem 3.9:

Theorem 4.4 *There exist constants $\psi_\infty > 0$ and $\overline{E} > 0$ such that the solution $(\psi, 0)$ of (4.17) at energy $E = E(\psi(0), \dot{\psi}(0)) > 0$ (that is, with ψ solving (4.18)) is torsionally stable provided that $\|\psi\|_\infty \le \psi_\infty$ or, equivalently, provided that $E \le \overline{E}$.*

Theorem 4.4 yields a theoretical complement to the numerical results obtained in Sect. 4.2. Figure 4.5 shows how the origin of the Poincaré section in the $(\dot{\theta}, \theta)$-plane loses stability for large energies. The same flutter (critical) energy is found for (4.19): when the energy of the solution of (4.18) reaches the threshold given by the Poincaré maps, the trivial solution of the Hill equation (4.19) becomes unstable. This statement is supported by numerical results. In Fig. 4.6 we plot the solutions of (4.17) with initial data

$$y(0) = \lambda = 10^4\theta(0)\,, \quad \dot{y}(0) = \dot{\theta}(0) = 0$$

for $\lambda = 1.045$ (left) and $\lambda = 1.05$ (right); respectively, these correspond to energies of $E \approx 3.54$ and $E \approx 3.58$. It can be noticed that no torsional oscillations appear in the left picture while they suddenly appear in the right picture. Therefore, it seems

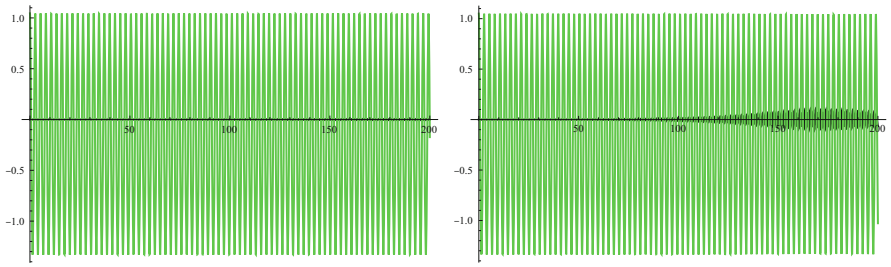

Fig. 4.6 Solutions of (4.17) with y (*green*) and θ (*black*): the energies are $E \approx 3.54$ (*left*) and $E \approx 3.58$ (*right*)

that for system (4.17) the flutter energy lies in the interval (3.54, 3.58). Not only this confirms the flutter energy of about 3.56 found with the Poincaré maps (see Fig. 4.5) but it also shows that the linearisation (4.3) is legitimate.

4.4 Interactions Between Multiple Cross Sections

We consider here a bridge described by finitely many cross sections (seen as rods acting as oscillators) linked by linear forces. This discretisation views a suspension bridge as in Fig. 4.7, where the red cross sections are the oscillators linked to the hangers (which act as nonlinear springs) while the grey part is a membrane connecting two adjacent oscillators. This model is the generalisation of the one displayed in Fig. 4.2 to the case of $n > 1$ parallel moving rods labeled by $i = 1, \dots, n$. We assume that each rod interacts with the two adjacent ones by means of attractive linear forces. For the i-th cross section ($i = 1, \dots, n$), we denote by y_i the downwards displacement of its midpoint and by θ_i its angle of deflection from horizontal. We assume that the mass of each rod modeling a cross section is $m = 1$ and its half-length is $\ell = 1$. We set $y_0 = y_{n+1} = \theta_0 = \theta_{n+1} = 0$ to model the connection between the bridge and the ground. We have the following system of $2n$ equations:

$$\begin{cases} \ddot{\theta}_i + 3U_{\theta_i}(\Theta, Y) = 0 \\ \ddot{y}_i + U_{y_i}(\Theta, Y) = 0 \end{cases} \qquad (i = 1, \dots, n)\,, \tag{4.20}$$

where

$$U(\Theta, Y) = \sum_{i=1}^{n} \Big[F(y_i + \sin\theta_i) + F(y_i - \sin\theta_i) \Big] + \sum_{i=0}^{n} \Big[\frac{K_y}{2}(y_i - y_{i+1})^2 + \frac{K_\theta}{2}(\theta_i - \theta_{i+1})^2 \Big]$$

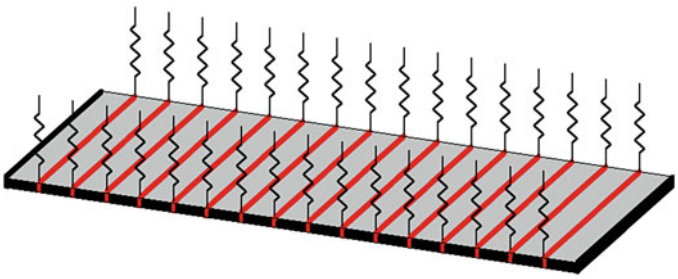

Fig. 4.7 The discretised suspension bridge

and $(\Theta, Y) = (\theta_1 \dots, \theta_n, y_1, \dots, y_n) \in \mathbb{R}^{2n}$. The constants $K_y, K_\theta > 0$ represent the vertical and torsional stiffness of the bridge. The conserved total energy of the system (4.20) is given by

$$E(\dot{\Theta}, \dot{Y}, \Theta, Y) = \frac{|\dot{\Theta}|^2}{6} + \frac{|\dot{Y}|^2}{2} + U(\Theta, Y)\,. \tag{4.21}$$

The choice of the nonlinear restoring force $f = F'$ is here more delicate since, according to [138, p. 1624], *...the failure of long hangers is less critical than the failure of short hangers*, which implies that hangers and restoring forces depend on the longitudinal position. Also, the sustaining cable links all the hangers, so that they cannot be considered to behave independently from each other. But, again, we numerically saw that the qualitative behavior of the system is not affected by the specific choice of the nonlinearity; so, we take again (4.10).

Let $\mathtt{dst} : \mathbb{R}^n \to \mathbb{R}^n$ be the discrete sine transform, that is, the linear invertible map defined for all $x \in \mathbb{R}^n$ by

$$x_i = \frac{2}{n+1} \sum_{j=1}^{n} (\mathtt{dst}x)_j \sin\left(\frac{\pi ij}{n+1}\right) \quad \text{and} \quad (\mathtt{dst}x)_j = \sum_{i=1}^{n} x_i \sin\left(\frac{\pi ij}{n+1}\right),$$

and note that, for any given $k \in \{1, \dots, n\}$ and $E_0 > 0$, there exists a unique $\alpha = \alpha(k, E_0) > 0$ such that $E\,(0, \alpha(k, E_0)\mathtt{dst}(e_k), 0, 0) = E_0$, where e_k is the $k-$th element of the canonical basis of $\mathbb{R}^n$. If f were linear, then the initial condition $(\dot{\Theta}, \dot{Y}, \Theta, Y)(0) = (0, \alpha(k, E_0)\mathtt{dst}(e_k), 0, 0)$ would raise a periodic solution of (4.20) for all k, E_0; such solution is usually called a (linear) normal mode of the system. If f is nonlinear, e.g. as in (4.10), by a minimisation algorithm we can compute numerically $Y^0(k, E_0), Y^1(k, E_0) \in \mathbb{R}^n$ such that

$$\begin{aligned} &I := |Y^0(k, E_0)| + |Y^1(k, E_0) - \alpha(k, E_0)\mathtt{dst}(e_k)| \ll 1\,, \quad I \to 0 \text{ as } E_0 \to 0\,, \\ &\big(0, Y^1(k, E_0), 0, Y^0(k, E_0)\big) \text{ lies on the orbit of a periodic solution of (4.20).} \end{aligned} \tag{4.22}$$

We may now define the nonlinear normal modes.

Definition 4.5 (Nonlinear Normal Modes) The periodic solution of (4.20) with initial data

$$(\dot{\Theta}, \dot{Y}, \Theta, Y)(0) = (0, Y^1(k, E_0), 0, Y^0(k, E_0))$$

is called the k-th nonlinear normal mode of (4.20) at energy E_0.

The continuous version of the first and second nonlinear normal modes are represented in the first two pictures of Fig. 1.18. Our purpose is to study the stability of the nonlinear normal modes under small perturbations of the null torsional initial data.

We consider (4.20) with $n = 16$ and $K_y = K_\theta = 320$. Let $Y^0(k, E_0), Y^1(k, E_0) \in \mathbb{R}^n$ be as in (4.22): Fig. 4.8 represents the solutions of the system (4.20) with initial conditions

$$\left(\dot{\Theta}, \dot{Y}, \Theta, Y\right)(0) = (\Theta^1, Y^1(k, E_0), 0, Y^0(k, E_0)) \tag{4.23}$$

where $\Theta^1 \in \mathbb{R}^{16}$ is a random vector whose components lie in the interval $[-5 \cdot 10^{-6}, 5 \cdot 10^{-6}]$, and with $(k, E_0) = (1, 516), (2, 500), (3, 6000)$.

In all the pictures the black and grey plots represent $\theta_i(t)$ and $y_i(t)$ respectively for $i = 1 \ldots, 8$ going from left to right; the first one is the closest to the towers whereas the eighth one is in the center of the span. We only display (θ_i, y_i) for $i = 1 \ldots, 8$ because $(\theta_i, y_i) \approx (\theta_{17-i}, y_{17-i})$ if k is odd and $(\theta_i, y_i) \approx -(\theta_{17-i}, y_{17-i})$ if k is even. In order to better explain the phenomenon, we enlarge the first picture of the second line, see Fig. 4.9 which looks quite similar to Fig. 4.3.

We observe that the (black) torsional oscillations are initially negligible with respect to the (grey) vertical oscillations but, suddenly, they become visible, and then larger and larger, and their maximum amplitude would suffice for an actual bridge to collapse. The delay in time may again be seen as a structural version of the Wagner effect [275].

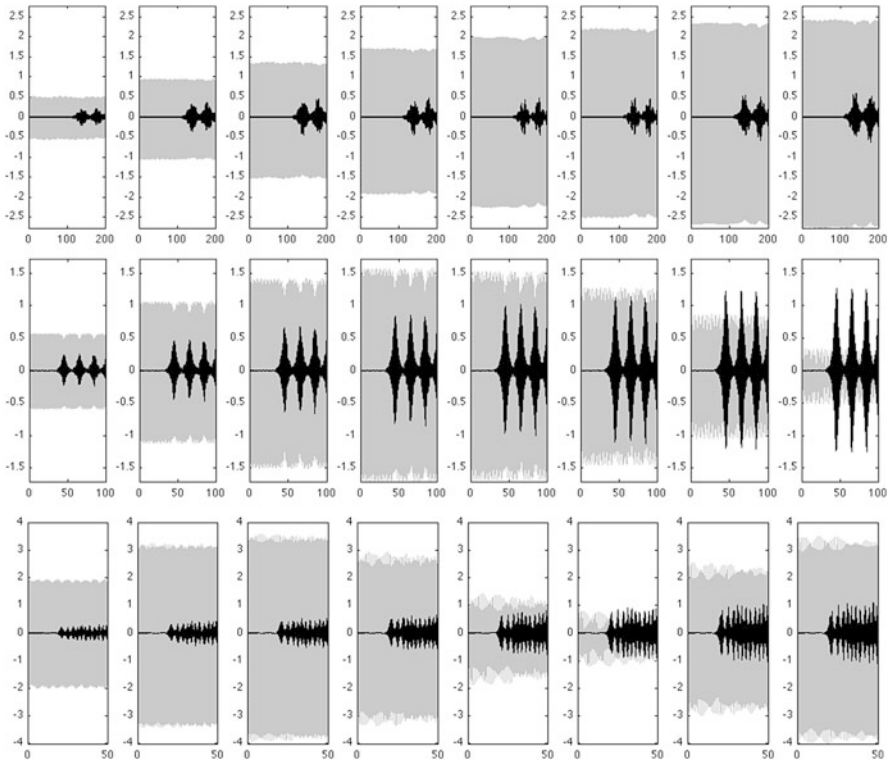

Fig. 4.8 Unstable torsional oscillations (*black*) and vertical oscillations (*grey*) of the cross sections

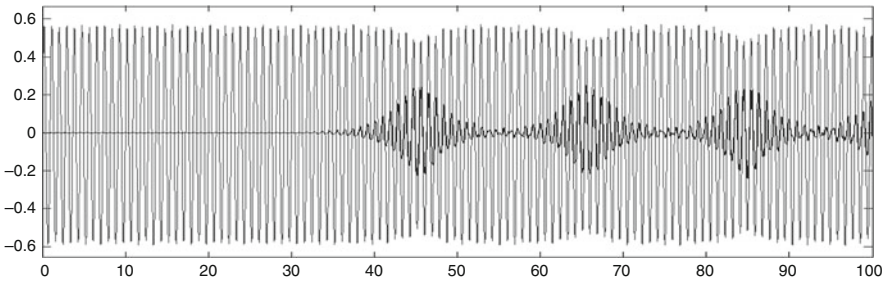

Fig. 4.9 Sudden appearance of torsional oscillations

Numerical experiments show that the sudden appearance of wide torsional oscillations as in Fig. 4.8 can be seen only if the energy is sufficiently large, that is, above the flutter energy. Above this threshold a very small perturbation of the k-th mode in any θ_i-variable can lead to a significant torsional motion, while below the threshold small initial torsional oscillations remain small for all time. In the latter case, the amplitudes of both the torsional and the vertical modes are constant, therefore the pictures are trivial and we do not display them.

We have also produced a dynamic representation of the solutions (Θ, Y) of (4.20)–(4.23). The movies available at [20] display the dynamics of the discretised bridge, and in particular the similarity with the original movie of the Tacoma Narrows Bridge collapse [253] and with the lowest picture in Fig. 1.18.

We now extend the results obtained in Sect. 4.2 to the full bridge model (4.20) where $n > 1$. For any mode $k \in \{1, \dots, n\}$ and any energy $E_0 > 0$ let $Y^1(k, E_0)$ and $Y^0(k, E_0)$ be as in (4.22). Let $T(k, E_0) > 0$ be the period of the k-th nonlinear normal mode of (4.20) at energy E_0 and let $\Psi^k_{E_0} : \mathbb{R}^{2n} \to \mathbb{R}^{2n}$ be the evolution map defined by

$$\Psi^k_{E_0}(\Theta^1, \Theta^0) = \left(\dot{\Theta}(T(k, E_0)), \Theta(T(k, E_0))\right) , \tag{4.24}$$

where $(\Theta(t), Y(t))$ is the solution of (4.20) with initial conditions

$$\left(\dot{\Theta}, \dot{Y}, \Theta, Y\right)(0) = (\Theta^1, Y^1(k, E_0), \Theta^0, Y^0(k, E_0)) .$$

We remark that the origin is a fixed point of $\Psi^k_{E_0}$ and that $\Psi^k_{E_0}$ is not a Poincaré map; in particular, the iteration time T does not depend on (Θ^1, Θ^0). One could compute a Poincaré map even in the full model case, but its construction is theoretically and computationally more complicated, and, due to the higher dimensionality of the problem, it would not provide any additional insights. The maps $\Psi^k_{E_0}$ enable us to generalise Definition 4.1 as follows:

Definition 4.6 (Torsional Stability) We say that the k-th nonlinear normal mode of (4.20) at energy $E_0 > 0$ is torsionally stable if the origin $(0, 0) \in \mathbb{R}^{2n}$ is stable for the evolution map $\Psi^k_{E_0}$. Otherwise, we say that it is torsionally unstable.

In order to evaluate the stability of the k-th nonlinear normal mode, we study the Jacobian $J\Psi^k_{E_0}(0,0)$ of $\Psi^k_{E_0}$ at $(\Theta^1,\Theta^0)=(0,0)$. To compute the derivatives of this map, we linearise (4.20) at $(\Theta,Y)=(0,\overline{Y}_k)$, where $\overline{Y}_k(t)$ is the k-th nonlinear normal mode of (4.20) at energy E_0. We are led to solve the system

$$\ddot{\xi}_i + 3\sum_{j=1}^{n} U_{\theta_i\theta_j}(0,\overline{Y}_k(t))\xi_j = 0 \qquad (i=1,\dots,n)\,, \tag{4.25}$$

where $\Xi(t)=(\xi_1(t),\dots,\xi_n(t))$ is the variation of $\Theta\equiv 0$. The l-th column of $J\Psi^k_{E_0}(0,0)$ is the solution $(\dot{\Xi}(T),\Xi(T))$ at time $T(k,E_0)$ of (4.25) with initial conditions $(\dot{\Xi},\Xi)(0)=\eta_l$ $(l=1,\dots,2n)$, where η_l is the l-th element of the canonical basis of $\mathbb{R}^{2n}$. The system (4.25) is the counterpart of (3.29).

In principle, when $n>1$ one cannot infer the full stability of the nonlinear normal mode $\overline{Y}_k$ from its linear stability, that is, when all the eigenvalues of $J\Psi^k_{E_0}(0,0)$ have modulus 1. On the other hand, we have numerical evidence that the model is torsionally stable if and only if all the eigenvalues of $J\Psi^k_{E_0}(0,0)$ lie on the unit circle. This leads to the following:

Criterion 4.7 *Let $\lambda_i=\lambda_i(k,E_0)$ $(i=1,\dots,2n)$ be the eigenvalues of $J\Psi^k_{E_0}(0,0)$. Then:*

(S) *If $\max_i|\lambda_i|=1$, then the k-th nonlinear normal mode of (4.20) at energy E_0 is torsionally stable.*

(U) *If $\max_i|\lambda_i|>1$, then the k-th nonlinear normal mode of (4.20) at energy E_0 is torsionally unstable.*

All our experiments have shown that a nonlinear normal mode is stable, that is small initial torsional data yield small torsional oscillations for all time, whenever it is linearly stable. Then, Criterion 4.7 enables us to provide a rigorous definition of the flutter energy of each mode.

Definition 4.8 (Flutter Energy) We call flutter energy $\overline{E}_k$ of the k-th nonlinear normal mode of (4.20) the positive number

$$\overline{E}_k := \inf\left\{E_0>0;\ \max_i|\lambda_i(k,E_0)|>1\right\}\,.$$

Figure 4.11 in next section shows that $\overline{E}_k$ depends on k and the effective flutter energy $\overline{E}$ of the bridge satisfies

$$\overline{E} \le \min_{1\le k\le n}\overline{E}_k\,.$$

In order to show further that this model well explains the behavior of suspension bridges and is able to reproduce the collapse of the TNB, we revisit the results trying to match the description by Farquharson [104] recalled in Sect. 1.4:

> The motion, which a moment before had involved a number of waves (nine or ten) had shifted almost instantly to two.

Let us first introduce a new definition.

Definition 4.9 (Fundamental Vibrations) For all $j = 1, \ldots, 16$ we call j-th vertical (respectively, torsional) fundamental vibration of a solution $(\Theta(t), Y(t))$ of (4.20) the function $t \mapsto (\mathtt{dst} Y(t))_j$ (respectively, the function $t \mapsto (\mathtt{dst}\Theta(t))_j$), that is, the j-th component of the discrete sine transform.

In Fig. 4.10 we plot a simple moving average of the first four (vertical and torsional) fundamental vibrations of a solution of (4.20) in the case $(k, E_0) = (2, 500)$. The graphs show that initially most of the dynamics is concentrated on the second vertical fundamental vibration, but at time $t \approx 50$ part of the energy is transferred to the first torsional fundamental vibration; then the second vertical and the first torsional fundamental vibrations begin a somehow periodic exchange of energy. All the other fundamental vibrations, vertical and torsional, appear to be almost unaffected. The above testimony by Farquharson tells us that, at the TNB, the appearance of torsional oscillations had changed the vertical oscillations from the ninth to the second fundamental vibration.

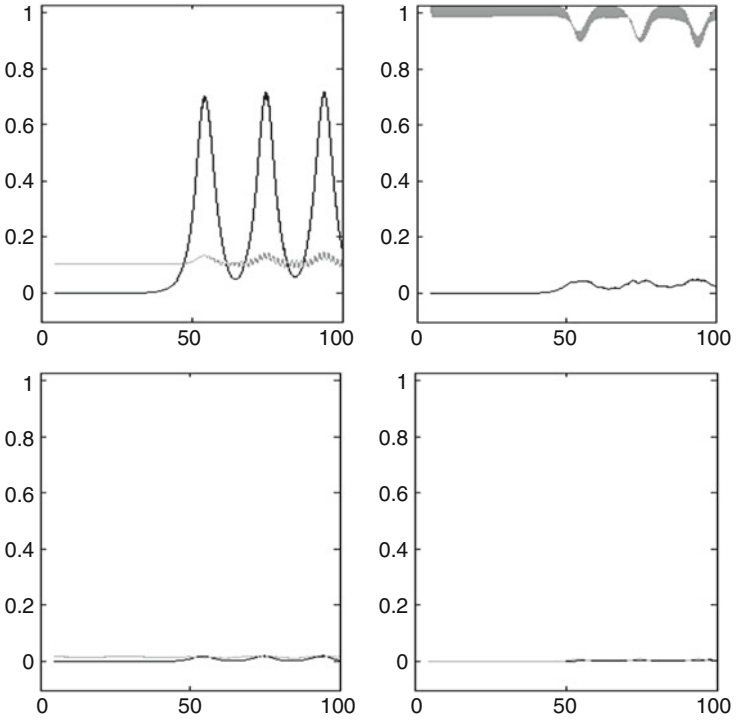

Fig. 4.10 The first four torsional (*black*) and vertical (*grey*) fundamental vibrations of a solution of (4.20)

4.5 Computation of the Flutter Energy

We take again (4.10) while we fix $n = 16$ and $K_y = K_\theta = 320$. In the graphs in Fig. 4.11 we display the largest modulus of the eigenvalues of $J\Psi^k_{E_0}(0,0)$ as a function of the energy E_0, with $k = 1, 2, 3$.

The graphs in Fig. 4.12 display the largest modulus of the eigenvalues of $J\Psi^k_{E_0}(0,0)$ as a function of the energy E_0, with $k = 4, 5, 6$.

These graphs confirm that for all k there exists $\overline{E}_k$ such that the periodic k-th mode is stable whenever $E < \overline{E}_k$ and it is unstable if E is slightly larger than $\overline{E}_k$. In fact, for higher energies, the system may become stable again, but this has a purely theoretical relevance: the bridge is safe as long as its internal energy is smaller than the least $\overline{E}_k$. This phenomenon was already observed by Rocard [234, p. 100] who writes

> . . .these special vibrations are excited, at least in a single or any given mode, by winds of only a rather narrow range of speeds and that stronger winds suppress them as much as lighter winds.

A qualitative but sound theoretical explanation of this phenomenon is given in Sect. 3.6. While analysing the impact of the speed of the wind on a bridge, Rocard states that *within the interval of speeds from V_1 to V_2 the bridge is "susceptible*

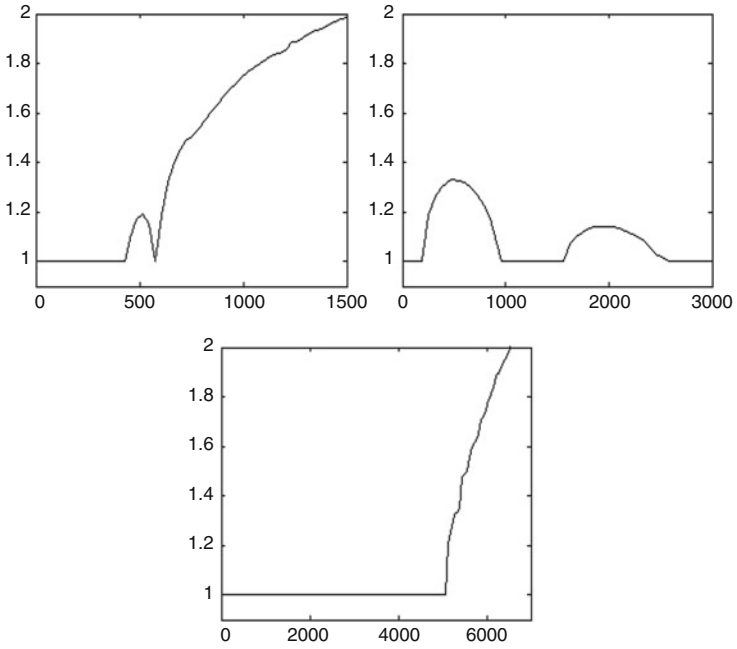

Fig. 4.11 Largest modulus of the eigenvalues of $J\Psi^k_{E_0}(0,0)$ versus the energy E_0, $k = 1, 2, 3$

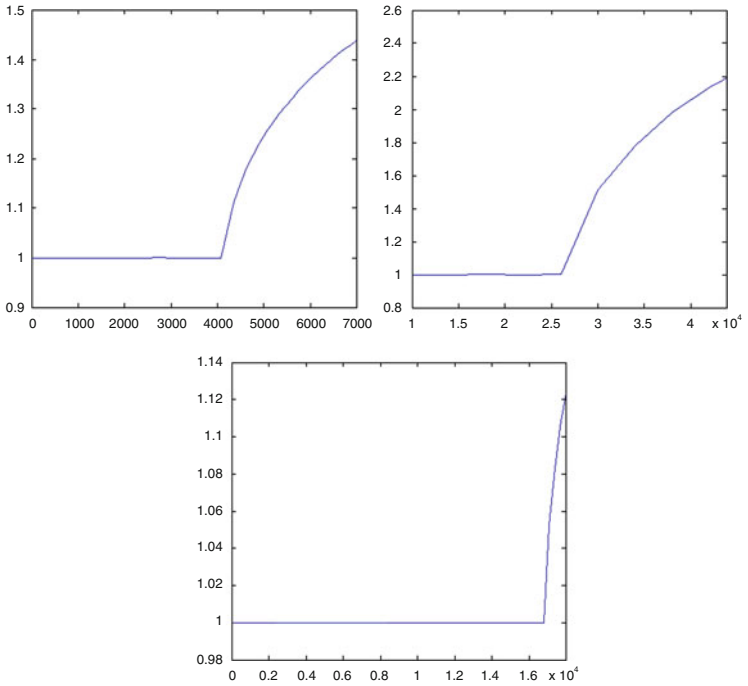

Fig. 4.12 Largest modulus of the eigenvalues of $J\Psi_{E_0}^k(0,0)$ versus the energy E_0, $k = 4, 5, 6$

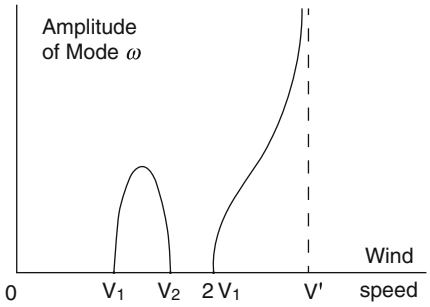

Fig. 4.13 Amplitude of mode versus wind speed (From [234, Fig. 64, p. 141], reproduced with the permission from Francis Rocard)

to the wind". He then claims that the amplitudes of oscillations of the bridge are close to 0 just outside this interval and that the bridge starts oscillating again if the speed is larger than $2V_1$ until a critical speed V' where the bridge collapses, see Fig. 4.13. This figure appears quite similar to Figs. 4.11 and 4.12 although they represent different phenomena. We have already underlined that our main concern is the internal energy and not the speed of the wind.

Table 4.1 Approximate value of the flutter energy $\overline{E}_k$

k	1	2	3	4	5	6	7	8
$\overline{E}_k$	450	195	5,100	4,160	28,000	17,500	64,000	36,000

By maintaining fixed all the parameters, Table 4.1 shows the approximate value of $\overline{E}_k$ for all $k = 1, \dots, 8$.

In order to test these results, one may follow a less rigorous but simpler procedure, inspired to the experiments for the single cross section, see (4.8)–(4.11). Consider (4.20) with initial data

$$10^4\theta_i(0) = y_i(0) = \overline{y}\sin\frac{ik\pi}{17}\,, \quad \dot{\theta}_i(0) = \dot{y}_i(0) = 0\,, \quad (i = 1, \dots, 16) \tag{4.26}$$

where k denotes the vertical fundamental vibration we wish to perturb and $\overline{y} > 0$ serves as a measure of the energy E_0. Numerical results show that if $|\overline{y}|$ is small then torsional oscillations remain small, whereas if $|\overline{y}|$ is sufficiently large then there is a sudden appearance of wide torsional oscillations θ_i. The energy value where this transition occurs strongly depends on the mode k and coincides with the values in Table 4.1. This procedure, which is much simpler than the one described above, does not allow to give a precise definition of the flutter energy.

Table 4.1 seems to show that the map $k \mapsto \overline{E}_k$ is increasing in the classes of odd and even modes which, respectively, correspond to the so-called asymmetric and symmetric modes. This monotonicity follows the rule that the bending energy is increasing with respect to the modes, see Sect. 2.7. Moreover, for the TNB it is shown on [9, p. 119] that the "prevailing mode" of motion increases with wind velocity (that is, the energy within the structure). We also see that two modes may have very different flutter energies. If a bridge is vertically oscillating on a mode having large flutter energy (such as $k = 8$) it remains stable also at high energies. On the contrary, little energy is enough to create a resonance within a vertical mode with a small flutter energy ($k = 2$) and to give rise to torsional oscillations, that is, to an energy transfer within modes.

4.6 Damped and Forced Systems

Let $\delta > 0$ and consider (4.20) with a damping term:

$$\begin{cases} \ddot{\theta}_i + \delta\dot{\theta}_i + 3U_{\theta_i}(\Theta, Y) = 0 \\ \ddot{y}_i + \delta\dot{y}_i + U_{y_i}(\Theta, Y) = 0 \end{cases} \qquad (i = 1, \dots, n). \tag{4.27}$$

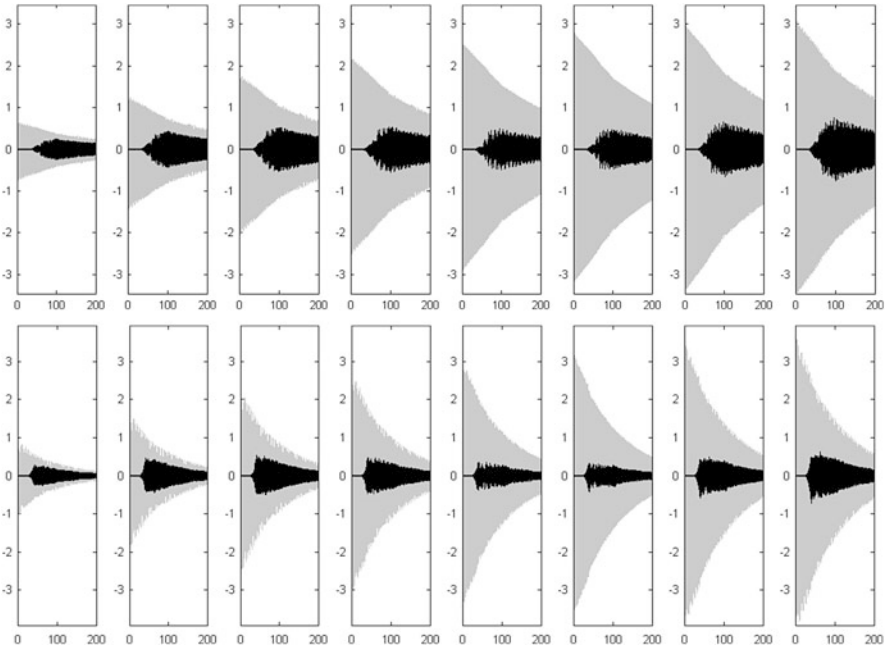

Fig. 4.14 The solution y_i (*black*) and θ_i (*grey*) ($i = 1, \ldots, 8$) of (4.27) and (4.28) for $(k, E(0)) = (1, 1000)$ with $\delta = 0.01$ (*first line*) and $(k, E(0)) = (1, 1500)$ with $\delta = 0.02$ (*second line*), $t \in [0, 200]$

Fix $k \in \{1, \ldots, n\}$ and let $(Y_1(k, E_0), Y_0(k, E_0))$ be as in (4.22). We take

$$\left(\dot{\Theta}, \dot{Y}, \Theta, Y\right)(0) = (\Theta^1, Y^1(k, E_0), \Theta^0, Y^0(k, E_0)) \text{ with } 0 < |(\Theta^1, \Theta^0)| < 10^{-6}. \tag{4.28}$$

We fix again $n = 16$. Figure 4.14 plots the solutions of (4.27) and (4.28) for $k = 1$, $\delta = 0.01$ and $\delta = 0.02$, and initial energy $E(0) > 500$, no wide torsion is visible for $E(0) = 500$. These plots should be compared with Fig. 4.8.

The numerical results for the damped system (4.27) suggest that for any $\delta > 0$ there exists a flutter energy $\overline{E}_{k,\delta}$ which, if exceeded by the initial energy $E(0) = E_0$ yields torsional instability of the k-th nonlinear normal mode $\overline{Y}_k(t)$ of (4.20) at energy E_0, while if $0 < E(0) < \overline{E}_{k,\delta}$ then the mode $\overline{Y}_k$ is torsionally stable. Large δ dissipate the energy very rapidly, preventing instability. It appears that the maps $\delta \mapsto \overline{E}_{k,\delta}$ are strictly increasing: by increasing δ from 0 to 0.1, the flutter energies $\overline{E}_{k,\delta}$ increase from 450 to 500 ($k = 1$), from 195 to 205 ($k = 2$), from 5,100 to 5,200 ($k = 3$). To compute $\overline{E}_{k,\delta}$ we use again the evolution map $\Psi^k_{E_0}$ defined in (4.24) with iteration time equal to the period $T = T(k, E_0)$ of the periodic k-th vertical mode of oscillation at energy $E_0 > 0$. We then compute the $2n$ eigenvalues $\lambda^k_1(E_0), \ldots, \lambda^k_{2n}(E_0)$ of its Jacobian $J\Psi^k_{E_0}(0, 0)$ at $(\Theta^1, \Theta^0) = (0, 0)$. In turn, the derivatives of $\Psi^k_{E_0}$ at $(0, 0)$ are computed by linearising (4.27) at $(\Theta, Y) = (0, \overline{Y}_k)$.

Denoting by $\Xi = (\xi_1, \ldots, \xi_n)$ the variation of $\Theta \equiv 0$, this yields the system

$$\ddot{\xi}_i + \delta\dot{\xi}_i + 3\sum_{j=1}^{n} U_{\theta_i\theta_j}(0, \overline{Y}_k(t))\xi_j = 0 \qquad (i = 1, \ldots, n). \tag{4.29}$$

The l-th column of $J\Psi^k_{E_0}(0,0)$ is the solution $(\dot{\Xi}, \Xi)(T)$ at time $T(k, E_0)$ of (4.29) with initial conditions $(\dot{\Xi}, \Xi)(0) = \eta_l$ $(l = 1, \ldots, 2n)$; here η_l is the l-th element of the canonical basis of $\mathbb{R}^{2n}$. It turns out that the solution of (4.27) with initial data (4.28) has small $(\dot{\Theta}, \Theta)(t)$ for all $t > 0$ if and only if $\max_l(|\lambda^k_l(E_0)|) \leq 1$. Therefore,

$$\overline{E}_{k,\delta} = \inf\left\{ E_0 > 0;\ \max_l(|\lambda^k_l(E_0)|) > 1 \right\}.$$

In Fig. 4.15 we plot the value of $\max_l(|\lambda^k_l(E_0)|)$ in dependence of the initial energy $E(0)$ for the first three vertical nonlinear normal modes.

Figure 4.15 should be compared with Fig. 4.11. The above results enable us to conclude that the suggested method to compute the flutter energy may be extended to damped models.

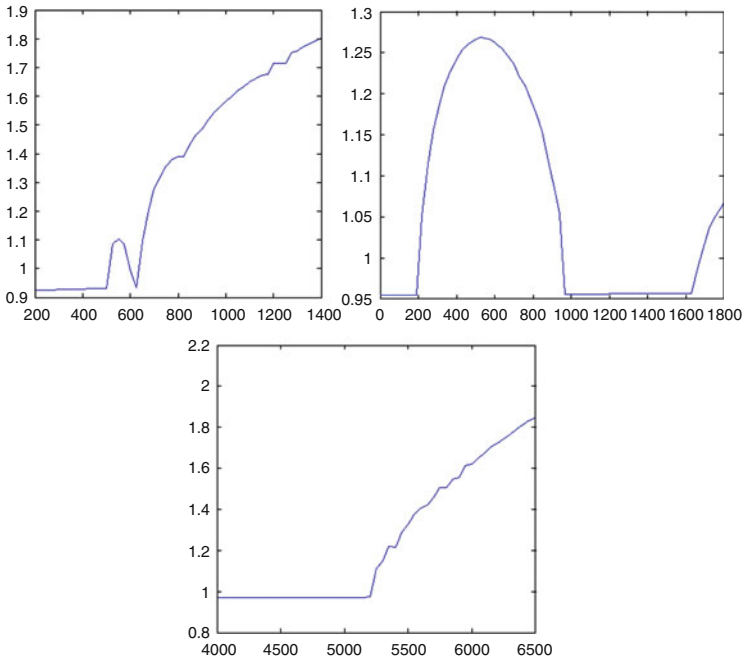

Fig. 4.15 Plot of $\max_l(|\lambda^k_l(E_0)|)$ versus $E(0) = E_0$ for $k = 1, 2, 3$ and $\delta = 0.1$

Let us now spend a few words on forced systems which appear much more delicate since the choice of the forcing term strongly influences the response of (4.20). In particular, it is shown in [144–146] that even simple mechanical systems may respond with frequencies different from the source: this creates new phenomena which are independent of the structure. In literature we essentially found periodic forcing but we prefer not to follow this trend for at least two reasons. First, the wind is random in nature and, for sure, it is not periodic; second, a periodic forcing may "pollute" the model by creating some artificial phenomena such as an external resonance, as discussed in Sect. 1.2. Moreover, in Sect. 1.4 we recalled a letter by Durkee [241, p. 63] stating that

> There appears to be no difference in the motion whether the wind is steady or gusty.

Let us also mention that it is not clear where the forcing term should be added in (4.20). The action of the wind is more likely to be horizontal and orthogonal to the centerline of the roadway. In Sect. 1.7.6 we have outlined the mechanism which creates vortices and, in turn, the lift with subsequent vertical oscillations of the bridge. Of course, the angle of attack may also be variable in time and generate further phenomena. McKenna [191] added a periodic forcing term in both the equations. Subsequently, McKenna-Tuama [195] claimed that it was not reasonable to introduce torsional forcing and considered a system with purely vertical periodic forcing: they showed that a purely vertical forcing could create a torsional response.

Following the suggestions of the above discussion, we introduce a purely vertical constant forcing $W \in \mathbb{R}$:

$$\begin{cases} \ddot{\theta}_i + 3U_{\theta_i}(\Theta, Y) = W \\ \ddot{y}_i + U_{y_i}(\Theta, Y) = 0 \end{cases} \qquad (i = 1, \dots, n)\,. \tag{4.30}$$

Even in the simplest case $n = 1$, a Poincaré map would be of no help, there is no energy conservation. But also an evolution map of the kind of (4.24) turned out to be useless, the computation of the eigenvalues did not appear reliable. So, we merely performed numerical experiments and we summarise the obtained results as follows.

- Starting with initial data (4.26) close to the k-th nonlinear normal mode with initial energy $E(0) < \overline{E}_k$ we could detect sudden appearance of torsional oscillations in (4.30) after some time. The plots looked like the ones in Fig. 4.8.
- There was no evident rule on the monotonicity with respect to W. Some small W gave rise to torsional oscillations while some larger W did not. Nor there was a clear pattern with respect to the sign of W. We suspect that this could be a phenomenon of resonance between the strength of forcing term W and the internal energy E.
- After adding aerodynamic forces depending linearly on $\dot{Y}$ (first equation) and $\dot{\Theta}$ (second equation) we could display similar phenomena to those described in Sect. 3.7.

Let us conclude by stating that, although deeper investigations appear necessary, also for nonlinear vertically forced systems such as (4.30) sudden torsional oscillations may appear. And the explanation seems to be the one suggested at the end of Sect. 4.2.

4.7 How to Construct the Poincaré Maps

A classical tool introduced in [223] by the French mathematician Henri Poincaré (1854–1912) is the so-called Poincaré map. We also refer to [135, Sect. 11.5] and [160, Sect. 1.4] for some applications.

In this section we describe in full detail the Poincaré map used to obtain the results in Sect. 4.2. The autonomous system (4.8) is conservative, its phase space is $\mathbb{R}^4$ and the variables are $(\dot\theta, \theta, \dot y, y)$. Its energy E in (4.9) is a constant of motion and, for any $E_0 > 0$, the three-dimensional manifold $E(\dot\theta, \dot y, \theta, y) = E_0$ is flow-invariant. We intersect this manifold with the three-dimensional hyperplane $y = 0$ but we consider only their points of intersection which have $\dot y > 0$.

Roughly speaking, the three-dimensional hypersurface $E(\dot\theta, \dot y, \theta, y) = E_0$ may be seen as the boundary of a domain in $\mathbb{R}^4$. Its intersection $\mathscr{C}$ with the hyperplane $y = 0$ is quite similar to an ellipsoid, see the left picture in Fig. 4.16. In order to define the Poincaré map P_{E_0} in (4.16), one fixes $E_0 > 0$ and takes initial data as in (4.15). This corresponds to fixing a point $M \in \mathscr{C}_+ := \mathscr{C} \cap \{\dot y > 0\}$ whose coordinates in the three-dimensional space $(\dot\theta, \dot y, \theta)$ are given by $M(\theta^1, y^1(E_0, \theta^1, \theta^0), \theta^0)$. The trajectory starts in M and always lives in the interior of $\mathscr{C}$; after some time $T = T(\theta^1, \theta^0) > 0$ it reaches again $\mathscr{C}_+$ at some point M', see the left picture in Fig. 4.16. Let $\mathscr{R}$ denote the orthogonal projection of $\mathbb{R}^3$ onto the plane $\mathbb{B}$ having equation $\dot y = 0$ so that $\mathscr{R}(M) = (\theta^1, \theta^0)$. Then the Poincaré map $P_{E_0} : \mathbb{B} \to \mathbb{B}$ is defined by $P_{E_0}(\mathscr{R}(M)) = \mathscr{R}(M')$, that is, by (4.16).

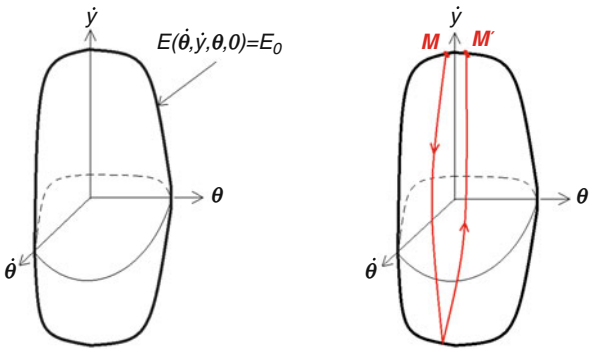

Fig. 4.16 Isoenergetic surface in the $(\dot\theta, \dot y, \theta)$-space and a cycle defining the Poincaré map

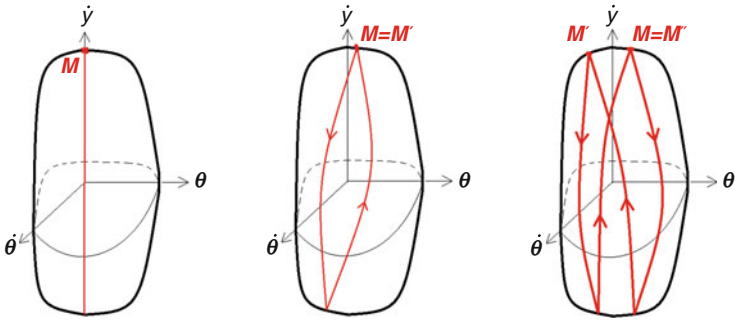

Fig. 4.17 Fixed and periodic points for the Poincaré map

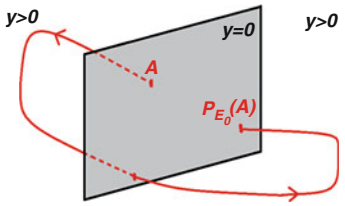

Fig. 4.18 The Poincaré map

Some situations are particularly meaningful. For all $y^1 > 0$, the initial data (4.14) gives rise to a periodic solution of system (4.8) which is represented in the left picture in Fig. 4.17 by the red segment. The trajectory starts in M whose coordinates in the three-dimensional space $(\dot{\theta}, \dot{y}, \theta)$ are given by $M(0, y^1, 0)$; the trajectory reaches periodically $\mathscr{C}_+$ at the point M. So, $M' = M$ and $(0, 0)$ is a fixed point of the Poincaré map. In the middle picture in Fig. 4.17, the point $\mathscr{R}(M)$ is also a fixed point for P_{E_0}. In the right picture in Fig. 4.17, $\mathscr{R}(M)$ transforms into $\mathscr{R}(M')$ which then transforms into $\mathscr{R}(M'')$: the point $\mathscr{R}(M)$ is a 2-periodic point for P_{E_0}, that is, a fixed point for the iterated map $P_{E_0}^2$. As we have seen in Sect. 4.2, these two latter cases may occur only when the total energy E is larger than the flutter energy $\overline{E}$: a bifurcation occurs and the two oscillators reach a resonance. In the first case (middle picture) we have a pitchfork bifurcation, in the second case (right picture) we have a period doubling bifurcation.

Another way of describing the Poincaré map is displayed in Fig. 4.18. The space represented is the three-dimensional manifold $E(\dot{\theta}, \dot{y}, \theta, y) = E_0$. The grey part is its intersection with the plane $y = 0$. The point A on this plane has coordinates $A(\dot{\theta}, \dot{y}, \theta, 0)$ with $\dot{y} > 0$. When the dynamics starts, the trajectory goes in the part of the manifold where $y > 0$, then it reaches a point where $\dot{y} = 0$ and comes back towards the plane $y = 0$; we are not interested in its first intersection (and crossing) of the plane because $\dot{y} < 0$, we have to wait until it comes back again from the part of the manifold where $y < 0$. At the second crossing, we have $\dot{y} > 0$ and we obtain the point $P_{E_0}(A)$. From this point, the same procedure is iterated. This is how we obtained the plots in Fig. 4.5.

4.8 Bibliographical Notes

The model described by Fig. 4.1 seems to have been first suggested by Bleich-McCullough-Rosecrans-Vincent [50, Figs. 39 and 75], see also [245, Fig. 10] and [234, p. 121].

The linear equation (4.5) is taken from [239], while some years later Scanlan [237] considers the same equation in a 3 degrees of freedom setting: vertical, torsional, and lateral swaying motions. The system (4.2) was introduced by Lazer-McKenna [168, Sect. 3.5] as a tentative model able to display torsional oscillations. They were mainly interested in periodic solutions with periodic sources. For a system without damping terms ($\delta_\theta = \delta_y = 0$) the problem becomes variational and the method of [70] enables to find multiple solutions. The system (4.2) was studied numerically in [151, 191, 194, 195] as reported in detail in Sect. 4.1. Numerical results displaying different kinds of bifurcations for (4.2) were obtained in [96].

Bartoli-Spinelli [30, (21)] consider a nonlinear stochastic version of (4.2) which includes damping and aerodynamic forces: they assume that the nonlinear behavior of the two hangers is only due to the sustaining cables. A related model was subsequently reconsidered by Plaut-Davis [220] who studied the case of asymmetric restoring hangers (as if one hanger failed) and nonlinear restoring forces f: as soon as an asymmetric behavior is assumed, torsional oscillations appear. We do not investigate this any further because we learned from Sect. 1.7.1 that a structural failure was not the cause of torsional oscillations at the TNB. A four-degrees-of-freedom model, describing the action of cables as well, is discussed in [220, Sect. 4] and, more recently, in [170]. Finally, let us mention that a variant of (4.2), with a fourth order equation describing also the torsional component was numerically studied in [151]; this system is related to the ones previously suggested in [1, 50, 234].

Section 4.2 gives an answer to [121, Problem 3] where we suggested to consider the isolated system with "doubly superlinear" forces such as (4.10); this was motivated by the self-excited behavior of solutions of some fourth order ODE's, see Sect. 2.6. The model described by Fig. 4.2 was suggested by Arioli-Gazzola [21, 22] from where we took all the remaining material of this chapter. The model described in Fig. 4.7 is also taken from [22] and is inspired to the celebrated model by Fermi-Pasta-Ulam [108], see also [18, 19, 23, 120].

Section 4.3 is new and unpublished. It is known that a combination between the Hill equation and the Poincaré sections is possible also in models of celestial mechanics, see e.g. [243]. Moreover, in recent engineering literature [65] one can find attempts to combine the tools from the Floquet theory, the Mathieu or Hill equation, the Poincaré maps, in order to study complex mechanical systems: these are the precisely the tools that we used in the present chapter and in the previous one. Theorem 4.4 is new and its proof may be obtained as for [36, Theorem 3]. We are grateful to Haïm Brezis for raising our attention on the work by Poincaré [222].

Chapter 5
Plate Models

The most natural way to describe the bridge roadway is to view it as a rectangular elastic plate. Rocard [234, p. 150] writes:

> The plate as a model is perfectly correct and corresponds mechanically to a vibrating suspension bridge.

In this chapter we make some attempts to model suspension bridges with nonlinear plate equations. We discuss both material nonlinearities, such as the behavior of the restoring force due to the hangers and the sustaining cables, and geometric nonlinearities due to possible wide oscillations which bring the plate (roadway) far away from its equilibrium position. The results in the present chapter should be seen as a prelude of more detailed studies aiming to increase the knowledge of the qualitative behavior of suspension bridges through plate models. Still, these results are sufficient to highlight a torsional instability and the existence of a flutter energy similar to those described in the previous chapters for different models.

The bending energy of a plate involves curvatures of the surface and this leads to fourth order PDE's. The choice of the boundary conditions is then quite delicate since it depends on the physical model considered. We review here several plate models and we adapt them to the roadway of a suspension bridge. As far as small deformations are involved, a linear model is accurate enough to describe the roadway: we recall the classical Kirchhoff-Love theory [154, 176]. Then we consider a celebrated quasilinear system due to von Kármán [271] and we study it with the boundary conditions modeling the behavior of the edges of the roadway. The oscillations of these plates are described by the spectrum of the linear operator and by the corresponding set of eigenfunctions: we classify them in two main categories, vertical and torsional. We perform a detailed analysis of the spectrum by using the parameters of the collapsed TNB and we provide an explanation why its oscillation switched from the tenth vertical mode to the second torsional mode. Through a finite-dimensional projection of the phase space, for an approximated semilinear equation we show that a characterization of the flutter energy is available.

F. Gazzola, *Mathematical Models for Suspension Bridges*, MS&A 15,
DOI 10.1007/978-3-319-15434-3_5

Finally, we study the role of the stretching energy and we introduce it into the equation under three different forms: as a linearised approximation, as an increment of surface, as a nonlocal term.

5.1 Linear or Nonlinear Models?

Nonlinearity is intrinsic in nature. Linear theories are only valid in circumstances which involve some assumption of "smallness" such as small strains or small displacements. Usually, linear theories are adopted because the solutions of linear equations are easier to compute and the computational cost is smaller. But nonlinear analysis becomes necessary if one exits the smallness regime and if one aims at a better understanding of the underlying physical phenomena.

A body is called elastic if it may be deformed by the application of suitable forces but returns to its original state after the forces are withdrawn. The simplest formulation of elasticity is based on the assumptions of a linear stress-strain law and of small displacements. Dropping these assumptions uncovers the two main sources of nonlinearity: the geometric and the material nonlinearities. Geometric nonlinearities in mechanical problems involve nonlinearities in kinematic quantities, such as the strain-displacement relations in solids, and occur for large deformations or large strains. In a plate, geometric nonlinearities appear for large displacements from equilibrium or large loads: in a bridge modeled by a plate, this corresponds to wide oscillations and to actions of hurricanes or earthquakes. Material nonlinearities occur when the stress-strain or force-displacement law is not linear, or when material properties change with the applied loads. For plates, the stress-strain nonlinearity essentially depends on the thickness: for thin plates a linear theory is enough to detect the main phenomena involved. For a bridge modeled by a plate, the thickness depends on the presence of a stiffening truss: roughly speaking, a thick stiffening truss forces a bridge to behave nonlinearly. In suspension bridges there is a further source of material nonlinearity, namely the interaction between the different components of the bridge, in particular the interaction between the roadway (plate) and the cables-hangers system. The nonlinear behavior of cables, see Chap. 2, is perhaps the main source of material nonlinearity in suspension bridges.

The first satisfactory linear theory of bending of plates was suggested by the German physicist and mathematician Gustav Robert Kirchhoff (1824–1887). In his seminal paper [154], published in 1850, he established the correct mathematical expressions for the potential energy and he showed that there are only two boundary conditions and not three, as was supposed by Poisson. The advent of this theory of plates has been a great step forward in the theory of elasticity. This theory was later complemented by the English mathematician and geophysicist Augustus Edward Hough Love (1863–1940) in his monograph [176] originally published in 1927 and is nowadays known as the Kirchhoff-Love linear theory for plates: in Sect. 5.2 we briefly recall it. Destuynder-Salaun [92, Sect. I.2] describe this modeling by

> Kirchhoff and Love have suggested to assimilate the plate to a collection of small pieces, each one being articulated with respect to the other and having a rigid-body behavior. It looks like these articulated wooden snakes that children have as toys. Hence the transverse shear strain remains zero, while the planar deformation is due to the articulation between small blocks. But this simplified description of a plate movement can be acceptable only if the components of the stress field can be considered to be negligible.

The above comment confirms that a linear theory should not be followed if the components of the stress field are not negligible. Destuynder-Salaun [92, Sect. I.2] also revisit an alternative model due to Naghdi [208] by using a mixed variational formulation. They refer to [204, 231, 232] for further details and modifications, and conclude by saying that none between the Kirchhoff-Love model or one of these alternative models is better than the others. Moreover, the definition of the transverse shear energy is not universally accepted; from [92, p. 149], we quote:

> this discussion has been at the origin of a very large number of papers from both mathematicians and engineers. But to our best knowledge, a convincing justification concerning which one of the two expressions is the more suitable for numerical purpose, has never been formulated in a convincing manner. This question is nevertheless a fundamental one.

Linear theories are reliable as long as the thickness of the plate is small and the vertical displacements are small when compared to the thickness. In the case of a suspension bridge, this is not the case: if large deformations occur, geometric nonlinearities arise and one should stick to nonlinear theories.

In 1910, the Hungarian physicist and engineer Theodore von Kármán (1881–1963) suggested a two-dimensional system in order to describe large deformations of a thin plate, see [271]. This theory was considered a breakthrough in several scientific communities, including in the National Advisory Committee for Aeronautics, an American federal agency during the twentieth century: the purpose of this agency was to undertake, to promote, and to institutionalise aeronautical research and the von Kármán equations were studied for a comparison between theoretical and experimental results, see [172, 173]. In his report, Levy [172] writes:

> In the design of thin plates that bend under lateral and edge loading, formulas based on the Kirchhoff theory which neglects stretching and shearing in the middle surface are quite satisfactory provided that the deflections are small compared with the thickness. If deflections are of the same order as the thickness, the Kirchhoff theory may yield results that are considerably in error and a more rigorous theory that takes account of deformations in the middle surface should therefore be applied. The fundamental equations for the more exact theory have been derived by von Kármán.

Several years later, in his autobiography [272], von Kármán states:

> If you define a great scientist as a man with great ideas, then you will have to rate Einstein first. He had four great ideas. ... All the other major scientists of our age are associated with just one, or at most two, great ideas. In my case I have had three great ideas. Maybe more. Yes, perhaps three and a half great ideas.

This attitude may be the reason why several doubts have been raised on the physical soundness of the von Kármán theory of plates. For instance, Truesdell [263, pp. 601–602] writes

> An analysis may regard that theory as handed out by some higher power (a Hungarian wizard, say) and study it as a matter of pure analysis. To do so for von Kármán theory is particularly tempting because nobody can make sense out of the "derivations"...

Then Truesdell continues by writing

> Being unable to explain just why the von Kármán theory has always made me feel a little nauseated as well as very slow and stupid, I asked an expert, Mr. Antman, what was wrong with it. I can do no better than paraphrase what he told me: it relies upon
>
> 1) "approximate geometry", the validity of which is assessable only in terms of some other theory.
> 2) assumptions about the way the stress varies over a cross-section, assumptions that could be justified only in terms of some other theory.
> 3) commitment to some specific linear constitutive relation - linear, that is, in some special measure of strain, while such approximate linearity should be outcome, not the basis, of a theory.
> 4) neglect of some components of strain - again, something that should be proved mathematically from an overriding, self-consistent theory.
> 5) an apparent confusion of the referential and spatial descriptions - a confusion that is easily justified for the classical linearised elasticity but here is carried over unquestioned, in contrast with all recent studies of the elasticity of finite deformations.

Finally, Truesdell concludes with a quite eloquent comment:

> These objections do not prove that anything is wrong with von Kármán strange theory. They merely suggest that it would be difficult to prove that there is anything right about it.

Let us invite the interested reader to have a careful look at the paper by Truesdell [263]; it contains several criticisms exposed in a highly ironic and exhilarating fashion and, hence, very effective.

In spite of these criticisms, many authors have studied the von Kármán system, see Sect. 5.8 for some references. In particular, Ciarlet [79] provides an important justification of the von Kármán equations. He makes an asymptotic expansion with respect to the thickness of a three-dimensional class of elastic plates under suitable loads. He then shows that the leading term of the expansion solves a system of equations equivalent to those of von Kármán: by referring to the above reported objections by Antman, he states [79, p. 350] that he is able to

> ...provide an effective strategy for embedding the von Kármán equations in a rational approximation scheme that overcomes objections 1, 2, 4 and 5.

Subsequently, Davet [88] pursued further and proved that the von Kármán equations may be justified by asymptotic expansion methods starting from very general three-dimensional constitutive laws. In Sect. 5.2.3 we recall the main points of the von Kármán theory while in Sect. 5.6 we adapt it to a suspension bridge model.

An attempt to classify nonlinear theories for plates is made by Mansfield [186, Chaps. 8–9]. He first considers approximate methods, then three classes of asymptotic plate theories: membrane theory, tension field theory, inextensional theory. Basically, which of the three theories should be followed depends on the ratio between the thickness of the plate and the typical planar dimension: for the

first two theories the ratio should be less than 10^{-3}, whereas for the third theory it should be less than 10^{-2}. Since the plate modeling the roadway of a bridge has a length of the order of 1 km, the width of the order of 10 m, even for the less stringent inextensional theory the thickness of the roadway should be less than 10 cm which, of course, appears unreasonable. As a conclusion, Mansfield [186, p. 183] makes the following meaningful comment:

> The exact large-deflection analysis of plates generally presents considerable difficulties.

Some alternative attempts to tackle nonlinear elasticity in particular situations were done by Antman [13, 14] (see also [15, 16]) who, however, appears quite skeptic on the possibility to have a general theory [13, p. 308]:

> general three-dimensional nonlinear theories have so far proved to be mathematically intractable.

Finally, let us also quote a couple of sentences written by Gurtin [137] about a general theory of nonlinear elasticity:

> Our discussion demonstrates why this theory is far more difficult than most nonlinear theories of mathematical physics. It is hoped that these notes will convince analysts that nonlinear elasticity is a fertile field in which to work.

What we have just seen suggests that classical and recent modeling of plates should be carefully revisited. For the beam model it took several decades before one could successfully face nonlinear problems and, for some particular models such as the Hill equation (1), it even took more than one century before tackling nonlinear versions. It seems that, for the plate model, we are still in the age where mathematics is guilty (see Sect. 2.7.2) being unable to be used by applied scientists. Since fully nonlinear plate equations appear intractable, and since linear equations fail to satisfy the requirements of the (GPCM), see Sect. 1.8, a first step could be to introduce models having some nonlinearity only in the lower order terms. This appears to be a good compromise between unreliable linear models and too complicated fully nonlinear models. This compromise is quite common in elasticity, see e.g. the book by Ciarlet [81, p. 322] who describes the method of asymptotic expansions for the thickness ε of a plate as a "partial linearisation"

> in that a system of quasilinear partial differential equations, i.e., with nonlinearities in the higher order terms, is replaced as $\varepsilon \to 0$ by a system of semilinear partial differential equations, i.e., with nonlinearities only in the lower order terms.

In Sect. 5.4 we follow this suggestion and analyse a semilinear equation where the nonlinearities merely appear in the zero order term. In Sect. 5.6 we study a modified von Kármán quasilinear static system which aims to better model large vertical displacements of the plate. Then in Sects. 5.7.3 and 5.7.4 we consider two quasilinear equations involving second order nonlinear differential operators while the highest order operator (fourth order) remains linear.

5.2 The Elastic Bending Energy of a Plate

5.2.1 The Plate as a Model for Suspension Bridges

A rectangular plate $\Omega = (0, L) \times (-\ell, \ell) \subset \mathbb{R}^2$ resists to transverse loads exclusively by means of bending. The flexural properties of a plate strongly depend on its thickness, which we denote by d, compared with its width 2ℓ and its length L. We assume here that $2\ell < L$ so that d has to be compared with 2ℓ. From Ventsel-Krauthammer [264, Sect. 1.1] we learn that plates may be classified according to the ratio $2\ell/d$:

- If $2\ell \leq 8d$ we have a thick plate and the analysis of these plates includes all the components of stresses, strains and displacements as for solid three-dimensional bodies.
- If $8d \leq 2\ell \leq 80d$ we have a thin plate which may behave in both linear and nonlinear regime according to how large is the ratio between its deflection and its thickness d.
- If $2\ell \geq 80d$ the plate behaves like a membrane and lacks of flexural rigidity.

Let us now turn to a suspension bridge. We view the roadway of the bridge as a long narrow rectangular plate, hinged on its short edges where the bridge is supported by the ground, and free on its long edges. If L denotes its length and 2ℓ denotes its width, a realistic assumption is that $2\ell \cong \frac{L}{100}$. For instance, the main span of the collapsed Tacoma Narrows Bridge had the measures

$$L = 2800\,\text{ft} \approx 853.44\,\text{m}, \quad 2\ell = 39\,\text{ft} \approx 11.89\,\text{m}, \quad d = 4\,\text{ft}4\tfrac{1}{2}'' \approx 1.33\,\text{m}, \tag{5.1}$$

see p. 11 and Drawings 2 and 3 in [9]. Therefore, $2\ell/d \approx 8.94$ and

the TNB may be considered as a thin plate.

It is clear that modern suspension bridges with their stiffening trusses are more similar to thick plates.

Which theory (linear or nonlinear) models a thin plate depends on the magnitude W of its maximal deflection. If we denote again by d its thickness, two cases may occur, according to Ventsel-Krauthammer [264, Sect. 1.1]:

- If $W/d \leq 0.2$ the plate is classified as stiff: these plates carry loads two dimensionally, mostly by internal bending, twisting moments and by transverse shear forces.
- If $W/d \geq 0.3$ the plate is classified as flexible: in this case, the deflections will be accompanied by stretching of the surface.

A fundamental feature of stiff plates is that the equation of static equilibrium for a plate element may be set up for an original (undeformed) configuration of the plate: in this case a linear theory describes with sufficient accuracy the behavior of

the plate. Flexible plates behave somehow in between membranes and stiff plates: when $W/d \gg 0.3$ the membrane action is dominant and the flexural stress can be neglected compared with the membrane stress. In this case, a linear theory is not enough to describe accurately the behavior of the plate and one has to stick to nonlinear theories.

According to Scott [241, pp. 49–51] (see also [9, p. 60] and the video [253]), the Board of Engineers stated that under pure vertical oscillations

> . . .the lateral deflection of the center bridge was not measured but did not appear excessive, perhaps four times the width of the yellow center line (about 2 ft.)

while, after the appearance of the torsional oscillation,

> . . .the roadway was twisting almost 45° from the horizontal, with one side lurching 8.5 m. above the other.

This means that it was $W = 2$ ft during the vertical oscillations without torsion and $W = 14$ ft when the torsional oscillation appeared at the TNB. In view of (5.1), we then have $W/d \approx 0.46$ under pure vertical oscillations and $W/d \approx 3.21$ in presence of torsional oscillations. The conclusion is that

the TNB oscillated in a nonlinear regime.

Which nonlinear model should be used is questionable. In what follows, we start by setting a reliable linear theory and then, in Sect. 5.4, we add some nonlinearity in order to reach a semilinear model. As already mentioned at the end of the previous section, this is good compromise between intractable fully nonlinear models and unreliable linear models. Then, in Sect. 5.6 we move a further step towards a fully nonlinear model: we study the quasilinear system suggested by von Kármán [271]. In spite of the criticisms reported in Sect. 5.1, this model has been considered in literature, see the references in Sect. 5.8.

We are now ready to start the modeling process for an elastic thin rectangular plate. In the next two subsections we introduce both linear and nonlinear models for plates and we discuss the main role of the bending energy. A further energy which appears in plates is the stretching energy, especially if the plate is thin and flexible. However, for narrow elongated plates with free edges this energy plays a minor role and, for a first approximation, it may be neglected. We discuss further this approximation and suggest some plate models including the stretching energy in Sect. 5.7.

5.2.2 A Linear Model for Small Deformations

After scaling, we may take $L = \pi$ and consider the plate

$$\Omega = (0, \pi) \times (-\ell, \ell) \subset \mathbb{R}^2 . \tag{5.2}$$

The bending energy of the plate Ω involves curvatures of the surface. Let κ_1 and κ_2 denote the principal curvatures of the graph of the (smooth) function u representing the vertical displacement of the plate, then a simple model for the bending energy of a deformed plate Ω of thickness $d > 0$ is

$$\mathbb{E}_B(u) = \frac{E\, d^3}{12(1-\sigma^2)} \int_\Omega \left(\frac{\kappa_1^2}{2} + \frac{\kappa_2^2}{2} + \sigma \kappa_1 \kappa_2 \right) dxdy \tag{5.3}$$

where σ is the Poisson ratio defined by $\sigma = \frac{\lambda}{2(\lambda+\mu)}$ and E is the Young modulus defined by $E = 2\mu(1+\sigma)$, with the so-called Lamé constants λ, μ that depend on the material. For physical reasons it holds that $\mu > 0$ and usually $\lambda > 0$ so that

$$0 < \sigma < \frac{1}{2}. \tag{5.4}$$

Moreover, it always holds true that $\sigma > -1$ although some exotic materials have a negative Poisson ratio, see [165]. For metals the value of σ lies around 0.3, see [176, p. 105], while for concrete $0.1 < \sigma < 0.2$; hence, we will assume (5.4). The Poisson ratio is the negative ratio of transverse to axial strain: when a material is compressed in one direction, it tends to expand in the other two directions. The Poisson ratio σ is a measure of this effect, it is the fraction of expansion divided by the fraction of compression for small values of these changes. Throughout this chapter we will intensively make use of the Monge-Ampère operator

$$[\phi, \psi] := \phi_{xx}\psi_{yy} + \phi_{yy}\psi_{xx} - 2\phi_{xy}\psi_{xy} \qquad \forall \phi, \psi \in H^2(\Omega)\,. \tag{5.5}$$

Note that, in particular, $[\phi, \phi] = 2\det(D^2\phi)$ where $D^2\phi$ is the Hessian matrix of ϕ.

For small deformations the terms in (5.3) are taken as approximations being purely quadratic with respect to the second order derivatives of u. More precisely, for small deformations u, one has

$$(\kappa_1 + \kappa_2)^2 \approx (\Delta u)^2\,, \quad \kappa_1\kappa_2 \approx \det(D^2 u) = \frac{[u,u]}{2}\,, \tag{5.6}$$

and therefore

$$\frac{\kappa_1^2}{2} + \frac{\kappa_2^2}{2} + \sigma\kappa_1\kappa_2 \approx \frac{1}{2}(\Delta u)^2 + \frac{\sigma - 1}{2}[u,u].$$

If f denotes the external vertical load (including both dead and live loads) acting on the plate Ω and if u is the corresponding (small) vertical displacement of the plate, then by (5.3) we have that the total energy $\mathbb{E}_T$ of the plate becomes

$$\begin{aligned} \mathbb{E}_T(u) &= \mathbb{E}_B(u) - \int_\Omega fu\, dxdy \\ &= \frac{E\, d^3}{12(1-\sigma^2)} \int_\Omega \left(\frac{1}{2}(\Delta u)^2 + \frac{\sigma - 1}{2}[u,u] \right) dxdy - \int_\Omega fu\, dxdy. \end{aligned} \tag{5.7}$$

Note that for $|\sigma| < 1$ the quadratic part of the functional (5.7) is positive. The unique minimiser u of $\mathbb{E}_T$, satisfies the Euler-Lagrange equation

$$\Delta^2 u = \frac{12(1-\sigma^2)}{E\, d^3}\, f \qquad \text{in } \Omega\,. \tag{5.8}$$

5.2.3 A Nonlinear Model for Large Deformations

If large deformations are involved, one does not have a linear strain-displacement relation resulting in (5.6). A possible nonlinear model was suggested by von Kármán [271] as we illustrate in this section. For a plate of uniform thickness $d > 0$, one assumes that the plate has a middle surface midway between its parallel faces that, in equilibrium, occupies the region Ω in the plane $z = 0$; the two faces are in the planes $z = \pm d/2$. Let $w = w(x, y)$, $v = v(x, y)$, $u = u(x, y)$ denote the components (respectively in the x, y, z directions) of the displacement vector of the particle of the middle surface which, when the plate is in equilibrium, occupies the position $(x, y) \in \Omega$: u is the component in the vertical z-direction which is related to bending while w and v are the in-plane stretching components, see Fig. 5.1. The "horizontal" displacements are small when compared with the (vertical) deflection:

$$|w| \ll |u|\,, \quad |v| \ll |u|\,. \tag{5.9}$$

For large deformations of Ω there is a coupling between u and (w, v). In order to describe it, we consider the two points $A(x, y, 0)$ and $B(x + dx, y, 0)$ of the undeformed middle surface Ω; after deformation, these points will be, respectively, in positions

$$A'(x+w, y+v, u)\,, \quad B'(x+dx+w+w_x dx, y+v+v_x dx, u+u_x dx)\,. \tag{5.10}$$

The distance between A' and B' is then

$$d(A', B') = \sqrt{(dx + w_x dx)^2 + (v_x dx)^2 + (u_x dx)^2}$$

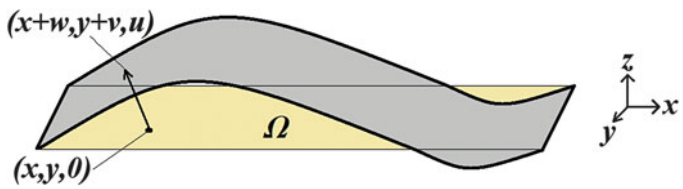

Fig. 5.1 Large deformation of the plate Ω: $(x, y, 0) \mapsto (x + w, y + v, u)$

and the relative stretching of the line segment AB of Ω in the x-direction is given by

$$\varepsilon_x = \frac{d(A',B') - d(A,B)}{d(A,B)} = \frac{\sqrt{(dx + w_x dx)^2 + (v_x dx)^2 + (u_x dx)^2} - dx}{dx}$$
$$= \sqrt{1 + 2w_x + w_x^2 + v_x^2 + u_x^2} - 1\,.$$

The quantities u_x, v_x, w_x are experimentally seen to be small compared to unity, see e.g. [74, 174, 246]. Therefore, we know that $w_x^2 \ll |w_x|$ and, by (5.9), we may also drop his companion v_x^2; we finally obtain $\varepsilon_x \approx w_x + u_x^2/2$. Depending on the deformation of Ω, each one of these terms may be the largest one and therefore we maintain both of them. Then we consider the two points $A(x, y, 0)$ and $C(x, y + dy, 0)$ of Ω; after deformation, the latter point will be in position

$$C'(x + w + w_y dy, y + dy + v + v_y dy, u + u_y dy)\,. \tag{5.11}$$

By computing the distance between A' and C' and performing the same approximations as for ε_x we find the stretching ε_y in the y direction. Summarising, we obtain the following form for the stretching in the x and y directions (see e.g. [264, (7.80)]):

$$\varepsilon_x \approx w_x + \frac{u_x^2}{2}\,, \quad \varepsilon_y =\approx v_y + \frac{u_y^2}{2}\,. \tag{5.12}$$

Let us now compute the shear strain that we denote by γ_{xy}. Consider again the points A, B, C and their new positions A', B', C' [see (5.10) and (5.11)] and let α be the angle between the segments $A'B'$ and $A'C'$: then $\gamma_{xy} = \frac{\pi}{2} - \alpha$. Since $\alpha \approx \frac{\pi}{2}$, we have

$$\gamma_{xy} \approx \sin\left(\frac{\pi}{2} - \alpha\right) = \cos\alpha\,. \tag{5.13}$$

From the triangle $A'B'C'$ we obtain

$$d(B',C')^2 = d(A',B')^2 + d(A',C')^2 - 2d(A',B')d(A',C')\cos\alpha\,,$$

that is,

$$\cos\alpha = \frac{d(A',B')^2 + d(A',C')^2 - d(B',C')^2}{2d(A',B')d(A',C')}\,.$$

By replacing the coordinates of the points in (5.10) and (5.11) and by simplifying the ratio by $2dxdy$ we obtain

$$\cos\alpha = \frac{(1+w_x)w_y + (1+v_y)v_x + u_x u_y}{\sqrt{(1+w_x)^2 + v_x^2 + u_x^2}\,\sqrt{(1+v_y)^2 + w_y^2 + u_y^2}}\,.$$

Since all these derivatives are small, the denominator can be approximated with 1 while in the numerator we may drop both the terms $w_x w_y$ and $v_y v_x$. The only information for the three remainder terms is (5.9) which is not enough to decide which is the leading term; indeed, depending on the deformation of Ω, each one of these terms may be the largest one and therefore we maintain all of them. We then obtain $\cos\alpha \approx w_y + v_x + u_x u_y$ which, combined with (5.13) finally yields (see e.g. [264, (7.81)]):

$$\gamma_{xy} \approx w_y + v_x + u_x u_y\,. \tag{5.14}$$

It is also convenient to introduce the so-called stress resultants which are the integrals of suitable components of the strain tensor (see e.g. [162, (1.22)]), namely,

$$N^x = \frac{Ed}{1-\sigma^2}\left(w_x + \sigma v_y + \frac{u_x^2}{2} + \frac{\sigma}{2}u_y^2\right), \quad N^y = \frac{Ed}{1-\sigma^2}\left(v_y + \sigma w_x + \frac{u_y^2}{2} + \frac{\sigma}{2}u_x^2\right),$$

$$N^{xy} = \frac{Ed}{2(1+\sigma)}\,(w_y + v_x + u_x u_y)\,, \tag{5.15}$$

so that

$$\varepsilon_x = \frac{N^x - \sigma N^y}{Ed}\,, \quad \varepsilon_y = \frac{N^y - \sigma N^x}{Ed}\,, \quad \gamma_{xy} = \frac{2(1+\sigma)}{Ed}\,N^{xy}\,.$$

We are now in a position to define the energy functional. The first term $\mathbb{E}_T(u)$ of the energy is due to pure bending and to external loads and was already computed in (5.7). For large deformations, one needs to consider also the interaction with the stretching components v and w and the total energy reads (see [163, (1.7)])

$$J(u,v,w) = \mathbb{E}_T(u) + \frac{E\,d}{2(1-\sigma^2)}\int_\Omega \left(\varepsilon_x^2 + \varepsilon_y^2 + 2\sigma\,\varepsilon_x\varepsilon_y + \frac{1-\sigma}{2}\,\gamma_{xy}^2\right) dxdy$$

which has to be compared with (5.7). In view of (5.2.3)–(5.14) the additional term $I := J - \mathbb{E}_T$ may also be written as

$$I(u,v,w) = \frac{E\,d}{2(1-\sigma^2)}\int_\Omega \left\{\left[w_x + \frac{u_x^2}{2}\right]^2 + \left[v_y + \frac{u_y^2}{2}\right]^2 + 2\sigma\left[w_x + \frac{u_x^2}{2}\right]\left[v_y + \frac{u_y^2}{2}\right]\right\} dxdy$$

$$+ \frac{E\,d}{4(1+\sigma)}\int_\Omega (w_y + v_x + u_x u_y)^2 dxdy\,.$$

The Euler-Lagrange equation characterises the critical points of J: we need to compute the variation δJ of J and to find triples (u, v, w) such that

$$\Big\langle \delta J(u,v,w), (\phi,\psi,\xi) \Big\rangle = \lim_{t\to 0} \frac{J(u+t\phi, v+t\psi, w+t\xi) - J(u,v,w)}{t} = 0$$

for all $\phi, \psi, \xi \in C_c^\infty(\Omega)$. After replacing N^x, N^y, N^{xy}, see (5.15), this yields

$$\begin{gathered}
\frac{E\,d^3}{12(1-\sigma^2)} \int_\Omega \big(\Delta u \Delta\phi + (\sigma-1)[u,\phi]\big)\,dxdy \\
+ \int_\Omega \big((N^x u_x + N^{xy} u_y)\phi_x + (N^y u_y + N^{xy} u_x)\phi_y\big)\,dxdy = \int_\Omega f\phi\,dxdy \quad \forall \phi \in C_c^\infty(\Omega) \\
\int_\Omega \big(N^y \psi_y + N^{xy}\psi_x\big)\,dxdy = 0 \qquad \forall \psi \in C_c^\infty(\Omega) \\
\int_\Omega \big(N^x \xi_x + N^{xy}\xi_y\big)\,dxdy = 0 \qquad \forall \xi \in C_c^\infty(\Omega).
\end{gathered}$$

Thanks to some integration by parts and by arbitrariness of the test functions, we may rewrite the above identities in strong form

$$\begin{gathered}
\tfrac{E\,d^3}{12(1-\sigma^2)} \Delta^2 u - (N^x u_x + N^{xy} u_y)_x - (N^y u_y + N^{xy} u_x)_y = f \qquad \text{in } \Omega\,, \\
N^y_y + N^{xy}_x = 0\,, \quad N^x_x + N^{xy}_y = 0 \qquad \text{in } \Omega\,.
\end{gathered} \tag{5.16}$$

The last two equations in (5.16) show that there exists a function Φ (called Airy stress function), unique up to an affine function, such that

$$\Phi_{yy} = N^x, \quad \Phi_{xx} = N^y, \quad \Phi_{xy} = -N^{xy}\,. \tag{5.17}$$

Then, after some tedious computations and by using the Monge-Ampère operator (5.5), (5.16) becomes

$$\begin{cases} \Delta^2 \Phi = -\frac{E\,d}{2}\,[u,u] & \text{in } \Omega \\ \Delta^2 u = \frac{12(1-\sigma^2)}{E\,d^3}([\Phi,u] + f) & \text{in } \Omega\,. \end{cases} \tag{5.18}$$

After reaching system (5.18), Ventsel-Krauthammer [264, Sect. 7.4.2] write

> Unfortunately, where realistic problems are concerned, solving these coupled, nonlinear, partial differential equations represents a stubborn mathematical task.

Although (5.18) appears theoretically difficult to tackle directly, one may use iterative and numerical methods in order to get approximate solutions. In particular, let us illustrate the *method of successive approximations* [264, Sect. 18.7.1]. In the first approximation one solves the system

$$\Delta^2 \Phi_1 = 0\,, \quad \Delta^2 u_1 = \frac{12(1-\sigma^2)}{E\,d^3}\,f \quad \text{in } \Omega$$

complemented with the boundary conditions describing the model. This system has as solution $\Phi_1 = 0$ and u_1 being the solution of the linear problem (5.8). Then one defines iteratively the sequence $\{u_n, \Phi_n\}$ as follows

$$\Delta^2 \Phi_{n+1} = -\frac{E\,d}{2}[u_n, u_n], \quad \Delta^2 u_{n+1} = \frac{12(1-\sigma^2)}{E\,d^3}([\Phi_n, u_n] + f) \quad \text{in } \Omega \quad \forall n \geq 1\,.$$

In particular, $u_2 = u_1$ and $\Phi_3 = \Phi_2$. Several investigations show that this sequence converges towards a solution of (5.18), the solution is found as a fixed point of the map implicitly defined by the iterative procedure. The convergence is fairly slow if the load f is small, in which case also the deformation u is small and hence close to a linear regime. But if f is large, and consequently u is large and in a full nonlinear regime, then the method has a satisfactory convergence rate.

In Sect. 5.6 we modify (5.18) in order to model wide oscillations in suspension bridges. We add the boundary conditions and we introduce in (5.18) both a prestressing constraint which may lead to buckling and the nonlinear restoring action due to the hangers. Instead of using the method of successive approximations we take advantage of tools from the calculus of variations, from critical point theory, and from bifurcation theory.

5.3 The Linear Equation with No Stretching Term

5.3.1 Variational Setting: Existence and Uniqueness

For small deformations of the plate, the energy may be reduced to $\mathbb{E}_T$, see (5.7). By replacing the load f with $\frac{Ed^3}{12(1-\sigma^2)} f$, and up to a constant multiplier, we have

$$\mathbb{E}_T(u) = \int_\Omega \left(\frac{(\Delta u)^2}{2} + \frac{\sigma - 1}{2}[u, u] - fu \right) dxdy \tag{5.19}$$

and the unique minimiser u of $\mathbb{E}_T$, satisfies the Euler-Lagrange equation

$$\Delta^2 u = f \qquad \text{in } \Omega\,. \tag{5.20}$$

The boundary conditions to be associated to (5.20) should represent the physical situation of a plate modeling a bridge. Due to the connection with the ground, the plate $\Omega = (0, \pi) \times (-\ell, \ell)$ is assumed to be hinged on its short edges and hence

$$u(0, y) = u_{xx}(0, y) = u(\pi, y) = u_{xx}(\pi, y) = 0 \quad y \in (-\ell, \ell)\,. \tag{5.21}$$

The long edges $y = \pm\ell$ are free and the boundary conditions there become (see e.g. [264, (2.40)])

$$u_{yy}(x,\pm\ell)+\sigma u_{xx}(x,\pm\ell)=u_{yyy}(x,\pm\ell)+(2-\sigma)u_{xxy}(x,\pm\ell)=0 \quad x\in(0,\pi). \tag{5.22}$$

These conditions arise when writing the variational formulation of (5.20), see Theorem 5.2. Summarising, the whole set of boundary conditions for a rectangular plate $\Omega = (0,\pi)\times(-\ell,\ell)$ modeling a suspension bridge is (5.21)–(5.22) and the boundary value problem reads

$$\begin{cases} \Delta^2 u = f & \text{in } \Omega \\ u(0,y)=u_{xx}(0,y)=u(\pi,y)=u_{xx}(\pi,y)=0 & y\in(-\ell,\ell) \\ u_{yy}(x,\pm\ell)+\sigma u_{xx}(x,\pm\ell)=u_{yyy}(x,\pm\ell)+(2-\sigma)u_{xxy}(x,\pm\ell)=0 & x\in(0,\pi). \end{cases} \tag{5.23}$$

Problem (5.23) requires a suitable variational framework which will also be useful for other equations containing additional terms. Let D^2w denote the Hessian matrix of a function $w\in H^2(\Omega)$. Thanks to the intermediate derivatives Theorem, see [3, Theorem 4.15], the space $H^2(\Omega)$ is a Hilbert space if endowed with the scalar product

$$(u,v)_{H^2} := \int_\Omega \left(D^2u\cdot D^2v + uv\right)\,dxdy \qquad \text{for all } u,v\in H^2(\Omega)\,.$$

We define the spaces

$$H^2_*(\Omega) := \left\{w\in H^2(\Omega);\ w=0 \text{ on } \{0,\pi\}\times(-\ell,\ell)\right\},$$

$$\mathscr{H}(\Omega) := \text{the dual space of } H^2_*(\Omega)$$

and denote by $\langle\cdot,\cdot\rangle$ the duality between $\mathscr{H}(\Omega)$ and $H^2_*(\Omega)$. Since we are in the plane, $H^2(\Omega)\subset C^0(\overline{\Omega})$ (see again [3]) so that the condition on $\{0,\pi\}\times(-\ell,\ell)$ in the definition of $H^2_*(\Omega)$ is satisfied pointwise and

$$L^p(\Omega)\subset\mathscr{H}(\Omega) \qquad \forall 1\le p\le\infty\,. \tag{5.24}$$

The following result states that on the closed subspace $H^2_*(\Omega)$ we may also define a different scalar product.

Lemma 5.1 *Assume* (5.4)*. On the space* $H^2_*(\Omega)$ *the two norms*

$$w\mapsto\|w\|_{H^2}\,,\quad w\mapsto\|w\|_{H^2_*} := \left[\int_\Omega\left((\Delta w)^2+(\sigma-1)[w,w]\right)dxdy\right]^{1/2}$$

are equivalent. Therefore, $H^2_*(\Omega)$ is a Hilbert space when endowed with the scalar product

$$(u,v)_{H^2_*} := \int_\Omega (\Delta u \Delta v + (\sigma-1)[u,v])\, dxdy\,. \tag{5.25}$$

For later use (see Sect. 5.7), we also introduce the space

$$H^1_*(\Omega) := \left\{ w \in H^1(\Omega);\ w = 0 \text{ on } \{0,\pi\} \times (-\ell,\ell) \right\}.$$

Since $H^1_*(\Omega) \not\subset C^0(\overline{\Omega})$ we need to define this space in a more rigorous way. Consider the space

$$C^\infty_*(\Omega) := \left\{ w \in C^\infty(\overline{\Omega});\ \exists \varepsilon > 0\,, w(x,y) = 0 \text{ if } x \in [0,\varepsilon] \cup [\pi-\varepsilon,\pi] \right\}$$

which is a normed vector space when endowed with the Dirichlet norm

$$\|u\|_{H^1_*} = \left[\int_\Omega |\nabla u|^2\, dxdy \right]^{1/2}. \tag{5.26}$$

The space $H^1_*(\Omega)$ is the completion of $C^\infty_*(\Omega)$ with respect to the norm $\|\cdot\|_{H^1_*}$; the scalar product in $H^1_*(\Omega)$ is defined by

$$(u,v)_{H^1_*} := \int_\Omega \nabla u \nabla v\, dxdy \qquad \forall (u,v) \in H^1_*(\Omega)\,. \tag{5.27}$$

In view of (5.24), if $f \in L^1(\Omega)$ then the functional $\mathbb{E}_T$ in (5.19) is well-defined in $H^2_*(\Omega)$, while if $f \in \mathscr{H}(\Omega)$ we need to replace $\int_\Omega fu$ with $\langle f,u\rangle$. The following somehow standard statement is the connection between minimisers of the energy functional $\mathbb{E}_T$ and weak solutions of (5.23). It shows that the variational setting is correct and it allows to derive the boundary conditions.

Theorem 5.2 *Assume (5.4) and let $f \in \mathscr{H}(\Omega)$. Then there exists a unique $u \in H^2_*(\Omega)$ such that*

$$(u,v)_{H^2_*} = \langle f,v\rangle \qquad \forall v \in H^2_*(\Omega)\,;$$

moreover, u is the minimiser of the convex functional $\mathbb{E}_T$ in (5.19). If $f \in L^2(\Omega)$ then $u \in H^4(\Omega)$, and if $u \in C^4(\overline{\Omega})$ then u is a classical solution of (5.23).

Since the thin plate representing the bridge roadway is a long narrow rectangle, that is $\ell \ll \pi$, it appears reasonable to consider forcing terms f which do not depend on y. If we assume that

$$f = f(x)\,, \qquad f \in L^2(0,\pi), \tag{5.28}$$

then the source f may be extended as an odd 2π-periodic function over $\mathbb{R}$ and then expanded in Fourier series, that is,

$$f(x) = \sum_{m=1}^{+\infty} \beta_m \sin(mx) , \qquad \beta_m = \frac{2}{\pi} \int_0^\pi f(x) \sin(mx)\, dx , \tag{5.29}$$

with the series converging in $L^2(0,\pi)$ to f. In this case, by separation of variables, one finds that the unique solution of (5.23) is given by

$$u(x,y) = \sum_{m=1}^{+\infty} \left[\frac{1}{m^4} + A\cosh(my) + Bmy \sinh(my) \right] \beta_m \sin(mx) \tag{5.30}$$

where

$$A = A(m,\ell) := \frac{\sigma}{1-\sigma} \frac{1}{m^4} \frac{(1+\sigma)\sinh(m\ell) - (1-\sigma)m\ell\cosh(m\ell)}{(3+\sigma)\sinh(m\ell)\cosh(m\ell) - (1-\sigma)m\ell} ,$$

$$B = B(m,\ell) := \sigma \frac{1}{m^4} \frac{\sinh(m\ell)}{(3+\sigma)\sinh(m\ell)\cosh(m\ell) - (1-\sigma)m\ell} .$$

These simple formulas describe the relationship between the Fourier components of f and the corresponding Fourier components of the solution of (5.23). Of course, they are available because we are dealing with a linear equation.

5.3.2 Vertical and Torsional Modes

In order to study the oscillating modes of the rectangular plate Ω in (5.2), one needs to consider the eigenvalue problem

$$\begin{cases} \Delta^2 w = \lambda w & \text{in } \Omega \\ w(0,y) = w_{xx}(0,y) = w(\pi,y) = w_{xx}(\pi,y) = 0 & y \in (-\ell,\ell) \\ w_{yy}(x,\pm\ell) + \sigma w_{xx}(x,\pm\ell) = w_{yyy}(x,\pm\ell) + (2-\sigma) w_{xxy}(x,\pm\ell) = 0 & x \in (0,\pi). \end{cases} \tag{5.31}$$

If (5.31) has a nontrivial solution w we say that λ is an eigenvalue for problem (5.31). The following complete description of the spectrum and of the eigenfunctions was obtained in [34, 111]:

Theorem 5.3 *Assume* (5.4). *Then the set of eigenvalues of* (5.31) *may be ordered in an increasing sequence* $\{\lambda_k\}$ *of strictly positive numbers diverging to* $+\infty$ *and any*

eigenfunction belongs to $C^\infty(\overline{\Omega})$*; the set of eigenfunctions of* (5.31) *is a complete system in* $H^2_*(\Omega)$*. Moreover:*

(*i*) *For any* $m \geq 1$*, there exists a unique eigenvalue* $\lambda = \mu_{m,1} \in ((1-\sigma)^2 m^4, m^4)$ *with corresponding eigenfunction*

$$\left[\left[\mu_{m,1}^{1/2} - (1-\sigma)m^2\right]\frac{\cosh\left[y\sqrt{m^2+\mu_{m,1}^{1/2}}\right]}{\cosh\left[\ell\sqrt{m^2+\mu_{m,1}^{1/2}}\right]} + \left[\mu_{m,1}^{1/2} + (1-\sigma)m^2\right]\frac{\cosh\left[y\sqrt{m^2-\mu_{m,1}^{1/2}}\right]}{\cosh\left[\ell\sqrt{m^2-\mu_{m,1}^{1/2}}\right]}\right]\sin(mx).$$

(*ii*) *For any* $m \geq 1$*, there exist infinitely many eigenvalues* $\lambda = \mu_{m,k} > m^4$ $(k \geq 2)$ *with corresponding eigenfunctions*

$$\left[\left[\mu_{m,k}^{1/2} - (1-\sigma)m^2\right]\frac{\cosh\left[y\sqrt{\mu_{m,k}^{1/2}+m^2}\right]}{\cosh\left[\ell\sqrt{\mu_{m,k}^{1/2}+m^2}\right]} + \left[\mu_{m,k}^{1/2} + (1-\sigma)m^2\right]\frac{\cos\left[y\sqrt{\mu_{m,k}^{1/2}-m^2}\right]}{\cos\left[\ell\sqrt{\mu_{m,k}^{1/2}-m^2}\right]}\right]\sin(mx).$$

(*iii*) *For any* $m \geq 1$*, there exist infinitely many eigenvalues* $\lambda = \nu_{m,k} > m^4$ $(k \geq 2)$ *with corresponding eigenfunctions*

$$\left[\left[\nu_{m,k}^{1/2} - (1-\sigma)m^2\right]\frac{\sinh\left[y\sqrt{\nu_{m,k}^{1/2}+m^2}\right]}{\sinh\left[\ell\sqrt{\nu_{m,k}^{1/2}+m^2}\right]} + \left[\nu_{m,k}^{1/2} + (1-\sigma)m^2\right]\frac{\sin\left[y\sqrt{\nu_{m,k}^{1/2}-m^2}\right]}{\sin\left[\ell\sqrt{\nu_{m,k}^{1/2}-m^2}\right]}\right]\sin(mx).$$

(*iv*) *For any* $m \geq 1$ *satisfying* $\ell m\sqrt{2}\coth(\ell m\sqrt{2}) > \left(\frac{2-\sigma}{\sigma}\right)^2$ *there exists an eigenvalue* $\lambda = \nu_{m,1} \in (\mu_{m,1}, m^4)$ *with corresponding eigenfunction*

$$\left[\left[\nu_{m,1}^{1/2} - (1-\sigma)m^2\right]\frac{\sinh\left[y\sqrt{m^2+\nu_{m,1}^{1/2}}\right]}{\sinh\left[\ell\sqrt{m^2+\nu_{m,1}^{1/2}}\right]} + \left[\nu_{m,1}^{1/2} + (1-\sigma)m^2\right]\frac{\sinh\left[y\sqrt{m^2-\nu_{m,1}^{1/2}}\right]}{\sinh\left[\ell\sqrt{m^2-\nu_{m,1}^{1/2}}\right]}\right]\sin(mx).$$

Finally, if the unique positive solution $s > 0$ *of the equation*

$$\tanh(\sqrt{2}s\ell) = \left(\frac{\sigma}{2-\sigma}\right)^2 \sqrt{2}s\ell \tag{5.32}$$

is not an integer, then the only eigenvalues and eigenfunctions are as in $(i) - (iv)$.

Of course, (5.32) has probability 0 to occur in a real bridge; if it occurs, there is an additional eigenvalue and eigenfunction, see [111]. The eigenvalues λ_k are solutions of explicit equations. More precisely,

(*i*) The eigenvalue $\lambda = \mu_{m,1}$ is the unique value $\lambda \in ((1-\sigma)^2 m^4, m^4)$ such that

$$\begin{aligned}&\sqrt{m^2-\lambda^{1/2}}\left(\lambda^{1/2} + (1-\sigma)m^2\right)^2 \tanh(\ell\sqrt{m^2-\lambda^{1/2}})\\ &= \sqrt{m^2+\lambda^{1/2}}\left(\lambda^{1/2} - (1-\sigma)m^2\right)^2 \tanh(\ell\sqrt{m^2+\lambda^{1/2}})\,.\end{aligned}$$

(*ii*) The eigenvalues $\lambda = \mu_{m,k}$ ($k \geq 2$) are the solutions $\lambda > m^4$ of the equation

$$\begin{aligned}&\sqrt{\lambda^{1/2}-m^2}\big(\lambda^{1/2}+(1-\sigma)m^2\big)^2\tan(\ell\sqrt{\lambda^{1/2}-m^2})\\&=-\sqrt{\lambda^{1/2}+m^2}\big(\lambda^{1/2}-(1-\sigma)m^2\big)^2\tanh(\ell\sqrt{\lambda^{1/2}+m^2})\,.\end{aligned}$$

(*iii*) The eigenvalues $\lambda = \nu_{m,k}$ ($k \geq 2$) are the solutions $\lambda > m^4$ of the equation

$$\begin{aligned}&\sqrt{\lambda^{1/2}-m^2}\big(\lambda^{1/2}+(1-\sigma)m^2\big)^2\tanh(\ell\sqrt{\lambda^{1/2}+m^2})\\&=\sqrt{\lambda^{1/2}+m^2}\big(\lambda^{1/2}-(1-\sigma)m^2\big)^2\tan(\ell\sqrt{\lambda^{1/2}-m^2})\,.\end{aligned}$$

(*iv*) The eigenvalue $\lambda = \nu_{m,1}$ is the unique value $\lambda \in ((1-\sigma)^2 m^4, m^4)$ such that

$$\begin{aligned}&\sqrt{m^2-\lambda^{1/2}}\big(\lambda^{1/2}+(1-\sigma)m^2\big)^2\tanh(\ell\sqrt{\lambda^{1/2}+m^2})\\&=\sqrt{\lambda^{1/2}+m^2}\big(\lambda^{1/2}-(1-\sigma)m^2\big)^2\tanh(\ell\sqrt{\lambda^{1/2}-m^2})\,.\end{aligned}$$

In particular, the least eigenvalue is $\lambda_1 = \mu_{1,1}$ and it is the unique value of $\lambda \in ((1-\sigma)^2, 1)$ such that

$$\frac{\sqrt{1-\sqrt{\lambda}}}{\big(\sqrt{\lambda}-1+\sigma\big)^2}\,\tanh(\ell\sqrt{1-\sqrt{\lambda}}\,) = \frac{\sqrt{1+\sqrt{\lambda}}}{\big(\sqrt{\lambda}+1-\sigma\big)^2}\,\tanh(\ell\sqrt{1+\sqrt{\lambda}}\,)\,; \tag{5.33}$$

the corresponding eigenspace is generated by the positive eigenfunction

$$\left\{(\sqrt{\lambda}+1-\sigma)\,\frac{\cosh\left(y\sqrt{1-\sqrt{\lambda}}\right)}{\cosh\left(\ell\sqrt{1-\sqrt{\lambda}}\right)} + (\sqrt{\lambda}-1+\sigma)\,\frac{\cosh\left(y\sqrt{1+\sqrt{\lambda}}\right)}{\cosh\left(\ell\sqrt{1+\sqrt{\lambda}}\right)}\right\}\,\sin x\,.$$

Whence, the first eigenfunction is of one sign over Ω and this fact is by far nontrivial. It is well-known that the first eigenfunction of some biharmonic problems may change sign. When Ω is a square, Coffman [83] proved that the first eigenfunction of the clamped plate problem changes sign, see also [158] for more general results and [123, Sect. 3.1.3] for the updated history of the problem. Hence, the positivity of the first eigenfunction is not for free. Due to the L^2-orthogonality of eigenfunctions, it is the only positive eigenfunction of (5.31).

The eigenfunctions in (*i*)–(*ii*) are even with respect to y whereas the eigenfunctions in (*iii*)–(*iv*) are odd. We call **vertical modes** the eigenfunctions of the kind (*i*)–(*ii*) and **torsional modes** the eigenfunctions of the kind (*iii*)–(*iv*). The reason is that, since ℓ is small, the former are essentially of the kind $c_m \sin(mx)$ whereas the latter are of the kind $c_m y \sin(mx)$. The pictures in Fig. 1.18 in Sect. 1.6 display (from top to bottom) the first two vertical eigenfunctions (approximately described by $c_1 \sin(x)$ and $c_2 \sin(2x)$) and the second torsional eigenfunction (approximately

described by $c_2 y \sin(2x)$). In each picture the displacement of the roadway is compared with equilibrium.

In general, the maximum and the minimum of the eigenfunctions are attained on the free edges. This behavior suggests that torsional oscillations appear because the free long edges are the weak part of the plate. In the next section we perform a detailed analysis with the parameters of the original Tacoma Narrows Bridge.

5.3.3 *Quantitative Analysis of the Oscillating Modes*

In this section we analyse Theorem 5.3 with the parameters of the collapsed TNB and we give an answer to a question raised in Sect. 1.6: why do torsional oscillations appear with a node at midspan? This was observed not only at the TNB, but also at the Menai Straits Bridge, at the Brighton Chain Pier, at the Wheeling Suspension Bridge, at the Matukituki Bridge, see Sects. 1.3 and 1.6.

The described one-node torsional oscillation is sketched in the lowest picture in Fig. 1.18, see also the front cover of this book. It seems that this particular kind of torsional oscillation is the only one ever seen in suspension bridges. From the Official Report [9, p. 31] we quote

> Prior to 10:00 A.M. on the day of the failure, there were no recorded instances of the oscillations being otherwise than the two cables in phase and with no torsional motions,

whereas from Smith-Vincent [245, p. 21] we learn that

> the only torsional mode which developed under wind action on the bridge or on the model is that with a single node at the center of the main span.

With the notations of Theorem 5.3, this torsional behavior of suspension bridges may be rephrased as follows

$$\begin{gathered}\text{the oscillations causing the collapse of a suspension bridge}\\ \text{are of the kind } c_2 y \sin(2x), \text{ as represented in the bottom picture of Fig. 1.18,}\\ \text{and correspond to the eigenvalue } \nu_{2,2}, \text{ as given by Theorem 5.3.}\end{gathered} \tag{5.34}$$

The eigenfunction corresponding to the eigenvalue $\nu_{1,1}$ is of the kind $c_2 y \sin(x)$ but, in general, this eigenvalue does not exist since the inequality in Theorem 5.3 (*iv*) is usually satisfied only for fairly large m.

We now fix the parameters. For metals the value of σ lies around 0.3, see [176, p. 105], while for concrete we have $0.1 < \sigma < 0.2$. Since the suspended structure of the Tacoma Bridge consisted of a "mixture" of concrete and metal (see [9, p. 13]), we take

$$\sigma = 0.2\,. \tag{5.35}$$

By (5.1) and after scaling we have $2\ell/\pi = 39/2800$. For simplicity, we fix

$$\ell = \frac{\pi}{150}\,. \tag{5.36}$$

Assuming (5.35)–(5.36), the eigenvalues of (5.31) reported in Table 5.1 were numerically obtained in [34]. We only quote the least 16 eigenvalues because we are mainly interested in the second torsional eigenvalue which is, precisely, the 16th.

These results are obtained with the parameters of the collapsed TNB. During the collapse, Farquharson [9, V-10] witnessed the events and wrote that

> The motions, which a moment before had involved a number of waves (nine or ten) had shifted almost instantly to two.

Note that the vertical eigenvalue immediately preceding the least torsional eigenvalue is $\mu_{10,1}$: it involves the function $\sin(10x)$ which has precisely "ten waves". This means that the torsional instability occurs when the bridge is vertically oscillating like $\sin(10x)$. Then, if no constraint acts on the roadway, the energy should transfer to the mode corresponding to $\nu_{1,2}$ which has a behavior like $y\sin(x)$. The reason is that the ratio $\nu_{1,2}/\mu_{10,1}$ between the frequencies is very close to 1 and this gives a strong instability, see Sect. 3.6. However, in the case of a suspension bridge, the sustaining cable yields a serious constraint. With a rude approximation, the cable may be considered as inextensible. A better point of view is that it is only "weakly extensible", which means that its elongation cannot bee too large. In Fig. 5.2 we represent the deformation of the cable in the two situations where the roadway behaves like $\sin(x)$ and like $\sin(2x)$. It turns out that the no-node behavior $\sin(x)$ (on the left) only allows small vertical displacements of the roadway

Table 5.1 Approximate value of the least 16 eigenvalues of (5.31) for $\sigma = 0.2$, $\ell = \frac{\pi}{150}$

Eigenvalue	λ_1	λ_2	λ_3	λ_4	λ_5	λ_6	λ_7	λ_8
Kind	$\mu_{1,1}$	$\mu_{2,1}$	$\mu_{3,1}$	$\mu_{4,1}$	$\mu_{5,1}$	$\mu_{6,1}$	$\mu_{7,1}$	$\mu_{8,1}$
$\sqrt{\text{Eigenvalue}} \approx$	0.98	3.92	8.82	15.68	24.5	35.28	48.02	62.73
Eigenvalue	λ_9	λ_{10}	λ_{11}	λ_{12}	λ_{13}	λ_{14}	λ_{15}	λ_{16}
Kind	$\mu_{9,1}$	$\mu_{10,1}$	$\nu_{1,2}$	$\mu_{11,1}$	$\mu_{12,1}$	$\mu_{13,1}$	$\mu_{14,1}$	$\nu_{2,2}$
$\sqrt{\text{Eigenvalue}} \approx$	79.39	98.03	104.61	118.62	141.19	165.72	192.21	209.25

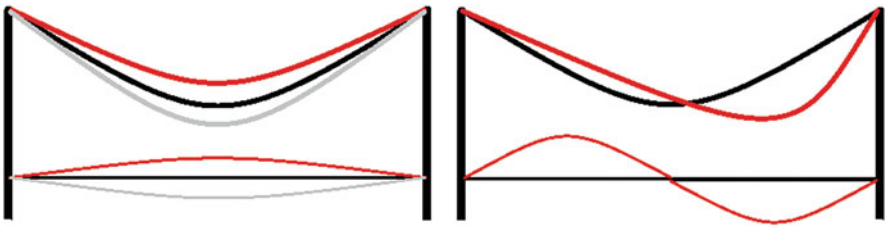

Fig. 5.2 Elongation of the cable generated by the oscillations of the roadway

(between the grey and red positions) and, therefore, small torsional oscillations of the kind $y\sin(x)$. On the contrary, the one-node behavior $\sin(2x)$ allows much larger torsional oscillations of the kind $y\sin(2x)$, see the right picture. A first explanation of the transition described by Farquharson is that when the vertical oscillation $\sin(10x)$ became sufficiently large, reaching the threshold of the torsional instability, the cable forced the transition to the mode $y\sin(2x)$ instead of $y\sin(x)$. This gives a sound explanation to (5.34) and reproduces what was seen during the oscillations at the Tacoma Bridge.

If we slightly modify the choices in (5.35)–(5.36), but remaining in the range of the Tacoma Bridge, the eigenvalues of (5.31) become as in Table 5.2.

After comparison with Table 5.1, one notices that all the eigenvalues have slightly decreased but the qualitative behavior, and hence the subsequent explanation, remain the same.

5.4 The Action of Cables and Hangers: Semilinear Equations

The roadway of the bridge is hooked to the hangers whose action is concentrated in the union of two thin parallel strips adjacent to the two long edges of the plate Ω in (5.2), i.e. in a set of the type

$$\omega := (0,\pi)\times\Big((-\ell,-\ell+\varepsilon)\cup(\ell-\varepsilon,\ell)\Big) \tag{5.37}$$

with $\varepsilon > 0$ small, see Fig. 5.3. In turn, the hangers are hooked to the sustaining cables. It is generally understood, see e.g. [233, p. 26], that the nonlinear behavior of a suspension bridge is mainly due to the changes of the cables geometry. Since the

Table 5.2 Approximate value of the least 16 eigenvalues of (5.31) for $\sigma = 0.25$, $\ell = \frac{\pi}{144}$

Eigenvalue	λ_1	λ_2	λ_3	λ_4	λ_5	λ_6	λ_7	λ_8
Kind	$\mu_{1,1}$	$\mu_{2,1}$	$\mu_{3,1}$	$\mu_{4,1}$	$\mu_{5,1}$	$\mu_{6,1}$	$\mu_{7,1}$	$\mu_{8,1}$
$\sqrt{\text{Eigenvalue}}\approx$	0.97	3.87	8.71	15.49	24.21	34.87	47.46	62
Eigenvalue	λ_9	λ_{10}	λ_{11}	λ_{12}	λ_{13}	λ_{14}	λ_{15}	λ_{16}
Kind	$\mu_{9,1}$	$\mu_{10,1}$	$\nu_{1,2}$	$\mu_{11,1}$	$\mu_{12,1}$	$\mu_{13,1}$	$\mu_{14,1}$	$\nu_{2,2}$
$\sqrt{\text{Eigenvalue}}\approx$	78.48	96.9	97.24	117.27	139.58	163.84	190.1	194.51

Fig. 5.3 The plate Ω and its subset ω (*dark grey*) where the hangers act

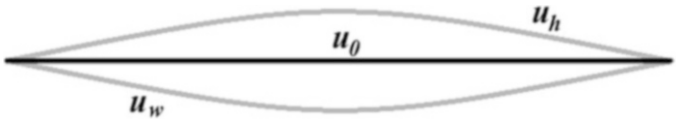

Fig. 5.4 Different positions of the bridge

cables are connected to the plate through the hangers, this means that a nonlinearity appears in the hangers, both because they are extensible nonlinear springs and because they transmit the nonlinearity of the cables.

Let us discuss different positions of the plate depending on the forces acting on it. If the plate had no mass (as a sheet of paper) and there were no loads acting on the plate, it would take the horizontal equilibrium position u_0, see Fig. 5.4. If the plate was only subject to its own weight w (dead load) it would take a $\cup$-position such as u_w in Fig. 5.4. If the plate had no weight but it was subject to the restoring force of the cables-hangers system, it would take a $\cap$-position such as u_h: this is also the position of the lower endpoints of the hangers before the roadway is installed. If both the weight and the action of the hangers are considered, the two effects cancel and the equilibrium position $u_0 \equiv 0$ is recovered. Since the bending energy of the plate vanishes when it is in position $u_0 \equiv 0$, the unknown function should be the displacement of the plate with respect to the equilibrium u_0. In Sect. 3.3.3 we illustrated the Augusti-Sepe [25] model for the restoring force, see Fig. 3.2. This lead us to consider the nonlinearity (3.14) and then to take $\gamma = 1$. Therefore, a suitable form of the restoring force due to the hangers is

$$h(y,u) = \Upsilon(y)\left(u + u^3\right) \tag{5.38}$$

where Υ is the characteristic function of the set $(-\ell, -\ell+\varepsilon) \cup (\ell-\varepsilon, \ell)$. The force h admits a potential energy given by $\int_\Omega H(y,u)\,dxdy$ where

$$H(y,u) := \int_0^u h(y,\tau)d\tau = \Upsilon(y)\left(\frac{u^2}{2} + \frac{u^4}{4}\right) \qquad \forall u \in \mathbb{R}\,. \tag{5.39}$$

The total static energy of the bridge is then obtained by adding the potential energy to the elastic energy (5.7) of the plate:

$$\mathbb{E}_T(u) = \frac{E\,d^3}{12(1-\sigma^2)}\int_\Omega \left(\frac{(\Delta u)^2}{2} + \frac{\sigma-1}{2}[u,u]\right) dxdy + \int_\Omega (H(y,u) - fu)\,dxdy \tag{5.40}$$

where d denotes the thickness of the plate, E is the Young modulus and σ is the Poisson ratio, see (5.4) and (5.35). The Euler-Lagrange equation is obtained by minimising this convex functional:

$$\begin{cases} \frac{E\,d^3}{12(1-\sigma^2)}\,\Delta^2 u + h(y,u) = f & \text{in } \Omega \\ u(0,y) = u_{xx}(0,y) = u(\pi,y) = u_{xx}(\pi,y) = 0 & y \in (-\ell,\ell) \\ u_{yy}(x,\pm\ell) + \sigma u_{xx}(x,\pm\ell) = u_{yyy}(x,\pm\ell) + (2-\sigma)u_{xxy}(x,\pm\ell) = 0 & x \in (0,\pi). \end{cases} \tag{5.41}$$

This problem deserves several comments in connection with Fig. 5.4. If we drop both the action of the hangers and the loads, the equation in (5.41) becomes $\Delta^2 u = 0$ which, with the boundary conditions, yields $u = 0$: this is the equilibrium position represented by u_0 in Fig. 5.4. If we merely drop the action of the hangers ($h \equiv 0$) we are back to problem (5.23) and the roadway goes to a position such as u_w in Fig. 5.4. If we assume that $h \neq 0$ but there are no loads ($f \equiv 0$, in particular no mass), then a new equilibrium position is obtained, see u_h in Fig. 5.4.

For $f \in \mathscr{H}(\Omega)$, we say that $u \in H^2_*(\Omega)$ is a weak solution of (5.41) if

$$\tfrac{E\,d^3}{12(1-\sigma^2)}\,(u,v)_{H^2_*} + (h(y,u),v)_{L^2} = \langle f, v\rangle \qquad \forall v \in H^2_*(\Omega)\,.$$

Then we have

Theorem 5.4 *Assume (5.4), let h be as in (5.38), and let $f \in \mathscr{H}(\Omega)$; then there exists a unique weak solution $u \in H^2_*(\Omega)$ of (5.41). If $\mathbb{E}_T$ denotes the energy defined in (5.40), this solution is the unique minimiser of the problem*

$$\min_{v \in H^2_*(\Omega)} \mathbb{E}_T(v)\,.$$

If the external force also depends on time, $f = f(x,y,t)$, and if m denotes the mass density of the plate, then the corresponding deformation u has a kinetic energy which should be added to the energy (5.40):

$$\mathscr{E}_u(t) := \frac{m}{2}\int_\Omega u_t^2\,dxdy + \mathbb{E}_T(u) \qquad \forall t > 0\,. \tag{5.42}$$

This is the total energy of a nonlinear dynamic bridge. As for the action, one has to take the difference between the kinetic energy and the potential energy and integrate over the time interval $\mathbb{R}_+ = (0,\infty)$. The evolution equation describing the motion of the bridge is obtained by taking critical points of the action functional:

$$m u_{tt} + \tfrac{E\,d^3}{12(1-\sigma^2)}\,\Delta^2 u + h(y,u) = f \qquad \text{in } \Omega \times \mathbb{R}_+\,.$$

Due to internal frictions, we also introduce a damping term and obtain

$$\begin{cases} mu_{tt}+\eta u_t+\frac{E\,d^3}{12(1-\sigma^2)}\Delta^2 u+h(y,u)=f & \text{in } \Omega\times\mathbb{R}_+ \\ u(0,y,t)=u_{xx}(0,y,t)=0 & (y,t)\in(-\ell,\ell)\times\mathbb{R}_+ \\ u(\pi,y,t)=u_{xx}(\pi,y,t)=0 & (y,t)\in(-\ell,\ell)\times\mathbb{R}_+ \\ u_{yy}(x,\pm\ell,t)+\sigma u_{xx}(x,\pm\ell,t)=0 & (x,t)\in(0,\pi)\times\mathbb{R}_+ \\ u_{yyy}(x,\pm\ell,t)+(2-\sigma)u_{xxy}(x,\pm\ell,t)=0 & (x,t)\in(0,\pi)\times\mathbb{R}_+ \\ u(x,y,0)=u_0(x,y)\,, \quad u_t(x,y,0)=u_1(x,y) & (x,y)\in\Omega \end{cases} \tag{5.43}$$

where $\eta>0$. If $f\in C^0(\mathbb{R}_+;L^2(\Omega))$ we say that

$$u\in C^0(\mathbb{R}_+;H^2_*(\Omega))\cap C^1(\mathbb{R}_+;L^2(\Omega))\cap C^2(\mathbb{R}_+;\mathscr{H}(\Omega)) \tag{5.44}$$

is a solution of (5.43) if it satisfies the initial conditions and if

$$m\langle u''(t),v\rangle+\eta(u'(t),v)_{L^2}+\tfrac{E\,d^3}{12(1-\sigma^2)}(u(t),v)_{H^2_*}+(h(y,u(t)),v)_{L^2}=(f(t),v)_{L^2}$$

for all $v\in H^2_*(\Omega)$ and all $t>0$. Then we have

Theorem 5.5 *Assume (5.4). Let $f\in C^0(\mathbb{R}_+;L^2(\Omega))$ and let $\eta>0$; let $u_0\in H^2_*(\Omega)$ and $u_1\in L^2(\Omega)$. Then:*

(i) There exists a unique solution of (5.43).
(ii) If $f\in L^2(\Omega)$ is independent of t, then the unique solution u of (5.43) satisfies

$$u(t)\to\overline{u}\quad \text{in } H^2_*(\Omega)\quad \text{and}\quad u'(t)\to 0\quad \text{in } L^2(\Omega)\quad \text{as } t\to+\infty$$

where $\overline{u}$ is the unique solution of the stationary problem (5.41).

Theorem 5.5 establishes the well-posedness of the evolution problem (5.43) and the convergence of the solution to an equilibrium. In the next section we sketch a proof in the case of an isolated system ($\eta=0$ and $f=0$).

5.5 Torsional Instability and Flutter Energy

5.5.1 Finite Dimensional Approximation of the Solution

For a different model of suspension bridges, Irvine [149, p. 176] ignores damping of both structural and aerodynamic origin. His purpose is to simplify as much as possible the model by maintaining its essence, that is, the conceptual design of bridges. Here we follow this suggestion: we consider the isolated version of (5.43)

(with $\eta = 0$ and $f = 0$) and we attempt for a slightly more quantitative model. As a first step we take a general plate $\Omega = (0, L) \times (-\ell, \ell)$ and we add coefficients to the nonlinearity in (5.38), that is, we consider

$$h(y, u) = \Upsilon(y) \left(k u + \delta u^3 \right); \tag{5.45}$$

the coefficients $k, \delta > 0$ reflect the elasticity of steel. The equation becomes

$$m\, u_{tt} + \tfrac{E\, d^3}{12(1-\sigma^2)}\, \Delta^2 u + \Upsilon(y)(k\, u + \delta u^3) = 0 \qquad \text{in } (0, L) \times (-\ell, \ell) \times \mathbb{R}_+. \tag{5.46}$$

We scale the plate and go back to (5.2) with the scaling factor π/L appearing within the equation. Then we divide (5.46) by k and obtain a unit coefficient in front of the linear term in the restoring force. Moreover, we scale in time and absorb the coefficient m/k in front of u_{tt}. Finally, we scale $u \to \alpha u$ for a suitable $\alpha > 0$ and also obtain a unit coefficient in front of the cubic term. Summarising, we put

$$u(x, y, t) \longrightarrow \sqrt{\frac{k}{\delta}}\, u\left(\frac{\pi x}{L}, \frac{\pi y}{L}, \sqrt{\frac{k}{m}}\, t \right) \qquad \text{and} \qquad \gamma = \frac{E\, d^3}{12k(1-\sigma^2)}\, \frac{\pi^4}{L^4} \tag{5.47}$$

where L is the original length of the plate (the length of the roadway). To obtain a quantitatively reasonable model we take the measures of the collapsed TNB, see [9]; we fix the short edge of the scaled plate to be $(-\frac{\pi}{150}, \frac{\pi}{150})$, see (5.36). Then, the amplitude of the strip ω [see (5.37)] containing the hangers at the TNB is

$$\varepsilon = \frac{\pi}{1500}\,, \tag{5.48}$$

see [9, p. 11]. Following all these steps, one reduces (5.46) to an equation where the only parameter is in front of the biharmonic term:

$$u_{tt} + \gamma\, \Delta^2 u + \Upsilon(y)(u + u^3) = 0 \qquad \text{in } (0, \pi) \times (-\tfrac{\pi}{150}, \tfrac{\pi}{150}) \times \mathbb{R}_+$$

and Υ is now the characteristic function of the set $(-\frac{\pi}{150}, -\frac{3\pi}{500}) \cup (\frac{3\pi}{500}, \frac{\pi}{150})$.

So far, we just need to bear in mind that $\gamma > 0$. Using (5.47) we find the dimensionless version of the problem under study

$$\begin{cases} u_{tt} + \gamma \Delta^2 u + \Upsilon(y)(u + u^3) = 0 & \text{in } \Omega \times \mathbb{R}_+ \\ u(0, y, t) = u_{xx}(0, y, t) = u(\pi, y, t) = u_{xx}(\pi, y, t) = 0 & \text{for } (y, t) \in (-\frac{\pi}{150}, \frac{\pi}{150}) \times \mathbb{R}_+ \\ u_{yy}(x, \pm\frac{\pi}{150}, t) + 0.2 \cdot u_{xx}(x, \pm\frac{\pi}{150}, t) = 0 & \text{for } (x, t) \in (0, \pi) \times \mathbb{R}_+ \\ u_{yyy}(x, \pm\frac{\pi}{150}, t) + 1.8 \cdot u_{xxy}(x, \pm\frac{\pi}{150}, t) = 0 & \text{for } (x, t) \in (0, \pi) \times \mathbb{R}_+ \\ u(x, y, 0) = u_0(x, y)\,, \quad u_t(x, y, 0) = u_1(x, y) & \text{for } (x, y) \in \Omega \end{cases} \tag{5.49}$$

where $\Omega = (0,\pi)\times(-\frac{\pi}{150},\frac{\pi}{150})$ and we assumed (5.35)–(5.36). The initial-boundary value problem (5.49) is isolated, which means that it has a conserved quantity. This quantity is the energy defined in (5.42) which is now constant in time:

$$\mathscr{E}_u(t) = \int_\Omega \left(\frac{u_t^2}{2} + \frac{\gamma}{2}(\Delta u)^2 - \frac{2\gamma}{5}[u,u] + H(y,u) \right) dxdy \tag{5.50}$$

where H is as in (5.39) and $[\cdot,\cdot]$ is as in (5.5). We say that u with the regularity (5.44) is a solution of (5.49) if it satisfies the initial conditions and if

$$\langle u''(t), v\rangle + \gamma(u(t),v)_{H^2_*} + (h(y,u(t)),v)_{L^2} = 0 \tag{5.51}$$

for all $v \in H^2_*(\Omega)$ and $t \in \mathbb{R}_+$; here h is as in (5.38). The following result holds.

Theorem 5.6 *Let $u_0 \in H^2_*(\Omega)$ and $u_1 \in L^2(\Omega)$. Then there exists a unique solution $u = u(t)$ of (5.49) and its energy (5.50) satisfies*

$$\mathscr{E}_u(t) \equiv \int_\Omega \left(\frac{u_1^2}{2} + \frac{\gamma}{2}(\Delta u_0)^2 - \frac{2\gamma}{5}[u_0,u_0] + H(y,u_0) \right) dxdy.$$

Sketch of the Proof of Theorem 5.6 It makes use of a Galerkin method, the solution of (5.49) is obtained as the limit (in a suitable topology) of a sequence of solutions of approximated problems in finite dimensional spaces. By Theorem 5.3 we may consider an orthogonal complete system $\{w_k\}_{k\geq 1} \subset H^2_*(\Omega)$ of eigenfunctions of (5.31) such that $\|w_k\|_{L^2} = 1$. Let $\{\lambda_k\}_{k\geq 1}$ be the corresponding eigenvalues and, for any $m \geq 1$, put $W_m := \text{span}\{w_1,\dots,w_m\}$. For any $m \geq 1$ let

$$u_0^m := \sum_{i=1}^m (u_0,w_i)_{L^2} w_i = \sum_{i=1}^m \lambda_i^{-1}(u_0,w_i)_{H^2_*} w_i \quad \text{and} \quad u_1^m = \sum_{i=1}^m (u_1,w_i)_{L^2} w_i$$

so that $u_0^m \to u_0$ in $H^2_*(\Omega)$ and $u_1^m \to u_1$ in $L^2(\Omega)$ as $m \to +\infty$. Fix $T > 0$; for any $m \geq 1$ one seeks a solution $u_m \in C^2([0,T]; W_m)$ of the variational problem

$$\begin{cases} (u''(t),v)_{L^2} + \gamma(u(t),v)_{H^2_*} + (h(y,u(t)),v)_{L^2} = 0 \\ u(0) = u_0^m\,, \quad u'(0) = u_1^m \end{cases} \tag{5.52}$$

for any $v \in W_m$ and $t \in (0,T)$. If we put

$$u_m(t) = \sum_{i=1}^m g_i^m(t) w_i \qquad \text{and} \qquad g^m(t) := (g_1^m(t),\dots,g_m^m(t))^T \tag{5.53}$$

then the vector valued function g^m solves

$$\begin{cases} (g^m(t))'' + \gamma\, \Lambda_m g^m(t) + \Phi_m(g^m(t)) = 0 \qquad \forall t \in (0,T) \\ g^m(0) = (u_0, w_1)_{L^2}, \ldots, (u_0, w_m)_{L^2})^T,\ (g^m)'(0) = ((u_1, w_1)_{L^2}, \ldots, (u_1, w_m)_{L^2})^T \end{cases} \tag{5.54}$$

where $\Lambda_m := \mathrm{diag}(\lambda_1, \ldots, \lambda_m)$ and $\Phi_m : \mathbb{R}^m \to \mathbb{R}^m$ is the map defined by

$$\Phi_m(\xi_1, \ldots, \xi_m) := \left(\left(h\Big(y, \sum_{j=1}^m \xi_j w_j\Big), w_1 \right)_{L^2}, \ldots, \left(h\Big(y, \sum_{j=1}^m \xi_j w_j\Big), w_m \right)_{L^2} \right)^T .$$

From (5.38) we deduce that $\Phi_m \in \mathrm{Lip}_{\mathrm{loc}}(\mathbb{R}^m; \mathbb{R}^m)$ and hence (5.54) admits a unique solution. We have shown that the function u_m in (5.53) belongs $C^2([0,T); H^2_*(\Omega))$ and is a solution of the problem

$$\begin{cases} u_m''(t) + \gamma\, L u_m(t) + P_m(h(y, u_m(t))) = 0 \qquad \text{for any } t \geq 0 \\ u_m(0) = u_0^m\,, \quad u_m'(0) = u_1^m \end{cases} \tag{5.55}$$

where $L : H^2_*(\Omega) \to \mathscr{H}(\Omega)$ is implicitly defined by $\langle Lu, v\rangle := (u,v)_{H^2_*}$ for any $u, v \in H^2_*(\Omega)$, and P_m is the orthogonal projection from $H^2_*(\Omega)$ onto W_m. Then one finds that the sequence $\{u_m\}$ converges in $C^0([0,T]; H^2_*(\Omega)) \cap C^1([0,T]; L^2(\Omega))$ to a solution of (5.49). □

The eigenfunctions described in Theorem 5.3 are the oscillating modes of the plate Ω. The above proof shows that the solution of (5.49) may be obtained as the limit of a finite dimensional analysis performed with a finite number of modes. Let us fix some value $E > 0$ for (5.50). Depending on the value of E, higher modes may be dropped, see Sect. 3.4.1. Our purpose is to study the torsional stability of the low modes in a sense that will be made precise in next section. The results obtained in Sect. 5.3.3 suggest to focus the attention on the lowest 16 modes, including the two least torsional modes.

5.5.2 A Theoretical Characterisation of Torsional Stability

In this section we give a precise definition of torsional stability. We point out that this is not the only possible definition, several different characterisations may also be given. However, the numerical results reported in Sect. 5.5.4 show that our characterisation well describes the instability.

We fix $m = 16$ to be the position of the second torsional mode. From Theorem 5.3 and Table 5.1 we know that the eigenvalues and the L^2-normalised eigenfunctions up to the 16th are given by

$$\lambda_k = \begin{cases} \mu_{k,1} & \text{if } 1 \le k \le 10 \\ \nu_{1,2} & \text{if } k = 11 \\ \mu_{k-1,1} & \text{if } 12 \le k \le 15 \\ \nu_{2,2} & \text{if } k = 16 \end{cases} \qquad w_k(x,y) = \begin{cases} \frac{v_k(y)\sin(kx)}{\omega_k} & \text{if } 1 \le k \le 10 \\ \frac{\theta_1(y)\sin(x)}{\bar\omega_1} & \text{if } k = 11 \\ \frac{v_{k-1}(y)\sin((k-1)x)}{\omega_{k-1}} & \text{if } 12 \le k \le 15 \\ \frac{\theta_2(y)\sin(2x)}{\bar\omega_2} & \text{if } k = 16 \end{cases}$$

with

$$v_k(y) := \left[\frac{k^2}{5} - \beta_k^-\right] \frac{\cosh\left(y\sqrt{\beta_k^+}\right)}{\cosh\left(\frac{\pi}{150}\sqrt{\beta_k^+}\right)} + \left[\beta_k^+ - \frac{k^2}{5}\right] \frac{\cosh\left(y\sqrt{\beta_k^-}\right)}{\cosh\left(\frac{\pi}{150}\sqrt{\beta_k^-}\right)} \quad (k = 1, \dots, 14),$$

$$\theta_k(y) := \left[\frac{k^2}{5} + \alpha_k^-\right] \frac{\sinh\left(y\sqrt{\alpha_k^+}\right)}{\sinh\left(\frac{\pi}{150}\sqrt{\alpha_k^+}\right)} + \left[\alpha_k^+ - \frac{k^2}{5}\right] \frac{\sin\left(y\sqrt{\alpha_k^-}\right)}{\sin\left(\frac{\pi}{150}\sqrt{\alpha_k^-}\right)} \qquad (k = 1, 2),$$

where $\beta_k^\pm := k^2 \pm \mu_{k,1}^{1/2}$ (for $k = 1, \dots, 14$), $\alpha_k^\pm := \nu_{k,2}^{1/2} \pm k^2$ (for $k = 1, 2$) and

$$\omega_k^2 = \pi \int_0^{\frac{\pi}{150}} v_k^2(y)\,dy \quad (k = 1, \dots, 14) \quad , \quad \bar\omega_k^2 = \pi \int_0^{\frac{\pi}{150}} \theta_k^2(y)\,dy \quad (k = 1, 2)\,. \tag{5.56}$$

Notice that the v_k are even with respect to y, while θ_1 and θ_2 are odd.

Following the Galerkin procedure described in the proof of Theorem 5.6, we seek solutions of (5.52) in the form

$$u(x,y,t) = \sum_{k=1}^{14} \varphi_k(t)\,\frac{v_k(y)\sin(kx)}{\omega_k} + \sum_{k=1}^{2} \tau_k(t)\,\frac{\theta_k(y)\sin(kx)}{\bar\omega_k}$$

where the functions φ_k and τ_k are to be determined. Take h as in (5.38) and, for all $(\varphi_1, \dots, \varphi_{14}, \tau_1, \tau_2) \in \mathbb{R}^{16}$, put

$$\Phi_k(\varphi_1, \dots, \varphi_{14}, \tau_1, \tau_2) = \left(h\Big(y, \sum_{j=1}^{14} \varphi_j \tfrac{v_j(y)\sin(jx)}{\omega_j} + \sum_{j=1}^{2} \tau_j \tfrac{\theta_j(y)\sin(jx)}{\bar\omega_j}\Big), \tfrac{v_k(y)\sin(kx)}{\omega_k}\right)_{L^2}$$

for $k = 1, \dots, 14$ and

$$\Gamma_k(\varphi_1, \dots, \varphi_{14}, \tau_1, \tau_2) = \left(h\Big(y, \sum_{j=1}^{14} \varphi_j \tfrac{v_j(y)\sin(jx)}{\omega_j} + \sum_{j=1}^{2} \tau_j \tfrac{\theta_j(y)\sin(jx)}{\bar\omega_j}\Big), \tfrac{\theta_k(y)\sin(kx)}{\bar\omega_k}\right)_{L^2}$$

for $k = 1, 2$. Then (5.55) becomes the system of ODE's:

$$\begin{cases} \varphi_k''(t) + \gamma\, \mu_{k,1}\varphi_k(t) + \Phi_k\big(\varphi_1(t), \dots, \varphi_{14}(t), \tau_1(t), \tau_2(t)\big) = 0 \ (k = 1, \dots, 14) \\ \tau_k''(t) + \gamma\, \nu_{k,2}\tau_k(t) + \Gamma_k\big(\varphi_1(t), \dots, \varphi_{14}(t), \tau_1(t), \tau_2(t)\big) = 0 \quad (k = 1, 2) \end{cases} \tag{5.57}$$

for all $t \in (0, T)$. For $1 \le k \le 14$, we also put $\Psi_k\big(\varphi_k(t)\big) = \Phi_k(0, \dots, \varphi_k(t), \dots, 0)$. By Lemma 3.6 and taking into account that v_k is even with respect to y, some computations yield

$$\Psi_k\big(\varphi_k(t)\big) = a_k\varphi_k(t) + b_k\varphi_k^3(t)\,, \tag{5.58}$$

where

$$a_k = \frac{\pi}{\omega_k^2}\int_{\frac{3\pi}{500}}^{\frac{\pi}{150}} v_k^2(y)\,dy \quad \text{and} \quad b_k = \frac{3\pi}{4\omega_k^4}\int_{\frac{3\pi}{500}}^{\frac{\pi}{150}} v_k^4(y)\,dy \qquad (k = 1, \dots, 14)\,. \tag{5.59}$$

In particular, by combining (5.59) with (5.56) we see that

$$a_k = \frac{\|v_k\|^2_{L^2(\frac{3\pi}{500}, \frac{\pi}{150})}}{\|v_k\|^2_{L^2(0, \frac{\pi}{150})}} < 1 \quad , \quad b_k = \frac{3}{4\pi}\,\frac{\|v_k\|^4_{L^4(\frac{3\pi}{500}, \frac{\pi}{150})}}{\|v_k\|^4_{L^2(0, \frac{\pi}{150})}}\,.$$

We may now define what we mean by vertical mode; what follows has to be compared with Definition 3.5. We point out that this is a classical definition in a linear regime while it is by no means standard how to characterise modes in nonlinear regimes; contrary to the linear case, the frequency of a nonlinear mode depends on the energy or, equivalently, on the amplitude of its oscillations.

Definition 5.7 (Vertical Mode) Let $1 \le k \le 14$, $\mathbb{R}^2 \ni (\phi_0^k, \phi_1^k) \ne (0, 0)$ and Ψ_k as in (5.58). We call kth vertical mode at energy $E(\phi_0^k, \phi_1^k) > 0$ the unique (periodic) solution $\overline{\varphi}_k$ of the Cauchy problem:

$$\begin{cases} \varphi_k''(t) + \gamma\mu_{k,1}\varphi_k(t) + \Psi_k(\varphi_k(t)) = 0 \qquad \forall t > 0 \\ \varphi_k(0) = \phi_0^k\,, \quad \varphi_k'(0) = \phi_1^k\,. \end{cases} \tag{5.60}$$

If it was $\Psi_k \equiv 0$ then Eq. (5.60) would be linear and Definition 5.7 would coincide with the usual one: in this case, there would be no need to emphasise the dependence on the energy since the solution with initial data $\varphi_k(0) = \varepsilon\phi_0^k$ and $\varphi_k'(0) = \varepsilon\phi_1^k$ (for any ε) would coincide with the solution of (5.60) multiplied by ε. In view of (5.58), we have instead a nonlinear equation and (5.60) becomes

$$\begin{cases} \varphi_k''(t) + (\gamma\mu_{k,1} + a_k)\varphi_k(t) + b_k\varphi_k^3(t) = 0 \qquad \forall t > 0 \\ \varphi_k(0) = \phi_0^k\,, \quad \varphi_k'(0) = \phi_1^k\,. \end{cases} \tag{5.61}$$

The system (5.61) admits the conserved quantity

$$E = \frac{(\varphi_k')^2}{2} + (\gamma\mu_{k,1} + a_k)\frac{\varphi_k^2}{2} + b_k\frac{\varphi_k^4}{4} \equiv E(\phi_0^k, \phi_1^k)$$
$$= \frac{(\phi_1^k)^2}{2} + (\gamma\mu_{k,1} + a_k)\frac{(\phi_0^k)^2}{2} + b_k\frac{(\phi_0^k)^4}{4}\,. \tag{5.62}$$

Any couple of initial data having the same energy leads to the same solution of (5.61) up to a time translation while it is no longer true that multiplying the initial data by a constant leads to proportional solutions; different energies yield different frequencies of the solution.

In order to define the torsional stability of a vertical mode $\overline{\varphi}_k$, we linearise the last two equations of system (5.57) around $(0, \dots, \overline{\varphi}_k(t), \dots, 0) \in \mathbb{R}^{16}$. These two equations correspond, respectively, to the first and second torsional mode. In both cases we obtain a Hill equation of the type

$$\xi''(t) + A_{l,k}(t)\xi(t) = 0\,, \tag{5.63}$$

where, for every $1 \le k \le 14$ and $l = 1, 2$, we set

$$A_{l,k}(t) = \gamma\nu_{l,2} + \bar{a}_l + d_{l,k}\overline{\varphi}_k^2(t) \tag{5.64}$$

with

$$\bar{a}_l = \frac{\pi}{\bar{\omega}_l^2}\int_{\frac{3\pi}{500}}^{\frac{\pi}{150}} \theta_l^2(y)\,dy = \frac{\|\theta_l\|^2_{L^2(\frac{3\pi}{500},\frac{\pi}{150})}}{\|\theta_l\|^2_{L^2(0,\frac{\pi}{150})}} < 1\,, \tag{5.65}$$

$$d_{l,k} = \begin{cases} \frac{9\pi}{4\omega_l^2\bar{\omega}_l^2}\int_{\frac{3\pi}{500}}^{\frac{\pi}{150}} v_l^2(y)\theta_l^2(y)\,dy \text{ if } l = k \\ \frac{3\pi}{2\omega_k^2\bar{\omega}_l^2}\int_{\frac{3\pi}{500}}^{\frac{\pi}{150}} v_k^2(y)\theta_l^2(y)\,dy \text{ if } l \neq k\,. \end{cases} \tag{5.66}$$

For the computation of these coefficients we have used Lemma 3.6 and the fact that the integrals containing odd powers of $\theta_l(y)$ vanish.

Since (5.63) is a linear equation with periodic coefficients, it is standard to define the stability of its trivial solution. This enables us to define the torsional stability of a vertical mode. The numerical results in [34] validate this definition.

Definition 5.8 (Torsional Stability) Fix $1 \le k \le 14$ and $l = 1, 2$. We say that the kth vertical mode $\overline{\varphi}_k$ at energy $E(\phi_0^k, \phi_1^k)$, namely the unique periodic solution of (5.61), is stable with respect to the lth torsional mode if the trivial solution of (5.63) is stable.

5.5.3 *Sufficient Conditions for the Torsional Stability*

It is well-known that the stability regions for the Hill equations may have strange shapes such as *pockets* and *resonance tongues*, see e.g. [60, 61]. Therefore, the theoretical stability analysis of any such equation has to deal with these shapes and with the lack of a precise characterisation of the stability regions. For (5.63), the theoretical obstruction is essentially related to the following condition

$$\sqrt{\frac{\gamma \nu_{l,2} + \bar{a}_l}{\gamma \mu_{k,1} + a_k}} \notin \mathbb{N} \tag{5.67}$$

where γ is defined in (5.47) while a_k and $\bar{a}_l$ are defined, respectively, in (5.59) and in (5.65). The usual difficulties are further increased for (5.63) which, instead of a single equation, represents *a family of Hill equations having coefficients with periods depending on the energy* of the original system (5.57).

Below we discuss in some detail assumption (5.67). But let us start the stability analysis with the following sufficient condition for the stability of a vertical mode.

Theorem 5.9 *Fix $1 \le k \le 14$, $l \in \{1, 2\}$ and assume that (5.67) holds. Then there exists $E_k^l > 0$ and a strictly increasing function Λ such that $\Lambda(0) = 0$ and such that the kth vertical mode $\overline{\varphi}_k$ at energy $E(\phi_0^k, \phi_1^k)$ (that is, the solution of (5.61)) is stable with respect to the lth torsional mode provided that*

$$E \le E_k^l$$

or, equivalently, provided that $\|\overline{\varphi}_k\|_\infty^2 \le \Lambda(E_k^l)$.

Theorem 5.9 is not a perturbation result: the proof given in [34] allows to determine explicit values of E_k^l and $\Lambda(E_k^l)$. Here we stated Theorem 5.9 in a qualitative form in order not to spoil the statement with too many constants.

Let us now discuss assumption (5.67). First of all, it is a generic assumption, it has probability 1 to occur among all random choices of the positive real numbers γ, $\nu_{l,2}$, $\bar{a}_l$, $\mu_{k,1}$, a_k. Moreover, (5.67) seems to hold for "reasonable" choices of these parameters as shown in [34]. Finally, even in the case where (5.67) fails we may obtain a sufficient condition for the torsional stability of vertical modes.

Theorem 5.10 *Fix $1 \le k \le 14$, $l \in \{1, 2\}$ and assume that*

$$\exists m \in \mathbb{N} \quad \text{such that} \quad \frac{\gamma \nu_{l,2} + \bar{a}_l}{\gamma \mu_{k,1} + a_k} = (m+1)^2 .$$

Assume moreover that

$$2\Big(2 + (m+1)\pi\Big) d_{l,k} < 3\pi (m+1)^3 b_k . \tag{5.68}$$

Then the same conclusions of Theorem 5.9 hold.

Theorem 5.10 raises the attention on the further technical assumption (5.68). Motivated by Theorem 3.14 in Sect. 3.6, we are confident that it might be improved and, perhaps, completely removed. However, we will not discuss (5.68) here.

Theorems 5.9 and 5.10 state that a crucial role is played by the amount of energy inside the system. In next section we quote some numerical results on the equations (5.63) and we study the stability of the least 14 vertical modes with the TNB parameters. Our results show that for each vertical mode there exists a critical energy threshold E_k^l under which the solution of (5.63) is stable while for larger energies the solution may be unstable: we also know that different initial data with the same total energy give the same stability response. Not only this enables us to numerically compute the threshold E_k^l and to evaluate the power of the sufficient condition given in Theorems 5.9 and 5.10, but also to define a flutter energy for each vertical mode as a threshold of stability.

Definition 5.11 (Flutter Energy) We call flutter energy of the kth vertical mode $\overline{\varphi}_k$ (that is, the solution of (5.60)) the positive number $\overline{E}_k$ being the supremum of the energies E_k^l such that the trivial solution of (5.63) is stable for both $l = 1$ and $l = 2$.

Compare this definition with Definitions 3.12 and 4.3. Concerning the bridge model, Theorems 5.9 and 5.10 lead to the conclusion that

if the internal energy E is smaller than the flutter energy then small initial torsional oscillations remain small for all time $t > 0$.

In next section we quote some numerical results in order to complement this statement with a description of what may happen for large energies.

5.5.4 Numerical Computation of the Flutter Energy

First, by using the eigenvalues found in Table 5.1, we numerically compute a_k and b_k in (5.59). Since all the a_k are equal to 0.1 up to an error of less than 10^{-3}, in Table 5.3 we quote the values of $10^4(a_k - 0.1)$. Moreover, all the b_k are equal to 1.1 up to an error of less than 10^{-1}: we quote the values of $10^2(b_k - 1.1)$.Then we compute $\bar{a}_l$ and $d_{l,k}$ as defined in (5.65)–(5.66). We find that both $\bar{a}_1 \approx 0.27$, $\bar{a}_2 \approx 0.27$. Moreover, $0 < d_{1,k} - d_{2,k} \approx 10^{-4}$ (for $k = 3, \ldots, 14$) so that, in Table 5.4, one does not see any difference between these coefficients: we put however the

Table 5.3 Numerical values of the parameters a_k and b_k

k	1	2	3	4	5	6	7	8	9	10	11	12	13	14
$10^4(a_k-0.1)$	0.05	0.2	0.45	0.8	1.24	1.78	2.42	3.14	3.96	4.86	5.85	6.92	8.06	9.28
$10^2(b_k-1.1)$	4	4.03	4.09	4.17	4.27	4.39	4.54	4.7	4.89	5.1	5.32	5.57	5.83	6.11

Table 5.4 Numerical values of the parameters $d_{1,k}$ and $d_{2,k}$

k	1	2	3	4	5	6	7	8	9	10	11	12	13	14
$d_{1,k}$	9.27	6.18	6.18	6.18	6.19	6.19	6.19	6.2	6.2	6.21	6.21	6.22	6.23	6.24
$d_{2,k}$	6.18	9.27	6.18	6.18	6.19	6.19	6.19	6.2	6.2	6.21	6.21	6.22	6.23	6.24

"exact" numerical values in the below numerical experiments.We solve (5.61) for $\varphi_k(0) = A > 0$ and $\varphi_k'(0) = 0$ for different values of A. Each A yields the kth vertical mode $\overline{\varphi}_k = \overline{\varphi}_k^A$ at energy $E(A, 0) > 0$, see Definition 5.7. We use $\overline{\varphi}_k^A$ to compute the function $A_{l,k}(t)$ in (5.64) and we replace it into (5.63). We start with $A = 0$ and we increase it until the trivial solution $\xi_0 \equiv 0$ of (5.63) becomes unstable. Since this is a delicate point, let us explain with great precision how we obtain the two sets of critical values of A (thresholds of instability) that we denote by $A_1(k)$ and $A_2(k)$. The results obtained in [38] for the Hamiltonian system (3.51) (leading to some Mathieu equations) suggest the conjecture that there exist two increasing and divergent sequences $\{A_l^n\}_{n=0}^{\infty}$ $(l = 1, 2)$ such that:

- If $A \in S := \cup_k (A_l^{2k}, A_l^{2k+1})$ then ξ_0 is stable.
- If $A \in U := \cup_k (A_l^{2k+1}, A_l^{2k+2})$ then ξ_0 is unstable.

Moreover, one expects the instability to become more evident if A is far from S: in particular, if $A \in (A_l^{2k+1}, A_l^{2k+2})$ for some $k \geq 0$ and $A_l^{2k+2} - A_l^{2k+1} > 0$ is small, then it could be hard to detect the instability of ξ_0.

Due to the unpredictable behavior of the stability regions for general Hill equations (see [60, 61]), these results appear difficult to reach for the particular Hamiltonian system (5.57). It is however reasonable to expect that somehow similar results and behaviors hold. In particular, we expect ξ_0 to be "weakly unstable" whenever A belongs to a narrow interval of instability, that is, nontrivial solutions of (5.63) blow up slowly in time: if A belongs to a narrow instability interval, then only a small amount of energy is transferred from the vertical mode $\overline{\varphi}_k^A$ to a torsional mode. From a physical point of view, this kind of instability is irrelevant, both because it has low probability to occur and because, even if it occurs, the torsional mode remains fairly small. From a mechanical point of view, we know from [239] that small torsional oscillations are harmless and the bridge would remain safe, see (3.13). For this reason, we compute the two sets of critical values $A_l(k)$ $(l = 1, 2)$ as the infimum of the first interval of instability having at least amplitude 0.2. These critical values measure the least height of the vertical mode $\overline{\varphi}_k$ which gives rise to a "strong" instability. It may happen that there exists some $A < A_l(k)$ leading to instability but if its instability interval is narrow, this generates a weak and harmless instability and we neglect it.

Let us describe qualitatively what is seen numerically. We vary A with step 0.1 and we determine $\overline{\varphi}_k^A$, then we solve (5.63) with $\xi(0) = \xi'(0) = 1$. In Fig. 5.5 we represent the corresponding solution ξ. In the first picture the behavior of ξ appears

periodic with, basically, oscillations of constant amplitude. If we increase A by 0.1, the function ξ still appears periodic but with oscillations of variable amplitude; this behavior is well visible in the second picture and always turned out to be the foreplay of instability. After a further increment of 0.1 to A we see that $\xi(t)$ oscillates with increasing amplitude and reaches a magnitude of the order of 10^9 for $t = 40$. The same phenomenon is accentuated at the subsequent step where $\xi(40)$ has an order of magnitude of 10^{14}. By increasing further A the magnitude was also increasing. The least A displaying instability is the value that we denote by $A_l(k)$ (l is the torsional mode, k is the vertical mode).

If one wishes to reproduce the TNB, all the parameters in (5.46) can be computed following the Report [9]. After these computations it is shown in [34], that $\gamma \ll 1$. We quote our results for $\gamma = 10^{-3}$ (Table 5.5,a) and $\gamma = 10^{-4}$ (Table 5.5,b) .

From the values of $A_1(k)$ and $A_2(k)$ in Table 5.5 one can compute the corresponding energies E_1 and E_2 as given by (5.62):

$$E_l(k) = (\gamma\mu_{k,1} + a_k)\frac{A_l(k)^2}{2} + b_k\frac{A_l(k)^4}{4} \qquad (l = 1, 2)\,.$$

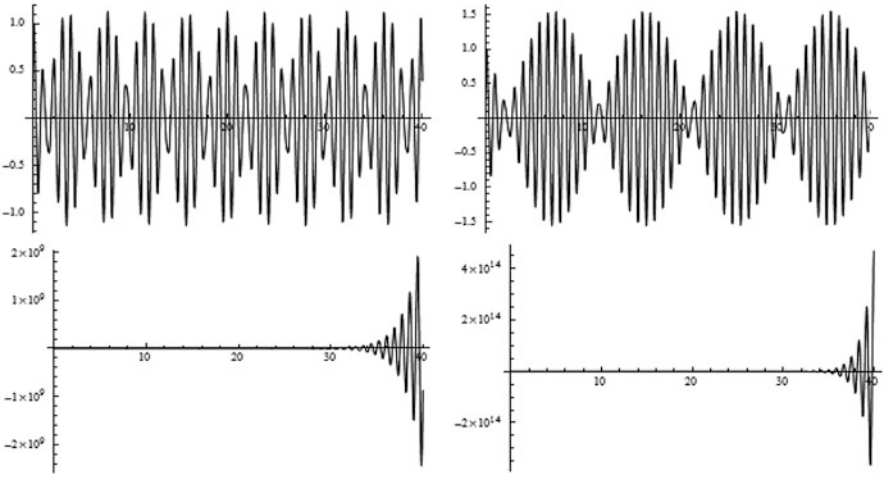

Fig. 5.5 Solutions of (5.63) with $\xi(0) = \xi'(0) = 1$, for A varying with step 0.1

Table 5.5 Critical amplitude of vertical oscillations for $\gamma = 10^{-3}$ (**a**); $\gamma = 10^{-4}$ (**b**)

	k	1	2	3	4	5	6	7	8	9	10	11	12	13	14
a	$A_1(k)$	4.7	3.0	3.0	2.9	2.7	2.4	1.5	>20	>20	>20	0.9	1.6	2.1	2.6
	$A_2(k)$	6.0	9.3	6.0	5.9	5.8	5.7	5.4	5.0	4.2	2.7	>20	>20	>20	>20
	k	1	2	3	4	5	6	7	8	9	10	11	12	13	14
b	$A_1(k)$	1.44	0.91	0.9	0.88	0.82	0.69	>10	>10	>10	>10	0.2	0.44	0.63	0.8
	$A_2(k)$	1.87	2.91	1.86	1.85	1.82	1.77	1.69	1.54	1.3	0.76	>10	>10	>10	>10

The flutter energy of the kth vertical mode $\overline{\varphi}_k$ (see Definition 5.11) is then

$$E_k = \min\{E_1(k), E_2(k)\}\,.$$

From Table 5.5 we deduce that, if $\gamma = 10^{-3}$ then $A_1(k) > A_2(k)$ provided that $k = 8, 9, 10$ while if $\gamma = 10^{-4}$ this happens provided that $k = 7, 8, 9, 10$. In these cases, the energy transfer occurs on the second torsional mode. On the contrary, for lower k, we have that $A_1(k) < A_2(k)$.

A few days prior to the TNB collapse, the project engineer L.R. Durkee wrote a letter (see [9, p.28]) describing the oscillations which were so far observed at the TNB. He wrote:

> Altogether, seven different motions have been definitely identified on the main span of the bridge, and likewise duplicated on the model. These different wave actions consist of motions from the simplest, that of no nodes, to the most complex, that of seven modes.

Hence, the TNB never oscillated with $k = 8, 9, 10$ before the day of the collapse. On the other hand, we have repeatedly recalled that on the day of the collapse the motion suddenly changed from the tenth vertical mode to the second torsional mode, see [9, V-10] and Sect. 5.3.3. Therefore, **the plate model studied in the present section is able to reproduce the very same change of oscillations as at the TNB**. And the above numerical results, combined with the conclusions of Sect. 5.5.3, confirm the behavior highlighted in the previous chapters for different models:

if the energy E in (5.62) is small enough then the kth vertical mode is stable (small initial torsional oscillations remain small for all time $t > 0$), whereas if E is large then the kth vertical mode may become unstable (small torsional oscillations may suddenly become wider).

5.6 The Quasilinear von Kármán Plate System

5.6.1 The Equations and the Boundary Conditions

By normalising the coefficients, the system (5.18) may be written as

$$\begin{cases} \Delta^2 \Phi = -[u,u] & \text{in } \Omega \\ \Delta^2 u = [\Phi,u] + f & \text{in } \Omega\,. \end{cases}$$

In a plate subjected to compressive forces along its edges, one should consider a prestressing constraint which may lead to buckling. Then the system (5.18) becomes

$$\begin{cases} \Delta^2 \Phi = -[u,u] & \text{in } \Omega \\ \Delta^2 u = [\Phi,u] + f + \lambda[F,u] & \text{in } \Omega\,. \end{cases} \tag{5.69}$$

The term $\lambda[F,u]$ in the right hand side of (5.69) represents the boundary stress. The parameter $\lambda \geq 0$ measures the magnitude of the compressive forces acting on $\partial\Omega$ while the smooth function F satisfies

$$F \in C^4(\overline{\Omega})\,, \quad \Delta^2 F = 0 \text{ in } \Omega\,, \quad F_{xx} = F_{xy} = 0 \text{ on } (0,\pi)\times\{\pm\ell\}\,, \tag{5.70}$$

see [43, pp. 228–229]: the term λF is the stress function in the plate resulting from the applied force if the plate were artificially prevented from deflecting and the boundary constraints in (5.70) physically mean that no external stresses are applied on the free edges of the plate. Following Knightly-Sather [157], we take

$$F(x,y) = \frac{\ell^2 - y^2}{2} \qquad \text{so that} \quad [F,u] = -u_{xx}\,.$$

Therefore, (5.69) becomes

$$\begin{cases} \Delta^2\Phi = -[u,u] & \text{in } \Omega \\ \Delta^2 u = [\Phi,u] + f - \lambda u_{xx} & \text{in } \Omega\,. \end{cases} \tag{5.71}$$

In literature, the system (5.71) is usually complemented with Dirichlet boundary conditions, see [82, Sect. 1.5] and [268, p. 514]. But since we aim to model a suspension bridge, these conditions are not the correct ones. As in Sect. 5.4, we view the roadway as a long narrow rectangular thin plate hinged at its two opposite short edges and free on the remaining two long edges: this leads to the boundary conditions (5.21)–(5.22). When (5.21) holds, Ventsel-Krauthammer [264, Example 7.4] suggest that $N^x = v = 0$ on $\{0,\pi\}\times(-\ell,\ell)$. In view of (5.15) this yields

$$0 = w_x + \sigma v_y + \frac{1}{2}u_x^2 + \frac{\sigma}{2}u_y^2 = w_x + \frac{1}{2}u_x^2 = \frac{Ed}{(1-\sigma^2)\sigma}N^y$$

where the condition $u_y = 0$ comes from the first of (5.21). In turn, by (5.17) this implies that $\Phi_{xx} = 0$ on $\{0,\pi\}\times(-\ell,\ell)$. For the second boundary condition we recall that $N^x = 0$ so that, by (5.17), also $\Phi_{yy} = 0$: since the Airy function Φ is defined up to the addition of an affine function, we may take $\Phi = 0$. Summarising, we also have

$$\Phi = \Phi_{xx} = 0 \qquad \text{on } \{0,\pi\}\times(-\ell,\ell)\,. \tag{5.72}$$

On the long edges the boundary condition (5.22) does not depend on λ; for the Airy stress function Φ, we take the usual Dirichlet boundary condition, see [42, 43]. Then

$$\Phi = \Phi_y = 0 \qquad \text{on } (0,\pi)\times\{\pm\ell\}\,. \tag{5.73}$$

These boundary conditions suggest to introduce the following subspace of $H^2_*(\Omega)$

$$H^2_{**}(\Omega) := \{u \in H^2_*(\Omega) : u = u_y = 0 \text{ on } (0,\pi)\times\{\pm\ell\}\},$$

which is a Hilbert space when endowed with the scalar product and norm

$$(u,v)_{H^2_{**}(\Omega)} := \int_\Omega \Delta u \Delta v\,, \qquad \|u\|_{H^2_{**}(\Omega)} := \left(\int_\Omega |\Delta u|^2\right)^{1/2}.$$

We denote the dual space of $H^2_{**}(\Omega)$ by $\mathscr{H}_{**}(\Omega)$.

By putting together the Euler-Lagrange equation (5.71) and the boundary conditions (5.21), (5.22), (5.72) and (5.73) we obtain the system

$$\begin{cases} \Delta^2\Phi = -[u,u] & \text{in } \Omega \\ \Delta^2 u = [\Phi,u] + f - \lambda u_{xx} & \text{in } \Omega \\ u = \Phi = u_{xx} = \Phi_{xx} = 0 & \text{on } \{0,\pi\}\times(-\ell,\ell) \\ u_{yy} + \sigma u_{xx} = u_{yyy} + (2-\sigma)u_{xxy} = 0 & \text{on } (0,\pi)\times\{\pm\ell\} \\ \Phi = \Phi_y = 0 & \text{on } (0,\pi)\times\{\pm\ell\}\,. \end{cases} \tag{5.74}$$

Finally, we also add the nonlinear restoring action due to the hangers. In view of the discussion in Sect. 3.3.3 we take here a compromise between (5.38) and the nonlinearity suggested in [196], that is, $\Upsilon(y)(ku+\delta u^3)^+$. This leads to the problem

$$\begin{cases} \Delta^2\Phi = -[u,u] & \text{in } \Omega \\ \Delta^2 u + \Upsilon(y)(ku+\delta u^3)^+ = [\Phi,u] + f - \lambda u_{xx} & \text{in } \Omega \\ u = \Phi = u_{xx} = \Phi_{xx} = 0 & \text{on } \{0,\pi\}\times(-\ell,\ell) \\ u_{yy} + \sigma u_{xx} = u_{yyy} + (2-\sigma)u_{xxy} = 0 & \text{on } (0,\pi)\times\{\pm\ell\} \\ \Phi = \Phi_y = 0 & \text{on } (0,\pi)\times\{\pm\ell\}\,. \end{cases} \tag{5.75}$$

After that a solution (u,Φ) of (5.74) or (5.75) is found, (5.15)–(5.17) yield

$$w_x + \sigma v_y = \frac{1-\sigma^2}{E\,d}\,\Phi_{yy} - \frac{1}{2}u_x^2 - \frac{\sigma}{2}u_y^2\,, \quad \sigma w_x + v_y = \frac{1-\sigma^2}{E\,d}\,\Phi_{xx} - \frac{1}{2}u_y^2 - \frac{\sigma}{2}u_x^2$$

which immediately gives w_x and v_y. Upon integration, this gives $w = w(x,y)$ up to the addition of a function only depending on y and $v = v(x,y)$ up to the addition of a function depending only on x. These two additive functions are determined by solving the last constraint given by (5.15)–(5.17), that is,

$$w_y + v_x = -\frac{2(1+\sigma)}{E\,d}\,\Phi_{xy} - u_x - u_y\,.$$

5.6.2 *Uniqueness and Multiplicity of the Equilibrium Positions*

With no further mention, we assume here that (5.4) holds. The first step to study (5.74) and (5.75) is to analyze the spectrum of the linear problem obtained

by taking $\Phi = f = k = \delta = 0$:

$$\begin{cases} \Delta^2 u + \lambda u_{xx} = 0 & \text{in } \Omega \\ u = u_{xx} = 0 & \text{on } \{0, \pi\} \times (-\ell, \ell) \\ u_{yy} + \sigma u_{xx} = u_{yyy} + (2-\sigma) u_{xxy} = 0 & \text{on } (0, \pi) \times \{\pm \ell\}\,. \end{cases} \tag{5.76}$$

The following result is proved in [130].

Theorem 5.12 *The problem* (5.76) *admits a sequence of divergent eigenvalues*

$$0 < \lambda_1 < \lambda_2 \le \ldots \le \lambda_k \le \ldots$$

whose corresponding eigenfunctions $\{\overline{e}_k\}$ *form a complete orthonormal system in* $H^2_*(\Omega)$. *Moreover, the least eigenvalue* λ_1 *is simple and is the unique value of* $\lambda \in ((1-\sigma)^2, 1)$ *such that*

$$\sqrt{1-\sqrt{\lambda}}\left(\sqrt{\lambda}+1-\sigma\right)^2 \tanh(\ell\sqrt{1-\sqrt{\lambda}}) = \sqrt{1+\sqrt{\lambda}}\left(\sqrt{\lambda}-1+\sigma\right)^2 \tanh(\ell\sqrt{1+\sqrt{\lambda}})$$

while the corresponding eigenspace is generated by the positive eigenfunction

$$\overline{e}_1(x,y) = \left\{ (\sqrt{\lambda}+1-\sigma)\frac{\cosh\left(y\sqrt{1-\sqrt{\lambda}}\right)}{\cosh\left(\ell\sqrt{1-\sqrt{\lambda}}\right)} + (\sqrt{\lambda}-1+\sigma)\frac{\cosh\left(y\sqrt{1+\sqrt{\lambda}}\right)}{\cosh\left(\ell\sqrt{1+\sqrt{\lambda}}\right)} \right\} \sin x.$$

Also for this problem the simplicity of the least eigenvalue and the positivity of the first eigenfunction were not to be expected. By mimicking Knightly-Sather [157, Sect. 3], let us analyse the eigenvalue problem for the fully hinged rectangular plate:

$$\Delta^2 u + \lambda u_{xx} = 0 \text{ in } \Omega = (0, \pi) \times (-\ell, \ell)\,, \qquad u = \Delta u = 0 \text{ on } \partial\Omega\,. \tag{5.77}$$

The eigenvalues and eigenfunctions are given by

$$\lambda_{m,n} = \frac{1}{m^2}\left(m^2 + \frac{n^2\pi^2}{4\ell^2}\right)^2, \qquad \sin(mx)\sin\left(\frac{n\pi}{2\ell}(\ell - y)\right).$$

The least eigenvalue is obtained for $n = 1$ and the following facts hold:

- If $\ell > \pi/2\sqrt{2}$ then the least eigenvalue is $\lambda_{1,1}$ and the first eigenfunction is of one sign.
- If $\ell = \pi/2\sqrt{2}$ then the least eigenvalue is double, $\lambda_{1,1} = \lambda_{2,1} = 9$.
- If $\ell < \pi/2\sqrt{2}$ then the least eigenvalue is $\lambda_{2,1}$ and the first eigenfunction changes sign.

Back to Theorem 5.12, the least eigenvalue λ_1 represents the critical buckling load. This eigenvalue is the same as for (5.31), see Theorem 5.3 and the characterisation in (5.33). Therefore,

$$\lambda_1 = \min_{v \in H^2_*(\Omega)} \frac{\|v\|^2_{H^2_*(\Omega)}}{\|v_x\|^2_{L^2(\Omega)}} = \min_{v \in H^2_*(\Omega)} \frac{\|v\|^2_{H^2_*(\Omega)}}{\|v\|^2_{L^2(\Omega)}} \tag{5.78}$$

and the critical buckling load for a rectangular plate equals the eigenvalue relative to the first eigenmode of the plate. In turn, the first eigenmode is also the first buckling deformation of the plate. From (5.78) we readily infer the Poincaré-type inequalities

$$\lambda_1 \|v_x\|^2_{L^2(\Omega)} \le \|v\|^2_{H^2_*(\Omega)}\,, \quad \lambda_1 \|v\|^2_{L^2(\Omega)} \le \|v\|^2_{H^2_*(\Omega)} \qquad \forall v \in H^2_*(\Omega)$$

with strict inequality unless v is a multiple of $\overline{e}_1$. By taking $v(x, y) = \sin x$ one finds that $\lambda_1 < 1$. We also mention that Theorem 5.12 may be complemented with the explicit form of all the eigenfunctions: they are $\sin(mx)$ ($m \in \mathbb{N}$) multiplied by trigonometric or hyperbolic functions with respect to y, see [130].

Next, we insert a live load f and we study the existence and multiplicity of solutions of (5.74).

Theorem 5.13 *For all $f \in L^2(\Omega)$ and $\lambda \ge 0$ (5.74) admits a solution $(u, \Phi) \in H^2_*(\Omega) \times H^2_{**}(\Omega)$. Moreover:*

- (*i*) *If $\lambda \le \lambda_1$ and $f = 0$, then (5.74) only admits the trivial solution $(u, \Phi) = (0, 0)$.*
- (*ii*) *If $\lambda \in (\lambda_k, \lambda_{k+1}]$ for some $k \ge 1$ and $f = 0$, then (5.74) admits at least k pairs of nontrivial solutions.*
- (*iii*) *If $\lambda < \lambda_1$ there exists $K > 0$ such that if $\|f\|_{L^2(\Omega)} < K$ then (5.74) admits a unique solution $(u, \Phi) \in H^2_*(\Omega) \times H^2_{**}(\Omega)$.*
- (*iv*) *If $\lambda > \lambda_1$ there exists $K > 0$ such that if $\|f\|_{L^2(\Omega)} < K$ then (5.74) admits at least three solutions.*

Theorem 5.13 gives both uniqueness and multiplicity results. Since the solutions are obtained as critical points of an action functional, they describe the stable and unstable equilibria positions of the plate. When both the buckling load λ and the external load f are small there is just one possible equilibrium position. If one of them is large then multiple equilibrium positions may exist.

The last step is to study the nonlinear plate modeling the suspension bridge, that is, with the action of the hangers and cables. We first define the constants

$$\alpha := \int_\Omega \Upsilon(y)\overline{e}_1^2\,, \qquad \overline{\lambda} := (\alpha k + 1)\lambda_1 > \lambda_1\,,$$

where λ_1 is the least eigenvalue and $\overline{e}_1$ denotes here the positive least eigenfunction normalised in $H^2_*(\Omega)$, see Theorem 5.12; Υ is as in (5.38). Then we have

Theorem 5.14 *For all* $f \in L^2(\Omega)$, $\lambda \geq 0$ *and* $k, \delta > 0$ *problem* (5.75) *admits a solution* $(u, \Phi) \in H^2_*(\Omega) \times H^2_{**}(\Omega)$. *Moreover:*

(*i*) *If* $\lambda < \lambda_1$ *there exists* $K > 0$ *such that if* $\|f\|_{L^2(\Omega)} < K$ *then* (5.75) *admits a unique solution* $(u, \Phi) \in H^2_*(\Omega) \times H^2_{**}(\Omega)$.

(*ii*) *If* $\lambda > \lambda_1$ *and* $f = 0$ *then* (5.75) *admits at least two solutions* $(u, \Phi) \in H^2_*(\Omega) \times H^2_{**}(\Omega)$ *and one of them is trivial and unstable.*

(*iii*) *If* $\overline{\lambda} < \lambda_2$ *and* $\overline{\lambda} < \lambda < \lambda_2$, *there exists* $K > 0$ *such that if* $\|f\|_{L^2(\Omega)} < K$ *then* (5.75) *admits at least three solutions* $(u, \Phi) \in H^2_*(\Omega) \times H^2_{**}(\Omega)$, *two being stable and one being unstable.*

Also Theorem 5.14 gives both uniqueness and multiplicity results. Item (*ii*) states that even in absence of a live load ($f = 0$), if the buckling load λ is sufficiently large then there exists at least two equilibrium positions; we conjecture that if we further assume that $\lambda < \overline{\lambda}$ then there exist no other solutions and that the equilibrium positions look like in Fig. 5.6. In the left picture we see the trivial equilibrium $u = 0$ which is unstable due to the buckling load. In the right picture we see the stable equilibrium for some $u < 0$ (above the horizontal position due to the downwards positive orientation). We conjecture that it is a negative multiple of the first eigenfunction $\overline{e}_1$, see Theorem 5.12; since ℓ is very small, a rough approximation shows that this negative multiple looks like $\approx C \sin(x)$ for some $C < 0$, which is the shape represented in the right picture. In this pattern, a crucial role is played by the positivity of $\overline{e}_1$. Our feeling is that the action functional corresponding to this case has a qualitative shape as described in Fig. 5.7, where O is the trivial unstable equilibrium and M is the stable equilibrium. If there were no

Fig. 5.6 Equilibrium positions of the buckled bridge

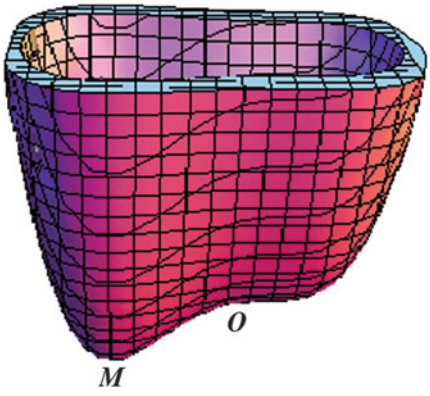

Fig. 5.7 Qualitative shape of the action functional for Theorem 5.14 (*ii*) when $\lambda < \overline{\lambda}$

hangers also the opposite position would be a stable equilibrium. But the presence of the restoring force requires a larger buckling term in order to generate a positive (downwards) displacement. Indeed, item (*iii*) states, in particular, that if $f = 0$ and the buckling load is large then there exist three equilibria: one is trivial and unstable, the second is the enlarged negative one already found in item (*ii*), the third should precisely be the positive one which appears because the buckling load λ is stronger than the restoring force due to the hangers. All these conjectures and qualitative explanations are supported by similar results for a simplified (one dimensional) beam equation, see Theorem 2.17.

5.7 Alternative Plate Models with Stretching Energy

5.7.1 Should the Stretching Energy Be Included in the Model?

In a plate $\Omega \subset \mathbb{R}^2$ stretching is most visible when the plate is fixed on the boundary $\partial\Omega$ and a deformation of Ω yields a variation of its surface. This is the two-dimensional version of the variation of length of a beam, see (2.2). If the elastic force is proportional to the increment of surface, the stretching energy for the plate whose vertical displacement is u reads

$$\mathbb{E}_S(u) = \int_\Omega \left(\sqrt{1 + |\nabla u|^2} - 1\right) dxdy. \tag{5.79}$$

By measuring the importance of the stretching energy through a coefficient $\delta \geq 0$, one is led to consider the energy

$$\mathbb{E}_T(u) + \delta \mathbb{E}_S(u) \tag{5.80}$$

where $\mathbb{E}_T(u)$ is the sum of the bending and potential energies, see (5.19).

Let us explain why we believe that, at least for a first approximation, the stretching energy may be left out, that is, $\delta = 0$. There are several reasons for this and, from a mathematical point of view, one simply has to notice that $H^2 \subset H^1$ and that the H^2-norm bounds the H^1-norm. Of course, this is a very rough argument and, as we shall see, deeper motivations come from structural engineering and physics.

From a physical point of view, one should notice that the axial force in the plate modeling the roadway is very small: the plate is very long and since two edges are free, only very small variations of the total surface are expected.

From an engineering point of view, it is known that concrete is weakly elastic and heavy loads can produce cracks while metals are more elastic and react to loads by bending. This is the reason why prestressed concrete structures have been conceived. According to [200, p. 28], the father of prestressed concrete bridges is the French engineer Eugène Freyssinet (1879–1962) and these bridges were first built around 1940. Prestressing metal tendons (generally of high tensile steel) are

used to provide a clamping load which produces a compressive stress that balances the tensile stress that the concrete compression member would otherwise experience due to a load. Prestressed concrete is obtained by casting concrete around tensioned tendons; this method produces a winning interaction between tendons and concrete since it protects the tendons from corrosion and allows for a direct transfer of tension. The concrete adheres and bonds to the bars and when the tension is released it is transferred to the concrete as compression by static friction. The idea, or even better, the necessity of having an "elasticized concrete" explains why stretching is negligible when computing the energy of the plate Ω. Indeed, if the prestressed plate increases its surface, it simply recovers its initial surface (before prestressing) and therefore, no effective stretching energy appears. Moreover, the plate is fixed only on its short edges so that it is free to move horizontally on the long edges which are free boundaries described by (5.22). And in such situation, we already pointed out that there is little stretching energy. So, the coefficient δ is very small and, as a first approximation, it can be neglected.

On the other hand, for a more accurate analysis one needs to take account of the stretching energy. In particular, in prestressed structures there is a competing effect between bending and stretching. We also saw in Sect. 5.2.3 that when large deformations of the plate are involved the stretching components (w, v) couple with the bending component u and modify the energy. In the following subsections we discuss some equations which take into account the stretching energy. Villaggio [268, Sect. 51] considers these equations as modifications of the quasilinear von Kármán system (5.18) discussed in Sects. 5.2.3 and 5.6:

> . . .the equations are derived from the principle of minimum energy, but by neglecting the strain energy resulting from the second invariant of the strains. The resulting equations are still nonlinear, but they can be decoupled. . .

5.7.2 *The Equation with a Linearised Stretching Term*

For small displacements u, the asymptotic expansion $(\sqrt{1+|\nabla u|^2}-1) \sim |\nabla u|^2/2$ allows to approximate (5.79) with the Dirichlet integral

$$\mathbb{E}_S(u) = \frac{1}{2}\int_\Omega |\nabla u|^2\, dxdy. \tag{5.81}$$

Then the resulting energy (5.80) reads

$$\mathbb{E}_f = \int_\Omega \left(\frac{(\Delta u)^2}{2} + \frac{\sigma-1}{2}[u,u]\right) dxdy + \frac{\delta}{2}\int_\Omega |\nabla u|^2 dxdy - \int_\Omega fu\, dxdy.$$

By minimising this energy, one obtains the following linear equation

$$\Delta^2 u - \delta\Delta u = f \qquad \text{in } \Omega\,. \tag{5.82}$$

In this section we study (5.82). By using the scalar products (5.25) and (5.27) we may formally link minimisers of the energy $\mathbb{E}_f$ and weak solutions of the equation.

Theorem 5.15 *Assume (5.4), let $\delta > 0$, and let $f \in \mathscr{H}$. Then there exists a unique $u \in H^2_*(\Omega)$ such that*

$$(u, v)_{H^2_*} + \delta(u, v)_{H^1_*} = \langle f, v \rangle \qquad \forall v \in H^2_*(\Omega)\,; \tag{5.83}$$

moreover, u is the minimiser of the convex functional $\mathbb{E}_f$. If $f \in L^2(\Omega)$ then $u \in H^4(\Omega)$. Finally, if $u \in C^4(\Omega) \cap C^3(\overline{\Omega})$ satisfies (5.83), then u is a classical solution of (5.82) complemented with the boundary conditions

$$u(0, y) = u_{xx}(0, y) = u(\pi, y) = u_{xx}(\pi, y) = 0$$
$$u_{yy}(x, \pm\ell) + \sigma u_{xx}(x, \pm\ell) = u_{yyy}(x, \pm\ell) + (2 - \sigma)u_{xxy}(x, \pm\ell) - \delta u_y(x, \pm\ell) = 0$$

for all $y \in (-\ell, \ell)$ and all $x \in (0, \pi)$.

From Theorem 5.15 we learn that the boundary conditions on the free edges $y = \pm\ell$ are modified by the stretching constant δ. If we assume again (5.28) and (5.29), then the unique solution of (5.82) is given by

$$u(x, y) = \sum_{m=1}^{\infty} \left[\frac{1}{m^2(m^2 + \delta)} + A_m \cosh(my) + B_m \cosh(\sqrt{m^2 + \delta}\, y) \right] \beta_m \sin(mx) \tag{5.84}$$

where the coefficients $A_m = A_m(\ell)$ and $B_m = B_m(\ell)$ are given by

$$A_m = \frac{-\sigma(1-\sigma)m}{\sqrt{m^2+\delta}[(1-\sigma)m^2+\delta]^2 \sinh(m\ell)\coth(\ell\sqrt{m^2+\gamma\delta}) - (1-\sigma)^2(m^2+\delta)m^3\cosh(m\ell)}$$

$$B_m = \frac{\sigma[(1-\sigma)m^2+\delta]}{[(1-\sigma)m^2+\delta]^2\cosh(\ell\sqrt{m^2+\delta}) - (1-\sigma)^2 m^3\sqrt{m^2+\delta}\coth(m\ell)\sinh(\ell\sqrt{m^2+\delta})} \frac{1}{m^2+\delta}.$$

To estimate the impact of the stretching energy, one should compare (5.84) with (5.30). These formulas also describe the dependence on y of the equilibrium when the forcing term merely depends on x. The y-dependence is a measure of the tendency to cross bending, which was the main cause of the collapse of the Tacoma Narrows Bridge, see [253]. The tendency to cross bending is well estimated by

$$u(x, \ell) - u(x, 0) = \sum_{m=1}^{\infty} \left[A_m(\cosh(m\ell) - 1) + B_m(\cosh(\ell\sqrt{m^2 + \delta}) - 1) \right] \sin(mx)\,.$$

It is quite standard (see [3]) that the embedding $H^2_*(\Omega) \subset H^1_*(\Omega)$ is compact and that the optimal embedding constant is given by

$$\Lambda := \min_{w \in H^2_*(\Omega)} \frac{\|w\|^2_{H^2_*}}{\|w\|^2_{H^1_*}}\,. \tag{5.85}$$

From a physical point of view, this constant determines a bound for the prestressing strength: we will see that, if exceeded, nontrivial equilibria appear giving rise to buckling. The characterisation in (5.85) yields the Poincaré-type inequality

$$\Lambda \|w\|^2_{H^1_*} \le \|w\|^2_{H^2_*} \qquad \forall w \in H^2_*(\Omega)\,; \tag{5.86}$$

this inequality is strict unless w minimises the ratio in (5.85), that is, w is a nontrivial solution of the eigenvalue problem

$$\begin{cases} \Delta^2 w + \Lambda \Delta w = 0 & \text{in } \Omega \\ w(0,y) = w_{xx}(0,y) = w(\pi,y) = w_{xx}(\pi,y) = 0 & y \in (-\ell,\ell) \\ w_{yy}(x,\pm\ell) + \sigma w_{xx}(x,\pm\ell) = 0 & x \in (0,\pi) \\ w_{yyy}(x,\pm\ell) + (2-\sigma) w_{xxy}(x,\pm\ell) + \Lambda w_y(x,\pm\ell) = 0 & x \in (0,\pi). \end{cases} \tag{5.87}$$

Problem (5.87) is similar to (5.82) with $\delta = -\Lambda$ and $f = 0$. By strict monotonicity of the function (of variable λ) on the left hand side, we know that there exists a unique $\lambda \in (0, \sqrt{\sigma})$ such that

$$\frac{\lambda}{(\lambda^2-\sigma)^2} \tanh(\ell\lambda) = \frac{1}{(1-\sigma)^2} \tanh(\ell)\,. \tag{5.88}$$

This number enables us to characterise the least eigenvalue of (5.87):

Theorem 5.16 *Let $\Lambda = \Lambda_1$ be as in (5.85) and let $\lambda \in (0, \sqrt{\sigma})$ be the unique solution of (5.88), then*

$$\Lambda = 1 - \lambda^2 \in (1-\sigma, 1)$$

and, up to a multiplicative constant, the unique solution of (5.87) is positive in Ω and is given by

$$\overline{w}(x,y) = \big\{(\sigma-\lambda^2)\cosh(\lambda\ell)\cosh(y) + (1-\sigma)\cosh(\ell)\cosh(\lambda y)\big\}\sin x.$$

Moreover, (5.87) admits a divergent sequence of eigenvalues

$$\Lambda_1 < \Lambda_2 \le \ldots \le \Lambda_k \le \ldots \tag{5.89}$$

whose corresponding eigenfunctions $\{\overline{w}_k\}$ form a complete orthonormal system in $H^2_*(\Omega)$.

Theorem 5.16 is far from trivial. First of all, the computation of the exact value of the least eigenvalue requires some effort; if $\sigma = 0.2$ and $\ell = \pi/150$ then $\Lambda \approx 0.96$. Secondly, and more important, a similar remark as for Theorem 5.3 holds: the results in [83] show that the positivity of $\overline{w}$ should not be considered an obvious result.

Last but not least, note that (5.87) is not a standard eigenvalue problem such as $Lu = \Lambda u$ for some linear operator L; some work is needed in order to exhibit a linear compact and self-adjoint operator, see [6].

5.7.3 The Surface Increment Quasilinear Equation

We study here the behavior of the plate without the linearisation (5.81) and subject to prestressing $\delta = -P < 0$. The energy becomes

$$\mathscr{E}_f(u) = \frac{1}{2}\|u\|^2_{H^2_*} - P\int_\Omega \left(\sqrt{1+|\nabla u|^2} - 1\right) dxdy - \langle f, u\rangle \tag{5.90}$$

where $\|\cdot\|_{H^2_*(\Omega)}$ is the norm defined in Lemma 5.1 and P is the axial force acting on the short edges of the plate (prestressing): we have $P > 0$ if the plate is compressed and $P < 0$ if the plate is stretched. The energy function $\mathscr{E}_f$ may not be convex, hence it may admit critical points different from the global minimiser: although the only stable equilibrium is the global minimiser, other unstable equilibria may exist. Critical points of the energy $\mathscr{E}_f$ solve the following (quasilinear) Euler-Lagrange equation:

$$\begin{cases} \Delta^2 u + P\,\nabla\cdot\left(\frac{\nabla u}{\sqrt{1+|\nabla u|^2}}\right) = f & \text{in } \Omega \\ u(0,y) = u_{xx}(0,y) = u(\pi,y) = u_{xx}(\pi,y) = 0 & y \in (-\ell,\ell) \\ u_{yy}(x,\pm\ell) + \sigma u_{xx}(x,\pm\ell) = 0 & x \in (0,\pi) \\ u_{yyy}(x,\pm\ell) + (2-\sigma)u_{xxy}(x,\pm\ell) - \delta(u)u_y(x,\pm\ell) = 0 & x \in (0,\pi) \end{cases} \tag{5.91}$$

where $\delta = \delta(u)$ is no longer constant and reads

$$\delta(u) = -\frac{P}{\sqrt{1+|\nabla u|^2}}\,.$$

For a given $f \in \mathscr{H}$ we say that $u \in H^2_*(\Omega)$ is a weak solution of (5.91) if

$$(u,v)_{H^2_*} - P\int_\Omega \frac{\nabla u\cdot\nabla v}{\sqrt{1+|\nabla u|^2}} dxdy = \langle f, v\rangle \qquad \forall v \in H^2_*(\Omega)\,. \tag{5.92}$$

We first consider the homogeneous case $f = 0$. In this case, we say that $u \in H^2_*(\Omega)$ is a weak solution of (5.91) if

$$(u,v)_{H^2_*} - P\int_\Omega \frac{\nabla u\cdot\nabla v}{\sqrt{1+|\nabla u|^2}} dxdy = 0 \qquad \forall v \in H^2_*(\Omega)\,. \tag{5.93}$$

Of course, $u = 0$ always solves (5.93) and the interesting question is whether nontrivial solutions also exist. In this respect, we state

Theorem 5.17 *Let Λ_k ($k \geq 1$) be as in (5.89) and put $\Lambda_0 = 0$. If*

$$P \in (\Lambda_k, \Lambda_{k+1}]$$

for some $k \geq 0$, then (5.93) admits at least k pairs of nontrivial solutions $\pm u_j$.

Theorem 5.17 states that large prestressing leads to buckling, that is, nontrivial solutions. The picture in Fig. 5.8 displays the qualitative behavior of the energy functional $\mathscr{E}_0$ when $P \in (\Lambda_1, \Lambda_2]$. There is an unstable equilibrium (at the origin) and two stable equilibria symmetric with respect to the origin. For $P > \Lambda_2$, Theorem 5.17 gives additional multiplicity and the qualitative graph of $\mathscr{E}_0$ becomes more complicated, with more unstable solutions.

For the nonhomogeneous problem our result is less precise. However, also when $f \neq 0$ we may state a result about uniqueness and multiplicity of solutions.

Theorem 5.18 *Let Λ be as in (5.85) (see Theorem 5.16).*

(*i*) *If $P \leq \Lambda$, then for all $f \in \mathscr{H}$ the problem (5.92) admits a unique solution $u \in H^2_*(\Omega)$.*
(*ii*) *If $P > \Lambda$, then for all $f \in \mathscr{H}$ the problem (5.92) admits at least a solution $u \in H^2_*(\Omega)$.*
(*iii*) *If $P > \Lambda$, there exists $\gamma = \gamma(P) > 0$ such that if $\|f\|_{\mathscr{H}} < \gamma$ then (5.92) admits at least three solutions.*

Theorem 5.18 deserves several important comments. From a physical point of view, it is not unexpected. If the prestressing constant is sufficiently small (that is, $P \leq \Lambda$), then there exists a unique equilibrium position for any given external forcing and this equilibrium is stable. But if prestressing is sufficiently large (that is, $P > \Lambda$) then other equilibria may appear. We conjecture that for increasing P (and

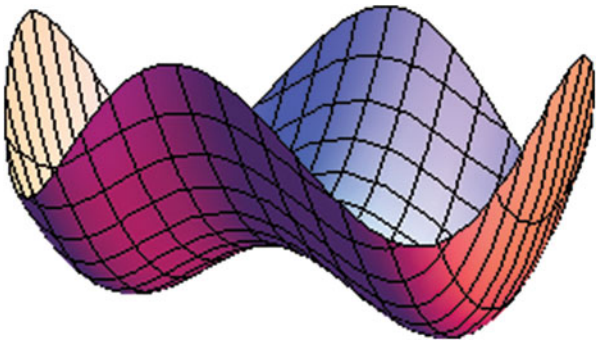

Fig. 5.8 Qualitative description of the energy $\mathscr{E}_0$ with three equilibria

given small f) the number of solutions also increases; in this respect, see the beam equation in Sect. 2.8.3.

The proof of Theorem 5.18 in [6] makes use of a perturbation argument. Therefore, if $P \in (\Lambda_1, \Lambda_2]$ the picture in Fig. 5.8 still displays the qualitative behavior of the energy functional $\mathscr{E}_f$: there is an unstable equilibrium (close to the origin) and two stable equilibria (nearly symmetric with respect to the origin). For larger P, further solutions may appear but they cannot be directly derived from Theorem 5.17 due to the instability of the solutions found there. Of course, if f belongs to some space related to the kernel of the second derivative of $\mathscr{E}_0$ one may also maintain the unstable solutions of the homogeneous problem; but we will not pursue this further.

The classical Fredholm alternative tells us that nonhomogeneous linear problems at resonance lack either existence or uniqueness of the solution. The simplest relevant example is the equation $\Delta u + \lambda u = f$ in a bounded domain $\Omega \subset \mathbb{R}^n$ ($n \geq 1$) under Dirichlet boundary conditions; if λ is an eigenvalue of the Laplacian, that is $-\Delta u = \lambda u$ admits a nontrivial solution $\overline{w} \in H_0^1(\Omega)$, the existence of solutions of the nonhomogeneous problem depends on $f \in H^{-1}(\Omega)$: there are no solutions if $\langle f, \overline{w} \rangle \neq 0$ and there are infinitely many solutions otherwise. Theorems 5.17 and 5.18 tell us that (5.91) admits a unique solution also at resonance, when $P = \Lambda$, for any $f \in \mathscr{H}$; this confirms the nonlinear nature of (5.91).

Let us now introduce the action of the hangers in this model. Consider again the functions h and H in (5.38) and (5.39). If we add the potential energy of the hangers (and cables) to the energy in (5.90) we obtain

$$\mathscr{E}_f(u) = \frac{1}{2}\|u\|^2_{H^2_*} - P \int_\Omega \left(\sqrt{1 + |\nabla u|^2} - 1 \right) dxdy + \int_\Omega H(y,u)\, dxdy - \langle f, u \rangle .$$

Critical points of the energy $\mathscr{E}_f(u)$ solve the quasilinear equation

$$\Delta^2 u + P\, \nabla \cdot \left(\frac{\nabla u}{\sqrt{1 + |\nabla u|^2}} \right) + h(y,u) = f \quad \text{in } \Omega \tag{5.94}$$

with the same boundary conditions as in (5.91). If the plate is weakly prestressed, then following result holds.

Theorem 5.19 *Let h be as in (5.38); assume that $P < \Lambda$. For any $f \in \mathscr{H}$ there exists a unique $u \in H^2_*(\Omega)$ such that*

$$(u, v)_{H^2_*} - P \int_\Omega \frac{\nabla u \cdot \nabla v}{\sqrt{1 + |\nabla u|^2}} dxdy + (h(y,u), v)_{L^2} = \langle f, v \rangle \qquad \forall v \in H^2_*(\Omega) .$$

If $u \in H^4(\Omega) \cap C^3(\overline{\Omega})$ then u is a strong solution of (5.94) and satisfies the boundary conditions in (5.91).

If the external force also depends on time, $f = f(x, y, t)$, and if m denotes the mass of the plate, then arguing as for (5.42) we find that the quasilinear evolution equation describing the motion of the bridge now reads

$$u_{tt} + \Delta^2 u + P\,\nabla \cdot \left(\frac{\nabla u}{\sqrt{1 + |\nabla u|^2}} \right) + h(y, u) = f \qquad \text{in } \Omega \times \mathbb{R}_+ .$$

Due to internal friction, we add a small damping term and obtain

$$\begin{cases} u_{tt} + \eta u_t + \Delta^2 u + P\nabla \cdot \left(\frac{\nabla u}{\sqrt{1+|\nabla u|^2}} \right) + h(y,u) = f & \text{in } \Omega \times \mathbb{R}_+ \\ u(0,y,t) = u_{xx}(0,y,t) = 0 & (y,t) \in (-\ell,\ell) \times \mathbb{R}_+ \\ u(\pi,y,t) = u_{xx}(\pi,y,t) = 0 & (y,t) \in (-\ell,\ell) \times \mathbb{R}_+ \\ u_{yy}(x,\pm\ell,t) + \sigma u_{xx}(x,\pm\ell,t) = 0 & (x,t) \in (0,\pi) \times \mathbb{R}_+ \\ u_{yyy}(x,\pm\ell,t) + (2-\sigma) u_{xxy}(x,\pm\ell,t) - \delta(u) u_y(x,\pm\ell,t) = 0 & (x,t) \in (0,\pi) \times \mathbb{R}_+ \\ u(x,y,0) = u_0(x,y)\,, \quad u_t(x,y,0) = u_1(x,y) & (x,y) \in \Omega \end{cases} \tag{5.95}$$

where $\eta > 0$. If $f \in C^0(\mathbb{R}_+; L^2(\Omega))$ we say that

$$u \in C^0(\mathbb{R}_+; H^2_*(\Omega)) \cap C^1(\mathbb{R}_+; L^2(\Omega)) \cap C^2(\mathbb{R}_+; \mathscr{H}(\Omega)) \tag{5.96}$$

is a solution of (5.95) if it satisfies the initial conditions and if

$$\langle u''(t), v \rangle + \eta (u'(t), v)_{L^2} + (u(t), v)_{H^2_*} - P \int_\Omega \frac{\nabla u \cdot \nabla v}{\sqrt{1 + |\nabla u|^2}} dxdy + (h(y, u(t)), v)_{L^2}$$

$$= (f(t), v)_{L^2} \quad \forall v \in H^2_*(\Omega)\,,\ \forall t > 0\,.$$

Then we have

Theorem 5.20 *Assume (5.4) and that $P < \Lambda$. Let $f \in C^0(\mathbb{R}_+; L^2(\Omega))$ and let $\eta > 0$; let $u_0 \in H^2_*(\Omega)$ and $u_1 \in L^2(\Omega)$. Then:*

(i) There exists a unique solution of (5.95).

(ii) If $f \in L^2(\Omega)$ is independent of t, then the unique solution u of (5.95) satisfies

$$u(t) \to \overline{u} \quad \text{in } H^2_*(\Omega) \quad \text{and} \quad u'(t) \to 0 \quad \text{in } L^2(\Omega) \quad \text{as } t \to +\infty$$

where $\overline{u}$ is the unique solution of the stationary problem (5.94).

5.7.4 A Nonlocal Quasilinear Equation

We study here the behavior of the plate subject to prestressing and we follow the model suggested by Berger [39]; see also the beam model suggested by Woinowsky-Krieger [279] and discussed in Sect. 2.8.3. The elastic energy to be considered reads

$$\mathscr{E}_f(u) = \frac{1}{2}\|u\|^2_{H^2_*} - \frac{P}{2}\|u\|^2_{H^1_*} + \frac{S}{4}\|u\|^4_{H^1_*} - \langle f, u\rangle \tag{5.97}$$

where $\|\cdot\|_{H^2_*}$ is the norm defined in Lemma 5.1 and $\|\cdot\|_{H^1_*}$ is the Dirichlet norm defined in (5.26). Here $S > 0$ depends on the elasticity of the material composing the roadway, $S\int_\Omega |\nabla u|^2$ measures the geometric nonlinearity of the plate due to its stretching and P is the prestressing constant. Again, we have $P > 0$ if the plate is compressed and $P < 0$ if the plate is stretched.

Critical points of the energy $\mathscr{E}_f(u)$ solve the following (quasilinear, nonlocal) Euler-Lagrange equation:

$$\Delta^2 u + \Big(P - S\int_\Omega |\nabla u|^2 dxdy\Big)\Delta u = f \ \text{ in } \Omega\,. \tag{5.98}$$

Note that the second order expansion

$$\sqrt{1+\varepsilon^2} - 1 = \frac{\varepsilon^2}{2} - \frac{\varepsilon^4}{8} + O(\varepsilon^6) \quad \text{as } \varepsilon \to 0$$

leads to an energy similar to (5.97) with

$$\frac{P}{8}\int_\Omega |\nabla u|^4 dxdy \quad \text{instead of} \quad \frac{S}{4}\left(\int_\Omega |\nabla u|^2 dxdy\right)^2; \tag{5.99}$$

these terms are quite similar and hence the energy (5.97) may be considered as a second order approximation of (5.90). Using (5.99) yields the quasilinear equation

$$\Delta^2 u + P\Delta u - \frac{P}{2}\Delta_4 u = f \ \text{ in } \Omega$$

where Δ_4 is the p-Laplacian operator with $p = 4$; this equation should be compared with (5.98).

For simplicity we put

$$\delta(u) = -P + S\int_\Omega |\nabla u|^2\, dxdy$$

so that the corresponding boundary value problem for (5.98) reads

$$\begin{cases} \Delta^2 u - \delta(u)\,\Delta u = f & \text{in } \Omega \\ u(0,y) = u_{xx}(0,y) = u(\pi,y) = u_{xx}(\pi,y) = 0 & y \in (-\ell,\ell) \\ u_{yy}(x,\pm\ell) + \sigma u_{xx}(x,\pm\ell) = 0 & x \in (0,\pi) \\ u_{yyy}(x,\pm\ell) + (2-\sigma) u_{xxy}(x,\pm\ell) - \delta(u) u_y(x,\pm\ell) = 0 & x \in (0,\pi)\,. \end{cases} \tag{5.100}$$

The problem (5.100) with a general $\delta = \delta(u)$ is also studied by Villaggio [268, (51.8)] as an approximation of the von Kármán system (5.18).

For a given $f \in \mathscr{H}$ we say that $u \in H^2_*(\Omega)$ is a weak solution of (5.100) if

$$(u,v)_{H^2_*} + \delta(u)(u,v)_{H^1_*} = \langle f, v\rangle \qquad \forall v \in H^2_*(\Omega)\,. \tag{5.101}$$

It appears quite instructive to deal first with the homogeneous case $f = 0$: the energy functional $\mathscr{E}_0$ has a rich structure. In this case, we say that $u \in H^2_*(\Omega)$ is a weak solution of (5.100) if

$$(u,v)_{H^2_*} + \delta(u)(u,v)_{H^1_*} = 0 \qquad \forall v \in H^2_*(\Omega)\,. \tag{5.102}$$

We then have a precise multiplicity result.

Theorem 5.21 *Let $S > 0$, let Λ_k ($k \geq 1$) be as in (5.89) and put $\Lambda_0 = 0$.*

(*i*) *If $P \in (\Lambda_k, \Lambda_{k+1}]$ for some $k \geq 0$ and at least one of the eigenvalues $\Lambda_2, \dots, \Lambda_k$ has multiplicity greater than 1, then (5.102) admits infinitely many solutions.*

(*ii*) *If $P \in (\Lambda_k, \Lambda_{k+1}]$ for some $k \geq 0$ and all the eigenvalues $\Lambda_2, \dots, \Lambda_k$ have multiplicity 1, then (5.102) admits exactly $2k+1$ solutions which are explicitly given by*

$$u_0 = 0\,, \qquad \pm u_j = \pm\sqrt{\frac{P-\Lambda_j}{S}}\,\overline{w}_j \quad (j = 1,\dots,k) \tag{5.103}$$

where $\overline{w}_j$ is an $H^1_*(\Omega)$-normalised eigenfunction of (5.87) corresponding to the eigenvalue Λ_j ($j = 1,\dots,k$). Moreover, for each solution the energy is given by

$$\mathscr{E}_0(u_0) = 0\,, \qquad \mathscr{E}_0(\pm u_j) = -\frac{(P-\Lambda_j)^2}{4S} \quad (j = 1,\dots,k) \tag{5.104}$$

and the Morse index M is given by

$$M(u_0) = k\,, \qquad M(\pm u_j) = j-1 \quad (j = 1,\dots,k)\,. \tag{5.105}$$

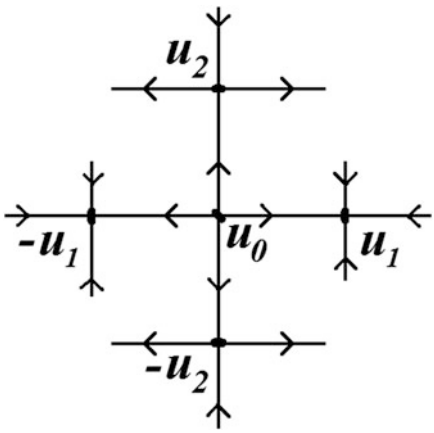

Fig. 5.9 Qualitative description of the energy $\mathscr{E}_0$ with five equilibria

The statement of Theorem 5.21 can be made more precise in the case of infinitely many solutions. Any simple eigenvalue Λ_j generates solutions satisfying (5.104) and (5.105). Multiple eigenvalues Λ_j generate infinitely many solutions which are linear combinations of the (multiple) related eigenfunctions, they still satisfy (5.104) but they are degenerate critical points for $\mathscr{E}_0$.

The picture in Fig. 5.8 displays again the qualitative behavior of the energy functional $\mathscr{E}_0$ when $P \in (\Lambda_1, \Lambda_2]$. However, in this case more details are available. If Λ_2 is simple, the picture of Fig. 5.9 represents the 2D space spanned by the first two eigenfunctions $\{\overline{w}_1, \overline{w}_2\}$ and the five solutions $\{u_0, \pm u_1, \pm u_2\}$; the arrows represent the directions where the energy $\mathscr{E}_0$ decreases. Theorem 5.21 [in particular, (5.105)] states that only $\pm u_1$ are stable (global minima) while all the other critical points of $\mathscr{E}_0$ are saddle points. By standard minimax techniques, one could try to link the two minima $\pm u_1$ in order to find further unstable (mountain pass) solutions. But Theorem 5.21 states that the only solutions are (5.103) so that the minimax point is one of the u_j's ($j = 0, \dots, k$) and no additional unstable solutions exist. From a physical point of view, the Morse index may be seen as a "measure of instability".

For the nonhomogeneous problem the result is similar to Theorem 5.18:

Theorem 5.22 *Let $S > 0$ and let Λ be as in (5.85) (see Theorem 5.16).*

(*i*) *If $P \leq \Lambda$, then for all $f \in \mathscr{H}$ the problem (5.101) admits a unique solution $u \in H^2_*(\Omega)$.*

(*ii*) *If $P > \Lambda$, then for all $f \in \mathscr{H}$ the problem (5.101) admits at least a solution $u \in H^2_*(\Omega)$; moreover, there exists $\gamma = \gamma(P) > 0$ such that if $\|f\|_{\mathscr{H}} < \gamma$ then (5.101) admits at least three solutions.*

The same comments and remarks following Theorem 5.18 apply also to Theorem 5.22. In particular, problem (5.100) displays the same prestressing and buckling features as (5.91). But a further remark about a priori estimates may be given here.

Of course, this makes sense in the case of a unique solution $P \leq \Lambda$. By taking $v = u$ in (5.101), we obtain

$$\|u\|_{H^2_*}^2 - P\|u\|_{H^1_*}^2 + S\|u\|_{H^1_*}^4 = \langle f, u\rangle \leq \|f\|_{\mathscr{H}}\|u\|_{H^2_*}\,. \tag{5.106}$$

If $P < \Lambda$, then by (5.86) this yields the following a priori estimate for the unique solution of (5.100):

$$\|u\|_{H^2_*} \leq \frac{\Lambda}{\Lambda - P}\|f\|_{\mathscr{H}}\,. \tag{5.107}$$

As $P \to \Lambda$ this estimate is of little interest and one may wonder whether a different a priori estimate may be obtained for $P = \Lambda$. But this is not the case, as shown by the following counterexample. Let $\overline{w}$ denote an $H^1_*(\Omega)$-normalised eigenfunction corresponding to Λ and let $f = \alpha\Delta\overline{w}$ for some $\alpha > 0$. By Theorem 5.22, the problem (5.100) admits a unique weak solution; one may check that

$$u = -\sqrt[3]{\frac{\alpha}{S}}\,\overline{w}$$

is the solution. Then

$$\|u\|_{H^2_*} = \sqrt{\Lambda}\,\|u\|_{H^1_*} = \frac{\sqrt{\Lambda}}{\sqrt[3]{S}}\,\sqrt[3]{\alpha}\,, \qquad \|f\|_{\mathscr{H}} = \alpha\|\Delta\overline{w}\|_{\mathscr{H}}\,,$$

so that no a priori estimate such as $\|u\|_{H^2_*(\Omega)} \leq C\|f\|_{\mathscr{H}}$ can hold; to be convinced, it suffices to let $\alpha \to 0$. On the other hand, for any $P > 0$, from (5.106) we infer that

$$\text{either} \qquad \|u\|_{H^1_*} \leq \sqrt{\frac{P}{S}} \qquad \text{or} \qquad \|u\|_{H^2_*} \leq \|f\|_{\mathscr{H}}$$

so that, by (5.86),

$$\|u\|_{H^1_*} \leq \max\left\{\sqrt{\frac{P}{S}}, \frac{\|f\|_{\mathscr{H}}}{\sqrt{\Lambda}}\right\}$$

and a kind of a priori estimate in the weaker norm $H^1_*(\Omega)$ is always available.

Note that by taking $v = u$ in (5.92), if $P < \Lambda$, we also obtain the a priori estimate (5.107) for the unique solution of (5.91). But contrary to (5.100), nothing can be said when $P \to \Lambda$ or when $P = \Lambda$.

If we introduce the action of the hangers in this model, the energy (5.97) becomes

$$\mathscr{E}_f(u) = \frac{1}{2}\|u\|_{H^2_*}^2 - \frac{P}{2}\|u\|_{H^1_*}^2 + \frac{S}{4}\|u\|_{H^1_*}^4 + \int_\Omega H(y,u)\,dxdy - \langle f, u\rangle$$

whereas the quasilinear Euler-Lagrange equation reads

$$\Delta^2 u - \delta(u)\,\Delta u + h(y,u) = f \quad \text{in } \Omega \tag{5.108}$$

with the same boundary conditions as in (5.100). If the plate is weakly prestressed, then the following result holds.

Theorem 5.23 *Let h be as in (5.38); assume that $P < \Lambda$. For any $f \in \mathscr{H}$ there exists a unique $u \in H^2_*(\Omega)$ such that*

$$(u,v)_{H^2_*} - \delta(u)(u,v)_{H^1_*} + (h(y,u),v)_{L^2} = \langle f, v\rangle \qquad \forall v \in H^2_*(\Omega)\,.$$

If $u \in H^4(\Omega) \cap C^3(\overline{\Omega})$ then u is a strong solution of (5.108) and satisfies the boundary conditions in (5.100).

If the external force also depends on time, $f = f(x,y,t)$, one may obtain a result completely similar to Theorem 5.20.

5.8 Bibliographical Notes

The first attempt to mathematically model a plate goes back to 1766 and is due to Euler in his masterpiece work [103]. These studies were performed just a few years before the experiment by Chladni [77] described in Sect. 1.3. The story continues in 1789 with the contribution [46] by the Swiss mathematician Jacques Bernoulli (1759–1789), also known as Jacques II Bernoulli. In 1811 the Italian mathematician Giuseppe Lodovico Lagrangia (1736–1813), better known as Joseph-Louis Lagrange, published his treatise of analytical mechanics, see [164]. It was the French mathematician Marie-Sophie Germain (1776–1831) who first derived in 1811 a fourth order differential equation to model plates; her equation was incomplete and the missing term was added by Lagrange in 1813. Her work [131] was published in 1821, see also Sect. 1.9 for more historical details. The Poisson ratio σ in (5.4) is named after the French mathematician Siméon Denis Poisson (1781–1840) who introduced it in 1829, see [224]. Further contributions in the theory of plates are mentioned throughout the present chapter.

The brief historical survey of models for plates given in Sect. 5.1 may be complemented with full details by referring to the monographs by Timoshenko [259] and Truesdell [262], see also [264, Sect. 1.2].

Part of the material in Sect. 5.2.1 is taken from [264, Sect. 1.1]. The Kirchhoff-Love theory reported in Sect. 5.2.2 may be derived from the original works [154, 176], see also [123, Sect. 1.1.2]. The variational formulation (5.19) should be attributed to Friedrichs [117], while for a discussion of the boundary value problems for a thin elastic plate in a somehow old fashioned notation we refer again to [154]. In 1910, von Kármán [271] described the large deflections and stresses produced in a

thin elastic plate subject to compressive forces along its edge by means of the fourth order quasilinear elliptic system (5.18). An interesting phenomenon associated with this nonlinear model is the appearance of buckling, namely the plate may deflect out of its plane when these forces reach a certain magnitude, see [41, Sect. 4.3B]. The linearisation of the von Kármán equations for an elastic plate over a planar domain Ω under pressure also leads to the eigenvalue equation (5.87), although with different boundary conditions. Miersemann [203] studied in some detail the corresponding eigenvalue problem. We also refer to [123, Sect. 1.3.2] for further information and more recent bibliography.

The part concerning the von Kármán quasilinear model in Sect. 5.2.3 is taken from Lagnese [162], see also [163]. For a precise physical interpretation of the Airy stress function Φ introduced in Sect. 5.2.3 we refer to [82, pp. 61–66]. Ciarlet [79, 80] and Davet [88] showed that the von Kármán equations (5.18) may be derived as the leading term of a formal asymptotic expansion in a thickness parameter of the exact equations of three-dimensional nonlinear elasticity, provided that the applied forces are suitably scaled in terms of the thickness parameter. These (stationary) equations have been widely studied in the mathematical literature, see e.g. [40, 42, 43, 82, 155, 156, 162, 163, 264], as well as in the engineering literature [160, Sect. 8.8.1], see also [86] for some numerical approaches. Concerning the evolution (wave-type) von Kármán equations, for the general theory we refer again to [162, 163]. The hinged boundary conditions (5.21) are named after Navier, from their first appearance in [209, p. 96], from where we took Fig. 5.10.

The deflection of the fully hinged rectangular plate Ω under the action of a distributed load has been solved by Navier [209], see also [186, Sect. 2.1]. Maybe Cauchy [71] had in mind the difference/analogy between bending, stretching, and torsion when he criticised the work by Navier by claiming that

> ...Navier ... avait considéré deux espèces de forces produites, les unes par la dilatation ou la contraction, les autres par la flexion de ce même plan. ... Il me parut que ces deux espèces de forces pouvaient être réduites à une seule...

Many years later, the general problem of a load on the rectangular plate Ω with hinged short edges was considered by Lévy [171], Zanaboni [283], and Nadai [207], see also [186, Sect. 2.2] for the analysis of different kinds of boundary conditions on the long edges $y = \pm\ell$. Further classical books of elasticity theory are due to Timoshenko [258], Ciarlet [81], Villaggio [268], see also [92, 207, 208, 260] for the

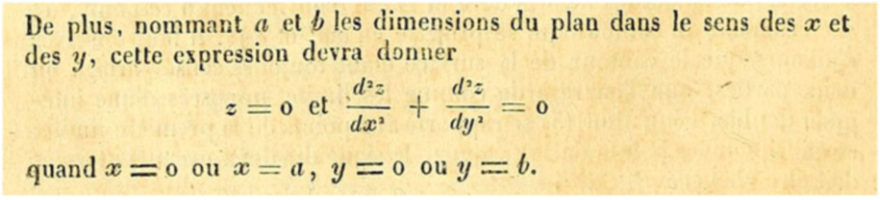
De plus, nommant a et b les dimensions du plan dans le sens des x et des y, cette expression devra donner

$$z = 0 \text{ et } \frac{d^2z}{dx^2} + \frac{d^2z}{dy^2} = 0$$

quand $x = 0$ ou $x = a$, $y = 0$ ou $y = b$.

Fig. 5.10 First appearance of Navier boundary conditions (1823)

theory of plates. Let us also mention a celebrated work by Ball [29] who analytically approached the real 3D boundary value problems for nonlinear elasticity. For the definition of Sobolev spaces and embedding properties such as (5.24), we refer to [3]. For the spaces introduced in (5.44) we refer to [254, Chap. II].

Sections 5.3.1 and 5.4 are entirely taken from a paper by Ferrero-Gazzola [111]. More general forms for h, other than (5.38), are considered in [111]. The explicit solution (5.30) may be obtained following [186, Sect. 2.2], see [111, Theorem 2]. A similar procedure can be used also for some forcing terms depending on y such as $e^{\pm y} f(x)$ or $y f(x)$, see [186]. When $\ell \to 0$, the plate Ω tends to become a one dimensional beam of length π: when $\ell \to 0$, the solution and the energy of the plate "tend to become" as for the beam, see [111, Theorem 3.3]. Equation (5.43) also arises in different contexts, see e.g. [118, (17)], and is sometimes called the Swift-Hohenberg equation. We refer to [277] for the study of the same equation but with a noncoercive nonlinearity.

The quantitative analysis of Sects. 5.3.2 and 5.3.3 is due to Berchio-Ferrero-Gazzola [34]. Sect. 5.5 is also taken from [34] while Sect. 5.5.4 contains some variants of the results in [34] where one can find many other numerical results validating the definition and the theoretical characterisation given in Sect. 5.5.2.

The pure plate model (5.69) is due to von Kármán [271] who derived the equations by an heuristic method in which he discarded certain terms that he regarded as physically or geometrically negligible. For several decades these equations remained of purely theoretical interest. Pioneering numerical experiments were performed in the mentioned engineering reports [172, 173] and by applied mathematicians some 20 years later, see [31]. At that time, some tools of nonlinear analysis were quickly developing and the first applications to the von Kármán equations should be attributed to Berger-Fife [42]. Critical point theory was then employed in the two milestone papers [40, 43] which gave rise to many further contributions. The adaptation of the von Kármán model (5.69) to suspension bridges as well as all the material in Sect. 5.6 comes from Gazzola-Wang [130].

Sections 5.7.2–5.7.4 come from AlGwaiz-Benci-Gazzola [6]. The proofs of Theorems 5.19 and 5.23 are straightforward and may be obtained by standard variational methods. Theorem 5.20 is new and, although it has time-dependent boundary conditions due to the presence of $\delta(u)$, its proof may be obtained as for Theorem 5.5 and 5.6, see [111].

Chapter 6
Conclusions

In the previous chapters we have analysed several different models for suspension bridges. Each model has highlighted a form of instability due to the presence of some nonlinearity. The purpose of this final chapter is to put all together the observed phenomena and to afford possible explanations as well as to give answers to the questions raised in Chap. 1.

6.1 Flutter Energy in Nonlinear Models

In Sect. 1.7.4 we recalled the usual definition of flutter: it is a form of instability depending on the velocity of the wind acting on the structure. Classical models assume that the forcing term describing the wind is periodic. Not only we believe that this assumption is incorrect (the wind is random in nature) but we also believe that it may create artificial phenomena and lead to incorrect conclusions. While analysing carefully the oscillations at the TNB, the project engineer Durkee [9, p. 28] comments the effects of the wind by writing:

- Motions of considerable magnitude . . . have been observed with wind velocities as low as three or four miles per hour.
- Motions of varying degrees of violence have been noted in winds up to 48 miles per hour. The violence of motion is not necessarily proportional to the velocity of wind.
- The bridge has remained motionless at times in wind velocities varying from zero to 35 miles per hour.
- There appears to be no difference in the motion whether the wind is steady or gusty.

Overall, Durkee states that what really counts is the **effective velocity** of the wind which is difficult to determine. We recall that the TNB has collapsed under a wind velocity of 42 mph. To justify the withstanding of the TNB under a wind of 48 mph, one may think of a Wagner effect [275] and claim that also the **duration** of the wind plays an important role.

F. Gazzola, *Mathematical Models for Suspension Bridges*, MS&A 15,
DOI 10.1007/978-3-319-15434-3_6

The instability generating flutter is usually attributed to the action of an external force, either by invoking a parametric resonance or self-oscillations, see Sect. 1.7.5. Arena-Lacarbonara [17] conclude their paper by writing

> The onset of flutter is very sensitive to the initial wind angle of attack, the damping ratio, and the bridge prestress condition caused by dead loads.

Thus flutter also depends on structural parameters and in this monograph we have focused our efforts precisely on the nonlinear structural features. We have seen that, in several isolated nonlinear models, the instability is caused by internal resonances between different oscillating modes.

In [121] we suggested that, for nonlinear models, the flutter speed could be replaced by a critical input of external energy. The models considered in the present book confirm that the mechanism which gives rise to self-excited oscillations within a nonlinear structure depends on the amount of energy present inside the structure. The mechanism occurs in four steps. First, the wind inserts energy inside the structure through the vortex shedding, then the so absorbed energy varies the nonlinear frequencies of the oscillating modes. When the internal energy reaches the flutter energy of the oscillating mode, a resonance is created and an uncontrolled energy transfer occurs. In other words, since the nonlinear frequencies vary with the amplitude of oscillations, the resonance appears only for sufficiently wide oscillations and creates a **structural instability**. The final step is the entrance of aerodynamic forces which exacerbate the structural instability, see Sect. 3.7.

Therefore, one should compute how much energy from the wind is absorbed by the structure. When the structure is "drunk", that is, it has absorbed a critical amount of energy that we call **flutter energy**, its oscillations are uncontrolled: the energy may transfer between different modes and give rise to destructive oscillations. The addition of stiffening trusses increases the resistance to the appearance of a torsional component in the oscillations. Whence, for suspension bridges, one may characterise the (structural) instability by a critical energy threshold.

The flutter energy of a structure subject to vibrations is the least energy which generates an energy transfer between different modes of oscillations.

This definition is valid for any structure, both when the air is still and the structure is moving in the air (as for an airfoil) or when the air is moving the structure (as for a bridge). Up to some factor and square root, this definition coincides with the classical one (flutter speed instead of flutter energy) if the vibrating structure is the airfoil of an aircraft for which the angle of attack is "almost constant". But for suspension bridges, it may be fairly different. One should then investigate which structural parameters enlarge the flutter energy and how to compute the input of energy from the wind in dependence of its character. In this respect, a hint is given in Sect. 3.6 while in Sect. 3.3.3 we saw that the flutter energy decreases for increasing nonlinearity while it tends to infinity if the nonlinearity tends to vanish.

6.2 Answers to the Main Questions

In Chap. 1 we analysed several bridges failures which showed the necessity of mathematical models able to explain the observed phenomena. Although most of these failures occurred long time ago and modern design provides nowadays secure bridges, it seems that the phenomena were not completely understood. For instance, there is no unanimously shared explanation of the TNB collapse. In particular, we still owe to the reader an answer to the following questions raised in Sect. 1.6:

(Q1) Why do torsional oscillations appear suddenly in suspension bridges?
(Q2) Why the self-induced oscillations did not appear at earlier occasions when high wind velocity prevailed?
(Q3) Why have self-induced oscillations not been observed in other modern bridges?

In Sect. 1.8 we recalled that suspension bridges exhibit both nonlinear and chaotic behaviors and that a **General Principle of Classical Mechanics** suggests how to model these behaviors: *neither linear differential equations nor systems of less than three first-order equations can exhibit chaos.*

In Chaps. 2–5 we analysed several different nonlinear models. The nonlinear beam-type equation considered in Sect. 2.6 shows the possibility of self-excited oscillations and how these may appear only in presence of suitable nonlinearities. Since one dimensional beams cannot display torsional oscillations, in Chap. 3 we analysed a fish-bone model, namely a beam complemented with rigid cross sections. Thanks to a Galerkin approximation we reproduced the sudden transition from purely vertical oscillations to torsional oscillations: this occurs only at certain energy levels which can be computed numerically and may be estimated theoretically through the Hill equation. The least of these energies is called flutter energy and only depends on the structural parameters. In Sect. 3.6 we gave a qualitative explanation of how to compute the flutter energy and how torsional modes are activated. Once the flutter energy is exceeded, we have seen in Sect. 3.7 that the aerodynamic forces contribute to vary further the energy.

In Sect. 4.2 we focused our attention to a unique cross section of the roadway: we studied a system which allows the use of Poincaré maps. This tool enabled us to give a precise description of the starting spark for the onset of torsional oscillations. At some energy levels a bifurcation occurs and creates a resonance among oscillators: when the oscillators are in resonance there may be a transfer of energy from the vertical oscillator to the torsional oscillator. This occurs in isolated systems, with no need of additional energy inputs from the exterior. This internal resonance phenomenon should not be confused with the well-known elementary phenomenon of external resonance displayed by the bridges discussed in Sect. 1.2. Although the Poincaré maps could not be used, we were able to highlight the same phenomenon within a more complicated model consisting of multiple cross sections, that is, with many degrees of freedom. Again, we computed numerically

the flutter energy, namely the least value of the internal energy where the instability is manifested. We also made a feeble attempt to evaluate the role of internal damping and external forces: it turned out that damping enlarges the threshold of instability but it does not modify the response while forcing adds noise to the response.

A model viewing the roadway as a thin plate is analysed in Chap. 5. Several fourth order nonlinear PDE's are derived and studied in detail. The Galerkin method is again used to show that the vibrating modes of the plate may transfer energy, provided enough energy is present within the structure. More sophisticated nonlinear models presumably displaying the same phenomena are also suggested.

All the models analysed in the present book yield the same conclusions which we now summarise. Since the models are nonlinear, the frequencies of the vibrating modes depend on the energy involved and resonances may occur only if a certain amount of energy is present in the structure, that is,

if the total energy within the structure is small, then the different modes weakly interact and only a negligible part of the energy of the vertical oscillations can be transferred to a torsional oscillation, whereas if the total energy is sufficiently large then the modes may enter in resonance and tiny torsional oscillations may suddenly become wide.

The existence of a flutter energy was highlighted in all the models considered and effective methods how to compute it were given.

We are now in position to give an answer to the above questions. Our answer to **(Q1)** is the following:

(A1) Torsional oscillations appear suddenly in suspension bridges because of internal resonances which occur when large energies are within the structure.

We believe that the TNB has collapsed because, on November 7, 1940, the wind inserted enough energy to overcome the flutter energy of its 10th (nonlinear) vertical mode. This gave rise to internal resonances that were the onset of the destructive torsional oscillations. Then the aerodynamic forces further excited these oscillations until the collapse of the bridge.

To **(Q2)** we answer by

(A2) No self-induced torsional oscillations appeared earlier because the flutter energy is a structural parameter and depends on the oscillating mode.

And, as remarked in the Report [9], the TNB never previously oscillated with the same mode as on November 7, 1940: that day the vertical motion prior to the appearance of torsional oscillations involved "nine or ten waves". The results in Sects. 5.3.2 and 5.5.4 explain why these oscillations are particularly prone to activate torsional oscillations.

To **(Q3)**, we answer by

(A3) Other modern bridges have a structure with larger flutter energies.

This is clearly due to different strengths of the stiffening structure, quantified by the constants appearing in the models, see again Sect. 3.6.

We hope that this book has suggested a different point of view on models for suspension bridges and that it has emphasised the necessity of mathematical models satisfying the (GPCM). Nonlinearity play a crucial role in the models and one should not be afraid of it: it is much better to suffer with some nonlinear model rather that to obtain unreliable responses. Some of the models of the present book raised the attention of the civil engineers from the Politecnico di Milano and in some master thesis [26, 44] it is shown that the answer **(A1)** may indeed explain the Tacoma collapse. We have no hope that this book might solve all the problems related to the stability of suspension bridges, much work is still necessary: more refined models should be investigated and correct values should be attributed to the parameters. But we do hope that this book might induce some researcher, both mathematicians and engineers, to investigate more deeply into these fascinating challenges.

References

1. A.M. Abdel-Ghaffar, Suspension bridge vibration: continuum formulation. J. Eng. Mech. **108**, 1215–1232 (1982)
2. D.M. Abrams, B. Eckhardt, A. McRobie, E. Ott, S.H. Strogatz, Crowd synchrony on the millennium bridge. Nat. Brief Commun. **438**, 43–44 (2005)
3. R.A. Adams, *Sobolev Spaces*. Pure and Applied Mathematics, vol. 65 (Academic, New York/London, 1975)
4. N.U. Ahmed, H. Harbi, Mathematical analysis of dynamic models of suspension bridges. SIAM J. Appl. Math. **58**, 853–874 (1998)
5. B. Akesson, *Understanding Bridges Collapses* (CRC Press/Taylor & Francis Group, London, 2008)
6. M. Al-Gwaiz, V. Benci, F. Gazzola, Bending and stretching energies in a rectangular plate modeling suspension bridges. Nonlinear Anal. T.M.A. **106**, 18–34 (2014)
7. C.J. Amick, J.F. Toland, Homoclinic orbits in the dynamic phase-space analogy of an elastic strut. Eur. J. Appl. Math. **3**, 97–114 (1992)
8. O.H. Ammann, Additional stiffening of Bronx-Whitestone bridge. Civil Eng. (March, 1946)
9. O.H. Ammann, T. von Kármán, G.B. Woodruff, *The Failure of the Tacoma Narrows Bridge* (Federal Works Agency, Washington, DC, 1941)
10. Anonymous, Fall of the Broughton suspension bridge, near Manchester. Manch. Guardian **9**(53), 384–389 (1831)
11. Anonymous, Fall of a suspension bridge over the Ostrawitza at Mahrisch-Ostrau. Proc. Inst. Civil Eng Lond. **87**, 479–480 (1886/87)
12. Anonymous, Stays and brakes check oscillation of Whitestone bridge. Eng. News Rec. (December 5, 1940)
13. S.S. Antman, Ordinary differential equations of nonlinear elasticity. I. Foundations of the theories of nonlinearly elastic rods and shells. Arch. Ration. Mech. Anal. **61**, 307–351 (1976)
14. S.S. Antman, Buckled states of nonlinearly elastic plates. Arch. Ration. Mech. Anal. **67**, 111–149 (1978)
15. S.S. Antman, *Nonlinear Problems of Elasticity*. Applied Mathematical Sciences, vol. 107 (Springer, New York, 2005)
16. S.S. Antman, W. Lacarbonara, Forced radial motions of nonlinearly viscoelastic shells. J. Elast. **96**, 155–190 (2009)
17. A. Arena, W. Lacarbonara, Nonlinear parametric modeling of suspension bridges under aeroelastic forces: torsional divergence and flutter. Nonlinear Dyn. **304**, 72–90 (2012)
18. G. Arioli, F. Gazzola, Existence and numerical approximation of periodic motions of an infinite lattice of particles. Zeit. Angew. Math. Phys. **46**, 898–912 (1995)

F. Gazzola, *Mathematical Models for Suspension Bridges*, MS&A 15,
DOI 10.1007/978-3-319-15434-3

19. G. Arioli, F. Gazzola, Periodic motions of an infinite lattice of particles with nearest neighbor interaction. Nonlinear Anal. T.M.A. **26**, 1103–1114 (1996)
20. G. Arioli, F. Gazzola, Numerical implementation of the model considered in the paper: a new mathematical explanation of what triggered the catastrophic torsional mode of the Tacoma narrows bridge collapse (2013), http://mox.polimi.it/~gianni/bridges.html
21. G. Arioli, F. Gazzola, Old and new explanations of the Tacoma narrows bridge collapse, in *Atti XXI Congresso AIMETA*, Torino, p. 10 (2013)
22. G. Arioli, F. Gazzola, A new mathematical explanation of what triggered the catastrophic torsional mode of the Tacoma narrows bridge collapse. Appl. Math. Model. **39**, 901–912 (2015)
23. G. Arioli, F. Gazzola, S. Terracini, Multibump periodic motions of an infinite lattice of particles. Math. Zeit. **223**, 627–642 (1996)
24. G. Augusti, M. Diaferio, V. Sepe, A "deformable section" model for the dynamics of suspension bridges. Part ii: nonlinear analysis and large amplitude oscillations. Wind Struct. **6**, 451–470 (2003)
25. G. Augusti, V. Sepe, A "deformable section" model for the dynamics of suspension bridges. Part i: model and linear response. Wind Struct. **4**, 1–18 (2001)
26. D. Baccarin, *Is Internal Parametric Resonance a Potential Failure Mode for Suspension Bridges?* Master thesis, Civil Engineering, Politecnico di Milano, Italy, 2013
27. J.M. Ball, Initial-boundary value problems for an extensible beam. J. Math. Anal. Appl. **42**, 61–90 (1973)
28. J.M. Ball, Stability theory for an extensible beam. J. Differ. Equ. **14**, 399–418 (1973)
29. J.M. Ball, Convexity conditions and existence theorems in nonlinear elasticity. Arch. Ration. Mech. Anal. **63**, 337–403 (1977)
30. G. Bartoli, P. Spinelli, The stochastic differential calculus for the determination of structural response under wind. J. Wind Eng. Ind. Aerodyn. **48**, 175–188 (1993)
31. L. Bauer, E. Reiss, Nonlinear buckling of rectangular plates. J. SIAM **13**, 603–626 (1965)
32. V. Benci, D. Fortunato, Existence of solitons in the nonlinear beam equation. J. Fixed Point Theory Appl. **11**, 261–278 (2012)
33. C. Bender, Historical sketch of the successive improvements in suspension bridges to the present time. Am. Soc. Civil Eng. **I**, 27–43 (1872)
34. E. Berchio, A. Ferrero, F. Gazzola, Structural instability of nonlinear plates modelling suspension bridges: mathematical answers to some long-standing questions, arXiv:1502.05851
35. E. Berchio, A. Ferrero, F. Gazzola, P. Karageorgis, Qualitative behavior of global solutions to some nonlinear fourth order differential equations. J. Differ. Equ. **251**, 2696–2727 (2011)
36. E. Berchio, F. Gazzola, A qualitative explanation of the origin of torsional instability in suspension bridges. Nonlinear Anal. T.M.A. (2015)
37. E. Berchio, F. Gazzola, The role of aerodynamic forces in a mathematical model for suspension bridges, arXiv:1409.1769
38. E. Berchio, F. Gazzola, C. Zanini, Which residual mode captures the energy of the dominating mode in second order Hamiltonian systems? arXiv:1410.2374
39. H.M. Berger, A new approach to the analysis of large deflections of plates. J. Appl. Mech. **22**, 465–472 (1955)
40. M.S. Berger, On von Kármán's equations and the buckling of a thin elastic plate, I. The clamped plate. Commun. Pure Appl. Math. **20**, 687–719 (1967)
41. M.S. Berger, *Nonlinearity and Functional Analysis*. Pure and Applied Mathematics (Academic, New York/London, 1977)
42. M.S. Berger, P.C. Fife, On von Kármán's equations and the buckling of a thin elastic plate. Bull. Am. Math. Soc. **72**, 1006–1011 (1966)
43. M.S. Berger, P.C. Fife, Von Kármán's equations and the buckling of a thin elastic plate, II. Plate with general edge conditions. Commun. Pure Appl. Math. **21**, 227–241 (1968)
44. P. Bergot, L. Civati, *Dynamic Structural Instability in Suspension Bridges*, Master thesis, Civil Engineering, Politecnico di Milano, 2014

45. J. Berkovits, P. Drábek, H. Leinfelder, V. Mustonen, G. Tajčová, Time-periodic oscillations in suspension bridges: existence of unique solutions. Nonlinear Anal. Real World Appl. **1**, 345–362 (2000)
46. J. Bernoulli Jr., Essai théorique sur les vibrations de plaques élastiques rectangulaires et libres. Nova Acta Acad. Petropolit. (St. Petersburg) **5**, 197–219 (1789)
47. K.Y. Billah, R.H. Scanlan, Resonance, tacoma narrows bridge failure, and undergraduate physics textbooks. Am. J. Phys. **59**, 118–124 (1991)
48. M.A. Biot, T. von Kármán, *Mathematical Methods in Engineering: An Introduction to the Mathematical Treatment of Engineering Problems*, vol. XII (McGraw-Hill, New York, 1940)
49. F. Bleich, Dynamic instability of truss-stiffened suspension bridges under wind action. Proc. ASCE **74**, 1269–1314 (1948)
50. F. Bleich, C.B. McCullough, R. Rosecrans, G.S. Vincent, *The Mathematical Theory of Vibration in Suspension Bridges* (U.S. Dept. of Commerce, Bureau of Public Roads, Washington, DC, 1950)
51. I. Bochicchio, C. Giorgi, E. Vuk, Long-term damped dynamics of the extensible suspension bridge. Int. J. Differ. Equ., 19 pp. (2010). Art. ID 383420
52. I. Bochicchio, C. Giorgi, E. Vuk, On some nonlinear models for suspension bridges, in *Proceedings of the Conference Evolution Equations and Materials with Memory*, Rome, 12–14 July 2010, ed. by D. Andreucci, S. Carillo, M. Fabrizio, P. Loreti, D. Sforza (2011)
53. I. Bochicchio, C. Giorgi, E. Vuk, Long-term dynamics of the coupled suspension bridge system. Math. Models Methods Appl. Sci. **22**, 22 (2012)
54. I. Bochicchio, C. Giorgi, E. Vuk, Asymptotic dynamics of nonlinear coupled suspension bridge equations. J. Math. Anal. Appl. **402**, 319–333 (2013)
55. J. Bodgi, S. Erlicher, P. Argoul, Lateral vibration of footbridges under crowd-loading: continuous crowd modeling approach. Key Eng. Mater. **347**, 685–690 (2007)
56. D. Bonheure, Multitransition kinks and pulses for fourth order equations with a bistable nonlinearity. Ann. Inst. H. Poincaré Anal. Non Linéaire **21**, 319–340 (2004)
57. D. Bonheure, L. Sanchez, Heteroclinic orbits for some classes of second and fourth order differential equations, in *Handbook of Differential Equation*, vol. III (Elsevier Science, Amsterdam, 2006), pp. 103–202
58. M. Braun, *Differential Equations and Their Applications: An Introduction to Applied Mathematics*, 4th edn. (Springer, New York, 1993)
59. B. Breuer, J. Hórak, P.J. McKenna, M. Plum, A computer-assisted existence and multiplicity proof for travelling waves in a nonlinearly supported beam. J. Differ. Equ. **224**, 60–97 (2006)
60. H.W. Broer, M. Levi, Geometrical aspects of stability theory for Hill's equations. Arch. Ration. Mech. Anal. **131**, 225–240 (1995)
61. H.W. Broer, C. Simó, Resonance tongues in Hill's equations: a geometric approach. J. Differ. Equ. **166**, 290–327 (2000)
62. J.M.W. Brownjohn, Observations on non-linear dynamic characteristics of suspension bridges. Earthq. Eng. Struct. Dyn. **23**, 1351–1367 (1994)
63. D. Bruno, V. Colotti, F. Greco, P. Lonetti, A parametric deformability analysis of long span bridge schemes under moving loads, in *Second International Conference on Bridge Maintenance, Safety and Management*, IABMAS04, Kyoto, 2004, pp. 735–737
64. V.I. Burdina, Boundedness of solutions of a system of differential equations (Russian). Dokl. Akad. Nauk. SSSR **92**, 603–606 (1953)
65. E.A. Butcher, S. Radkar, S.C. Sinha, Order reduction of nonlinear systems with time periodic coefficients using invariant manifolds. J. Sound Vib. **284**, 985–1002 (2005)
66. E.I. Butikov, Subharmonic resonances of the parametrically driven pendulum. J. Phys. A: Math. Gen. **35**, 6209–6231 (2002)
67. J.R. Cash, D. Hollevoet, F. Mazzia, A.M. Nagy, Algorithm 927: the MATLAB code bvptwp.m for the numerical solution of two point boundary value problems. ACM Trans. Math. Softw. **39**(2) (2013). Article 15
68. C.A. Castigliano, Nuova teoria intorno all'equilibrio dei sistemi elastici. Atti Acc. Sci. Torino Cl. Sci. Fis. Mat. Nat. **11**, 127–286 (1875/1876)

69. C.A. Castigliano, *Théorie de l'équilibre des systèmes élastiques et ses applications* (A.F. Negro, Torino, 1879)
70. A. Castro, A.C. Lazer, Critical point theory and the number of solutions of a nonlinear Dirichlet problem. Ann. Mat. Pura Appl. **70**, 113–137 (1979)
71. A. Cauchy, Recherches sur l'équilibre et le mouvement intérieur des corps solides ou fluides, élastiques ou non élastiques. Bulletin des Sciences de la Société Philomathique de Paris, 9–13 (1823)
72. L. Cesari, *Asymptotic Behavior and Stability Problems in Ordinary Differential Equations* (Springer, Berlin, 1971)
73. A.R. Champneys, P.J. McKenna, On solitary waves of a piecewise linear suspended beam model. Nonlinearity **10**, 1763–1782 (1997)
74. X. Chen, J.W. Hutchinson, A family of herringbone patterns in thin films. Scr. Mater. **50**, 797–801 (2004)
75. Y. Chen, P.J. McKenna, Traveling waves in a nonlinearly suspended beam: theoretical results and numerical observations. J. Differ. Equ. **136**, 325–355 (1997)
76. C. Chicone, *Ordinary Differential Equations with Applications*. Texts in Applied Mathematics, vol. 34, 2nd edn. (Springer, New York, 2006)
77. E. Chladni, *Entdeckungen über die theorie des klanges* (Weidmanns Erben und Reich, Leipzig, 1787)
78. Q.H. Choi, T. Jung, P.J. McKenna, The study of a nonlinear suspension bridge equation by a variational reduction method. Appl. Anal. **50**, 73–92 (1993)
79. P.G. Ciarlet, A justification of the von Kármán equations. Arch. Ration. Mech. Anal. **73**, 349–389 (1980)
80. P.G. Ciarlet, *Plates and Junctions in Elastic Multi-Structures: An Asymptotic Analysis*. Recherches en mathématiques appliquées, vol. 14 (Masson, Paris, 1990)
81. P.G. Ciarlet, *Mathematical Elasticity. Vol. II, Theory of Plates*. Studies in Mathematics and its Applications, vol. 27 (North-Holland, Amsterdam, 1997)
82. P.G. Ciarlet, P. Rabier, *Les équations de von Kármán*. Studies in Mathematics and its Applications, vol. 27 (Springer, Berlin, 1980)
83. C.V. Coffman, On the structure of solutions to $\Delta^2 u = \lambda u$ which satisfy the clamped plate conditions on a right angle. SIAM J. Math. Anal. **13**, 746–757 (1982)
84. M. Como, in *Stabilità aerodinamica dei ponti di grande luce. Introduzione all'ingegneria strutturale*, ed. by E. Giangreco (UTET, Torino, 2002)
85. M. Como, S. Del Ferraro, A. Grimaldi, A parametric analysis of the flutter instability for long span suspension bridges. Wind Struct. **8**, 1–12 (2005)
86. H. Dai, X. Yue, S.N. Atluri, Solutions of the von Kármán plate equations by a Galerkin method, without inverting the tangent stiffness matrix. J. Mech. Mater. Struct. **9**, 195–226 (2014)
87. L. D'Ambrosio, J.P. Lessard, A. Pugliese, Blow-up profile for solutions of a fourth order nonlinear equation. Nonlinear Anal. T.M.A. (2015, to appear)
88. J.L. Davet, Justification de modèles de plaques nonlinéaires pour des lois de comportment générales. Mod. Math. Anal. Num. **20**, 147–192 (1986)
89. M. de Miranda, M. Petrequin, Storebaelt East bridge: aspetti del montaggio e della realizzazione. Costruzioni Metalliche **6**, 27–42 (1998)
90. K. Deckelnick, H.-Ch. Grunau, Boundary value problems for the one-dimensional Willmore equation. Calc. Var. **30**, 293–314 (2007)
91. N.J. Delatte, *Beyond Failure* (ASCE Press, Reston, 2009)
92. P. Destuynder, M. Salaun, *Mathematical Analysis of Thin Plate Models*. Mathématiques & Applications (Springer, Berlin, 1996)
93. R.W. Dickey, Free vibrations and dynamic buckling of the extensible beam. J. Math. Anal. Appl. **29**, 443–454 (1970)
94. R.W. Dickey, Dynamic stability of equilibrium states of the extensible beam. Proc. Am. Math. Soc. **41**, 94–102 (1973)

95. Z. Ding, On nonlinear oscillations in a suspension bridge system. Trans. Am. Math. Soc. **354**, 65–274 (2001)
96. S.H. Doole, S.J. Hogan, Non-linear dynamics of the extended Lazer-McKenna bridge oscillation model. Dyn. Stab. Syst. **15**, 43–58 (2000)
97. P. Drábek, P. Nečesal, Nonlinear scalar model of a suspension bridge: existence of multiple periodic solutions. Nonlinearity **16**, 1165–1183 (2003)
98. P. Drábek, G. Holubová, Bifurcation of periodic solutions in symmetric models of suspension bridges. Topol. Methods Nonlinear Anal. **14**, 39–58 (1999)
99. P. Drábek, G. Holubová, A. Matas, P. Nečesal, Nonlinear models of suspension bridges: discussion of the results. Appl. Math. **48**, 497–514 (2003)
100. P. Drábek, H. Leinfelder, G. Tajčová, Coupled string-beam equations as a model of suspension bridges. Appl. Math. **44**, 97–142 (1999)
101. Dupuit, Mery de Contades, Hougan, Roland, and Mahyer. Rapport de la commission d'enquête nommée par arrêté de M. le Préfet de Maine-et-Loire, en date du 20 avril 1850, pour rechercher les causes et les circonstances qui ont amené la chute du pont suspendu de la Baisse-Chaîne. Annales des ponts et chaussées, Tome XX: Partie technique **237**, 394–411 (1850)
102. L. Euler, *Methodus inveniendi lineas curvas maximi minimive proprietate gaudentes sive solutio problematis isoperimetrici latissimo sensu accepti* (Marcum Michaelem Bousquet & Socios, Lausanne/Geneva, 1744)
103. L. Euler, De motu vibratorio tympanorum. Novi Commentarii Acad. Sci. Petropolitanae **10**, 243–260 (1766)
104. F.B. Farquharson, Letter to the Editor. ENR, 3 July 1941, p. 37
105. F.B. Farquharson, *Aerodynamic Stability of Suspension Bridges: With Special Reference to the Tacoma Narrows Bridge, Part I: Investigations Prior to October 1941*. Investigation Conducted by the Structural Research Laboratory, University of Washington (University of Washington Press, Seattle, 1949)
106. F.B. Farquharson, *Aerodynamic Stability of Suspension Bridges: With Special Reference to the Tacoma Narrows Bridge, Part III: The Investigation of the Original Tacoma Narrows Bridge*. Investigation Conducted by the Structural Research Laboratory, University of Washington (University of Washington Press, Seattle, 1952)
107. F.B. Farquharson, *Aerodynamic Stability of Suspension Bridges: With Special Reference to the Tacoma Narrows Bridge, Part IV: Model Investigations which Influence the Design of the New Tacoma Narrows Bridge*. Investigation Conducted by the Structural Research Laboratory, University of Washington (University of Washington Press, Seattle, 1954)
108. E. Fermi, J. Pasta, S. Ulam, *Studies of Nonlinear Problems*. Los Alamos Rpt. LA, n.1940 (also in "Collected Works of E. Fermi" University of Chicago Press, Chicago. 1965, vol II, pp. 978–988), 1955. http://www.physics.utah.edu/~detar/phys6720/handouts/fpu/FermiCollectedPapers1965.pdf
109. L. Fernández Troyano, *Bridge Engineering: A Global Perspective*. Madrid: Colegio de ingenieros de caminos, canales y puertos (Thomas Telford, London, 2003)
110. V. Ferreira, E. Moreira dos Santos, On the finite space blow up of the solutions of the Swift-Hohenberg equation. Calc. Var. (2015, to appear). Available online at http://link.springer.com/article/10.1007/s00526-015-0821-6
111. A. Ferrero, F. Gazzola, A partially hinged rectangular plate as a model for suspension bridges. Discrete Continuous Dyn. Syst. A **35** (2015)
112. J. Finley, *A Description of the Patent Chain Bridge*. The Port Folio, vol. III (Bradford & Inskeep, Philadelphia, 1810)
113. A. Fonda, Z. Schneider, F. Zanolin, Periodic oscillations for a nonlinear suspension bridge model. J. Comput. Appl. Math. **52**, 113–140 (1994)
114. L. Franck, P. Lestuzzi, A. Low, *Synchronous Lateral Excitation of Footbridges*. IMAC-EPFL (Swiss Federal Institute of Technology, Lausanne, 2009)
115. F.L. Freiman, N. Schlager, *Failed Technology: True Stories of Technological Disasters*, vol. 2, UXI (1995)

116. D. Frenkel, R. Portugal, Algebraic methods to compute Mathieu functions. J. Phys. A: Math. Gen. **34**, 3541–3551 (2001)
117. K. Friedrichs, Die randwert und eigenwertprobleme aus der theorie der elastischen platten (anwendung der direkten methoden der variationsrechnung). Math. Ann. **98**, 205–247 (1927)
118. P. Galenko, D. Danilov, V. Lebedev, Phase-field-crystal and Swift-Hohenberg equations with fast dynamics. Phys. Rev. E **79**, 11 (2009)
119. B.G. Galerkin, Sterzhni i plastinki: reydy v nekotorykh voprosakh uprugogo ravnovesiya sterzhney i plastinok. Vestnik Inzhenerov **1**(19), 897–908 (1915)
120. F. Gazzola, Periodic motions of a lattice of particles with singular forces. Differ. Integr. Equ. **10**, 245–264 (1997)
121. F. Gazzola, Nonlinearity in oscillating bridges. Electron. J. Differ. Equ. **211**, 1–47 (2013)
122. F. Gazzola, H.-Ch. Grunau, Radial entire solutions for supercritical biharmonic equations. Math. Ann. **334**, 905–936 (2006)
123. F. Gazzola, H.-Ch. Grunau, G. Sweers, *Polyharmonic Boundary Value Problems*. Lecture Notes in Mathematics, vol. 1991 (Springer, Berlin, 2010)
124. F. Gazzola, M. Jleli, B. Samet, On the Melan equation for suspension bridges. J. Fixed Point Theory Appl. **16** (2014)
125. F. Gazzola, P. Karageorgis, Refined blow-up results for nonlinear fourth order differential equations. Commun. Pure Appl. Anal. **12**, 677–693 (2015)
126. F. Gazzola, R. Pavani, Blow up oscillating solutions to some nonlinear fourth order differential equations. Nonlinear Anal. T.M.A. **74**, 6696–6711 (2011)
127. F. Gazzola, R. Pavani, Blow-up oscillating solutions to some nonlinear fourth order differential equations describing oscillations of suspension bridges, in *Sixth International Conference on Bridge Maintenance, Safety and Management*, IABMAS12, Stresa, 2012, pp. 3089–3093
128. F. Gazzola, R. Pavani, Wide oscillations finite time blow up for solutions to nonlinear fourth order differential equations. Arch. Ration. Mech. Anal. **207**, 717–752 (2013)
129. F. Gazzola, R. Pavani, The impact of nonlinear restoring forces acting on hinged elastic beams. Bull. Belgian Math. Soc. (2015)
130. F. Gazzola, Y. Wang, Modeling suspension bridges through the von Kármán quasilinear plate equations, in *Progress in Nonlinear Differential Equations and Their Applications*. Contributions to Nonlinear Elliptic Equations and Systems: a tribute to Djairo Guedes de Figueiredo on occasion of his 80th birthday (Springer, 2015)
131. M.S. Germain, *Recherches sur la théorie des surfaces élastiques* (Huzard-Courcier, Libraire pour les Sciences, Paris, 1821)
132. M. Gerner, *Chakzampa Thangtong Gyalpo, Architect, Philosopher and Iron Chain Bridge Builder* (The Centre for Bhutan Studies, Bhutan, 2007)
133. D. Gilbert, On the mathematical theory of suspension bridges, with tables for facilitating their construction. Philos. Trans. R. Soc. Lond. **30**, 202–218 (1826)
134. J. Glover, A.C. Lazer, P.J. McKenna, Existence and stability of large scale nonlinear oscillations in suspension bridges. Zeit. Angew. Math. Phys. **40**, 172–200 (1989)
135. H. Goldstein, C. Poole, J. Safko, *Classical Mechanics*, 3rd edn. (Addison Wesley, San Francisco, 2002)
136. D. Green, W.G. Unruh, Tacoma bridge failure—a physical model. Am. J. Phys. **74**, 706–716 (2006)
137. M.E. Gurtin, On the nonlinear theory of elasticity, in *Contemporary Developments in Continuum Mechanics and Partial Differential Equations*, ed. by G.M. de la Penha, L.A. Medeiros (North-Holland, Amsterdam, 1978), pp. 237–253
138. M. Haberland, S. Hass, U. Starossek, Robustness assessment of suspension bridges, in *Sixth International Conference on Bridge Maintenance, Safety and Management*, IABMAS12, Stresa, 2012, pp. 1617–1624
139. M. Hayden, *The Book of Bridges* (Galahad Books, New York, 1976)
140. G. Herrmann, W. Hauger, On the interrelation of divergence, flutter and auto-parametric resonance. Ing. Arch. **42**, 81–88 (1973)

141. G.W. Hill, On the part of the motion of the lunar perigee which is a function of the mean motions of the sun and the moon. Acta Math. **8**, 1–36 (1886)
142. G. Holubová, A. Matas, Initial-boundary value problem for the nonlinear string-beam system. J. Math. Anal. Appl. **288**, 784–802 (2003)
143. L.D Humphreys, P.J. McKenna, Multiple periodic solutions for a nonlinear suspension bridge equation. IMA J. Appl. Math. **63**, 37–49 (1999)
144. L.D. Humphreys, P.J. McKenna, When a mechanical model goes nonlinear: unexpected responses to low-periodic shaking. Am. Math. Mon. **112**, 861–875 (2005)
145. L.D. Humphreys, P.J. McKenna, K.M. O'Neill, High frequency shaking induced by low frequency forcing: periodic oscillations in a spring-cable system. Nonlinear Anal. Real World Appl. **11**, 4312–4325 (2010)
146. L.D. Humphreys, R. Shammas, Finding unpredictable behavior in a simple ordinary differential equation. Coll. Math. J. **31**, 338–346 (2000)
147. G.W. Hunt, H.M. Bolt, J.M.T. Thompson, Localisation and the dynamical phase-space analogy. Proc. R. Soc. Lond. A **425**, 245–267 (1989)
148. D. Imhof, *Risk Assessment of Existing Bridge Structure*, Ph.D. Dissertation, University of Cambridge, see also http://www.bridgeforum.org/dir/collapse/type/ for the update of the Bridge failure database, 2004
149. H.M. Irvine, *Cable Structures*. MIT Press Series in Structural Mechanics (MIT Press, Cambridge, 1981)
150. I.V. Ivanov, D.S. Velchev, M. Kneć, T. Sadowski, Computational models of laminated glass plate under transverse static loading, in *Shell-Like Structures, Non-Classical Theories and Applications*, ed. by H. Altenbach, V. Eremeyev. Advanced Structured Materials, vol. 15 (Springer, Berlin, 2011), pp. 469–490
151. D. Jacover, P.J. McKenna, Nonlinear torsional flexings in a periodically forced suspended beam. J. Comput. Appl. Math. **52**, 241–265 (1994)
152. A. Jenkins, Self-oscillation. Phys. Rep. **525**, 167–222 (2013)
153. T. Kawada, *History of the Modern Suspension Bridge: Solving the Dilemma Between Economy and Stiffness* (ASCE Press, Reston, 2010)
154. G.R. Kirchhoff, Über das gleichgewicht und die bewegung einer elastischen scheibe. J. Reine Angew. Math. **40**, 51–88 (1850)
155. G.H. Knightly, An existence theorem for the von Kármán equations. Arch. Ration. Mech. Anal. **27**, 233–242 (1967)
156. G.H. Knightly, D. Sather, On nonuniqueness of solutions of the von Kármán equations. Arch. Ration. Mech. Anal. **36**, 65–78 (1970)
157. G.H. Knightly, D. Sather, Nonlinear buckled states of rectangular plates. Arch. Ration. Mech. Anal. **54**, 356–372 (1974)
158. V.A. Kozlov, V.A. Kondratiev, V.G. Maz'ya, On sign variation and the absence of strong zeros of solutions of elliptic equations. Math. USSR Izvestiya **34**, 337–353 (1990) (Russian original in: Izv. Akad. Nauk SSSR Ser. Mat. **53**, 328–344 (1989))
159. M.G. Krein, V.A. Yakubovich, Hamiltonian systems of linear differential equations with periodic coefficients (Russian), in *Analytic Methods in the Theory of Non-linear Vibrations - Proceedings of International Symposium on Non-linear Vibrations, Izdat. Akad. Nauk Ukrain. SSR, Kiev*, vol. I (1961), pp. 277–305
160. W. Lacarbonara, *Nonlinear Structural Mechanics* (Springer, New York, 2013)
161. W. Lacarbonara, V. Colone, Dynamic response of arch bridges traversed by high-speed trains. J. Sound Vib. **304**, 72–90 (2007)
162. J.E. Lagnese, *Boundary Stabilization of Thin Plates*. Studies in Applied Mathematics (SIAM, Philadelphia, 1989)
163. J.E. Lagnese, J.L. Lions, *Modelling Analysis and Control of Thin Plates*. Collection RMA (Masson, Paris, 1988)
164. J.L. Lagrange, *Mécanique Analytique* (Courcier, Paris, 1811). Reissued by Cambridge University Press, Cambridge, 2009
165. R.S. Lakes, Foam structures with a negative Poisson's ratio. Science **235**, 1038–1040 (1987)

166. A. Larsen, Aerodynamics of the Tacoma narrows bridge—60 years later. Struct. Eng. Int. **4**, 243–248 (2000)
167. A.C. Lazer, P.J. McKenna, Large scale oscillatory behaviour in loaded asymmetric systems. Ann. Inst. H. Poincaré Anal. Non Linear **4**, 243–274 (1987)
168. A.C. Lazer, P.J. McKenna, Large-amplitude periodic oscillations in suspension bridges: some new connections with nonlinear analysis. SIAM Rev. **32**, 537–578 (1990)
169. A.C. Lazer, P.J. McKenna, On travelling waves in a suspension bridge model as the wave speed goes to zero. Nonlinear Anal. T.M.A. **74**, 3998–4001 (2011)
170. M. Lepidi, V. Gattulli, Parametric interactions in the nonlinear sectional dynamics of suspended and cable-stayed bridges, in *Atti XXI Congresso AIMETA*, Torino, 2013, p. 100
171. M. Lévy, Sur l'équilibre élastique d'une plaque rectangulaire. C. R. Acad. Sci. Paris **129**, 535–539 (1899)
172. S. Levy, Bending of rectangular plates with large deflections. National Advisory Committee for Aeronautics, Washington. Report no. 737 (1942), pp. 139–157
173. S. Levy, D. Goldenberg, G. Zibritosky, Simply supported long rectangular plate under combined axial load and normal pressure. National Advisory Committee for Aeronautics, Washington. Technical Note 949 (1944), p. 24
174. P.-C. Lin, S. Yang, Spontaneous formation of one-dimensional ripples in transit to highly ordered twodimensional herringbone structures through sequential and unequal biaxial mechanical stretching. Appl. Phys. Lett. **90**, 241903 (2007)
175. M.F. Liu, T.P. Chang, D.Y. Zeng, The interactive vibration behavior in a suspension bridge system under moving vehicle loads and vertical seismic excitations. Appl. Math. Model. **35**, 398–411 (2011)
176. A.E.H. Love, *A Treatise on the Mathematical Theory of Elasticity*, 4th edn. (Cambridge University Press, Cambridge, 1927)
177. J.L. Luco, J. Turmo, Effect of hanger flexibility on dynamic response of suspension bridges. J. Eng. Mech. **136**, 1444–1459 (2010)
178. A.M. Lyapunov, Problème général de la stabilité du mouvement. Ann. Fac. Sci. Toulouse **2**(9), 203–474 (1907)
179. J.H.G. Macdonald, Lateral excitation of bridges by balancing pedestrians. Proc. R. Soc. A Math. Phys. Eng. Sci. **465**, 1055–1073 (2009)
180. W. Magnus, S. Winkler, *Hill's Equation* (Dover, New York, 1979)
181. Mail Items. Thames Star. Issue 5531, XVIII:3, 18 October 1886
182. J. Malík, Instability of oscillations in cable-stayed bridges. Appl. Math. **50**, 503–525 (2005)
183. J. Malík, Sudden lateral asymmetry and torsional oscillations in the original Tacoma suspension bridge. J. Sound Vib. **332**, 3772–3789 (2013)
184. I.G. Malkin, *Some Problems in the Theory of Nonlinear Oscillations (Russian)* (Gostekhizdat, Moscow, 1956)
185. H.A. Mann, A History of the Development of the Suspension Bridge, Bachelor thesis, Armour Institute of Technology, Chicago, IL, 1921
186. E.H. Mansfield, *The Bending and Stretching of Plates*, 2nd edn. (Cambridge University Press, Cambridge, 2005)
187. A. Matas, J. Očenášek, Modelling of suspension bridges. Proc. Comput. Mech. **2**, 275–278 (2002)
188. E. Mathieu, Mémoire sur le mouvement vibratoire d'une membrane de forme elliptique. J. Math. Pures Appl. **13**, 137–203 (1868)
189. M. Matsumoto, H. Matsumiya, S. Fujiwara, Y. Ito, New consideration on flutter properties basing on sbs-fundamental flutter mode, similar Selberg's formula, torsional divergence instability, and new coupled flutter phenomena affected by structural coupling, in *BBAA VI International Colloquium on: Bluff Bodies Aerodynamics & Applications*, Milan, 2008
190. M. Matsumoto, H. Shirato, T. Yagi, R. Shijo, A. Eguchi, H. Tamaki, Effects of aerodynamic interferences between heaving and torsional vibration of bridge decks: the case of the Tacoma narrows bridge. J. Wind Eng. **91**, 1547–1557 (2003)

191. P.J. McKenna, Torsional oscillations in suspension bridges revisited: fixing an old approximation. Am. Math. Mon. **106**, 1–18 (1999)
192. P.J. McKenna, Large-amplitude periodic oscillations in simple and complex mechanical systems: outgrowths from nonlinear analysis. Milan J. Math. **74**, 79–115 (2006)
193. P.J. McKenna, Oscillations in suspension bridges, vertical and torsional. Discrete Continuous Dyn. Syst. S **7**, 785–791 (2014)
194. P.J. McKenna, K.S. Moore, The global structure of periodic solutions to a suspension bridge mechanical model. IMA J. Appl. Math. **67**, 459–478 (2002)
195. P.J. McKenna, C.Ó. Tuama, Large torsional oscillations in suspension bridges visited again: vertical forcing creates torsional response. Am. Math. Mon. **108**, 738–745 (2001)
196. P.J. McKenna, W. Walter, Nonlinear oscillations in a suspension bridge. Arch. Ration. Mech. Anal. **98**, 167–177 (1987)
197. P.J. McKenna, W. Walter, Travelling waves in a suspension bridge. SIAM J. Appl. Math. **50**, 703–715 (1990)
198. N.W. McLachlan, *Theory and Application of Mathieu Functions* (Dover Publications, New York, 1964)
199. J. Melan, *Theory of Arches and Suspension Bridges* (Myron Clark, London, 1913). German original: *Handbuch der Ingenieurwissenschaften*, vol. 2 (1906)
200. C. Menn, *Prestressed Concrete Bridges* (Birkhäuser, Basel, 1990)
201. A.M. Micheletti, A. Pistoia, C. Saccon, Nontrivial solutions for a floating beam equation. Ricerche Mat. **48**, 187–197 (1999)
202. A.M. Micheletti, C. Saccon, Multiple nontrivial solutions for a floating beam equation via critical point theory. J. Differ. Equ. **170**, 157–179 (2001)
203. E. Miersemann, Über positive Lösungen von Eigenwertgleichungen mit Anwendungen auf elliptische Gleichungen zweiter Ordnung und auf ein Beulproblem für die Platte. Z. Angew. Math. Mech. **59**, 189–194 (1979)
204. R. Mindlin, Influence of rotatory inertia and shear on flexural motions of isotropic elastic plates. J. Appl. Mech. **18**, 31–38 (1951)
205. K.S. Moore, Large torsional oscillations in a suspension bridge: multiple periodic solutions to a nonlinear wave equation. SIAM J. Math. Anal. **33**, 1411–1429 (2002)
206. B. Moran, A bridge that didn't collapse. Am. Herit. Invent. Technol. **15**, 10–18 (1999)
207. A. Nadai, *Die Elastischen Platten* (Springer, Berlin, 1968)
208. P.M. Naghdi, The theory of shells and plates, in *Handbuch der Physik*, ed. by S. Flügge, C. Truesdell, vol. 6a/2 (Springer, Berlin, 1972), pp. 425–640
209. C.L. Navier, Extraits des recherches sur la flexion des plans élastiques. Bulletin des Sciences de la Société Philomathique de Paris 92–102 (1823)
210. C.L. Navier, *Mémoire sur les ponts suspendus* (Imprimerie Royale, Paris, 1823)
211. New York Times, Big Tacoma Bridge crashes 190 Feet into Puget Sound. November 8, 1940
212. New York Times, A Great Bridge Falls. November 9, 1940
213. R. Ortega, The stability of the equilibrium of a nonlinear Hill's equation. SIAM J. Math. Anal. **25**, 1393–1401 (1994)
214. D. Parker, Marching pedestrians blamed for bridge sway. New Civil Eng., 22 June 2000. http://www.nce.co.uk/marching-pedestrians-blamed-for-bridge-sway/826781.article
215. E.L. Pavlo, Widening and stiffening Whitestone bridge. Eng. News-Rec., 2 October 1947
216. L.A. Peletier, W.C. Troy, Spatial patterns, in *Higher Order Models in Physics and Mechanics*. Progress in Nonlinear Differential Equations and Their Applications, vol. 45 (Birkhäuser, Boston, 2001)
217. M.A. Peletier, Sequential buckling: a variational analysis. SIAM J. Math. Anal. **32**, 1142–1168 (2001)
218. B.G. Pittel, V.A. Yakubovich, Application of the theory of parametric resonance to explain the collapse of the Tacoma narrows bridge (Russian). Uspekhi Mat. Nauk. **15**, 183–184 (1961)
219. B.G. Pittel, V.A. Yakubovich, A mathematical analysis of the stability of suspension bridges based on the example of the Tacoma bridge (Russian). Vestnik Leningrad Univ. **24**, 80–91 (1969)

220. R.H. Plaut, F.M. Davis, Sudden lateral asymmetry and torsional oscillations of section models of suspension bridges. J. Sound Vib. **307**, 894–905 (2007)
221. W. Podolny, Cable-Suspended Bridges, in *Structural Steel Designer's Handbook: AISC, AASHTO, AISI, ASTM, AREMA, and ASCE-07 Design Standards*, ed. by R.L. Brockenbrough, F.S. Merritt, 5th edn. (McGraw-Hill, New York, 2011)
222. H. Poincaré, Introduction to the collected mathematical works of George William Hill, vol. I (Carnegie Institution, Washington, 1905), pp. vii–xviii
223. H. Poincaré, *Les méthodes nouvelles de la mécanique céleste* (Dover Publications, New York, 1957)
224. S.D. Poisson, Mémoire sur l'équilibre et le mouvement des corps élastiques. Mémoires de l'Académie Royale des Sciences de l'Institut de France **8**, 357–570 (1829)
225. W.A. Provis, Observations on the effect of wind on the suspension bridge over Menai Strait. Min. Proc. Inst. Civil Eng. **1**, 74–77 (1841)
226. W.A. Provis, Observations on the effects produced by wind on the suspension bridge over the Menai Strait, more especially as relates to the injuries sustained by the roadways during the storm of January, 1839; together with brief notices of various suggestions for repairing the structure. Trans. Inst. Civil Eng. **3**, 357–370 (1842)
227. A. Pugsley, *The Theory of Suspension Bridges* (Edward Arnold, London, 1968)
228. P. Radu, D. Toundykov, J. Trageser, Finite time blow-up in nonlinear suspension bridges models. J. Differ. Equ. **257**, 4030–4063 (2014)
229. W.J.M. Rankine, *A Manual of Applied Mechanics* (Charles Griffin & Company, London, 1858)
230. W. Reid, A short account of the failure of a part of the Brighton chain pier, in the gale of the 30th of November 1836. Papers on subjects connected with the duties of the corps of royal engineers, Professional Papers of the Corps of Royal Engineers, vol. I (1844)
231. E. Reissner, On the theory of bending elastic plates. J. Math. Phys. **23**, 184–191 (1944)
232. E. Reissner, The effect of transverse shear deformations on the bending of elastic plates. J. Appl. Mech. **12**, 69–77 (1945)
233. A.R. Robinson, H.H. West, *A re-examination of the theory of suspension bridges*. Civil Engineering Series, Structural Research Series no. 322, Doctoral Dissertation, Urbana, Illinois, 1967
234. Y. Rocard, *Dynamic Instability: Automobiles, Aircraft, Suspension Bridges* (Crosby Lockwood, London, 1957)
235. J.S. Russell, On the vibration of suspension bridges and other structures; and the means of preventing injury from this cause. Trans. R. Scott. Soc. Arts **1**, 304–314 (1841)
236. K. Sanderson, Millennium bridge wobble explained. Nature, Published online. Accessed 17 December 2008
237. R.H. Scanlan, The action of flexible bridges under wind, I: flutter theory, II: buffeting theory. J. Sound Vib. **60**, 187–199, 201–211 (1978)
238. R.H. Scanlan, Developments in low-speed aeroelasticity in the civil engineering field. AIAA J. **20**, 839–844 (1982)
239. R.H. Scanlan, J.J. Tomko, Airfoil and bridge deck flutter derivatives. J. Eng. Mech. **97**, 1717–1737 (1971)
240. F.K. Schleyer, Analysis of cables, cable nets, and cable structures, in *Tensile Structures*, ed. by F. Otto, vol. 2 (MIT Press, Cambridge, 1969)
241. R. Scott, *In the Wake of Tacoma: Suspension Bridges and the Quest for Aerodynamic Stability* (ASCE Press, Reston, 2001)
242. A. Selberg, *Oscillation and Aerodynamic Instability of Suspension Bridges*. Civil Engineering and Construction Series, vol. 13 (Acta Polytechnica Scandinavica, Trondheim, 1961)
243. C. Simó, T.J. Stuchi, Central stable/unstable manifolds and the destruction of KAM tori in the planar Hill problem. Physica D **140**, 1–32 (2000)
244. R. Sips, Repŕsentation asymptotique des fonctions de Mathieu et des fonctions d'onde sphéroidales. Trans. Am. Math. Soc. **66**, 93–134 (1949)

245. F.C. Smith, G.S. Vincent, *Aerodynamic Stability of Suspension Bridges: With Special Reference to the Tacoma Narrows Bridge, Part II: Mathematical Analysis*. Investigation conducted by the Structural Research Laboratory, University of Washington (University of Washington Press, Seattle, 1950)
246. J. Song, H. Jiang, W.M. Choi, D.Y. Khang, Y. Huang, J.A. Rogers, An analytical study of two-dimensional buckling of thin films on compliant substrates. J. Appl. Phys. **103**, 014303 (2008)
247. V.M. Starzhinskii, Survey of works on conditions of stability of the trivial solution of a system of linear differential equations with periodic coefficients. Am. Math. Soc. Translat. **2**(1), 189–237 (1955)
248. D.B. Steinman, *A Practical Treatise on Suspension Bridges, Their Design, Construction and Erection* (Wiley, New York, 1922)
249. D.B. Steinman, Letter to the editor. ENR **14**, 41–59 (1941)
250. D.B. Steinman, Design of bridges against wind: IV, aerodynamic instability—prevention and cure. Civil Eng. ASCE 20–23 (January, 1946)
251. D.B. Steinman, S.R. Watson, *Bridges and Their Builders*, 2nd edn. (Dover, New York, 1957)
252. R. Sweetman, *Above the City: A History of Otago Boys' High School 1863–2013* (Otago Boys' High School Foundation, Dunedin, 2013)
253. Tacoma Narrows Bridge Collapse (1940), http://www.youtube.com/watch?v=3mclp9qmcgs (Video)
254. R. Temam, *Infinite-Dimensional Dynamical Systems in Mechanics and Physics*. Applied Mathematical Sciences, vol. 68 (Springer, New York, 1997)
255. The Intelligencer, Destruction of the Wheeling Suspension Bridge, vol. 2, no. 225:3, Wheeling, VA, 18 May 1854, Thursday
256. T. Theodorsen, General theory of aerodynamic instability and the mechanism of flutter. National Advisory Committee for Aeronautics, Report no. 496, (1935)
257. S.P. Timoshenko, Theory of suspension bridges—part I. J. Frankl. Inst. **235**, 213–238 (1943)
258. S.P. Timoshenko, *Theory of Elasticity* (McGraw-Hill, New York, 1951)
259. S.P. Timoshenko, *History of Strengths of Materials* (McGraw-Hill, New York, 1953)
260. S.P. Timoshenko, S. Woinowsky-Krieger, *Theory of Plates and Shells* (McGraw-Hill, New York, 1959)
261. S.P. Timoshenko, D.H. Young, *Theory of Structures* (McGraw-Hill Kogakusha, Tokyo, 1965)
262. C. Truesdell, *Essays in the History of Mechanics* (Springer, Berlin, 1968)
263. C. Truesdell, Some challenges offered to analysis by rational thermomechanics, in *Contemporary Developments in Continuum Mechanics and Partial Differential Equations*, ed. by G.M. de la Penha, L.A. Medeiros (North-Holland, Amsterdam, 1978), pp. 495–603
264. E. Ventsel, T. Krauthammer, *Thin Plates and Shells: Theory, Analysis, and Applications* (Marcel Dekker, New York, 2001)
265. F. Verantii, Machinae Novae. Venetiis cum Privilegiis (1595)
266. F. Verhulst, *Nonlinear Differential Equations and Dynamical Systems* (Springer, Berlin, 1990)
267. F. Verhulst, Perturbation analysis of parametric resonance, in *Encyclopedia of Complexity and Systems Science*, pp. 6625–6639 (Springer, 2009)
268. P. Villaggio, *Mathematical Models for Elastic Structures* (Cambridge University Press, Cambridge, 1997)
269. G.S. Vincent, *Aerodynamic Stability of Suspension Bridges: With Special Reference to the Tacoma Narrows Bridge, Part V: Extended Studies: Logarithmic Decrement Field Damping*. Investigation conducted by the Structural Research Laboratory, University of Washington (University of Washington Press, Seattle, 1954)
270. Volgograd Bridge Oscillations (2010), http://www.bbc.co.uk/news/10138398 (Video)
271. T. von Kármán, Feestigkeitsprobleme in maschinenbau, in *Encycl. der Mathematischen Wissenschaften*, ed. by F. Klein, C. Müller, vol. IV/4C (Leipzig, 1910), pp. 48–352
272. T. von Kármán, L. Edson, *The Wind and Beyond: Theodore von Kármán, Pioneer in Aviation and Pathfinder in Space* (Little, Brown and Company, Boston, 1967)
273. J.A.L. Waddell, *Bridge Engineering* (Wiley, New York, 1916)

274. L.A. Waddell, *Lhasa and its Mysteries: With a Record of the British Tibetan Expedition of 1903–1904* (John Murray, London, 1905)
275. H. Wagner, Über die entstehung des dynamischen auftriebes von tragflügeln. Zeit. Angew. Mathematik und Mechanik **5**, 17–35 (1925)
276. R. Walther, B. Houriet, W. Isler, P. Moïa, J.-F. Klein, *Cable Stayed Bridges*, 2nd edn. (Thomas Telford Publishing, London, 1999)
277. Y. Wang, Finite time blow-up and global solutions for fourth order damped wave equations. J. Math. Anal. Appl. **418**, 713–733 (2014)
278. K. Wardhana, F.C. Hadipriono, Analysis of recent bridge failures in the United States. J. Perform. Constr. Facil. **17**, 144–150 (2003)
279. S. Woinowsky-Krieger, The effect of an axial force on the vibration of hinged bars. J. Appl. Mech. **17**, 35–36 (1950)
280. G.P. Wollmann, Preliminary analysis of suspension bridges. J. Bridge Eng. **6**, 227–233 (2001)
281. V.A. Yakubovich, On the dynamic stability of elastic systems (Russian). Dokl. Akad. Nauk SSSR **121**, 602–605 (1958)
282. V.A. Yakubovich, V.M. Starzhinskii, *Linear Differential Equations with Periodic Coefficients* (Russian original: Izdat. Nauka, Moscow, 1972) (Wiley, New York, 1975)
283. O. Zanaboni, Risoluzione, in serie semplice, della lastra rettangolare appoggiata, sottoposta all'azione di un carico concentrato comunque disposto. Ann. Mat. Pura Appl. **19**, 107–124 (1940)
284. N.E. Zhukovskii, Finiteness conditions for integrals of the equation $d^2y/dx^2 + py = 0$ (Russian). Math. Sb. **16**, 582–591 (1892)
285. S. Živanović, I.M. Díaz, A. Pavić, Influence of walking and standing crowds on structural dynamic properties, in *Proceedings of the IMAC-XXVII* (Society for Experimental Mechanics, Orlando, 2009)

Index

F. Gazzola, *Mathematical Models for Suspension Bridges*, MS&A 15,
DOI 10.1007/978-3-319-15434-3

Author Index

F. Gazzola, *Mathematical Models for Suspension Bridges*, MS&A 15,
DOI 10.1007/978-3-319-15434-3

Bridges Index

F. Gazzola, *Mathematical Models for Suspension Bridges*, MS&A 15,
DOI 10.1007/978-3-319-15434-3

Historical Biographies

1551–1617: Fausto Veranzio, 2
1654–1705: Jacques Bernoulli, 99
1707–1783: Leonhard Euler, 99
1709–1790: Giordano Riccati, 99
1736–1813: Joseph-Louis Lagrange, 229
1756–1827: Ernst Chladni, 10
1756–1828: James Finley, 4
1759–1789: Jacques II Bernoulli, 229
1773–1829: Thomas Young, 99
1776–1831: Marie-Sophie Germain, 229
1776–1852: Samuel Brown, 40
1781–1840: Siméon Denis Poisson, 229
1785–1836: Claude-Louis Navier, 44
1791–1858: William Reid, 8
1820–1872: William John Macquorn Rankine, 45
1824–1887: Gustav Robert Kirchhoff, 178
1847–1884: Carlo Alberto Castigliano, 45
1854–1912: Henri Poincaré, 174
1854–1938: John Alexander Low Waddell, 1
1854–1941: Joseph Melan, 45
1863–1940: Augustus Edward Hough Love, 179
1873–1943: Leon Moisseif, 21
1879–1962: Eugène Freyssinet, 217
1881–1963: Theodore von Kármán, 179
1886–1960: David Bernard Steinman, 45
1900–1982: Herbert Alois Wagner, 125
1903–1992: Yves-André Rocard, 101

F. Gazzola, *Mathematical Models for Suspension Bridges*, MS&A 15,
DOI 10.1007/978-3-319-15434-3